Radiative Corrections to Rare B-Decays, Computational Tools, and Higher Order Perturbative Calculations

---

Dissertation

zur

Erlangung der naturwissenschaftlichen Doktorwürde
(Dr. sc. nat.)

vorgelegt der

Mathematisch-naturwissenschaftlichen Fakultät

der

Universität Zürich

von

Tobias Huber

aus

Deutschland

Promotionskomitee:

Prof. Dr. Daniel Wyler (Vorsitz)
Prof. Dr. Thomas Gehrmann
Prof. Dr. Ulrich Straumann

Zürich, 2006

Contents

List of Figures

List of Tables

Zusammenfassung

Das zu Grunde liegende Modell der Teilchenphysik, das Standardmodell, beschreibt die Wechselwirkungen der Elementarteilchen basierend auf einer $SU(3)_C \times SU(2)_L \times U(1)_Y$-Eichsymmetrie. Es erklärt die Phänomene der Teilchenphysik bis zu den heute an Beschleunigern erzeugten Energien sehr erfolgreich und liefert korrekte Vorhersagen zu vielen Präzisionstests. Es gibt jedoch Hinweise, auf Grund derer man davon überzeugt ist, dass es bei höheren Energien "neue Physik", also Physik jenseits des Standardmodells, gibt.

Mit im Zentrum der heutigen Forschung stehen unter anderem die Experimente an den beiden B-Fabriken am SLAC (USA) und am KEK (Japan), sowie am Fermilab Tevatron (USA), die den Flavorsektor des Standardmodells mit dem Ziel untersuchen, Effekte von neuer Physik auf indirektem Wege zu finden. Weiterhin sollen am Hadronbeschleuniger LHC am CERN (Schweiz) bisher unentdeckte Teilchen durch Proton-Proton Kollisionen bei hohen Energien direkt erzeugt und nachgewiesen werden. Für all diese Experimente sind Präzisionsrechnungen auf theoretischer Seite notwendig, um die Prozesse so gut wie möglich zu verstehen und das Potential dieser Beschleuniger bestmöglich auszuschöpfen.

Der erste Teil der vorliegenden Arbeit beschäftigt sich mit dem inklusiven seltenen Zerfall $\bar{B} \to X_s \ell^+ \ell^-$, der im Standardmodell auf Born-Niveau verboten ist und nur über Schleifendiagramme induziert wird. Er ist damit sensitiv für Physik jenseits des Standardmodells. Im Fall von $\bar{B} \to X_s \ell^+ \ell^-$ betrachtet man das in der invarianten Masse des Leptonpaars differentielle Verzweigungsverhältnis und die vorwärts-rückwärts Asymmetrie. Im Rahmen einer effektiven Theorie werden QED-Korrekturen zu diesen Größen betrachtet. In der führenden Ordnung in QED sind sowohl das Verzweigungsverhältnis als auch die vorwärts-rückwärts Asymmetrie direkt proportional zu $\alpha^2_{\text{em}}(\mu)$, dessen Skalenabhängigkeit von $\pm 4\%$ unter der Variation der perturbativen Skala μ von $\mu \simeq m_b$ nach $\mu \simeq M_W$ aufgrund der bereits erreichten NNLO QCD-Präzision nicht vernachlässigt werden kann. In renormierungsgruppen-verbesserter Störungstheorie werden QED-Korrekturen zu diesen Größen berechnet. Die QED-Korrekturen verringern zum einen die erwähnte Skalenabhängigkeit, zum anderen liefern die QED-Matrixelemente der Operatoren logarithmisch verstärkte Korrekturen proportional zu $\ln(m_b^2/m_\ell^2)$, die ebenfalls numerisch relevant sind. In der abschließenden ausführlichen phänomenologischen Analyse werden all diese Korrekturen berücksichtigt. Weiterhin wird durch einen Wechsel des Renormierungsschemas für die Quarkmassen die Unsicherheit, die von diesen Parametern herrührt, reduziert.

Der zweite Teil der Arbeit behandelt mathematische und rechentechnische Methoden der theoretischen Teilchenphysik. Zunächst wird das `Mathematica`-Paket `HypExp` vorgestellt. Es ermöglicht die Entwicklung von hypergeometrischen Funktionen ${}_JF_{J-1}$ um ganzzahlige Parameter in einer kleinen Größe ϵ zu beliebiger Ordnung. Daneben sind im Paket Ergebnisse gewisser Klassen von Integralen implementiert, die bisher mit `Mathematica` nicht direkt zu berechnen waren. Die Entwicklung von hypergeometrischen Funktionen in deren Parametern taucht bereits in der Berechnung der QED-Matrixelemente zu $\bar{B} \to X_s \ell^+ \ell^-$ in der Phasenraumintegration auf, wird aber auch in vielen Schleifenintegralen im Zusammenhang mit dimensionaler Regularisierung benötigt. Nach einer Einführung in die Anwendung des Pakets wird die Integrationsmethode vorgestellt. Diese ist ein Algorithmus, der zur Entwicklung von ${}_2F_1$-Funktionen bis zur Ordnung $\mathcal{O}(\epsilon^4)$ im Paket implementiert ist.

Zwei Anwendungen des `HypExp`-Programms schließen sich an. Es werden zuerst der Quark-Formfaktor $\gamma^* \to q\bar{q}$ und der Gluon-Formfaktor $H \to gg$ (effektiver Vertex) auf Zwei-Schleifen Niveau in dimensionaler Regularisierung betrachtet. Die Zwei-Schleifen-Basisintegrale werden in exakter Form im Regularisierungsparameter ϵ berechnet, und die bereits bekannten Formfaktoren werden als exakte Funktionen der Basisintegrale angegeben. Im Ergebnis stehen hypergeometrische Funktionen ${}_JF_{J-1}$ vom Argument $z = 1$. Die Zwei-Schleifen-Formfaktoren können somit mit dem `HypExp`-Paket zu beliebiger Ordnung in ϵ entwickelt werden.

Das letzte Kapitel beschäftigt sich mit den Drei-Schleifen-Basisintegralen zu obigen Formfaktoren. Diese Integrale sind wesentliche Bestandteile der Formfaktoren zur Ordnung $\mathcal{O}(\alpha_s^3)$. An künftigen Hadronbeschleunigern wie dem LHC wird die Kenntnis von Observablen zu dieser Präzision von Bedeutung sein. Einige der Drei-Schleifen-Basisintegrale können wiederum zu allen Ordnungen in ϵ angegeben und mit `HypExp` entwickelt werden. Andere werden in Form eines mehrfachen Mellin-Barnes-Integrals dargestellt, aus dem die Koeffizienten der ϵ-Entwicklung Ordnung für Ordnung berechnet werden können. Hierbei sind alle Koeffizienten bis einschließlich Transzendentalität sechs in der Riemannschen Zeta-Funktion zu berechnen.

Summary

The underlying model of particle physics, the Standard Model, describes the interactions among elementary particles based on an $SU(3)_C \times SU(2)_L \times U(1)_Y$ gauge symmetry. It is very successful in explaining the phenomena of particle physics up to energies that are accessible by contemporary acceleration facilities, and yields correct predictions to numerous precision tests. There are, however, indications that convince people that there is "new physics" at higher energies, i.e. physics beyond the Standard Model.

In the center of present-day research are among others the experiments at the two B-factories at SLAC (USA), at KEK (Japan), as well as at the Fermilab Tevatron (USA). They explore the flavor sector of the Standard Model and search indirectly for new physics. Furthermore, the hadron collider LHC at CERN (Switzerland) is designed to produce and detect yet unobserved particles directly by means of proton-proton collisions at very high energies. The processes that are investigated in these experiments require precise theoretical predictions in order to fully exploit the discovery potential of these facilities.

The first part of the present thesis deals with the inclusive rare decay $\bar{B} \to X_s \ell^+ \ell^-$, which is forbidden at tree-level in the Standard Model. It occurs, however, via loop diagrams and is thus sensitive to new physics beyond the Standard Model. In the case of $\bar{B} \to X_s \ell^+ \ell^-$ one considers the differential – with respect to the invariant mass squared of the final state lepton pair – branching ratio and the forward-backward asymmetry. In the framework of an effective theory we consider QED corrections to these quantities. At the leading order (LO) in QED both the differential branching ratio and the forward-backward asymmetry are directly proportional to $\alpha_{\rm em}^2(\mu)$ which exhibits a $\pm 4\%$ scale uncertainty upon varying the perturbative scale μ from $\mu \simeq m_b$ to $\mu \simeq M_W$. This scale uncertainty cannot be neglected since it is as large as the already achieved NNLO QCD precision. We evaluate the QED corrections to these quantities in renormalization-group improved perturbation theory. The QED corrections reduce the aforementioned scale uncertainty. In addition, the QED matrix elements of the operators result in logarithmically enhanced corrections proportional to $\ln(m_b^2/m_\ell^2)$ which are also numerically relevant. All these corrections are included in the concluding extensive phenomenological analysis. Furthermore, we perform a change of renormalization scheme for the quark masses which reduces the uncertainties stemming from these parameters.

The second part of the thesis addresses mathematical and computational methods of theoretical particle physics. We first present the `Mathematica` package `HypExp`. It allows to expand hypergeometric functions ${}_JF_{J-1}$ about integer-valued parameters in a small quantity ϵ to arbitrary order. Furthermore, the package provides results of a certain class of integrals that were not yet implemented in `Mathematica`. The task of expanding hypergeometric functions in their parameters appears already in the phase space integration during the computation of QED matrix elements in $\bar{B} \to X_s \ell^+ \ell^-$. However, in the context of dimensional regularization this kind of expansion is required frequently in loop and phase space integrals. After an introduction on the usage of the package we present the method of integration. This method is an algorithm that is implemented in the package for the expansion of ${}_2F_1$-functions up to order $\mathcal{O}(\epsilon^4)$.

We continue the second part of the thesis by presenting two applications of the `HypExp` package. We first consider the quark form factor $\gamma^* \to q\bar{q}$ and the gluon form factor

$H \to gg$ (effective vertex) at two-loop precision in dimensional regularization. The two-loop master integrals will be calculated to all orders in the regularization parameter ϵ, and the already known form factors will be given as exact functions of the master integrals. The result contains hypergeometric functions ${}_JF_{J-1}$ of unit argument. Hence, the two-loop form factors can be expanded by means of `HypExp` to arbitrary order in ϵ.

In the last chapter we will deal with the three-loop master integrals to the aforementioned form factors. The integrals are essential ingredients to these form factors at order $\mathcal{O}(\alpha_s^3)$. The knowledge of observables to this precision will be of importance at future hadron colliders like the LHC. Some of the master integrals can again be displayed in a closed form in terms of hypergeometric functions of unit argument, and subsequently be expanded by means of the `HypExp` package. Integrals that do not reveal a closed form are displayed as multiple Mellin-Barnes integrals. These representations allow to compute the coefficients of the ϵ-expansion order by order. At this, all coefficients up to and including transcendentality six in the Riemann zeta-function have to be extracted.

Chapter 1

Introduction

It is the essence and the goal of physics to investigate processes in Nature by means of systematic observations and experiments, and to subsume the observed phenomena in physical laws, the latter being most often formulated in the language of mathematics. It is the aim to formulate these laws as general as possible in order to describe many apparently unrelated processes by a common law, and to make predictions for new and yet unobserved phenomena. One can find numerous examples in history where such a *unification* of seemingly disparent phenomena has led to a major breakthrough which oftentimes also catalyzes the development of important technology.

One of the first examples of this kind is Isaac Newton's discovery that planetary motion and the law of falling bodies can both be incorporated into a single law of gravitation. Another impressive example comes from the 19th century physicist James Clerk Maxwell, who formulated his famous equations which unify electricity and magnetism. These equations also allow one to postulate electromagnetic waves which propagate with the speed of light. Based on that Maxwell considered light as a form of electromagnetic waves. The experimental confirmation was rendered by Heinrich Hertz in the 1880's. He discovered the electromagnetic waves, thereby also showing that their properties, such as velocity of propagation, reflection, refraction and polarisation were the same as those of light. These discoveries have had a major impact on subsequent scientific and technical developments, and these achievements affect our lives more than ever.

It is remarkable that these and many other physical laws are quite often based on only a few underlying principles such as symmetries and invariance (or covariance) conditions, thereby exhibiting a certain beauty. These principles are often also the driving force for establishing physical laws that unify various phenomena that until now have seemed unrelated. It should be mentioned though, that physical laws, irrespective of their increasing generality, can only have the claim of *describing*, or at most *explaining*, processes in Nature. They do not answer the question *why* things are the way they are, and it is not their claim. Understanding in physics means – as explained above – that a large number of phenomena can be described in a unified way by means of laws which are based on fundamental principles.

In the field of particle physics the process of combining apparently unrelated phenomena into a common framework has taken place several times in history. It was the combined effort of theorists and experimentalists that ensured the extraordinary success this field has achieved since the late 19th century. The 1897 by J. J. Thomson discovered electron was the first truly elementary particle to be uncovered. In the years thereafter, the quan-

tum theory and relativity were formulated by Planck and Einstein, and the quantization of electromagnetic radiation in the form of the photon was found. The next mile-stones thereafter was the scattering experiment by Rutherford in 1911 whose interpretation led to the atomic model of a positively charged nucleus with surrounding electrons. Furthermore, the discovery of the electron's antiparticle, the positron, in 1932 was another breakthrough. It was already proposed by Dirac in 1928. He established a relativistic quantum theory of spin-1/2 particles which as a consequence of the underlying covariance principle predicted the existence of antiparticles. More examples of this kind, where new particles are predicted from symmetries and invariance principles, shall follow. The neutrino, for instance, was predicted in 1930 by Pauli in order explain the observed continuous electron spectrum in nuclear β-decay and to cure the apparent violation of energy conservation. A few years later, the neutrino was embedded in Fermi's theory of β-decay and weak interaction. It took until 1956 when the neutrino was discovered experimentally in the so-called inverse β-decay.

Until the 1950's, many experimental discoveries in particle physics were based on cosmic rays or nuclear processes. The development of new techniques and the construction of the first acceleration facilities offered the possibility to investigate particle dynamics systematically in a laboratory environment. These machines gave access to higher and higher energies and triggered the discovery of many new particles. The measurement of lifetimes and decay products with the help of sophisticated detector techniques revealed new patterns and gave further insight into particle properties. It was found that the proton and the neutron are compound states. This led, together with other discoveries, to the picture of partons and quarks.

On the theoretical side new ideas and techniques coming for instance from the theory of groups and their representations (e.g. flavor-$SU(3)$ and the "Eightfold Way" founded by Gell-Mann et. al.) or the principle of local (abelian and non-abelian) gauge symmetries came up and led the way to a unified picture of elementary particles and their interactions. Also the discrete symmetries of parity (P), charge conjugation (C), and time reversal (T), as well as their breaking, played an important part.

In the 1960's the picture of quarks (so far u, d, s) became accepted and mesons and baryons were explained as bound states of a quark and an anti-quark and three quarks, respectively. The discovery of the spin-3/2 Δ^{++} and its interpretation as a uuu bound state, together with the Pauli exclusion principle, led to a new quantum number, the color charge. The latter became essential for the development of a theory of strong interaction. In this field, the development of QCD and the discovery of asymptotic freedom by Gross, Wilczek, and Politzer in 1973 can be regarded as additional mile-stones.

In 1970, Glashow, Iliopoulos and Maiani (GIM) predicted the existence of a fourth quark (charm, c) in order to explain the rareness of strangeness-changing neutral current processes. The discovery of the charm quark in the J/Ψ meson in two independent experiments in 1974 was therefore highly appreciated.

In 1973, Kobayashi and Maskawa pointed out the possibility of a third fermion generation to explain the phenomenon of CP violation, which was discovered in the decays of neutral Kaons in 1964 by Fitch and Cronin. Nevertheless, the discovery of the τ-lepton in 1974 and its correct interpretation as a lepton of the third generation came unexpected. However, this discovery triggered the search for a corresponding third quark family, since the theory can only be free of anomalies if there is an equal number of quark and lepton generations. The first member of the third quark family, the bottom (b) quark, was then

found in 1977. The other members of the third fermion family, the τ-neutrino and the top (t) quark, were only discovered two decades later.

It was yet already a few years earlier, in the 1960's, when the seminal step of unifying the electromagnetic and the weak interaction was achieved by Glashow, Salam, and Weinberg. After the introduction of gauge fields $(W_\mu^{(1)}, W_\mu^{(2)}, W_\mu^{(3)})$ for the group $SU(2)_L$ and B_μ for the group $U(1)_Y$, the combinations

$$W_\mu^\pm = \frac{1}{\sqrt{2}} (W_\mu^{(1)} + i\, W_\mu^{(2)}) \tag{1.1}$$

represent the charged gauge bosons coupling to the left-handed fermions. Neither of the fields $W_\mu^{(3)}$) and B_μ can be identified with the photon field, since for instance, their coupling to the neutrino is non-zero. However, the vanishing of the photon's coupling to the neutrino can be put into effect by the combinations

$$A_\mu = B_\mu \cos\theta_W + W_\mu^{(3)} \sin\theta_W \,, \tag{1.2}$$

$$Z_\mu = -B_\mu \sin\theta_W + W_\mu^{(3)} \cos\theta_W \,, \tag{1.3}$$

where A_μ and Z_μ are the photon- and the Z-boson field, respectively, and θ_W is the weak mixing or Weinberg angle. In this framework, the gauge bosons are still massless. This is fine for the photon, but not for $W^\pm$ and Z. The latter acquire a mass through the coupling to the Higgs-boson. The Higgs field is introduced as a doublet

$$\phi = \begin{pmatrix} \phi^+ \\ \phi^0 \end{pmatrix} \tag{1.4}$$

under $SU(2)_L$ and undergoes spontaneous symmetry breaking. The neutral component thereby acquires a non-zero vacuum expectation value, whereas that of the charged one vanishes. This procedure ensures that the heavy gauge bosons $W^\pm$ and Z acquire their masses, whereas the photon remains massless. Via this procedure the simple relation between the masses of the heavy gauge bosons can be derived,

$$M_W = M_Z \cos\theta_W \,. \tag{1.5}$$

All these discoveries and unification processes finally led to today's underlying model of particle physics, the so-called *Standard Model*. It describes the interactions among elementary particles based on an $SU(3)_C \times SU(2)_L \times U(1)_Y$ local gauge symmetry. $SU(3)_C$ is the color group of quarks and gluons, $SU(2)_L$ stands for the group of weak isospin, and $U(1)_Y$ is the hypercharge group. In order for the particles to acquire a mass, the $SU(2)_L \times U(1)_Y$ symmetry is spontaneously broken to the electromagnetic $U(1)_Q$ symmetry,

$$SU(3)_C \times SU(2)_L \times U(1)_Y \stackrel{\text{SSB}}{\longrightarrow} SU(3)_C \times U(1)_Q \,, \tag{1.6}$$

where Q is the generator of the electromagnetic charge. Gauge bosons and fermions obtain their masses by interacting with the Higgs field. It was a great success when 't Hooft and Veltman proved that non-abelian gauge theories are renormalizable. Table 1.1 shows the particle content of the Standard Model together with their quantum numbers. We will not go into more details here. Much more can be said about the Standard Model and its dynamics, and we refer the reader to the textbooks, c. f. Refs. [1–3].

	Generation 1	2	3	$SU(3)_C$ Rep.	$SU(2)_L$ Rep.	I_W^3	Y	Q
Quarks	$\begin{pmatrix} u_L^\alpha \\ d_L^\alpha \end{pmatrix}$	$\begin{pmatrix} c_L^\alpha \\ s_L^\alpha \end{pmatrix}$	$\begin{pmatrix} t_L^\alpha \\ b_L^\alpha \end{pmatrix}$	**3**	**2**	$1/2$ $-1/2$	$1/3$	$2/3$ $-1/3$
	u_R^α, d_R^α	c_R^α, s_R^α	t_R^α, b_R^α	**3**	**1**	0	$4/3$, $-2/3$	$2/3$, $-1/3$
Leptons	$\begin{pmatrix} \nu_{e\,L} \\ e_L \end{pmatrix}$	$\begin{pmatrix} \nu_{\mu\,L} \\ \mu_L \end{pmatrix}$	$\begin{pmatrix} \nu_{\tau\,L} \\ \tau_L \end{pmatrix}$	**1**	**2**	$1/2$ $-1/2$	-1	0 -1
	e_R	μ_R	τ_R	**1**	**1**	0	-2	-1

Boson field	$SU(3)_C$ Rep.	$SU(2)_L$ Rep.	I_W^3	Y	Q
$W_\mu^\pm$	**1**	**3**	± 1	0	± 1
$W_\mu^{(3)}$	**1**	**3**	0	0	0
B_μ	**1**	**1**	0	0	0
G_μ^a	**8**	**1**	0	0	0
$\phi = \begin{pmatrix} \phi^+ \\ \phi^0 \end{pmatrix}$	**1**	**2**	$1/2$ $-1/2$	1	1 0

Table 1.1: Particle content of the Standard Model and transformation properties. L (R) denotes left-handed (right-handed) fields. The superscripts a and α are color indices. I_W^3 stands for the third component of the weak isospin. Q is the electromagnetic charge in units of e, and Y is the weak hypercharge. Antiparticles are not shown explicitly.

In addition, concepts such as effective field theories, renormalization group equations, and calculations in perturbation theory (Feynman rules, Feynman diagrams) gained importance and can be regarded as mile-stones towards the precise computation and automatization of processes on a computer.

At the time the Standard Model was formulated, not all of its particles were yet discovered. Among the gauge bosons, it was – after the photon – the gluon which was first discovered at DESY in Hamburg in 1979 through the observation of three-jet events in e^+e^--collisions. The heavy gauge bosons $W^\pm$ and Z^0 were discovered at CERN in 1983. The experiments at LEP in the 1990's yielded precise values for many quantities in the Standard Model. Precision measurements of the W- and Z-mass became available, and the gauge structure of the Standard Model was explored. From the decay width of the Z^0 one could infer that there are three light generations of neutrinos. The remaining bricks that were still missing for a full confirmation of the Standard Model picture were discovered a few years later – with the exception of the Higgs boson. The top quark was experimentally confirmed at the Tevatron in 1995, five years later, the τ-neutrino was discovered at the DONUT experiment, also at Fermilab. All discoveries confirmed the

Standard Model picture based on spontaneously broken local gauge symmetries.

At the turn of the millenium, new accelerator facilities such as the B-factories at SLAC (USA) and KEK (Japan) were built in order to investigate the flavor sector of the Standard Model. Also several other accelerators have their own flavor program. One seeks to understand the mechanism of flavor and CP violation, and also to search for indirect evidence for physics beyond the Standard Model. In the year 2000, 36 years after the discovery of CP violation in the K-system, this phenomenon was also found in the B-system by the experiments at SLAC and KEK. The experiments at the B factories have also confirmed the Kobayashi-Maskawa mechanism quantitatively to a high precision. Also the lepton flavor sector has been explored. The discovery of neutrino oscillations and other phenomena related to neutrino physics also render important contributions to contemporary particle physics research.

The Higgs boson is the only yet unobserved particle of the Standard Model. It escaped direct detection at LEP, which led to a lower bound of $M_{\text{Higgs}} \geq 114.4$ GeV for the Higgs mass. There are also ongoing searches for the Higgs-boson at the experiments at the Fermilab Tevatron, but until the present day without success. The large hadron collider (LHC) at CERN will collide protons at a center-of-mass energy of $\sqrt{s} = 14$ TeV and is therefore designed to find the Higgs boson and/or new degrees of freedom beyond the Standard Model, and physicists are looking forward to this exciting and perhaps also surprising era.

Despite its tremendous success, the Standard Model has also its weaknesses. The most uncomfortable one is certainly the large number of parameters that enter the theory and that are not predicted by symmetries but have to be determined experimentally. Among these are the masses of the twelve fundamental fermions, the coupling constants of the strong and the weak interaction, the weak mixing angle, and the Higgs vacuum expectation value. Furthermore, the entries of the CKM and PMNS matrix, as discussed in the next section. Problems arise also when one tries to embed the Standard Model in more fundamental theories; the flavor problem, the hierarchy problem and the unification of gauge couplings can be mentioned here. Moreover, the amount of CP violation that the Standard Model can account for is too small to explain the observed matter-antimatter asymmetry in the universe.

One way of addressing these problems is by investigating the flavor sector of the Standard Model to high precision, since this can give insight into the mechanism of flavor and CP violation and also allows one to extract information on physics models beyond the Standard Model. The present thesis' contributions are precision calculations of rare flavor changing neutral current processes, which are in particular sensitive to physics beyond the Standard Model. Moreover, we calculate higher order perturbative corrections to quantites whose precise knowledge will be relevant at hadron colliders such as the LHC. We want to emphasize that the precise determination of observables, both on theoretical and experimental side, is an essential ingredient to fully exploit the discovery potential of present and future acceleration facilities.

As a closing remark, we want to mention the connection between very small scales that are investigated at contemporary and future particle colliders, and very large scales relevant for the dynamics of the universe. From the exploration of heavy particles and the search for unification of the gauge couplings one can draw conclusions about dark matter or the conditions in the early universe.

1.1 Weak interactions of quarks and the CKM matrix

In the flavor sector of the Standard Model, the charged current weak interactions between fermions and the $W^{\pm}$ bosons plays a crucial rôle. The corresponding Lagrangian density reads

$$\mathcal{L}_{CC} = \frac{g_2}{2\sqrt{2}} \left(J_\mu^+ \, W^{+\mu} + J_\mu^- \, W^{-\mu} \right) \,, \tag{1.7}$$

where g_2 is the $SU(2)_L$ coupling constant and

$$J_\mu^+ = (\bar{u} d')_{V-A} + (\bar{c} s')_{V-A} + (\bar{t} b')_{V-A} + \sum_{l=e,\mu,\tau} (\bar{\nu}_l \, l)_{V-A} \tag{1.8}$$

denotes the charged current.[1] The fields (d', s', b') are the weak eigenstates. They are connected to the mass eigenstates (d, s, b) of the down-type quarks via the *Cabibbo-Kobayashi-Maskawa (CKM) matrix*

$$\begin{pmatrix} d' \\ s' \\ b' \end{pmatrix} = \begin{pmatrix} V_{ud} & V_{us} & V_{ub} \\ V_{cd} & V_{cs} & V_{cb} \\ V_{td} & V_{ts} & V_{tb} \end{pmatrix} \cdot \begin{pmatrix} d \\ s \\ b \end{pmatrix} \equiv V_{CKM} \cdot \begin{pmatrix} d \\ s \\ b \end{pmatrix} \quad . \tag{1.9}$$

The CKM matrix is a unitary matrix, which ensures the absence of flavor changing neutral current (FCNC) processes at tree-level in the SM. This is at the bottom of the famous GIM mechanism [4].

Not all the entries in the CKM matrix are independent physical quantities since we can impose rotations on the quark fields and consequently on the CKM matrix that leave the Lagrangian density invariant. One can show that for N quark generations the CKM matrix has

$$\frac{1}{2} \, N \, (N-1) \tag{1.10}$$

independent Euler angles and

$$\frac{1}{2} \, (N-1) \, (N-2) \tag{1.11}$$

independent complex phases, the latter are a necessary ingredient for oberving CP violating effects. It follows that for $N = 2$ the CKM matrix is real and can be parameterized by merely one single angle – the Cabibbo angle θ_C [5]. Hence, for CP violation at least three generations of quarks are required [6]. For $N = 3$ we have three independent Euler angles and one phase, and the CKM matrix can be parameterized by

$$V_{CKM} = \begin{pmatrix} c_{12} \, c_{13} & s_{12} \, c_{13} & s_{13} \, e^{-i\delta} \\ -s_{12} \, c_{23} - c_{12} \, s_{23} \, s_{13} \, e^{i\delta} & c_{12} \, c_{23} - s_{12} \, s_{23} \, s_{13} \, e^{i\delta} & s_{23} \, c_{13} \\ s_{12} \, s_{23} - c_{12} \, c_{23} \, s_{13} \, e^{i\delta} & -s_{23} \, c_{12} - s_{12} \, c_{23} \, s_{13} \, e^{i\delta} & c_{23} \, c_{13} \end{pmatrix} \,, \tag{1.12}$$

with $c_{ij} = \cos\theta_{ij}$ and $s_{ij} = \sin\theta_{ij}$. δ is the phase that is necessary, yet not sufficient for observing CP violating effects in the SM.

The parameterization (1.12) is *exact*. We now make the following change of variables [7]

$$s_{12} = \lambda \,, \qquad s_{23} = A \, \lambda^2 \,, \qquad s_{13} \, e^{-i\delta} = A \, \lambda^3 \, (\rho - i\eta) \,. \tag{1.13}$$

[1] We neglect lepton flavor mixing coming from a PMNS matrix.

Rewriting Eq. (1.12) in terms of these newly defined parameters renders the CKM matrix as a function of (λ, A, ρ, η), which still satisfies unitary exactly. However, from phenomenological applications we know that s_{13} as well as s_{23} are small numbers: $\mathcal{O}(10^{-3})$ and $\mathcal{O}(10^{-2})$ respectively. This implies that also λ has to be small, and allows us to expand the newly parameterized CKM matrix in this quantity, yielding the famous Wolfenstein parameterization [8]

$$V_{CKM} = \begin{pmatrix} 1-\lambda^2/2 & \lambda & \lambda^3 A\,(\rho - i\eta) \\ -\lambda & 1-\lambda^2/2 & \lambda^2 A \\ \lambda^3 A\,(1-\rho-i\eta) & -\lambda^2 A & 1 \end{pmatrix} + \mathcal{O}\left(\lambda^4\right) \ . \tag{1.14}$$

The expansion in λ can even be performed to higher orders. While V_{ub} remains unchanged by definition, the corrections to V_{us} and V_{cb} appear only at $\mathcal{O}(\lambda^7)$ and $\mathcal{O}(\lambda^8)$, respectively. For the full set of V_{ij} to subleading terms in λ we refer the reader to Refs. [7, 9].

From semileptonic kaon decays one extracts $|V_{us}| = 0.2257 \pm 0.0021$ [10, 11], justifying the validity of the expansion in λ.

From the unitarity condition of the CKM matrix follow six normalization and six orthogonality conditions. Of the latter, two are in particular interesting, namely

$$V_{ub}^* V_{ud} + V_{cb}^* V_{cd} + V_{tb}^* V_{td} = 0 \ , \tag{1.15}$$

$$V_{ub}^* V_{tb} + V_{us}^* V_{ts} + V_{ud}^* V_{td} = 0 \ , \tag{1.16}$$

since each product is of the same order $\mathcal{O}(\lambda^3)$. The vanishing of a sum of three complex numbers can be displayed as a triangle in the complex plane. At the leading non-vanishing order in λ the triangles of the two conditions (1.15) and (1.16) are identical. There are, however, differences at subleading orders in λ, see Refs. [12, 13]. We will focus on the first of the above orthogonality relations. Introducing

$$\bar{\rho} \equiv \rho \left(1 - \frac{\lambda^2}{2}\right) \ , \qquad \bar{\eta} \equiv \eta \left(1 - \frac{\lambda^2}{2}\right) \ , \tag{1.17}$$

and including terms of order $\mathcal{O}(\lambda^5)$, we obtain [13]

$$\left[(\bar{\rho} + i\,\bar{\eta}) + (-1) + (1 - \bar{\rho} - i\,\bar{\eta})\right] A\,\lambda^3 + \mathcal{O}(\lambda^7) = 0 \ . \tag{1.18}$$

The three terms in the square bracket build up what is nowadays referred to as the standard Unitarity Triangle. It is displayed in Figure 1.1 together with the labelling of the angles.

One of the main goals in contemporary particle physics related to the flavor sector of the SM is the precise determination of the V_{ij} and the sides and angles of the Unitarity Triangle (UT) with the goal to overconstrain the latter. If the Unitarity Triangle does not close we have evidence for new physics. If it – to whatever precision will be reached – closes, there can still be new physics (NP). For example, the apex extracted from B-decays could in principle be different from the one obtained from K-decays if there are additional sources of flavor violation besides the CKM mechanism. At any rate, the precise determination of UT quantities allows to constrain the parameter space of existing NP models. Below, we present a short and by far not exhaustive list of processes out of which the V_{ij} and the UT quantities can be extracted [10, 11].

- $|V_{ud}|$: From nuclear β-decays, the lifetime of the free neutron, or the decay of a charged pion.

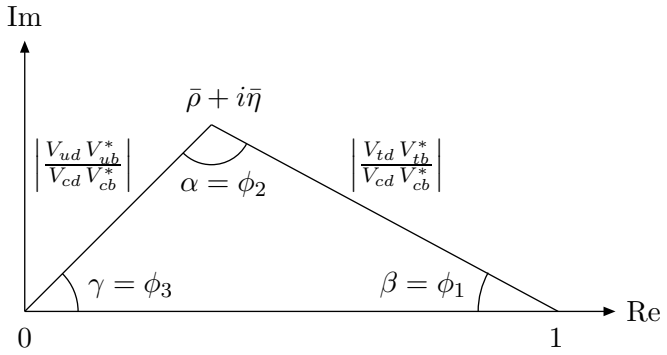

Figure 1.1: Unitarity Triangle

- $|V_{us}|$: From semileptonic kaon decays, leptonic kaon decays, hyperon- and τ decays.
- $|V_{cb}|$: From inclusive $\bar{B} \to X_c\,\ell\,\nu$ decays, and also from exclusive decays of B-mesons to charm.
- $|V_{ub}|$: From inclusive $\bar{B} \to X_u\,\ell\,\nu$ decays, and also from exclusive $B \to \rho\,\ell\,\nu$ and $B \to \pi\,\ell\,\nu$ decays.
- $|V_{td}V_{ts}^*|$: Clean theoretical extraction from the rare decays $K^+ \to \pi^+\nu\bar{\nu}$ and $K_L^0 \to \pi^0\nu\bar{\nu}$.
- $|V_{td}/V_{ts}|$: From ΔM_d and recent ΔM_s measurement [15–17].
- α (ϕ_2): From time-dependent CP asymmetries in $B \to \rho\rho$, $B \to \rho\pi$, $B \to \pi\pi$.
- β (ϕ_1): From tree-level transitions such as $B \to J/\Psi\,K_S$ (gold plated mode) and from pengiun transitions like $B \to \phi\,K_S$.
- γ (ϕ_3): From $B \to D\,K$ decays. $2\beta + \gamma$ also from $B \to D^{(*)}\,\pi$ decays.

Figure 1.2 shows the current status of the Unitarity Triangle [14] with the quantities and their error bars indicated by circles, hyperbolic bands and straight lines. The B-factories and future experiments like LHCb and a possible Super-B factory will further pursue the goal of determining the relevant parameters with ever higher precision. On the theoretical side calculations to ever higher order in perturbation theory and improved understanding of non-perturbative effects are required to achieve a precision that is comparable to the experimental one. Combined effort of theorists and experimentalists is necessary if one seeks for finding new physics in the flavor sector of the SM.

1.2 Effective Field Theory

Effective field theories have proven to be a powerful tool in physical calculations and are therefore widely used. In the context of B-physics they are a dedicated tool in theoretical calculations since there are at least two widely separated scales; a heavy one $M_H \simeq \mathcal{O}(M_W, M_Z, m_t)$ and a light one $M_L \simeq \mathcal{O}(m_b, m_c)$, satisfying $M_H \gg M_L$. The

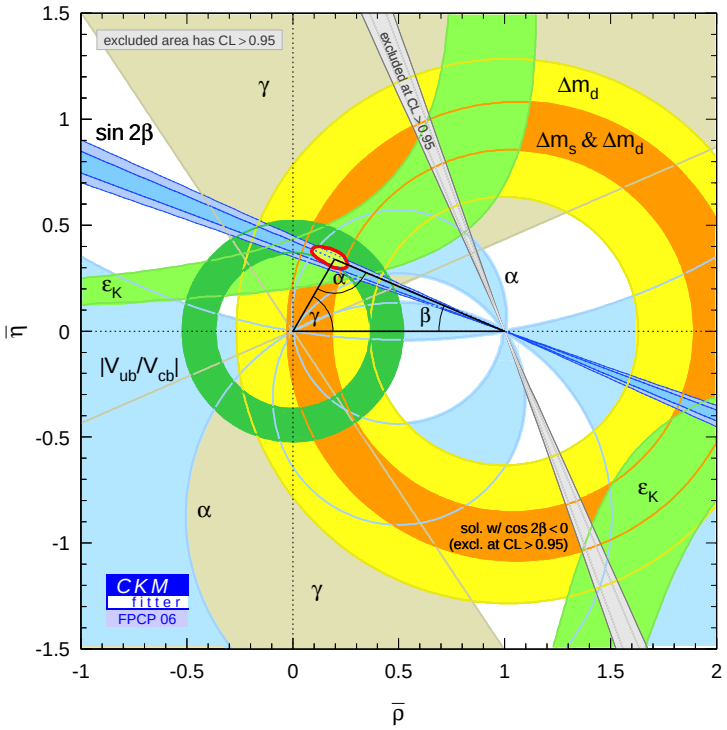

Figure 1.2: The Unitarity Triangle: Constraints in the $(\bar{\rho},\bar{\eta})$ plane [14].

effective theory allows one to separate short distance contributions arising from physics at the scale M_H and long distance contributions from processes associated with M_L. The former can be calculated order by order in perturbation theory. The effective theory is in particular well-suited for taking into account QCD corrections, since large QCD logarithms $\alpha_s^n \ln^n(M_H^2/M_L^2)$ (LO), $\alpha_s^n \ln^{n-1}(M_H^2/M_L^2)$ (NLO) etc. can be resummed order by order in perturbation theory.

1.2.1 Operator Product Expansion

Following Ref. [7], we will show in the next paragraphs how the heavy degrees of freedom which are of order $\mathcal{O}(M_H \simeq M_W, M_Z, m_t)$ get removed upon the transition from the full theory (the Standard Model) to the effective theory. The latter therefore describes the physics at scales of order $\mathcal{O}(M_L \simeq m_b, m_c)$ entirely in terms of light degrees of freedom.

We shall consider the quark-level decay $b \to c\,\bar{u}\,d$, whose tree-level Standard Model (SM) Feynman graph is shown on the left of Fig. 1.3. The amplitude associated with this diagram reads

$$\mathcal{A}_{full} = \frac{g_2^2}{2} V_{cb} V_{ud}^* (\bar{d}_L \gamma_\mu u_L) \frac{g^{\mu\nu}}{q^2 - M_W^2} (\bar{c}_L \gamma_\nu b_L) \,. \tag{1.19}$$

In the above equation, q denotes the four-momentum flowing through the W-propagator, see Fig. 1.3. Its square is kinematically restricted to the interval

$$(m_u + m_d)^2 \leq q^2 \leq (m_b - m_c)^2 \tag{1.20}$$

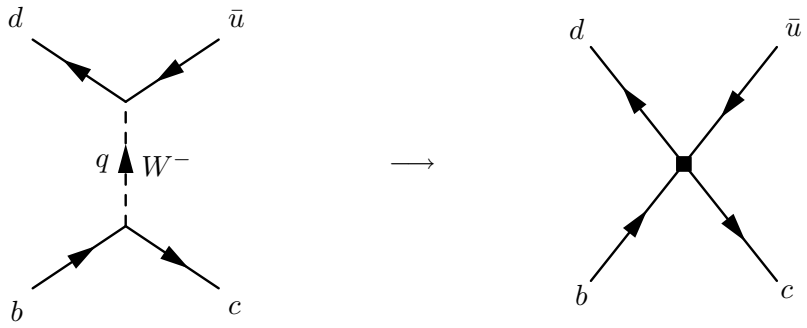

Figure 1.3: The tree-level process $b \to c\,\bar{u}\,d$ in the full (left) and effective (right) theory.

and therefore satisfies $q^2 \ll M_W^2$. We can thus expand $\mathcal{A}_{full}$ in Eq. (1.19) in powers of $q^2/M_W^2 \ll 1$, yielding

$$\mathcal{A}_{full} = -\frac{g_2^2}{2M_W^2}\, V_{cb}\, V_{ud}^* \left[(\bar{d}_L \gamma_\mu u_L)\, (\bar{c}_L \gamma^\mu b_L) + \mathcal{O}(q^2/M_W^2) \right] . \tag{1.21}$$

Since $q^2/M_W^2 \ll 1$, we can safely neglect terms of order $\mathcal{O}(q^2/M_W^2)$, and the full amplitude can be approximated by the first term on the r.h.s. of Eq. (1.21). Now the result of (1.21) can equally well be obtained from

$$\mathcal{H}_{eff} = -\frac{4\,G_F}{\sqrt{2}}\, V_{cb}\, V_{ud}^* \Big[\underbrace{(\bar{d}_L \gamma_\mu u_L)\, (\bar{c}_L \gamma^\mu b_L)}_{\text{dimension-six operator}} + \text{higher dim. operators} \Big] , \tag{1.22}$$

where G_F is the Fermi constant,

$$G_F = \frac{g_2^2}{4\sqrt{2}\, M_W^2} . \tag{1.23}$$

The interaction given by $\mathcal{H}_{eff}$ corresponds to the diagram on the right in Fig. 1.3. The higher dimensional operators in Eq. (1.22), typically involving derivative terms, correspond to $\mathcal{O}(q^2/M_W^2)$ terms in Eq. (1.21). Neglecting the latter corresponds to dropping higher dimensional operators. In this thesis, as in most calculations, we will neglect higher dimensional operators, keeping only operators of dimension five and six.

A more rigorous way of deriving the operators of the effective Hamiltonian is given by the path integral approach. In this approach the heavy degrees of freedom are *integrated out*. The corresponding source terms in the generating functional can be neglected. The integrals over their field components are then of Gaussian type and can be performed analytically. This removes these particles as dynamical degrees of freedom from the Lagrangian. The results are the same as in our derivation (1.19) – (1.22). We will not perform the explicit calculation in the path integral approach here but refer the reader to section 5.3 of Ref. [7].

Our example was a very simple one and served to illustrate the idea of the operator product expansion (OPE), namely that the product of two charged current operators gets expanded into a series of local operators. Due to the interplay of strong and electroweak interactions, the effective Hamiltonian consists of several terms, and quite generally assumes the form

$$\mathcal{H}_{eff} = -\frac{4\,G_F}{\sqrt{2}} \sum_i V_{\rm CKM}^i\, C_i(\mu)\, \mathcal{O}_i(\mu) . \tag{1.24}$$

The effective Hamiltonian relevant for $\bar{B} \to X_s \ell^+ \ell^-$ will be given later in Eq. (2.6). Equation (1.24) exhibits several crucial properties. The $C_i(\mu)$ are the so-called Wilson-coefficients, and μ is referred to as the renormalization scale. The $C_i(\mu)$ summarize the physics contributions from scales higher than μ. For $\mu = \mathcal{O}(M_W)$ they can be calculated in fixed-order perturbation theory. This is done by requiring the amplitude of a given process to be equal in the full theory (in which all particles are present as dynamical degrees of freedom) and in the effective theory (in which the heavy particles have been integrated out) order by order in the coupling constants,

$$\mathcal{A}_{full} = \mathcal{A}_{eff} = -\frac{4\,G_F}{\sqrt{2}} \sum_i V^i_{\rm CKM}\, C_i(\mu)\, \langle \mathcal{O}_i(\mu) \rangle \ . \tag{1.25}$$

This procedure is called the *matching* of the full theory onto the effective one. It renders the $C_i(\mu)$ at a scale $\mu = \mathcal{O}(M_W)$ as an expansion in the perturbative couplings, and each coefficient is a function of the masses of the heavy particles, which in the SM are the W and the Z boson as well as the top quark. An example of a matching calculation can again be found in Ref. [7]. It should be stressed that the $C_i(\mu)$ are process independent in the same manner in which the usual gauge couplings are universal and process independent.

The renormalization scale μ can be chosen arbitrarily. It serves to separate the physics contribution to a given decay amplitude into short-distance contributions at scales higher than μ and long-distance contributions corresponding to scales lower than μ. Usually, one chooses μ to be of the order of the mass of the decaying hadron, in our case $\mu \simeq m_b$.

The virtue of finding the Wilson coefficients first at the high scale $\mu = \mathcal{O}(M_W)$ is that logarithms $\ln(M_H^2/\mu^2)$ are small at this scale, which permits a fixed-order perturbative expansion of the C_i. By evolving this scale from $\mu = \mathcal{O}(M_W)$ down to $\mu = \mathcal{O}(m_b)$ one transforms the physics contributions from scales higher than μ from the matrix elements $\langle \mathcal{O}_i(\mu) \rangle$ into the Wilson coefficients. We will see below how the evolution of the Wilson coefficients from $\mu = \mathcal{O}(M_W)$ down to $\mu = \mathcal{O}(m_b)$ proceeds and want to make two comments here. The total amplitude is independent of μ, and therefore the μ-dependence of the Wilson coefficients has to cancel the μ-dependence of the matrix elements $\langle \mathcal{O}_i(\mu) \rangle$. This cancellation involves generally several terms in the expression (1.25). Furthermore, the total amplitude is also renormalization scheme independent. Any renormalization scheme dependence present in the $C_i(\mu)$ will be compensated by a corresponding scheme dependence in the matrix elements. Again, this cancellation is non-trivial.

1.2.2 Renormalization and Renormalization Group

Like in the case of the Standard Model the Wilson coefficients and the operators in the effective theory undergo renormalization beyond tree-level. At this, the usual counterterm method can be used, supplemented by the introduction of so-called evanescent operators. The latter vanish in four dimensions but are required for a consistency in dimensional regularization. An important feature of the operators in the effective Hamiltonian is that they mix under renormalization. This means that the renormalization of an operator $\mathcal{O}_i$ in general requires also counterterms proportional to the other operators.

From the μ-independence of the effective Hamiltonian one can derive a renormalization group equation for the Wilson coefficients:

$$\mu \frac{d}{d\mu} \vec{C}(\mu) = \hat{\gamma}^T(\mu)\, \vec{C}(\mu) \ , \tag{1.26}$$

where $\hat{\gamma}(\mu)$ is the anomalous dimension of the operators. It decribes the anomalous scaling of the operators with respect to the classical level. Since the operators mix under renormalization, the anomalous dimension adopts the form of a matrix. Equation (1.26) describes the evolution of the Wilson coefficients from the scale $\mu = \mathcal{O}(M_W)$ down to $\mu = \mathcal{O}(m_b)$, with the initial condition for $C_i(\mu)$ taken from the matching calculation at $\mu = \mathcal{O}(M_W)$. The renormalization group equation (1.26) can be solved order by order in perturbation theory. In this way, the Wilson coefficients at the low scale $\mu = \mathcal{O}(m_b)$ are obtained and large logarithms get resummed, resulting in renormalization group improved perturbation theory. More details on this can be found in chapter 2 and in Ref. [7].

1.3 Rare decays

The precise test of the flavor structure and the mechanism of CP violation of the Standard Model (SM) is at the center of today's research in high energy physics. By definition, flavor physics deals with that part of the SM that distinguishes between the three generations of fundamental fermions. At this, the B system represents an ideal framework for the study of flavor physics. The fact that flavor physics is governed by the interplay of strong and electroweak physics makes this field in particular interesting and challenging.

There are several dedicated experiments that explore B physics with increasing sensitivity and within various experimental setups. Apart from the CLEO experiment in Cornell (USA), two B factories running at the $\Upsilon(4S)$ resonance in an asymmetric mode are running successfully at SLAC (USA) and KEK (Japan). Furthermore, the hadronic facilities at Fermilab (USA) and soon the LHC (CERN, Geneva, Switzerland) have their own B physics programs. All these experiments will yield new and precise measurements of observables related to the flavor sector of the SM. The most spectacular recent result of the mass difference in B_s^0 – $\bar{B}_s^0$ mixing came from the experiments CDF [15, 16] and D0 [17] at the Fermilab Tevatron.

Among the decays of B-mesons, the ones that do not occur through the dominant $b \to c$ transition are commonly referred to as rare decays. These include both semileptonic and hadronic $b \to u$ decays that are suppressed at leading order by the small CKM matrix element V_{ub}, as well as higher order $b \to s$ processes such as electroweak and gluonic penguin decays. Among the former, the decays into charmless two-body hadronic final states like $B \to \pi\,\pi$ or $B \to K\,\pi$ are experimentally clean, and provide good opportunities to probe new physics and search for indirect and direct CP violation. Decays into vector mesons such as $B \to \rho\,\rho$ allow for measurements of polarizations and angular distributions of the final state. These are crucial for the extraction of the CKM angle α and for getting insight into both weak- and strong-interaction dynamics in B-decays. These $b \to u$ decays offer a large variety of observables and can be described theoretically in the sophisticated frameworks of QCD factorization [18–20] and soft-collinear effective theory (SCET) [21–27]. However, in this thesis we will be dealing with a decay of the second type. These processes represent flavor changing neutral currents (FCNC) and are forbidden in the SM at tree-level. They do, however, occur at the loop-level.

The B system is well suited for the study of flavor physics. In loop diagrams of B decays and $B - \bar{B}$ mixing, the GIM suppression is not active due to the large top quark mass which satisfies the relation $m_t > M_W \gg m_c,\, m_u$. This is an important difference compared to processes where charmed D-mesons are involved. There, down-type quarks

enter the loop and the GIM suppression is effective due to the relation m_d, m_s, $m_b \ll M_W$. In the case of a unitary CKM matrix and equal masses of quarks of a given charge there would be a complete GIM cancellation. In addition, the structure of the CKM elements entering D processes is less favorable than in the B system. Moreover, the mass of the bottom quark is much larger than the typical scale $\Lambda_{\rm QCD}$ of strong interaction, and many non-perturbative effects can be estimated using heavy mass expansion or heavy quark effective theory (HQET) (c.f. [28–30]).

Among the FCNC processes in B physics, decays associated with the quark level transitions $b \to s\,\gamma$ and $b \to s\,\ell^+\,\ell^-$ play a crucial rôle. Exclusive decay channels such as $\bar{B} \to K^*\,\gamma$ and $\bar{B} \to K^{(*)}\,\ell^+\,\ell^-$ are relatively easy to access experimentally, but difficult to treat on the theoretical side. The hadronic final state involves non-perturbative long-distance effects that are usually modeled by means of form factors. This model dependence is a source of large theoretical uncertainties. Approaches such as lattice QCD, QCD factorization, SCET, QCD sum rules or $1/N_c$-expansions are possible methods to access the exclusive modes theoretically. The problem of long-distance hadronic matrix elements restricts the opportunities in flavor physics significantly. In some cases it is possible to largely circumvent this problem by building ratios of observables in which the unknown long-distance matrix elements cancel. There are, however, also exclusive rare B-decays such as $B_s^0 \to \mu^+\,\mu^-$ that are theoretically rather clean.

In contrast to the exclusive rare B-decay modes, the inclusive ones are theoretically clean observables, because no specific model is needed to describe the hadronic final states. The decay widths $\Gamma(\bar{B} \to X_s\,\gamma)$ and $\Gamma(\bar{B} \to X_s\,\ell^+\,\ell^-)$ are well approximated by the respective partonic decay rate, which can be analyzed within the framework of renormalization group improved perturbation theory. Non-perturbative contributions play only a subdominant rôle and can be calculated in a model-independent way using the heavy mass expansion. The part played by inclusive rare decays is twofold. On the one hand they are useful for the determination of CKM matrix elements. On the other hand, they are particularly sensitive to new physics beyond the SM since additional contribtions from new physics degrees of freedom can result in sizable corrections to the SM predictions. In this way one could find indirect evidence for new physics, or at least constrain the parameter space and explore the flavor structure of new physics models.

However, in life there is no free lunch, which becomes manifest in the fact that fully inclusive measurements are difficult to achieve experimentally. In the case of $\bar{B} \to X_s\,\ell^+\,\ell^-$, with which we will deal in great detail in this work, one has to impose cuts on the hadronic invariant mass M_X. They are required to reduce background coming from $b \to c\,\ell^-\,\bar{\nu}_\ell$ and subsequent $c \to s\,\ell^+\nu_\ell$, yielding $b \to s\,\ell^+\ell^-$ plus missing energy. We will elaborate more on this in chapter 2. Both the exclusive $\bar{B} \to K^{(*)}\,\ell^+\ell^-$ and inclusive $\bar{B} \to X_s\,\ell^+\,\ell^-$ modes of this decay have been measured at BaBar [31,32] and Belle [33–35]. The inclusive results are obtained via a sum over exclusive modes. At BaBar (Belle), the hadronic system X_s consists of one $K^\pm$ or K_S^0 and up to two (four) pions, with at most one π^0. The inclusive result is then obtained under the assumption that the contribution from modes containing a K_L^0 is equal to that of containing a K_S^0. According to Babar and Belle, the missing states that remain unaccounted for represent $\sim 30\%$.

One of the virtues of the inclusive decay $\bar{B} \to X_s\,\ell^+\,\ell^-$ is the fact that it represents a complementary and more complex SM test compared to $B \to X_s\,\gamma$. Kinematical observables such as the dilepton invariant mass spectrum and the forward backward asymmetry provide clean information on short-distance couplings not accessible in $\bar{B} \to X_s\,\gamma$.

Despite the fact that experiments on flavor physics focus largely on B physics, there are also interesting and complementary opportunities offered by the D and the K system. CLEO for instance has a dedicated charm program. In the K system the rare decays $K^+ \to \pi^+ \nu \bar{\nu}$ and $K_L^0 \to \pi^0 \nu \bar{\nu}$ have been studied very intensively in recent years [36–38] and provide another example of theoretically clean exclusive decays.

Future experiments at LHCb and a possible Super-B factory will reach far higher statistics that allow to further constrain the quantities related to the Unitarity Triangle and to explore the flavor structure of the Standard Model or even beyond. These experiments will yield complementary information to the other LHC experiments that are dedicated to find the Higgs boson and to perform a direct search of physics beyond the SM, such as supersymmetry, extra dimensions, Two-Higgs-Doublet models etc.

This thesis consists of two parts and is organized as follows. In the first part, chapter 2 we will be dealing with the inclusive rare decay $\bar{B} \to X_s \ell^+ \ell^-$. We will consider QED corrections to the differential branching ratio and forward backward asymmetry. We will also present an updated phenomenological analysis that includes logarithmically enhanced corrections that emerge in the calculation of QED corrections to four-fermion operators.

In the second part of the thesis we first present the `Mathematica` package `HypExp` in chapter 3. It allows to expand hypergeometric functions ${}_JF_{J-1}$ about integer-valued parameters in a small quantity ϵ to arbitrary order and provides results of a certain class of integrals that were as yet been not implemented in `Mathematica`. The task of expanding hypergeometric functions in their parameters appears frequently in loop and phase space integrations in the context of dimensional regularization.

We continue the second part of the thesis by presenting two applications of the `HypExp` package. In chapter 4 we first consider the quark form factor $\gamma^* \to q\bar{q}$ and the gluon form factor $H \to gg$ (effective vertex) at two-loop precision in dimensional regularization. These form factors contribute to processes relevant at hadronic facilities such as the LHC. We give the results for the two-loop master integrals and for the form factors to all orders in the regularization parameter ϵ and expand the result by means of the `HypExp` package.

In chapter 5 we will deal with the three-loop master integrals to the aforementioned form factors. The integrals are essential ingredients to these form factors at $\mathcal{O}(\alpha_s^3)$ precison. Some of the master integrals can be displayed in a closed form in terms of hypergeometric functions of unit argument, and subsequently be expanded by means of the `HypExp` package. Integrals that do not reveal a closed form are displayed as multiple Mellin-Barnes integrals. These representations allow to compute the coefficients of the ϵ-expansion order by order.

Chapter 2

The Rare Decay $\bar{B} \to X_s \ell^+ \ell^-$: Effects of Logarithmically Enhanced QED Corrections[1]

2.1 Introduction

2.1.1 General Aspects

The inclusive rare decay $\bar{B} \to X_s \ell^+ \ell^-$ with $\ell = e$ or μ is known to be a sensitive probe of new physics at the electroweak scale. Since the Standard Model (SM) does not allow for tree-level flavor-changing neutral current (FCNC) transitions the quark level decay $b \to s\ell^+\ell^-$ can only occur at the loop level. Possible Feynman diagrams are shown in Fig. 2.1 – one of the box-type (left) and one of the penguin-type (middle). In models beyond the SM new degrees of freedom propagating in the loop can give additional contributions that could, in principle, result in quite sizable corrections to the SM predictions and yield indirect evidence for physics beyond the SM. The third diagram in Fig. 2.1 shows an example where supersymmetric particles – in the shown case squarks and charginos – form the loop.

In order to find evidence for new physics in rare decays the SM predictions as well as the results of experimental analyses have to be as precise as possible. On the theoretical side this requires calculations to higher orders in the perturbative expansion as well as control over non-perturbative effects. On the experimental side high statistics and sophisticated techniques in soft- and hardware yield measurements with ever shrinking error bars. One of the virtues of the $\bar{B} \to X_s \ell^+ \ell^-$ decay is that precise SM predictions on the one hand and precise measurements on the other hand can be achieved with contemporary techniques. Furthermore, $\bar{B} \to X_s \ell^+ \ell^-$ serves as a complementary SM test with respect to $\bar{B} \to X_s \gamma$.

The two most important quantities related to the decay $\bar{B} \to X_s \ell^+ \ell^-$ are the differential branching ratio (BR) and the forward backward asymmetry (FBA). The former can be written as a function of the differential decay width $d\Gamma[\bar{B} \to X_s \ell^+ \ell^-]/dq^2$,

$$\frac{d\mathcal{B}(\bar{B} \to X_s \ell^+ \ell^-)}{dq^2} = \frac{\mathcal{B}(B \to X_c e \bar{\nu})_{\rm exp}}{C} \left|\frac{V_{ub}}{V_{cb}}\right|^2 \frac{1}{\Gamma(B \to X_u e \bar{\nu})} \frac{d\Gamma[\bar{B} \to X_s \ell^+ \ell^-]}{dq^2} \,. \quad (2.1)$$

[1] The content of this chapter has been published, in part, in Ref. [39]

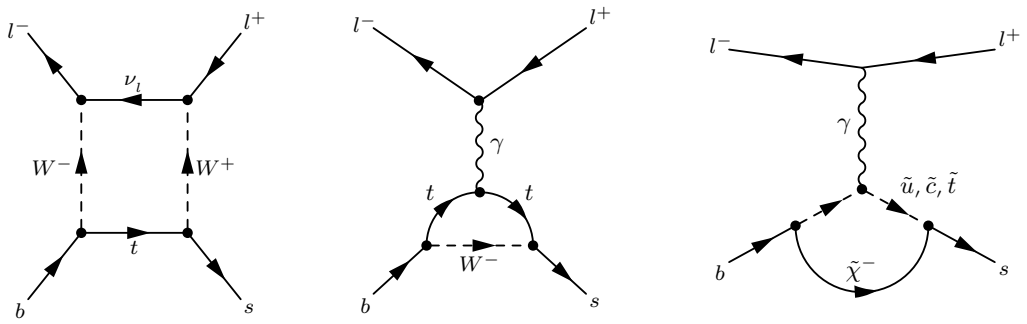

Figure 2.1: Examples of SM (left and middle) and SUSY (right) diagrams contributing to $\bar{B} \to X_s \ell^+ \ell^-$

We will explain this formula in great detail in sections 2.6 and 2.7. The latter reads in its so-called normalized form

$$\bar{\mathcal{A}}_{FB}(q^2) \equiv \frac{d\Gamma/dq^2(\cos\theta_l > 0) \; - \; d\Gamma/dq^2(\cos\theta_l < 0)}{d\Gamma/dq^2(\cos\theta_l > 0) \; + \; d\Gamma/dq^2(\cos\theta_l < 0)} \,. \tag{2.2}$$

In the above equations $q^2 = (p_{\ell^+} + p_{\ell^-})^2$ denotes the invariant mass squared of the final state lepton pair, and θ_l is the angle between the directions of the decaying $\bar{B}$ and the positvely charged lepton in the center of mass frame of the final state lepton pair. In Eq. (2.2) the notation $d\Gamma/dq^2(\cos\theta_l \gtrless 0)$ stands for

$$\begin{aligned} d\Gamma/dq^2(\cos\theta_l < 0) &\equiv \int_{-1}^{0} dz \left(\frac{d^2\Gamma[\bar{B} \to X_s \ell^+ \ell^-]}{dq^2 dz} \right) , \\ d\Gamma/dq^2(\cos\theta_l > 0) &\equiv \int_{0}^{1} dz \left(\frac{d^2\Gamma[\bar{B} \to X_s \ell^+ \ell^-]}{dq^2 dz} \right) , \end{aligned} \tag{2.3}$$

with $z = \cos\theta_l$. The so-called unnormalized FBA corresponds to Eq. (2.2) without the denominator. In Fig. 2.2 the two quantities are displayed as functions of q^2. One distinguishes four regions of q^2 which are separated by blue vertical lines in Fig. 2.2. Each of the regions has its virtues and its drawbacks. The region between the two blue arrows, satisfying 1 GeV$^2 \leq q^2 \leq 6$ GeV^2, is known as the low-q^2 region. There, the rate is relatively high, and the FBA has a zero. The latter, as it turns out, is almost insensitive to hadronic uncertainties. Furthermore, the shape of the curves in this region is sensitive to the interference terms $C_7 \cdot C_9$ (BR), $C_7 \cdot C_{10}$ (FBA), and $C_9 \cdot C_{10}$ (FBA) of Wilson coefficients[2], as we will describe in more detail later in this chapter. Such interference effects are not present in $\bar{B} \to X_s \, \gamma$ whose decay width is proportional to $|C_7|^2$. Another advantage of the low-q^2 region is the fact that $\Lambda_{\rm QCD}/m_b$-type and $\Lambda_{\rm QCD}/m_c$-type power corrections to the quark-level decay rate and FBA are small, which makes the perturbatively calculated partonic q^2-spectrum very clean. These power corrections start in the first place at order $\mathcal{O}(\Lambda^2_{\rm QCD}/m^2_{b,c})$.

On the other hand, the theoretical predictions in this region suffer from rather large scale dependences. Moreover, a fully inclusive measurement in this region is impossible in the forseeable future because of cuts on the hadronic invariant mass M_X. These cuts are

[2]See section 2.2.1 for the definitions of the corresponding operators.

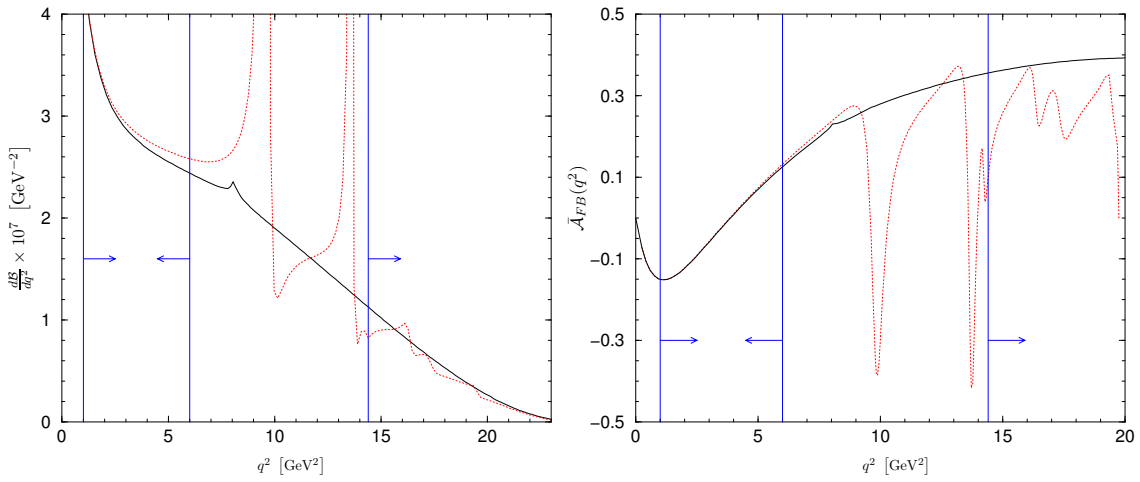

Figure 2.2: NNLO QCD predictions of $d\mathcal{B}/dq^2$ and $\bar{\mathcal{A}}_{FB}(q^2)$ with (dotted red line) and without (solid black line) $c\bar{c}$ effects. Plots courtesy of the authors of Ref. [45].

needed in order to reduce background coming from $b \to c\,\ell^-\bar{\nu}_\ell$ and subsequent $c \to s\,\ell^+\nu_\ell$, yielding $b \to s\,\ell^+\ell^-$ plus missing energy. Currently, one has $M_X \leq 2.0$ GeV at Belle [33] and $M_X \leq 1.8$ GeV at BaBar [31]. The effect of the cuts is an important issue. So far, it has been studied in the Fermi-motion model [40] and recently by using universality of shape functions together with soft-collinear effective theory (SCET) [41, 42].

The region at the very right, satisfying $q^2 \geq 14.4$ GeV^2, is called the high-q^2 region. The BR in this region is dominated by $|C_{10}|^2$. The latter is independent of m_c, and scale independent as far as QCD corrections are concerned. Furthermore, a fully inclusive measurement is easier due to the limited amount of phase space available (small hadronic invariant mass). On the other hand, the $\Lambda_{\rm QCD}/m_b$-type corrections are sizable and there is even a breakdown of that expansion at the endpoint [43, 44]. This breakdown is due to the special kinematical situation and cannot be cured by a partial resummation into a shape function [44]. However, there is an expansion in inverse powers of an effective mass $m_b^{\rm eff} = m_b - (q_i^2)^{1/2}$ for the integrated dilepton mass spectrum, as was shown in [45]. q_i^2 denotes the lower cut in the high-q^2 region. In addition, the rate in the high-q^2 region is much lower compared to the low-q^2 region. This is partly compensated by higher efficiency.

In between the low- and the high-q^2 region intermediate $c\bar{c}$ resonances such as the J/Ψ and the Ψ' show up as peaks in the spectrum. These effects can be modeled [46], but a theoretical calculation from first principles is not possible. The effect of higher $c\bar{c}$ resonances in the high-q^2 region is more pronounced in the FBA compared to the BR [45].

In the very low q^2-region with $q^2 < 1$ GeV^2, the branching ratio is entirely dominated by the contribution from almost real intermediate photons, and it contains essentially the same information on new physics as is already known from the $\bar{B} \to X_s\gamma$ measurements.

2.1.2 Theoretical Aspects

In this thesis we consider the decay $\bar{B} \to X_s\ell^+\ell^-$ in the Standard Model. We will first present the theoretical status of the considered quantities and motivate the necessity of including NLO QED corrections. We will also explain the organization of the perturbative expansion. The computation of the NLO QED corrections and an updated phenomeno-

logical analysis will be the main results of this chapter.

The theoretical predictions of $\bar{B} \to X_s \ell^+ \ell^-$ are well under control because the inclusive hadronic $\bar{B} \to X_s \ell^+ \ell^-$ decay rate is well approximated by the perturbatively calculable partonic $b \to X_s^{\text{parton}} \ell^+ \ell^-$ decay rate. Thanks to the recent (practically) complete calculation [45, 47–52] of the Next-to-Next-to-Leading Order (NNLO) QCD corrections, the perturbative uncertainties are now below 10%. On the experimental side the errors in the branching ratio are expected to be substantially reduced in the near future, calling also for a further improvement of the theoretical precision.

The branching ratio and the forward backward asymmetry are proportional to $\alpha_{em}^2(\mu)$ whose scale dependence cannot be neglected. Indeed, the uncertainty that stems from taking $\alpha_{em}(\mu_0)$ with $\mu_0 = \mathcal{O}(M_W)$ or $\alpha_{em}(\mu_b)$ with $\mu_b = \mathcal{O}(m_b)$ is $\pm 4\%$ and hence as large as the scale uncertainty after the inclusion of NNLO QCD corrections. For example, at the leading order in QED, the low-q^2 integrated BR $\mathcal{B}(B \to X_s \ell^+ \ell^-)$ changes from $1.54 \cdot 10^{-6}$ to $1.65 \cdot 10^{-6}$ when the renormalization scale of α_{em} is changed from $\mu = \mathcal{O}(m_b)$ to $\mu = \mathcal{O}(M_W)$. This uncertainty is removed by calculating those QED corrections that are enhanced by large logarithms $\ln(M_H^2/M_L^2)$, where $M_H \sim M_W, m_t$ and $M_L \sim m_b, \sqrt{q^2}$.

In Ref. [52], the QED corrections to the Wilson coefficients were calculated, thereby giving most of the electromagnetic corrections that are enhanced by $\ln(M_H^2/M_L^2)$. As a result, the authors find a branching ratio of $1.56 \cdot 10^{-6}$, [3] which incidentally corresponds to setting $\alpha_{\text{em}}^2 = \alpha_{\text{em}}^2(\mu \sim m_b)$ at the leading order in QED. In Ref. [39] all the two-loop anomalous dimension matrices that determine the size of the $\ln(M_H^2/M_L^2)$-enhanced electromagnetic corrections were calculated and the results of Ref. [52] confirmed.

However, there are additional QED corrections that get enhanced by large logarithms, namely $\ln(m_b^2/m_\ell^2)$. These corrections are the new result of the present chapter. They originate from these parts of the QED bremsstrahlung corrections where the photon is collinear with one of the outgoing leptons. They disappear after integration over the whole available phase space but survive and remain numerically important when q^2 is restricted to either the low-q^2 or the high-q^2 region.

Such logarithmic corrections are found under the assumption that no collinear photons are included in the definition of the dilepton invariant mass. This turns out to be a very good approximation for the muons in the current BaBar and Belle setups [53]. In this case, the enhancement of the low-q^2 integrated branching ratio by the collinear logarithms amounts to around 2%. The corresponding effect for the electrons would reach around 5%. However, in that case, the logarithm of the electron mass gets replaced by the BaBar and Belle angular cut parameters and the integrated branching ratio for the electrons is expected to be close to that for the muons. We shall describe this issue in more detail in section 2.5. In all other sections, our analytical and numerical results will correspond to the case of perfect separation of electrons and energetic collinear photons.

Before we come to the details of the calculation and the results, some comments on its systematics are in order. Due to the different scales involved, the perturbative corrections come not only with increasing powers of some coupling constant, but also with increasing powers of the large logarithm $L = \ln(M_H^2/M_L^2)$. The perturbative calculation results in an expansion in the product of the coupling with L rather than in the coupling alone.

Because α_s is relatively large, all powers of $c_s = \alpha_s L$ must be resummed at a given order of the perturbative expansion, which is achieved using the renormalization group

[3] The number quoted by the authors of Ref. [52] and on which we agree is $1.57 \cdot 10^{-6}$. In the text we give the result obtained using the updated experimental inputs summarized in Table 2.6.

technology. Within this framework, all the logarithms L are absorbed into $c_s = \mathcal{O}(1)$. Consequently, each electromagnetic logarithm $\alpha_{em}L = c_s\alpha_{em}/\alpha_s$ of the conventional perturbative expansion gets replaced by $f(c_s)\alpha_{em}/\alpha_s$, where the function $f(c_s)$ is found by solving the renormalization group equations. Such a replacement of the electromagnetic logarithm is not a matter of convenience but an unavoidable consequence of resumming the QCD logarithms and not resumming the QED ones. Resummation of the QED logarithms would be technically more difficult and also unnecessary, because $\alpha_{em}L \ll 1$. Thus, the conventional expansion in α_s and α_{em} is replaced by an expansion in α_s and in $\kappa \equiv \alpha_{em}/\alpha_s$. Each order of this expansion is calculated exactly in c_s.

The amplitude of $B \to X_s\ell^+\ell^-$ is proportional to α_{em}. The Leading Order (LO) contributions come from loops and are of order κ (the electromagnetic logarithm comes from a loop). Higher order terms that are proportional to $\kappa\alpha_s$ and $\kappa\alpha_s^2$ are conventionally called the NLO and NNLO QCD contributions, respectively. However, since $\kappa\alpha_s = \alpha_{em}$, the NLO contributions contain purely electroweak terms, too. Since these NLO terms are enhanced by $m_t^2/(M_W^2 \sin^2\theta_W)$ while the LO terms are accidentally suppressed, the two contributions turn out to be very similar in size. An analogous effect occurs at order κ^2: the terms of order $\kappa^2\alpha_s^1$ are larger than the $\kappa^2\alpha_s^0$ ones. For this reason, also high terms in the $\alpha_s^n\kappa^m$-expansion remain numerically important.

The corrections to be considered here (and also in Ref [52]) are of order κ^2 and $\kappa^2\alpha_s$ in the amplitude. Contributions corresponding to $\kappa^2\alpha_s^2 \simeq \alpha_{em}^2$ in the amplitude will be included only if they are enhanced by $\ln(m_b^2/m_\ell^2)$ or by an additional factor of $m_t^2/(M_W^2 \sin^2\theta_W)$. We will come back to this in more detail in section 2.7.

This chapter is organized as follows. In section 2.2, which is quite technical, we introduce the effective theory used for resummation of large QCD logarithms. It includes the list of the relevant operators, the matching conditions for the Wilson coefficients, the renormalization group equations, the anomalous dimension matrices, and the Wilson coefficients at the low scale. Sections 2.3 and 2.4 contain a detailed description of the four-fermion operator matrix element calculation. In section 2.5 we discuss the rôle of the angular cuts. Master formulae for the branching ratio are summarized in section 2.6. In section 2.7 we summarize the numerical results for the branching ratio, focusing on the low-q^2 region. We also explain details of the $\kappa^n\alpha_s^m$-expansion there. Afterwards in sections 2.9 and 2.8 we will give the log-enhanced corrections valid for the FBA and the high-q^2 region of the BR, respectively. We conclude this chapter in section 2.10, where we discuss possible impacts on new physics scenarios. Appendix A contains the loop functions that appear in the text as well as some quantities for the evolution of Wilson coefficients.

2.2 The effective theory

2.2.1 Operator basis

Resummation of large QCD logarithms is most conveniently performed in the framework of a low-energy effective theory [7]. There are ten operators that need to be considered at

the leading order in the electroweak interactions. They can be chosen as follows:

$$\begin{aligned}
P_1 &= (\bar{s}_L \gamma_\mu T^a c_L)(\bar{c}_L \gamma^\mu T^a b_L), \\
P_2 &= (\bar{s}_L \gamma_\mu c_L)(\bar{c}_L \gamma^\mu b_L), \\
P_3 &= (\bar{s}_L \gamma_\mu b_L) \textstyle\sum_q (\bar{q} \gamma^\mu q), \\
P_4 &= (\bar{s}_L \gamma_\mu T^a b_L) \textstyle\sum_q (\bar{q} \gamma^\mu T^a q), \\
P_5 &= (\bar{s}_L \gamma_{\mu_1} \gamma_{\mu_2} \gamma_{\mu_3} b_L) \textstyle\sum_q (\bar{q} \gamma^{\mu_1} \gamma^{\mu_2} \gamma^{\mu_3} q), \\
P_6 &= (\bar{s}_L \gamma_{\mu_1} \gamma_{\mu_2} \gamma_{\mu_3} T^a b_L) \textstyle\sum_q (\bar{q} \gamma^{\mu_1} \gamma^{\mu_2} \gamma^{\mu_3} T^a q), \\
P_7 &= \tfrac{e}{16\pi^2} m_b (\bar{s}_L \sigma^{\mu\nu} b_R) F_{\mu\nu}, \\
P_8 &= \tfrac{g}{16\pi^2} m_b (\bar{s}_L \sigma^{\mu\nu} T^a b_R) G^a_{\mu\nu}, \\
P_9 &= (\bar{s}_L \gamma_\mu b_L) \textstyle\sum_l (\bar{l} \gamma^\mu l), \\
P_{10} &= (\bar{s}_L \gamma_\mu b_L) \textstyle\sum_l (\bar{l} \gamma^\mu \gamma_5 l).
\end{aligned} \tag{2.4}$$

In P_3, ..., P_6 the quark flavors are $q = u, d, s, c, b$. In P_9 and P_{10} all the three lepton flavors are present. Contrary to other analyses [54,55], we have not included any gauge couplings in the normalization of P_9 and P_{10}. Including them would give only a minor simplification in the present investigation.

Once QED corrections are considered, five more operators need to be taken into account. They can be chosen as

$$\begin{aligned}
P_{3Q} &= (\bar{s}_L \gamma_\mu b_L) \textstyle\sum_q Q_q (\bar{q} \gamma^\mu q), \\
P_{4Q} &= (\bar{s}_L \gamma_\mu T^a b_L) \textstyle\sum_q Q_q (\bar{q} \gamma^\mu T^a q), \\
P_{5Q} &= (\bar{s}_L \gamma_{\mu_1} \gamma_{\mu_2} \gamma_{\mu_3} b_L) \textstyle\sum_q Q_q (\bar{q} \gamma^{\mu_1} \gamma^{\mu_2} \gamma^{\mu_3} q), \\
P_{6Q} &= (\bar{s}_L \gamma_{\mu_1} \gamma_{\mu_2} \gamma_{\mu_3} T^a b_L) \textstyle\sum_q Q_q (\bar{q} \gamma^{\mu_1} \gamma^{\mu_2} \gamma^{\mu_3} T^a q), \\
P_b &= \tfrac{1}{12} \left[(\bar{s}_L \gamma_{\mu_1} \gamma_{\mu_2} \gamma_{\mu_3} b_L)(\bar{b} \gamma^{\mu_1} \gamma^{\mu_2} \gamma^{\mu_3} b) - 4 (\bar{s}_L \gamma_\mu b_L)(\bar{b} \gamma^\mu b) \right].
\end{aligned} \tag{2.5}$$

where Q_q are the electric charges of the corresponding quarks ($Q_u = +\frac{2}{3}$ and $Q_d = -\frac{1}{3}$).

The Lagrangian of the effective theory reads

$$\begin{aligned}
\mathcal{L}_{eff} &= \mathcal{L}_{QCD \times QED}(u, d, s, c, b, e, \mu, \tau) \\
&\quad + \frac{4 G_F}{\sqrt{2}} V_{ts}^* V_{tb} \left[\sum_{i=1}^{10} C_i(\mu) P_i + \sum_{i=3}^{6} C_{iQ}(\mu) P_{iQ} + C_b(\mu) P_b \right].
\end{aligned} \tag{2.6}$$

2.2.2 Matching conditions

The Wilson coefficients at the matching scale $\mu_0 \sim M_W, m_t$ are expanded as follows

$$\begin{aligned}
C_k(\mu_0) &= C_k^{(00)}(\mu_0) + \widetilde{\alpha}_s(\mu_0)\, C_k^{(10)}(\mu_0) + \widetilde{\alpha}_s(\mu_0)^2\, C_k^{(20)}(\mu_0) \\
&\quad + \widetilde{\alpha}_s(\mu_0) \kappa(\mu_0)\, C_k^{(11)}(\mu_0) + \widetilde{\alpha}_s(\mu_0)^2 \kappa(\mu_0)\, C_k^{(21)}(\mu_0) + \mathcal{O}(\widetilde{\alpha}_s^3, \kappa^2 \widetilde{\alpha}_s^2),
\end{aligned} \tag{2.7}$$

where $\widetilde{\alpha}_s = \alpha_s / 4\pi$. Note, that at the low scale $\mu_b \sim m_b, \sqrt{q^2}$, also terms of order κ, κ^2 and $\kappa^2 \alpha_s$ arise and are included whenever necessary.

The values of the Wilson coefficients are found from the requirement that all the effective theory Green functions[4] match to the full SM ones at the leading order in M_L^2/M_H^2. At the order we consider, the following non-vanishing contributions to Eq. (2.7) must be taken into account for the four-fermion operators ($s_W^2 \equiv \sin^2\theta_W$):

$$C_2^{(00)}(\mu_0) = 1 , \tag{2.8}$$

$$C_1^{(10)}(\mu_0) = 15 + 6\ln\frac{\mu_0^2}{M_W^2} , \tag{2.9}$$

$$C_4^{(10)}(\mu_0) = E(x_t) - \frac{2}{3} + \frac{2}{3}\ln\frac{\mu_0^2}{M_W^2} , \tag{2.10}$$

$$C_2^{(11)}(\mu_0) = -\frac{7}{3} - \frac{4}{3}\ln\frac{\mu_0^2}{M_Z^2} , \tag{2.11}$$

$$C_3^{(11)}(\mu_0) = \frac{2}{9s_W^2}\left[X(x_t) - 2Y(x_t)\right] , \tag{2.12}$$

$$C_5^{(11)}(\mu_0) = -\frac{1}{18s_W^2}\left[X(x_t) - 2Y(x_t)\right] , \tag{2.13}$$

$$C_9^{(11)}(\mu_0) = \frac{1}{s_W^2}Y(x_t) + W(x_t) + \frac{4}{9} - \frac{4}{9}\ln\frac{\mu_0^2}{m_t^2} , \tag{2.14}$$

$$C_{10}^{(11)}(\mu_0) = -\frac{1}{s_W^2}Y(x_t) , \tag{2.15}$$

$$C_{3Q}^{(11)}(\mu_0) = \frac{2}{3s_W^2}\left[X(x_t) + Y(x_t)\right] - W(x_t) - \frac{4}{9} + \frac{4}{9}\ln\frac{\mu_0^2}{m_t^2} , \tag{2.16}$$

$$C_{5Q}^{(11)}(\mu_0) = -\frac{1}{6s_W^2}\left[X(x_t) + Y(x_t)\right] , \tag{2.17}$$

$$C_b^{(11)}(\mu_0) = -\frac{1}{2s_W^2}S(x_t) , \tag{2.18}$$

$$C_i^{(20)}(\mu_0) = C_i^{t(2)}(\mu_0) - C_i^{c(2)}(\mu_0) \quad \text{for} \quad i = 1, ..., 6 , \tag{2.19}$$

$$C_i^{(21)}(\mu_0) = C_i^{t(2)}(\mu_0) - C_i^{c(2)}(\mu_0) \quad \text{for} \quad i = 9, 10 , \tag{2.20}$$

$$C_9^{(22)}(\mu_0) = -\frac{x_t^2}{32s_W^4}\,(4s_W^2 - 1)\,\left[3 + \tau_b^{(2)}(x_{ht}) - \Delta_t(x_{ht})\right] , \tag{2.21}$$

$$C_{10}^{(22)}(\mu_0) = -\frac{x_t^2}{32s_W^4}\left[3 + \tau_b^{(2)}(x_{ht}) - \Delta_t(x_{ht})\right] . \tag{2.22}$$

All the one-loop coefficients $C_i^{(1m)}(\mu_0)$ above have been evaluated in the $\overline{\text{MS}}$ scheme.[5] The functions $E(x)$, $X(x)$, $Y(x)$, $W(x)$, $S(x)$ are collected in appendix A. All of the above contributions can be found in the literature. The one-loop coefficient $C_2^{(11)}$ is from Ref. [56]. The other one-loop ones have been known since many years (see, e.g., Ref. [57]). For $C_i^{(20)}$ and $C_i^{(21)}$, the relevant top ($C_i^{t(2)}$) and charm ($C_i^{c(2)}$) contributions to the two-loop matching conditions can be found in section 2 of Ref. [47]. The functions $\tau_b^{(2)}$ and

[4]For the on-shell 1PR functions, the operators from section 2.2.1 are sufficient. However, it is often more convenient to find the Wilson coefficients by matching the off-shell 1PI functions. Then, additional operators are necessary — see Eq. (73) of Ref. [47].

[5]Beyond tree-level, the Wilson coefficients usually depend on the choice of evanescent operators. Our choice is the same as in Refs. [50–52].

Δ_t, where $x_t \equiv (m_t^{\overline{MS}}/M_W)^2$ and $x_{ht} \equiv (M_h/m_t^{\overline{MS}})^2$, can be found in Ref. [58]. We take $M_h = 120$ GeV. We include also the contributions to $C_{i(Q)}^{(21)}(\mu_0)$ that were calculated in Refs. [47, 59]. Transforming the results of Ref. [59] to our operator basis is non-trivial.[6]

2.2.3 Renormalization Group Equations

In the effective theory, the RGE for the gauge couplings read[7]

$$\begin{aligned} \mu\frac{d\widetilde{\alpha}_{\rm s}}{d\mu} &= -2\widetilde{\alpha}_{\rm s}^2 \sum_{n,m=0} \beta^s_{nm} \widetilde{\alpha}_{\rm s}^n \widetilde{\alpha}_{\rm e}^m, \\ \mu\frac{d\widetilde{\alpha}_{\rm e}}{d\mu} &= +2\widetilde{\alpha}_{\rm e}^2 \sum_{n,m=0} \beta^e_{nm} \widetilde{\alpha}_{\rm e}^n \widetilde{\alpha}_{\rm s}^m, \end{aligned} \tag{2.23}$$

where $\widetilde{\alpha}_e = \alpha_{\rm em}/4\pi$. The solution for $\widetilde{\alpha}_{\rm s}(\mu)$ with the initial condition at $\mu = \mu_0$ is found perturbatively in $\widetilde{\alpha}_{\rm s}(\mu_0)$ and $\widetilde{\alpha}_{\rm e}(\mu_0)$ but exactly in $v_s = 1+2\beta^s_{00}\widetilde{\alpha}_{\rm s}(\mu_0)\ln\frac{\mu}{\mu_0}$ and $v_e = 1-2\beta^e_{00}\widetilde{\alpha}_{\rm e}(\mu_0)\ln\frac{\mu}{\mu_0}$. Including all the three-loop contributions, and, in addition, the four-loop pure-QCD term, one obtains

$$\begin{aligned} \widetilde{\alpha}_{\rm s}(\mu) &= \frac{\widetilde{\alpha}_{\rm s}(\mu_0)}{v_s} - \frac{\widetilde{\alpha}_{\rm s}(\mu_0)^2}{v_s^2}\left(\frac{\beta^s_{10}}{\beta^s_{00}}\ln v_s - \frac{\beta^s_{01}}{\beta^e_{00}}\ln v_e\right) \\ &+ \frac{\widetilde{\alpha}_{\rm s}(\mu_0)^3}{v_s^3}\left[\frac{\beta^s_{20}}{\beta^s_{00}}(1-v_s) + \left(\frac{\beta^s_{10}}{\beta^s_{00}}\right)^2\left(\ln^2 v_s - \ln v_s + v_s - 1\right)\right. \\ &\qquad \left. + \left(\frac{\beta^s_{01}}{\beta^e_{00}}\right)^2 \ln^2 v_e + \frac{\beta^s_{01}\beta^s_{10}}{\beta^s_{00}\beta^e_{00}}\left(-2\ln v_s \ln v_e + \rho\, v_e \ln v_e\right)\right] \\ &+ \frac{\widetilde{\alpha}_{\rm s}(\mu_0)^4}{v_s^4}\left[\frac{\beta^s_{30}}{\beta^s_{00}}\frac{1-v_s^2}{2} + \frac{\beta^s_{20}\beta^s_{10}}{(\beta^s_{00})^2}\left((2v_s-3)\ln v_s + v_s^2 - v_s\right)\right. \\ &\qquad \left. + \left(\frac{\beta^s_{10}}{\beta^s_{00}}\right)^3\left(-\ln^3 v_s + \frac{5}{2}\ln^2 v_s + 2(1-v_s)\ln v_s - \frac{1}{2}(v_s-1)^2\right)\right] \\ &+ \frac{\widetilde{\alpha}_{\rm s}(\mu_0)^2\widetilde{\alpha}_{\rm e}(\mu_0)}{v_s^2 v_e}\left[\frac{\beta^s_{02}}{\beta^e_{00}}(v_e-1) + \frac{\beta^s_{11}}{\beta^s_{00}}\rho\, v_e \ln\frac{v_e}{v_s} + \frac{\beta^s_{01}\beta^e_{10}}{(\beta^e_{00})^2}\left(\ln v_e - v_e + 1\right)\right. \\ &+ \left.\frac{\beta^s_{01}\beta^s_{10}}{(\beta^s_{00})^2}\rho\ln v_s + \frac{\beta^s_{01}\beta^e_{01}}{\beta^s_{00}\beta^e_{00}}\left(\rho\, v_e \ln\frac{v_s}{v_e} - \ln v_s\right)\right] + \widetilde{\alpha}_{\rm s}^2 \times \mathcal{O}(\widetilde{\alpha}_{\rm s}^3, \widetilde{\alpha}_{\rm e}^2, \widetilde{\alpha}_{\rm s}\widetilde{\alpha}_{\rm e}), \end{aligned} \tag{2.24}$$

where $\rho = \beta^s_{00}\widetilde{\alpha}_{\rm s}(\mu_0)/(\beta^s_{00}\widetilde{\alpha}_{\rm s}(\mu_0) + \beta^e_{00}\widetilde{\alpha}_{\rm e}(\mu_0))$. The corresponding solution for $\widetilde{\alpha}_{\rm e}(\mu)$ can be found by obvious replacements: $v_s \leftrightarrow v_e$, $\widetilde{\alpha}_{\rm s} \leftrightarrow \widetilde{\alpha}_{\rm e}$ and $\beta^s_{ij} \leftrightarrow -\beta^e_{ij}$ (also inside the ratio ρ).

The $\overline{\rm MS}$ values of the pure-QCD coefficients β^s_{i0} can be found in Refs. [60, 61]. After substituting $C_A = N = 3$, $C_F = \frac{4}{3}$, $t_F = \frac{1}{2}$ and $n_f = 5$, one finds $\beta^s_{00} = \frac{23}{3}$, $\beta^s_{10} = \frac{116}{3}$,

[6] We thank Ulrich Haisch for providing us with the relevant transformation matrices.

[7] The equations and solutions of subsection 2.2.3 have been kindly provided by my collaborators from Ref. [39].

$\beta^s_{20} = \frac{9769}{54}$ and $\beta^s_{30} = \frac{352864}{81}\zeta(3) - \frac{598391}{1458}$. The remaining beta-function coefficients that enter into Eq. (2.24) read

$$\begin{aligned}
\beta^s_{01} &= -4t_F\overline{Q^2} = -\tfrac{22}{9}, & \beta^e_{00} &= \tfrac{4}{3}\left(\overline{Q^2}N + 3Q_l^2\right) = \tfrac{80}{9},\\
\beta^s_{11} &= (4C_F - 8C_A)\,t_F\overline{Q^2} = -\tfrac{308}{27} & \beta^e_{10} &= 4\left(\overline{Q^4}N + 3Q_l^4\right) = \tfrac{464}{27},\\
\beta^s_{02} &= \tfrac{11}{3}t_F\overline{Q^2}\beta^e_{00} + 2t_F\overline{Q^4} = \tfrac{4945}{243} & \beta^e_{01} &= 4C_F N\overline{Q^2} = \tfrac{176}{9},
\end{aligned} \tag{2.25}$$

where $Q_l = -1$, $Q_u = \frac{2}{3}$, $Q_d = -\frac{1}{3}$ and $\overline{Q^n} = 2Q_u^n + 3Q_d^n$. All of them except β^s_{11} can be found by modifying the color and charge factors in the pure QCD results. β^s_{11} was found by an explicit three-loop calculation of my collaborators from Ref. [39]. To our knowledge, no result for this coefficient has been published before.

The RGE for the Wilson coefficients reads

$$\mu\frac{d}{d\mu}\vec{C}(\mu) = \hat{\gamma}^T(\mu)\vec{C}(\mu), \tag{2.26}$$

where the Anomalous Dimension Matrix (ADM) has the following expansion:

$$\hat{\gamma}(\mu) = \sum_{\substack{n,m=0\\ n+m\geq 1}} \hat{\gamma}^{(nm)}\widetilde{\alpha}_{\rm s}(\mu)^n\widetilde{\alpha}_{\rm e}(\mu)^m. \tag{2.27}$$

In Eq. (2.24), we have made no use of the fact that $\widetilde{\alpha}_{\rm e} \ll \widetilde{\alpha}_{\rm s}$. Now we shall take this relation into account, and solve the RGE (2.26) perturbatively in

$$\lambda \equiv \frac{\beta^e_{00}\,\widetilde{\alpha}_{\rm e}(\mu_0)}{\beta^s_{00}\,\widetilde{\alpha}_{\rm s}(\mu_0)} \qquad \text{and} \qquad \omega \equiv 2\beta^s_{00}\widetilde{\alpha}_{\rm s}(\mu_0), \tag{2.28}$$

neglecting terms of order $\mathcal{O}(\omega^3, \lambda^3, \omega^2\lambda^2)$. Let us introduce the following short-hand notation:

$$\begin{aligned}
b_1 &= \frac{\beta^s_{10}}{2(\beta^s_{00})^2}, \qquad b_2 = \frac{\beta^s_{20}}{4(\beta^s_{00})^3} - b_1^2, \qquad b_3 = \frac{\beta^s_{01}}{2\beta^s_{00}\beta^e_{00}},\\
b_4 &= \frac{\beta^s_{11}}{4(\beta^s_{00})^2\beta^e_{00}} - 2b_1b_3, \qquad b_5 = \frac{\beta^e_{01}}{2\beta^s_{00}\beta^e_{00}} - b_1, \qquad \hat{W}^{(nm)} = \frac{\left(\hat{\gamma}^{(nm)}\right)^T}{(2\beta^s_{00})^n(2\beta^e_{00})^m}.
\end{aligned} \tag{2.29}$$

The known evolution of the gauge couplings (2.24) allows us to rewrite the RGE (2.26) in terms of the variable $\eta = \widetilde{\alpha}_{\rm s}(\mu_0)/\widetilde{\alpha}_{\rm s}(\mu)$

$$\frac{d}{d\eta}\vec{C} = \frac{1}{\eta}\left[\hat{W}^{(10)} \;+\; \sum_{k=-2}^{2}\hat{B}^{(k)}\eta^k \;+\; \lambda^2\omega b_5\hat{W}^{(01)}\eta\ln\eta \;+\; \mathcal{O}(\omega^3, \lambda^3, \omega^2\lambda^2)\right]\vec{C}. \tag{2.30}$$

where the matrices $\hat{B}^{(k)}$ are η-independent

$$\hat{B}^{(-2)} = \omega^2\left(\hat{W}^{(30)} - b_1\hat{W}^{(20)} - b_2\hat{W}^{(10)}\right), \tag{2.31}$$

$$\hat{B}^{(-1)} = \omega\left(\hat{W}^{(20)} - b_1\hat{W}^{(10)}\right) + \omega^2\lambda\left(\hat{W}^{(21)} - b_1\hat{W}^{(11)} - b_2\hat{W}^{(01)} - b_3\hat{W}^{(20)} - b_4\hat{W}^{(10)}\right), \tag{2.32}$$

$$\hat{B}^{(0)} = \omega\lambda(1-\lambda)\left(\hat{W}^{(11)} - b_1\hat{W}^{(01)} - b_3\hat{W}^{(10)}\right), \tag{2.33}$$

$$\hat{B}^{(1)} = \lambda(1-\lambda)\hat{W}^{(01)} + \omega\lambda^2\left(\hat{W}^{(02)} + \hat{W}^{(11)} - (b_1+b_3)\hat{W}^{(01)} - b_3\hat{W}^{(10)}\right), \tag{2.34}$$

$$\hat{B}^{(2)} = \lambda^2\hat{W}^{(01)}. \tag{2.35}$$

The solution to Eq. (2.30) reads

$$\vec{C}(\mu) = \hat{V} \left[\hat{D}(\eta) + \sum_{k=-2}^{2} \hat{F}^{(k)}(\eta) + \sum_{k,l=-2}^{2} \hat{G}^{(kl)}(\eta) + \sum_{k,l,m=-2}^{2} \hat{H}^{(klm)}(\eta) + \hat{R}(\eta) + \mathcal{O}(\omega^3, \lambda^3, \omega^2\lambda^2) \right] \hat{V}^{-1} \vec{C}(\mu_0), \tag{2.36}$$

where $\hat{V}$ is the matrix that diagonalizes $\hat{W}^{(10)}$

$$\left[\hat{V}^{-1} \hat{W}^{(10)} \hat{V} \right]_{ij} = a_{\underline{i}} \delta_{ij}. \tag{2.37}$$

The eigenvalues a_i and entries of the matrix $\hat{V}$ are given numerically in appendix A. The matrices $\hat{D}(\eta)$, $\hat{F}^{(k)}(\eta)$, $\hat{G}^{(kl)}(\eta)$, $\hat{H}^{(klm)}(\eta)$ and $\hat{R}(\eta)$ depend on the a_i and on products $\hat{E}^{(k)} \equiv \hat{V}^{-1} \hat{B}^{(k)} \hat{V}$. They read

$$\hat{D}_{ij}(\eta) = \eta^{a_{\underline{i}}} \delta_{ij}, \qquad \hat{F}^{(k)}_{ij}(\eta) = \hat{E}^{(k)}_{ij} f^{(k)}_{\underline{ij}}(\eta), \qquad \hat{G}^{(kl)}_{ij}(\eta) = \sum_p \hat{E}^{(k)}_{ip} \hat{E}^{(l)}_{pj} g^{(kl)}_{\underline{ipj}}(\eta),$$

$$\hat{H}^{(klm)}_{ij}(\eta) = \sum_{p,q} \hat{E}^{(k)}_{ip} \hat{E}^{(l)}_{pq} \hat{E}^{(m)}_{qj} h^{(klm)}_{\underline{ipqj}}(\eta), \qquad \hat{R}_{ij}(\eta) = \lambda^2 \omega b_5 \left(\hat{V}^{-1} \hat{W}^{(01)} \hat{V} \right)_{ij} r^{(1)}_{\underline{ij}}(\eta). \tag{2.38}$$

The functions $f^{(k)}_{ij}(\eta)$, $g^{(kl)}_{ipj}(\eta)$, $h^{(klm)}_{ipqj}(\eta)$ and $r^{(k)}_{ij}(\eta)$ are given by

$$f^{(k)}_{ij}(\eta) = \begin{cases} \eta^{a_i} \ln \eta, & \text{when } a_j + k - a_i = 0, \\ \frac{1}{a_j + k - a_i} \left(\eta^{a_j + k} - \eta^{a_i} \right), & \text{otherwise,} \end{cases} \tag{2.39}$$

$$r^{(k)}_{ij}(\eta) = \begin{cases} \frac{1}{2} \eta^{a_i} \ln^2 \eta, & \text{when } a_j + k - a_i = 0, \\ \frac{1}{a_j + k - a_i} \left(\eta^{a_j + k} \ln \eta - f^{(k)}_{ij}(\eta) \right), & \text{otherwise,} \end{cases} \tag{2.40}$$

$$g^{(kl)}_{ipj}(\eta) = \begin{cases} r^{(k)}_{ip}(\eta) & \text{when } a_j + l - a_p = 0, \\ \frac{1}{a_j + l - a_p} \left(f^{(k+l)}_{ij}(\eta) - f^{(k)}_{ip}(\eta) \right), & \text{otherwise,} \end{cases} \tag{2.41}$$

$$h^{(klm)}_{ipqj}(\eta) = \begin{cases} \frac{1}{6} \eta^{a_i} \ln^3 \eta, & \text{when } a_p + k - a_i = a_q + l - a_p = a_j + m - a_q = 0, \\ \frac{1}{a_p + k - a_i} \left(\frac{1}{2} \eta^{a_p + k} \ln^2 \eta - r^{(k)}_{ip}(\eta) \right), & \text{when } a_p + k - a_i \neq 0 \text{ and } a_q + l - a_p = a_j + m - a_q = 0, \\ \frac{1}{a_q + l - a_p} \left(r^{(k+l)}_{iq}(\eta) - g^{(kl)}_{ipq}(\eta) \right), & \text{when } a_q + l - a_p \neq 0 \text{ and } a_j + m - a_q = 0, \\ \frac{1}{a_j + m - a_q} \left(g^{(k,l+m)}_{ipj}(\eta) - g^{(kl)}_{ipq}(\eta) \right), & \text{when } a_j + m - a_q \neq 0. \end{cases} \tag{2.42}$$

2.2.4 Anomalous dimension matrices

In the present section, we give the ADM's for the four-fermion operators. The calculation and the results of the one- and two-loop ADM matrices were again kindly provided

by my collaborators from Ref [39]. We checked that they agree with results from the literature, see Refs. [47, 52, 54, 55, 62–64]. When the operators are ordered as in the list $\{P_1, ..., P_6, P_9, P_{10}, P_{3Q}, ..., P_{6Q}, P_b\}$, then the matrices that enter Eq. (2.27) have the following generic structure:

$$\hat{\gamma}^{(nm)} = \begin{bmatrix} (\hat{\gamma}^{(nm)}_{CC})_{2\times2} & (\hat{\gamma}^{(nm)}_{CP})_{2\times4} & (\hat{\gamma}^{(nm)}_{CL})_{2\times2} & (\hat{\gamma}^{(nm)}_{CQ})_{2\times4} & 0_{2\times1} \\ 0_{4\times2} & (\hat{\gamma}^{(nm)}_{PP})_{4\times4} & (\hat{\gamma}^{(nm)}_{PL})_{4\times2} & (\hat{\gamma}^{(nm)}_{PQ})_{4\times4} & 0_{4\times1} \\ 0_{2\times2} & (\hat{\gamma}^{(nm)}_{LP})_{2\times4} & (\hat{\gamma}^{(nm)}_{LL})_{2\times2} & (\hat{\gamma}^{(nm)}_{LQ})_{2\times4} & 0_{2\times1} \\ 0_{4\times2} & (\hat{\gamma}^{(nm)}_{QP})_{4\times4} & (\hat{\gamma}^{(nm)}_{QL})_{4\times2} & (\hat{\gamma}^{(nm)}_{QQ})_{4\times4} & 0_{4\times1} \\ 0_{1\times2} & (\hat{\gamma}^{(nm)}_{BP})_{1\times4} & (\hat{\gamma}^{(nm)}_{BL})_{1\times2} & (\hat{\gamma}^{(nm)}_{BQ})_{1\times4} & (\hat{\gamma}^{(nm)}_{BB})_{1\times1} \end{bmatrix}. \tag{2.43}$$

However, the pure-QCD ADM's have a much simpler structure

$$\hat{\gamma}^{(n0)} = \begin{bmatrix} (\hat{\gamma}^{(n0)}_{CC})_{2\times2} & (\hat{\gamma}^{(n0)}_{CP})_{2\times4} & 0_{2\times2} & 0_{2\times4} & 0_{2\times1} \\ 0_{4\times2} & (\hat{\gamma}^{(n0)}_{PP})_{4\times4} & 0_{4\times2} & 0_{4\times4} & 0_{4\times1} \\ 0_{2\times2} & 0_{2\times4} & 0_{2\times2} & 0_{2\times4} & 0_{2\times1} \\ 0_{4\times2} & (\hat{\gamma}^{(n0)}_{QP})_{4\times4} & 0_{1\times2} & (\hat{\gamma}^{(n0)}_{QQ})_{4\times4} & 0_{4\times1} \\ 0_{1\times2} & (\hat{\gamma}^{(n0)}_{BP})_{1\times4} & 0_{1\times2} & 0_{1\times4} & (\hat{\gamma}^{(n0)}_{BB})_{1\times1} \end{bmatrix}. \tag{2.44}$$

Moreover, four additional blocks vanish in $\hat{\gamma}^{(01)}$

$$\hat{\gamma}^{(01)}_{CP} = 0, \qquad \hat{\gamma}^{(01)}_{PP} = 0, \qquad \hat{\gamma}^{(01)}_{LP} = 0, \qquad \hat{\gamma}^{(01)}_{BP} = 0. \tag{2.45}$$

We need to know all the non-vanishing blocks of $\hat{\gamma}^{(10)}$ and $\hat{\gamma}^{(20)}$:

$$\hat{\gamma}^{(10)}_{CC} = \begin{bmatrix} -4 & \frac{8}{3} \\ 12 & 0 \end{bmatrix}, \quad \hat{\gamma}^{(10)}_{CP} = \begin{bmatrix} 0 & -\frac{2}{9} & 0 & 0 \\ 0 & \frac{4}{3} & 0 & 0 \end{bmatrix}, \quad \hat{\gamma}^{(10)}_{PP} = \begin{bmatrix} 0 & -\frac{52}{3} & 0 & 2 \\ -\frac{40}{9} & -\frac{100}{9} & \frac{4}{9} & \frac{5}{6} \\ 0 & -\frac{256}{3} & 0 & 20 \\ -\frac{256}{9} & \frac{56}{9} & \frac{40}{9} & -\frac{2}{3} \end{bmatrix},$$

$$\hat{\gamma}^{(10)}_{QP} = \begin{bmatrix} 0 & -\frac{8}{9} & 0 & 0 \\ 0 & \frac{16}{27} & 0 & 0 \\ 0 & -\frac{128}{9} & 0 & 0 \\ 0 & \frac{184}{27} & 0 & 0 \end{bmatrix}, \quad \hat{\gamma}^{(10)}_{QQ} = \begin{bmatrix} 0 & -20 & 0 & 2 \\ -\frac{40}{9} & -\frac{52}{3} & \frac{4}{9} & \frac{5}{6} \\ 0 & -128 & 0 & 20 \\ -\frac{256}{9} & -\frac{160}{3} & \frac{40}{9} & -\frac{2}{3} \end{bmatrix},$$

$$\hat{\gamma}^{(10)}_{BB} = [4], \qquad \hat{\gamma}^{(10)}_{BP} = \begin{bmatrix} 0 & \frac{4}{3} & 0 & 0 \end{bmatrix}, \tag{2.46}$$

$$\hat{\gamma}^{(20)}_{CC} = \begin{bmatrix} -\frac{355}{9} & -\frac{502}{27} \\ -\frac{35}{3} & -\frac{28}{3} \end{bmatrix}, \qquad \hat{\gamma}^{(20)}_{CP} = \begin{bmatrix} -\frac{1412}{243} & -\frac{1369}{243} & \frac{134}{243} & -\frac{35}{162} \\ -\frac{416}{81} & \frac{1280}{81} & \frac{56}{81} & \frac{35}{27} \end{bmatrix},$$

$$\hat{\gamma}^{(20)}_{QQ} = \begin{bmatrix} -\frac{404}{9} & -\frac{3077}{9} & \frac{32}{9} & \frac{1031}{36} \\ -\frac{2698}{81} & -\frac{8035}{27} & -\frac{49}{162} & \frac{4493}{216} \\ -\frac{19072}{9} & -\frac{14096}{9} & \frac{1708}{9} & \frac{1622}{9} \\ \frac{32288}{81} & -\frac{15976}{27} & -\frac{6692}{81} & -\frac{2437}{54} \end{bmatrix}, \hat{\gamma}^{(20)}_{QP} = \begin{bmatrix} \frac{832}{243} & -\frac{4000}{243} & -\frac{112}{243} & -\frac{70}{81} \\ \frac{3376}{729} & \frac{6344}{729} & -\frac{280}{729} & \frac{55}{486} \\ \frac{2272}{243} & -\frac{72088}{243} & -\frac{688}{243} & -\frac{1240}{81} \\ \frac{45424}{729} & \frac{84236}{729} & -\frac{3880}{729} & \frac{1220}{243} \end{bmatrix},$$

$$\hat{\gamma}^{(20)}_{PP} = \begin{bmatrix} -\frac{4468}{81} & -\frac{31469}{81} & \frac{400}{81} & \frac{3373}{108} \\ -\frac{8158}{243} & -\frac{59399}{243} & \frac{269}{486} & \frac{12899}{648} \\ -\frac{251680}{81} & -\frac{128648}{81} & \frac{23836}{81} & \frac{6106}{27} \\ \frac{58640}{243} & -\frac{26348}{243} & -\frac{14324}{243} & -\frac{2551}{162} \end{bmatrix}, \qquad \hat{\gamma}^{(20)}_{BP} = \begin{bmatrix} -\frac{1576}{81} & \frac{446}{27} & \frac{172}{81} & \frac{40}{27} \end{bmatrix},$$

$$\hat{\gamma}^{(20)}_{BB} = \begin{bmatrix} \frac{325}{9} \end{bmatrix}. \tag{2.47}$$

Almost all the blocks of $\hat{\gamma}^{(01)}$ are necessary:

$$\hat{\gamma}^{(01)}_{CC} = \begin{bmatrix} -\frac{8}{3} & 0 \\ 0 & -\frac{8}{3} \end{bmatrix}, \quad \hat{\gamma}^{(01)}_{CL} = \begin{bmatrix} -\frac{32}{27} & 0 \\ -\frac{8}{9} & 0 \end{bmatrix}, \quad \hat{\gamma}^{(01)}_{BL} = \begin{bmatrix} \frac{16}{9} & 0 \end{bmatrix},$$

$$\hat{\gamma}^{(01)}_{CQ} = \begin{bmatrix} \frac{32}{27} & 0 & 0 & 0 \\ \frac{8}{9} & 0 & 0 & 0 \end{bmatrix}, \quad \hat{\gamma}^{(01)}_{LL} = \begin{bmatrix} 8 & -4 \\ -4 & 0 \end{bmatrix},$$

$$\hat{\gamma}^{(01)}_{PQ} = \begin{bmatrix} \frac{76}{9} & 0 & -\frac{2}{3} & 0 \\ -\frac{32}{27} & \frac{20}{3} & 0 & -\frac{2}{3} \\ \frac{496}{9} & 0 & -\frac{20}{3} & 0 \\ -\frac{512}{27} & \frac{128}{3} & 0 & -\frac{20}{3} \end{bmatrix}, \quad \hat{\gamma}^{(01)}_{PL} = \begin{bmatrix} -\frac{16}{9} & 0 \\ \frac{32}{27} & 0 \\ -\frac{112}{9} & 0 \\ \frac{512}{27} & 0 \end{bmatrix}, \quad \hat{\gamma}^{(01)}_{QL} = \begin{bmatrix} -\frac{272}{27} & 0 \\ -\frac{32}{81} & 0 \\ -\frac{2768}{27} & 0 \\ -\frac{512}{81} & 0 \end{bmatrix}. \tag{2.48}$$

From $\hat{\gamma}^{(02)}$ we need only the mixing of P_1, ..., P_6 into P_9 and P_{10}:

$$\hat{\gamma}^{(02)}_{CL} = \begin{bmatrix} -\frac{11680}{2187} & -\frac{416}{81} \\ -\frac{2920}{729} & -\frac{104}{27} \end{bmatrix}, \qquad \hat{\gamma}^{(02)}_{PL} = \begin{bmatrix} -\frac{39752}{729} & -\frac{136}{27} \\ \frac{1024}{2187} & -\frac{448}{81} \\ -\frac{381344}{729} & -\frac{15616}{27} \\ \frac{24832}{2187} & -\frac{7936}{81} \end{bmatrix}. \tag{2.49}$$

The necessary entries of $\hat{\gamma}^{(11)}$ read:

$$\hat{\gamma}^{(11)}_{CC} = \begin{bmatrix} \frac{169}{9} & \frac{100}{27} \\ \frac{50}{3} & -\frac{8}{3} \end{bmatrix}, \quad \hat{\gamma}^{(11)}_{CP} = \begin{bmatrix} 0 & \frac{254}{729} & 0 & 0 \\ 0 & \frac{1076}{243} & 0 & 0 \end{bmatrix},$$

$$\hat{\gamma}^{(11)}_{CQ} = \begin{bmatrix} \frac{2272}{729} & \frac{122}{81} & 0 & \frac{49}{81} \\ -\frac{1952}{243} & -\frac{748}{27} & 0 & \frac{82}{27} \end{bmatrix}, \quad \hat{\gamma}^{(11)}_{PP} = \begin{bmatrix} 0 & \frac{11116}{243} & 0 & -\frac{14}{3} \\ \frac{280}{27} & \frac{18763}{729} & -\frac{28}{27} & -\frac{35}{18} \\ 0 & \frac{111136}{243} & 0 & -\frac{140}{3} \\ \frac{2944}{27} & \frac{193312}{729} & -\frac{280}{27} & -\frac{175}{9} \end{bmatrix},$$

$$\hat{\gamma}_{PQ}^{(11)} = \begin{bmatrix} -\frac{23488}{243} & \frac{6280}{27} & \frac{112}{9} & -\frac{538}{27} \\ \frac{31568}{729} & \frac{9481}{81} & -\frac{92}{27} & -\frac{1012}{81} \\ -\frac{233920}{243} & \frac{68848}{27} & \frac{1120}{9} & -\frac{5056}{27} \\ \frac{352352}{729} & \frac{116680}{81} & -\frac{752}{27} & -\frac{10147}{81} \end{bmatrix}, \quad \hat{\gamma}_{PL}^{(11)} = \begin{bmatrix} -\frac{6752}{243} & 0 \\ -\frac{2192}{729} & 0 \\ -\frac{84032}{243} & 0 \\ -\frac{37856}{729} & 0 \end{bmatrix},$$

$$\hat{\gamma}_{QL}^{(11)} = \begin{bmatrix} -\frac{24352}{729} & 0 \\ \frac{54608}{2187} & 0 \\ -\frac{227008}{729} & 0 \\ \frac{551648}{2187} & 0 \end{bmatrix}, \qquad \hat{\gamma}_{CL}^{(11)} = \begin{bmatrix} -\frac{2272}{729} & 0 \\ \frac{1952}{243} & 0 \end{bmatrix}, \quad \hat{\gamma}_{LL}^{(11)} = \begin{bmatrix} 0 & 16 \\ 16 & 0 \end{bmatrix},$$

$$\hat{\gamma}_{BL}^{(11)} = \begin{bmatrix} -\frac{8}{9} & 0 \end{bmatrix}. \tag{2.50}$$

Finally, the relevant three-loop anomalous dimensions are taken from Ref. [51] and yield

$$\hat{\gamma}_{CC}^{(30)} = \begin{bmatrix} -\frac{12773}{18} + \frac{1472\zeta(3)}{3} & \frac{745}{9} - \frac{4288\zeta(3)}{9} \\ \frac{1177}{2} - 2144\zeta(3) & 306 - 224\zeta(3) \end{bmatrix}, \quad \hat{\gamma}_{CL}^{(21)} = \begin{bmatrix} -\frac{1359190}{19683} + \frac{6976\,\zeta(3)}{243} & 0 \\ -\frac{229696}{6561} - \frac{3584\,\zeta(3)}{81} & 0 \end{bmatrix}, \tag{2.51}$$

$$\hat{\gamma}_{CP}^{(30)} = \begin{bmatrix} \frac{63187}{13122} & -\frac{981796}{6561} & -\frac{202663}{52488} & -\frac{24973}{69984} \\ \frac{110477}{2187} & \frac{133529}{8748} & -\frac{42929}{8748} & \frac{354319}{11664} \end{bmatrix} + \zeta(3) \begin{bmatrix} -\frac{1360}{81} & -\frac{776}{81} & \frac{124}{81} & \frac{100}{27} \\ \frac{2720}{27} & -\frac{2768}{27} & -\frac{248}{27} & -\frac{110}{9} \end{bmatrix}, \tag{2.52}$$

$$\hat{\gamma}_{PP}^{(30)} = \begin{bmatrix} -\frac{3572528}{2187} & -\frac{58158773}{8748} & \frac{552601}{4374} & \frac{6989171}{11664} \\ -\frac{1651004}{6561} & -\frac{155405353}{52488} & \frac{1174159}{52488} & \frac{10278809}{34992} \\ -\frac{147978032}{2187} & -\frac{168491372}{2187} & \frac{11213042}{2187} & \frac{17850329}{2916} \\ \frac{136797922}{6561} & -\frac{72614473}{13122} & -\frac{9288181}{6561} & -\frac{16664027}{17496} \end{bmatrix}$$

$$+\zeta(3) \begin{bmatrix} -\frac{608}{27} & \frac{61424}{27} & -\frac{496}{27} & -\frac{2821}{9} \\ \frac{88720}{81} & \frac{54272}{81} & -\frac{9274}{81} & -\frac{3100}{27} \\ \frac{87040}{27} & \frac{324416}{27} & -\frac{13984}{27} & -\frac{31420}{9} \\ \frac{721408}{81} & -\frac{166432}{81} & -\frac{95032}{81} & -\frac{7552}{27} \end{bmatrix}, \quad \hat{\gamma}_{PL}^{(21)} = \begin{bmatrix} -\frac{1290092}{6561} + \frac{3200\,\zeta(3)}{81} & 0 \\ -\frac{819971}{19683} - \frac{19936\,\zeta(3)}{243} & 0 \\ -\frac{16821944}{6561} + \frac{30464\,\zeta(3)}{81} & 0 \\ -\frac{17787368}{19683} - \frac{286720\,\zeta(3)}{243} & 0 \end{bmatrix}. \tag{2.53}$$

The three-loop ADM's have no influence on the logarithmically-enhanced QED corrections at the considered order but are necessary for the NNLO QCD corrections.

2.2.5 Wilson coefficients at the low scale

From the solution to the RGE in section 2.2.3, we obtain the Wilson coefficients at the scale $\mu_b \sim m_b$ as a truncated series in $\widetilde{\alpha}_{\rm s}(\mu_0)$ and $\kappa(\mu_0)$. We then use Eq. (2.24) to express the couplings at the high scale in terms of $\widetilde{\alpha}_{\rm s}(\mu_b)$ and $\kappa(\mu_b)$. For $\widetilde{\alpha}_{\rm s}$, the simple relation

$$\widetilde{\alpha}_{\rm s}(\mu_0) = \eta\, \widetilde{\alpha}_{\rm s}(\mu_b) \tag{2.54}$$

holds to all orders. In order to obtain the running of κ, we invert Eq. (2.24), treating v_s and η as quantities of order $\mathcal{O}(1)$, which gives

$$\kappa(\mu_0) = \frac{\kappa(\mu_b)}{\eta} + \frac{\beta_{00}^e}{\beta_{00}^s}\,\frac{1-\eta}{\eta^2}\,\kappa^2(\mu_b) + \frac{\ln\eta}{\eta}\left[\frac{\beta_{00}^e\,\beta_{10}^s}{(\beta_{00}^s)^2} - \frac{\beta_{01}^e}{\beta_{00}^s}\right]\widetilde{\alpha}_{\rm s}(\mu_b)\,\kappa^2(\mu_b) + \mathcal{O}(\kappa^2\widetilde{\alpha}_{\rm s}^2, \kappa^3)\,. \tag{2.55}$$

The final expression for the Wilson coefficients at the low scale is:

$$C_k(\mu_b) = \sum_{n,m=0}^{2} \widetilde{\alpha}_{\rm s}(\mu_b)^n \kappa(\mu_b)^m\, C_k^{(nm)}(\mu_b) + \mathcal{O}(\widetilde{\alpha}_{\rm s}^3, \kappa^3)\,, \tag{2.56}$$

where $\vec{C}^{(n,m)}$ are functions of only $\eta = \widetilde{\alpha}_{\rm s}(\mu_0)/\widetilde{\alpha}_{\rm s}(\mu_b)$, s_W^2 and ratios of the heavy masses. At order $\mathcal{O}(\widetilde{\alpha}_{\rm s}^2\kappa^2)$, we keep only those contributions to C_9 and C_{10} that are proportional to $m_t^4/(M_W^4 s_W^4)$.

The matching conditions, anomalous dimensions and RG-equations presented in sections 2.2.2–2.2.4 do not include the two dipole operators $P_{7,8}$. For those two operators, it is more convenient to consider the so-called effective coefficients

$$\begin{aligned} C_7^{\rm eff}(\mu_b) &\equiv C_7(\mu_b) + \sum_{i=3}^{6} y_i \left[C_i(\mu_b) - \frac{1}{3}C_{iQ}(\mu_b)\right] \\ &= C_7^{(00)\rm eff}(\mu_b) + \widetilde{\alpha}_{\rm s}(\mu_b)\, C_7^{(10)\rm eff}(\mu_b) + \kappa(\mu_b)\, C_7^{(01)\rm eff}(\mu_b) \\ &\quad + \widetilde{\alpha}_{\rm s}(\mu_b)\kappa(\mu_b)\, C_7^{(11)\rm eff}(\mu_b) + \mathcal{O}(\widetilde{\alpha}_{\rm s}^2, \kappa^2)\,, \end{aligned} \tag{2.57}$$

$$C_8^{\rm eff}(\mu_b) \equiv C_8(\mu_b) + \sum_{i=3}^{6} z_i \left[C_i(\mu_b) - \frac{1}{3}C_{iQ}(\mu_b)\right] = C_8^{(00)\rm eff}(\mu_b) + \mathcal{O}(\widetilde{\alpha}_{\rm s}, \kappa) \tag{2.58}$$

where, in dimensional regularization with fully anticommuting γ_5 [47, 48, 65],

$$y = (0, 0, -\frac{1}{3}, -\frac{4}{9}, -\frac{20}{3}, -\frac{80}{9}) \quad \text{and} \quad z = (0, 0, 1, -\frac{1}{6}, 20, -\frac{10}{3})\,.$$

The effective coefficients $C_7^{(00)\rm eff}(\mu_b)$, $C_7^{(10)\rm eff}(\mu_b)$ and $C_8^{(00)\rm eff}(\mu_b)$ can be found in Eqs. (10)–(22) of Ref. [66], while $C_7^{(01)\rm eff}(\mu_b)$ can be found in Eq. (12) of Ref. [64].

Following Ref. [52], we take into account the *complete* $\mathcal{O}(\widetilde{\alpha}_{\rm s}\kappa)$ term in $C_7^{\rm eff}(\mu_b)$ rather than only its $m_t^2/(M_W^2 s_W^2)$-enhanced part (as sections 2.1.2 and 2.7 would imply). An explicit expression for $C_7^{(11)\rm eff}(\mu_b)$ can be found in Eq. (30) of Ref. [56]. In Tables 2.1 – 2.3, we present the relevant $C_k^{(nm)}(\mu_b)$. We fix the input parameters to their central values (specified in sec. 2.7) and choose $\mu_b = [2.5, 5, 10]$ GeV and $\mu_0 = 120$ GeV.

2.3 Matrix elements I

Once $\vec{C}^{(n,m)}(\mu_b)$ is found, one needs to calculate the on-shell $b \to s l^+ l^-$ matrix elements $\langle P_i \rangle$ of the corresponding operators. In the present section, we consider those parts of the matrix elements that originate from diagrams with no photons inside loops and/or bremsstrahlung photons. These parts are unrelated to the $\ln(m_b^2/m_\ell^2)$-enhanced correction

	(00)	(01)	(10)
$C_1^{(nm)}$	[-0.763 , -0.544 , -0.379]	[-0.180, -0.0835, -0.0378]	[13.764 , 14.943 , 16.066]
$C_2^{(nm)}$	[1.054 , 1.029 , 1.015]	[0.248, 0.158, 0.101]	[-1.746 , -1.376 , -1.050]
$C_3^{(nm)}$	[-1.10 , -0.571 , -0.283]10^{-2}	[-1.22, -0.400, -0.125]10^{-3}	[5.28 , 7.98 , 8.38]10^{-2}
$C_4^{(nm)}$	[-0.113 , -0.0741 , -0.0486]	[-1.62, -0.697, -0.297]10^{-2}	[-0.690 , -0.343 , -0.143]
$C_5^{(nm)}$	[1.04 , 0.547 , 0.274]10^{-3}	[1.17, 0.387, 0.122]10^{-4}	[-1.60 , -1.55 , -1.36]10^{-2}
$C_6^{(nm)}$	[2.32 , 1.17 , 0.563]10^{-3}	[2.51, 0.801, 0.245]10^{-4}	[-0.656 , -1.92 , -2.17]10^{-2}
$C_{3Q}^{(nm)}$	0	[-5.03, -3.72, -2.66]10^{-2}	0
$C_{4Q}^{(nm)}$	0	[-2.13, -1.04, -0.49]10^{-2}	0
$C_{5Q}^{(nm)}$	0	[-6.08, -1.71, -0.30]10^{-6}	0
$C_{6Q}^{(nm)}$	0	[2.12, 1.03, 0.485]10^{-3}	0
$C_b^{(nm)}$	0	0	0

Table 2.1: Numerical values of the relevant $C_k^{(nm)}(\mu_b)$ $(k \neq 7,8,9,10)$ for $\mu_b = [2.5, 5, 10]\,\text{GeV}$.

	$C_7^{(nm)}(\mu_b)$	$C_8^{(nm)}(\mu_b)$
(00)	[-0.362 , -0.320 , -0.285]	[-0.168 , -0.151 , -0.138]
(01)	[3.20 , 3.33 , 2.82]10^{-2}	–
(10)	[1.625 , 1.171 , 0.690]	–
(11)	[4.132 , 4.314 , 4.397]	–

Table 2.2: Numerical values of the relevant $C_{7,8}^{(nm)}(\mu_b)$ for $\mu_b = [2.5, 5, 10]\,\text{GeV}$.

to the decay width. In the following sections, we use frequently instead of $q^2 = (p_{\ell^+} + p_{\ell^-})^2$ the notations $s = q^2$ and $\hat{s} = s/m_{b,pole}^2$.

One-loop penguin contractions of the four-fermion operators give the following contributions to the matrix elements:

$$\langle P_i \rangle^{\text{peng}} = M_i^9 \langle P_9 \rangle_{\text{tree}} + M_i^7 \frac{\langle P_7 \rangle_{\text{tree}}}{\widetilde{\alpha}_s(\mu_b)\kappa(\mu_b)} + M_i^{10} \langle P_{10} \rangle_{\text{tree}} \,. \tag{2.59}$$

The above formula holds also for the tree-level matrix element of P_7, the one-loop matrix element of P_8, and for those parts of the two-loop $\mathcal{O}(\alpha_s \alpha_{\text{em}})$ matrix elements of the four-quark operators where the gluon couples to the closed quark loop. The coefficients M_i^A are summarized in Table 2.4 in terms of the functions $F_i^A(\hat{s})$ and

$$f_i(\hat{s}) = \gamma_{i9}^{(01)} \ln \frac{m_b}{\mu_b} + \rho_i^c \left(g(y_c) + \frac{8}{9} \ln \frac{m_b}{m_c} \right) + \rho_i^b g(y_b) + \rho_i^0 \left(\ln \hat{s} - i\pi \right) + \rho_i^{\#} \tag{2.60}$$

$$f_9^{\text{pen}}(\hat{s}) = 8 \ln \frac{m_b}{\mu_b} - 3 \left(g(y_\tau) + \frac{8}{9} \ln \frac{m_b}{m_\tau} \right) + \frac{8}{3} \left(\ln \hat{s} - i\pi \right) - \frac{40}{9} \,. \tag{2.61}$$

Here, $y_a = 4m_{a,\text{pole}}^2/s$, the function $g(y)$ is given in appendix A, and the numbers ρ are collected in Table 2.5. The pure QCD ones can be derived from Refs. [47, 48, 65]. ρ^c and ρ^b for the P_i^Q are obtained by inserting obvious charge factors in ρ^c and ρ^b for the P_i. The remaining ones were kindly provided by my collaborators of Ref. [39]. The functions $F_i^A(\hat{s})$

	$C_9^{(nm)}(\mu_b)$	$C_{10}^{(nm)}(\mu_b)$
(00)	0	0
(01)	[5.025 , 3.722 , 2.664]10^{-2}	0
(10)	0	0
(11)	[2.003 , 1.934 , 1.863]	[-4.222 , -4.222 , -4.222]
(20)	0	0
(02)	[0.376 , 0.208 , 0.104]10^{-2}	[1.081 , 0.489 , 0.218]10^{-2}
(12)	[-6.614 , -4.317 , -2.810]	[-5.854 , -3.798 , -2.458]
(21)	[5.645 , 3.538 , 1.193]	[5.105 , 6.380 , 7.631]
(22)	[36.814 , 27.320 , 20.275]	[-32.014 , -36.090 , -39.764]

Table 2.3: Numerical values of the relevant $C_{9,10}^{(nm)}(\mu_b)$ for $\mu_b = [2.5, 5, 10]\,\mathrm{GeV}$.

	M_i^9	M_i^7	M_i^{10}
i=1,2	$\widetilde{\alpha}_s\kappa\ f_i(\hat{s}) - \widetilde{\alpha}_s^2\kappa\ F_i^9(\hat{s})$	$-\widetilde{\alpha}_s^2\kappa\ F_i^7(\hat{s})$	0
i=3-6,3Q-6Q,b	$\widetilde{\alpha}_s\kappa\ f_i(\hat{s})$	0	0
i=7	0	$\widetilde{\alpha}_s\kappa$	0
i=8	$-\widetilde{\alpha}_s^2\kappa\ F_8^9(\hat{s})$	$-\widetilde{\alpha}_s^2\kappa\ F_8^7(\hat{s})$	0
i=9	$1 + \widetilde{\alpha}_s\kappa\ f_9^{\rm pen}(\hat{s})$	0	0
i=10	0	0	1

Table 2.4: Coefficients M_i^A that appear in Eq. (2.59). Here, $\widetilde{\alpha}_s$ and κ are taken at the scale μ_b.

can be found in Eqs. (54)–(56), (71) and (72) of Ref. [48] where they are given in terms of an expansion in $\hat{s}$ up to $\mathcal{O}(\hat{s}^3)$. In the low-$\hat{s}$ region, the accuracy of these expansions is excellent, as can be seen in Figs. 4 and 5 of Ref. [45] where the same functions are numerically evaluated for arbitrary $\hat{s}$. The functions $F_8^A(\hat{s})$ can also be found analytically since the double integral in Eqs. (4.17) and (4.18) of Ref. [45] can be carried out explicitly.

For what concerns the remaining contributions to the NLO and NNLO QCD matrix elements of $P_{7,9,10}$, the virtual and real corrections can be effectively taken into account via the following redefinitions of the squared tree-level matrix elements in the expression for the decay width:

$$|\langle P_9\rangle_{\rm tree}|^2 \implies |\langle P_9\rangle_{\rm tree}|^2 \left[1 + 8\ \widetilde{\alpha}_s\ \omega_{99}^{(1)}(\hat{s}) + 16\ \widetilde{\alpha}_s^2\ \omega_{99}^{(2)}(\hat{s})\right]\ , \quad (2.62)$$

$$|\langle P_{10}\rangle_{\rm tree}|^2 \implies |\langle P_{10}\rangle_{\rm tree}|^2 \left[1 + 8\ \widetilde{\alpha}_s\ \omega_{1010}^{(1)}(\hat{s})\right]\ , \quad (2.63)$$

$$|\langle P_7\rangle_{\rm tree}|^2 \implies |\langle P_7\rangle_{\rm tree}|^2 \left[1 + 8\ \widetilde{\alpha}_s\ \omega_{77}^{(1)}(\hat{s})\right]\ , \quad (2.64)$$

$$\mathrm{Re}\left(\langle P_7\rangle_{\rm tree}\langle P_9\rangle_{\rm tree}^*\right) \implies \mathrm{Re}\left(\langle P_7\rangle_{\rm tree}\langle P_9\rangle_{\rm tree}^*\right) \left[1 + 8\ \widetilde{\alpha}_s\ \omega_{79}^{(1)}(\hat{s})\right]\ , \quad (2.65)$$

where the functions $\omega_{ij}^{(n)}(\hat{s})$ calculated in Refs. [48, 52] are listed in appendix A.

The remaining contributions to the NNLO matrix elements of the four-quark operators originate from diagrams where the gluon does not couple to the quark loop. Thus, they are given by the same functions of $\hat{s}$ as in Eq. (2.62).

	P_1	P_2	P_3	P_4	P_5	P_6	P_3^Q	P_4^Q	P_5^Q	P_6^Q	P^b
ρ^c	$\frac{4}{3}$	1	6	0	60	0	4	0	40	0	0
ρ^b	0	0	$-\frac{7}{2}$	$-\frac{2}{3}$	-38	$-\frac{32}{3}$	$\frac{7}{6}$	$\frac{2}{9}$	$\frac{38}{3}$	$\frac{32}{9}$	-2
ρ^0	0	0	$\frac{2}{9}$	$\frac{8}{27}$	$\frac{32}{9}$	$\frac{128}{27}$	$-\frac{74}{27}$	$-\frac{8}{81}$	$-\frac{752}{27}$	$-\frac{128}{81}$	0
$\rho^\#$	$-\frac{16}{27}$	$-\frac{4}{9}$	$\frac{2}{27}$	$\frac{8}{81}$	$-\frac{136}{27}$	$\frac{320}{81}$	$\frac{358}{81}$	$-\frac{8}{243}$	$\frac{1144}{81}$	$-\frac{320}{243}$	$\frac{26}{27}$

Table 2.5: Numbers that occur in the four-quark operator matrix elements in Eq. (2.60).

2.4 Matrix elements II

In this section, we calculate those electromagnetic corrections to the matrix elements of the four-fermion operators that are responsible for the $\ln(m_b^2/m_\ell^2)$-enhanced correction to the decay width. In section 2.4.1, we cover in great detail the calculation of QED corrections to $\langle P_9 \rangle$. In section 2.4.2, we give the logarithmically enhanced QED corrections to the matrix elements of P_i with $i \neq 9$.

2.4.1 Corrections to $\langle P_9 \rangle$

Electromagnetic corrections to the matrix element of P_9 are infrared divergent and must be considered together with the corresponding bremsstrahlung. The dilepton invariant mass differential decay width is not an infrared safe object with respect to emission of collinear photons. Hence, electromagnetic corrections contain an explicit collinear logarithm $\ln(m_b^2/m_\ell^2)$. The coefficient of this logarithm vanishes when integrated over the whole phase space but does not if we restrict it to either the low- or the high-$\hat{s}$ region.

In this calculation, we adopt the NDR scheme with $D = 4 - 2\epsilon$. The NDR scheme is suitable for our calculation since no Levi-Civita tensor survives in divergent terms proportional to $1/\epsilon$ or $1/\epsilon^2$. Thus, all the Levi-Civita tensors can be evaluated in $D = 4$ and are therefore well-defined.

In the first step, all the external particles are taken to be on-shell, and, in addition, all the final state particles are treated as massless ($m_s = m_\ell = 0$). This implies that all the collinear divergences are dimensionally regularized, and that the collinear logarithm appears as a residual $1/\epsilon$. Later, we will be able to re-express such a residue in terms of $\ln(m_b^2/m_\ell^2)$ using the photonic splitting function of the lepton.

In the next two subsections, we present the calculation of virtual and bremsstrahlung corrections. A third subsection will be devoted to some technical details of the bremsstrahlung calculation. In the fourth and last subsection, we show how to change the collinear regulator from dimensional to the physical mass regularization.

The calculation involves the following kinematical invariants: $\hat{s}_{ij} = 2\, p_i \cdot p_j / m_b^2$, where $i, j \in \{l^+, l^-, s, b, \gamma\} \equiv \{1, 2, s, b, q\}$.[8]

2.4.1.1 Virtual corrections

In order to obtain the virtual corrections, one has to consider one-loop diagrams of the current-current type. There are in total six such diagrams, one of which is shown on the left

[8] We slightly change our notation here: q denotes the photon momentum, $s_{12} = (p_1 + p_2)^2$ the lepton invariant mass squared.

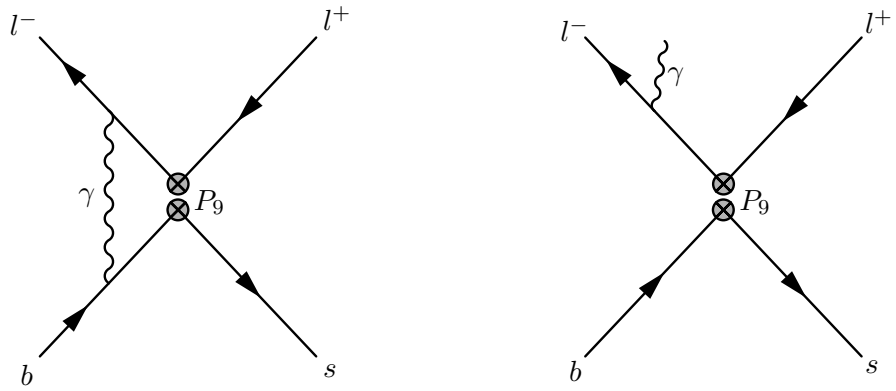

Figure 2.3: Examples of diagrams contributing to the virtual (left) and real (right) electromagnetic corrections to the matrix element of P_9.

in Figure 2.3. The sum of the six diagrams contains infrared and ultraviolet divergences. The latter cancel after the addition of counterterms. The next step is then to compute its interference with $\langle P_9 \rangle_{\text{tree}}$ which yields an expression $K_V(\hat{s}_{12}, \hat{s}_{1s}, \hat{s}_{2s})$. Finally, one has to integrate K_V over the phase space. The phase space measure for a three particle massless final state in D dimensions is given explicitly in [67]. Since K_V does not depend on angular variables we can immediately integrate them out

$$\begin{aligned}
\widetilde{dPS_3} &\equiv \tilde{\mu}^{4\epsilon} \int_\Omega dPS_3 = \tilde{\mu}^{4\epsilon} M_3(\hat{s}_{12}, \hat{s}_{1s}, \hat{s}_{2s})\, d\hat{s}_{12}\, d\hat{s}_{1s}\, d\hat{s}_{2s} \\
&= \tilde{\mu}^{4\epsilon} \frac{2^{-8+6\epsilon} \pi^{-\frac{5}{2}+2\epsilon} (m_b^2)^{1-2\epsilon}}{\Gamma(\frac{3}{2}-\epsilon)\,\Gamma(1-\epsilon)} (\hat{s}_{12}\,\hat{s}_{1s}\,\hat{s}_{2s})^{-\epsilon} \delta(1-\hat{s}_{12}-\hat{s}_{1s}-\hat{s}_{2s})\, d\hat{s}_{12}\, d\hat{s}_{1s}\, d\hat{s}_{2s}\,.
\end{aligned} \tag{2.66}$$

By means of this expression we obtain the final contribution from virtual corrections via

$$\begin{aligned}
T_V &\equiv \int \frac{\widetilde{dPS_3}}{d\hat{s}_{12}}\, K_V(\hat{s}_{12}, \hat{s}_{1s}, \hat{s}_{2s}) \\
&= \tilde{\mu}^{4\epsilon} \cdot \frac{2^{-8+6\epsilon}\, \pi^{-\frac{5}{2}+2\epsilon}\, (m_b^2)^{1-2\epsilon}}{\Gamma(\frac{3}{2}-\epsilon)\,\Gamma(1-\epsilon)}\, (\hat{s}_{12})^{-\epsilon} \\
&\quad \times \int_0^{1-\hat{s}_{12}} d\hat{s}_{1s}\, (\hat{s}_{1s})^{-\epsilon} (1-\hat{s}_{12}-\hat{s}_{1s})^{-\epsilon} \cdot K_V(\hat{s}_{12}, \hat{s}_{1s}, 1-\hat{s}_{12}-\hat{s}_{1s}) \\
&= -\frac{\widetilde{\alpha}_e\, m_b^6\, \left(Q_d^2 + 2\,Q_l^2\right) (1-\hat{s}_{12})^2\, (1+2\,\hat{s}_{12})}{96\,\pi^3\,\epsilon^2} \\
&\quad + \frac{\widetilde{\alpha}_e\, m_b^6\, (1-\hat{s}_{12})^2\, (1+2\,\hat{s}_{12})}{96\,\pi^3\,\epsilon} \left\{ Q_d^2 \left[\ln \hat{s}_{12} + 4 \ln(1-\hat{s}_{12}) - 6\,L - \frac{31}{6} - \frac{1}{1+2\,\hat{s}_{12}} \right] \right. \\
&\qquad \left. + Q_l^2 \left[4 \ln \hat{s}_{12} + 4 \ln(1-\hat{s}_{12}) - 12\,L - \frac{25}{3} - \frac{2}{1+2\,\hat{s}_{12}} \right] \right\} \\
&\quad - \frac{\widetilde{\alpha}_e\, m_b^6\, (1-\hat{s}_{12})^2\, (1+2\,\hat{s}_{12})}{192\,\pi^3}
\end{aligned}$$

$$
\begin{aligned}
\times\Bigg\{ Q_d^2 \Bigg[& 36\,L^2 + \ln^2\hat{s}_{12} + 16\ln^2(1-\hat{s}_{12}) + 4Li_2(\hat{s}_{12}) - \frac{5}{6}\pi^2 - 12\,L\cdot\ln\hat{s}_{12} \\
& -48\,L\cdot\ln(1-\hat{s}_{12}) + 62\,L + 8\ln\hat{s}_{12}\cdot\ln(1-\hat{s}_{12}) + \frac{350}{9} - \frac{31}{3}\ln\hat{s}_{12} \\
& -\frac{112}{3}\ln(1-\hat{s}_{12}) + \frac{37+36\,L-6\ln\hat{s}_{12}-6\ln(1-\hat{s}_{12})}{3\,(1+2\hat{s}_{12})}\Bigg] + 12\,Q_d\,Q_l \\
+Q_l^2 \Bigg[& 72\,L^2 + 8\ln^2\hat{s}_{12} + 8\ln^2(1-\hat{s}_{12}) - \frac{13}{3}\pi^2 - 48\,L\cdot\ln\hat{s}_{12} \\
& -48\,L\cdot\ln(1-\hat{s}_{12}) + 100\,L + 16\ln\hat{s}_{12}\cdot\ln(1-\hat{s}_{12}) + \frac{532}{9} - \frac{100}{3}\ln\hat{s}_{12} \\
& -\frac{100}{3}\ln(1-\hat{s}_{12}) + \frac{62+72\,L-24\ln\hat{s}_{12}-24\ln(1-\hat{s}_{12})}{3\,(1+2\hat{s}_{12})}\Bigg]\Bigg\}. \qquad (2.67)
\end{aligned}
$$

In the above expression Q_d and Q_l are defined as in Eq. (2.25), furthermore, $L \equiv \ln(\mu/m_b)$. $\tilde{\mu}^2 = \mu^2 \cdot \exp[\gamma_E - \ln(4\pi)]$ is introduced in the $\overline{\text{MS}}$ scheme and ensures the cancellation of all γ_E and $\ln(4\pi)$ terms.

2.4.1.2 Real corrections

In order to cancel the infrared singularities present in T_V one has to add the corresponding bremsstrahlung contribution. There are four diagrams, one of which is shown on the right in Figure 2.3. Contrary to the case of gluon bremsstrahlung, the photon couples to all external legs, which makes the calculation more involved. The sum of the four amplitudes has to be squared, yielding an expression $K_R(\hat{s}_{12}, \hat{s}_{1s}, \hat{s}_{2s}, \hat{s}_{1q}, \hat{s}_{2q}, \hat{s}_{sq}, \hat{s}_{tri})$, where

$$\hat{s}_{tri} \equiv 1 - \hat{s}_{12} - \hat{s}_{1s} - \hat{s}_{2s} = \hat{s}_{1q} + \hat{s}_{2q} + \hat{s}_{sq} \qquad (2.68)$$

is the triple invariant. The corresponding phase space measure for the four particle final state can also be found in [67]. After integration over angular variables, it reads

$$
\begin{aligned}
\widetilde{dPS_4} \equiv \tilde{\mu}^{6\epsilon}\int_\Omega dPS_4 \;\; = \;\; & \tilde{\mu}^{6\epsilon}\cdot\frac{2^{-12+10\epsilon}\,\pi^{-5+3\epsilon}\,(m_b^2)^{2-3\epsilon}}{\Gamma(\frac{3}{2}-\epsilon)\,\Gamma(1-\epsilon)\Gamma(\frac{1}{2}-\epsilon)}\,d\hat{s}_{12}\,d\hat{s}_{1s}\,d\hat{s}_{1q}\,d\hat{s}_{2s}\,d\hat{s}_{2q}\,d\hat{s}_{sq} \\
& \times(-\Delta_4)^{-\frac{1}{2}-\epsilon}\cdot\Theta(-\Delta_4)\cdot\delta(1-\hat{s}_{12}-\hat{s}_{1s}-\hat{s}_{1q}-\hat{s}_{2s}-\hat{s}_{2q}-\hat{s}_{sq})\,. \qquad (2.69)
\end{aligned}
$$

In the above equation, the Gram determinant is given by

$$\Delta_4 = (\hat{s}_{12}\hat{s}_{sq})^2 + (\hat{s}_{1s}\hat{s}_{2q})^2 + (\hat{s}_{1q}\hat{s}_{2s})^2 - 2\,(\hat{s}_{12}\hat{s}_{1s}\hat{s}_{2q}\hat{s}_{sq} + \hat{s}_{1s}\hat{s}_{1q}\hat{s}_{2s}\hat{s}_{2q} + \hat{s}_{12}\hat{s}_{1q}\hat{s}_{2s}\hat{s}_{sq}). \quad (2.70)$$

The phase space measure is completely symmetric in $\{1, 2, s, q\}$, but since we stay differential in $\hat{s}_{12}$ we can only make use of the symmetries $1 \leftrightarrow 2$ and $s \leftrightarrow q$.[9] The use of these symmetries is, however, essential since the number of distinct terms in K_R gets reduced significantly. In addition, all terms of the form $A/(\hat{s}_{1q}\hat{s}_{sq})$ and $A/(\hat{s}_{2q}\hat{s}_{sq})$ as well as $B/(\hat{s}_{1q}\hat{s}_{tri})$ and $B/(\hat{s}_{2q}\hat{s}_{tri})$ drop out by means of the $1 \leftrightarrow 2$ symmetry.

[9] In the terms containing $\hat{s}_{tri}$ in the denominator, only the $1 \leftrightarrow 2$ symmetry can be used.

Another crucial point is to choose for each term in K_R the order of integration in a suitable way in order to ensure that all terms through order $\mathcal{O}(\epsilon^0)$ can be found analytically. Section 2.4.1.3 is devoted to this rather technical issue. The QED bremsstrahlung contribution finally reads

$$
\begin{aligned}
T_R \;\equiv\;& \int \frac{\widetilde{dPS_4}}{d\hat{s}_{12}}\, K_R(\hat{s}_{12},\hat{s}_{1s},\hat{s}_{2s},\hat{s}_{1q},\hat{s}_{2q},\hat{s}_{sq},\hat{s}_{tri}) \\
=\;& \frac{\widetilde{\alpha}_e\, m_b^6\, \left(Q_d^2+2\,Q_l^2\right)(1-\hat{s}_{12})^2\,(1+2\,\hat{s}_{12})}{96\,\pi^3\,\epsilon^2} \\
& -\frac{\widetilde{\alpha}_e\, m_b^6\,(1-\hat{s}_{12})^2\,(1+2\,\hat{s}_{12})}{96\,\pi^3\,\epsilon}\Bigg\{ Q_d^2\left[\ln\hat{s}_{12}+4\ln(1-\hat{s}_{12})-6\,L-\frac{31}{6}-\frac{1}{1+2\,\hat{s}_{12}}\right] \\
& \qquad +Q_l^2\left[8\ln(1-\hat{s}_{12})-12\,L-11+2\cdot\frac{\hat{s}_{12}-\hat{s}_{12}^2+\ln\hat{s}_{12}}{(1-\hat{s}_{12})^2\,(1+2\,\hat{s}_{12})}\right]\Bigg\} \\
& -\frac{\widetilde{\alpha}_e\, m_b^6\,(1-\hat{s}_{12})^2\,(1+2\,\hat{s}_{12})}{192\,\pi^3} \\
& \times\Bigg\{ Q_d^2\left[\frac{19}{3}\ln\hat{s}_{12}-36\,L^2-\ln^2\hat{s}_{12}-16\ln^2(1-\hat{s}_{12})+4Li_2(\hat{s}_{12})+48\,L\cdot\ln(1-\hat{s}_{12})\right. \\
& \qquad -4\ln\hat{s}_{12}\cdot\ln(1-\hat{s}_{12})-\frac{377}{9}-62\,L+\frac{39}{18}\,\pi^2+12\,L\cdot\ln\hat{s}_{12}+\frac{124}{3}\ln(1-\hat{s}_{12}) \\
& \qquad \left.-\frac{19+36\,L+42\ln\hat{s}_{12}-24\ln(1-\hat{s}_{12})}{3\,(1+2\hat{s}_{12})}-\frac{8(1-\hat{s}_{12})+4(7\hat{s}_{12}-5)\ln\hat{s}_{12}}{(1-\hat{s}_{12})^2\,(1+2\hat{s}_{12})}\right] \\
& +Q_l^2\Bigg[-72\,L^2+4\ln^2\hat{s}_{12}-32\ln^2(1-\hat{s}_{12})+7\pi^2-8Li_2(\hat{s}_{12})-132\,L \\
& \qquad +96\,L\cdot\ln(1-\hat{s}_{12})-8\ln\hat{s}_{12}\cdot\ln(1-\hat{s}_{12})-\frac{281}{3}+88\ln(1-\hat{s}_{12}) \\
& \qquad -\frac{22+24\,L+16\ln\hat{s}_{12}-16\ln(1-\hat{s}_{12})}{(1+2\hat{s}_{12})} \\
& \qquad +\frac{30+24\,L+28\ln\hat{s}_{12}-16\ln(1-\hat{s}_{12})}{(1-\hat{s}_{12})(1+2\hat{s}_{12})} \\
& \qquad \left.-\frac{8\pi^2-72\,L\cdot\ln\hat{s}_{12}+18\ln^2\hat{s}_{12}-42\ln\hat{s}_{12}-48Li_2(\hat{s}_{12})}{3(1-\hat{s}_{12})^2(1+2\hat{s}_{12})}\Bigg]\Bigg\}. \qquad (2.71)
\end{aligned}
$$

In the sum of T_V and T_R the $1/\epsilon^2$ terms cancel as well as the Q_d^2 part of the $1/\epsilon$ terms, whereas the collinear divergences proportional to Q_l^2/ϵ remain.

2.4.1.3 Details of the bremsstrahlung calculation

Before we proceed in the main line of the calculation, we present some technical details of the bremsstrahlung calculation. We will integrate the sample kernel $K_R = \hat{s}_{1q}^{-1}\hat{s}_{2q}^{-1}$ over the four particle phase space, show how the Gram determinant factorizes, and explain how to extract all terms through order $\mathcal{O}(\epsilon^0)$ analytically. Omitting bothersome prefactors and,

in addition, removing all hats from the invariants $\hat{s}_{ij}$ we consider the expression

$$\begin{aligned} A &:= ds_{12} \int_0^1 ds_{1s}\, ds_{1q}\, ds_{2q}\, ds_{2s}\, ds_{sq}\, \delta(1 - s_{12} - s_{1s} - s_{1q} - s_{2s} - s_{2q} - s_{sq}) \\ &\quad \times (-\Delta_4)^{-\frac{1}{2}-\epsilon}\, \Theta(-\Delta_4) s_{1q}^{-1} s_{2q}^{-1} \,, \end{aligned} \tag{2.72}$$

where the Gram determinant is given by

$$\Delta_4 = (s_{12}s_{sq})^2 + (s_{1s}s_{2q})^2 + (s_{1q}s_{2s})^2 - 2\,(s_{12}s_{1s}s_{2q}s_{sq} + s_{1s}s_{1q}s_{2s}s_{2q} + s_{12}s_{1q}s_{2s}s_{sq}). \tag{2.73}$$

The first integration is over the δ-function. It is done by means of the variable s_{sq}, yielding

$$\begin{aligned} A &= ds_{12} \int_0^{1-s_{12}} ds_{1s} \int_0^{1-s_{12}-s_{1s}} ds_{1q} s_{1q}^{-1} \int_0^{1-s_{12}-s_{1s}-s_{1q}} ds_{2q} s_{2q}^{-1} \int_0^{1-s_{12}-s_{1s}-s_{1q}-s_{2q}} ds_{2s} \\ &\qquad \times (-\Delta_4)^{-\frac{1}{2}-\epsilon}\, \Theta(-\Delta_4) \Big|_{s_{sq}=1-s_{12}-s_{1s}-s_{1q}-s_{2q}-s_{2s}} . \end{aligned} \tag{2.74}$$

Substituting $s_{sq} = 1 - s_{12} - s_{1s} - s_{1q} - s_{2q} - s_{2s}$ in the Gram determinant yields an object that can be transformed into a quadratic polynomial in either of the variables s_{1s}, s_{1q}, s_{2s} or s_{2q}, i.e. in either variable that does not accompany s_{sq} in the quadratic piece of the Gram determinant. We choose this polynomial to be quadratic in s_{2s}:

$$-\Delta_4 = -(s_{12} + s_{1q})^2 \left[s_{2s}^2 + 2\,B\, s_{2s} + C\right] = (s_{12} + s_{1q})^2 (s_{2s}^+ - s_{2s})(s_{2s} - s_{2s}^-) \,, \tag{2.75}$$

where $s_{2s}^\pm$ are the roots of the quadratic polynomial:

$$s_{2s}^\pm = -B \pm \sqrt{B^2 - C} \equiv -B \pm \sqrt{\Xi}. \tag{2.76}$$

The Θ-function now requires these roots to be real, otherwise $-\Delta_4$ would be negative for all s_{2s}. This is equivalent to the condition $\Xi \geq 0$. From the latter inequality we conclude

$$s_{2q} \leq z\,(1 - s_{12} - s_{1s} - s_{1q}) \qquad \text{with} \qquad z = \frac{s_{12} + s_{1q}}{s_{12} + s_{1q} + s_{1s}} \leq 1\,. \tag{2.77}$$

The above roots now fulfill the inequality $0 \leq s_{2s}^- \leq s_{2s}^+ \leq 1 - s_{12} - s_{1s} - s_{1q} - s_{2q}$ which leads to the following new limits of integration:

$$\begin{aligned} A &= ds_{12} \int_0^{1-s_{12}} ds_{1s} \int_0^{1-s_{12}-s_{1s}} ds_{1q} s_{1q}^{-1} (s_{12} + s_{1q})^{-1-2\epsilon} \\ &\quad \times \int_0^{z(1-s_{12}-s_{1s}-s_{1q})} ds_{2q} s_{2q}^{-1} \int_{s_{2s}^-}^{s_{2s}^+} ds_{2s}\, (s_{2s}^+ - s_{2s})^{-\frac{1}{2}-\epsilon} (s_{2s} - s_{2s}^-)^{-\frac{1}{2}-\epsilon} \,. \end{aligned} \tag{2.78}$$

Substituting $s_{2s} = (s_{2s}^+ - s_{2s}^-)\chi + s_{2s}^-$, the subsequent χ-integration can be done trivially in terms of Γ-functions.

As a general strategy for the choice of the order of integration, we suggest the following. The variable of the first integration (δ-function) must not be contained in the term of K_R that one considers. If possible, this term should also be free of the variable that one uses to factorize the Gram determinant (s_{2s} in our case). If the latter is not possible as for instance in $K_R = s_{1s} s_{2s} s_{1q}^{-1} s_{2q}^{-1}$, one should at least factorize the Gram determinant in a variable that does not appear in the denominator of K_R. This procedure ensures that the first two integrations can be done in terms of Γ-functions, and it avoids hypergeometric functions to emerge at this stage of the calculation.

The choice of the subsequent order of integration is governed by the aim to extract all divergences as early as possible. This is the reason for which we solved the condition $\Xi \geq 0$ for s_{2q}. We now substitute $s_{2q} = z(1 - s_{12} - s_{1s} - s_{1q})\, t$ and perform the t-integration, yielding again only Γ-functions. After simplification, we obtain

$$A = -\frac{\pi}{\epsilon}\, ds_{12}\, s_{12}^{-\epsilon} \times \int_0^{1-s_{12}} ds_{1s}\, s_{1s}^{-\epsilon} \int_0^{1-s_{12}-s_{1s}} ds_{1q} s_{1q}^{-1-\epsilon} (s_{12}+s_{1q})^{-1} (s_{12}+s_{1q}+s_{1s})^{\epsilon} (1-s_{12}-s_{1s}-s_{1q})^{-2\epsilon} \,. \quad (2.79)$$

We now proceed as follows:

- Perform an expansion into partial fractions via $\dfrac{1}{s_{1q}(s_{12}+s_{1q})} = \dfrac{1}{s_{12}\, s_{1q}} - \dfrac{1}{s_{12}(s_{12}+s_{1q})}$.
- Substitute $s_{1q} = (1 - s_{12} - s_{1s})(1-u)$. The u-integration can be carried out in the first term of the above expansion.
- Substitute $s_{1s} = (1 - s_{12})(1-v)$. Again, the v-integration can be done in the first term.

In this way one obtains the following expression:

$$\begin{aligned} A &= -\frac{\pi}{\epsilon}\, ds_{12}\, s_{12}^{-1-\epsilon} (1-s_{12})^{1-4\epsilon} \left\{ \frac{\Gamma(1-2\epsilon)\Gamma(-\epsilon)\Gamma(1-\epsilon)}{\Gamma(2-4\epsilon)}\, {}_2F_1(-\epsilon, 1-2\epsilon; 2-4\epsilon; 1-s_{12}) \right. \\ &\quad \left. -(1-s_{12}) \int_0^1 du \int_0^1 dv\, \frac{u^{-2\epsilon}(1-u)^{-\epsilon}\, v^{1-3\epsilon}(1-v)^{-\epsilon}}{s_{12} + (1-s_{12})\, v\, (1-u)} \left[1 - (1-s_{12})\, u\, v\right]^{\epsilon} \right\}. \quad (2.80) \end{aligned}$$

We now carry out a two-dimensional variable transformation from (u, v) to (y, w) via

$$y = 1 - u\, v\,, \qquad \text{and} \qquad y\, w = v\,(1-u)\,. \quad (2.81)$$

The w-integration can now be performed, resulting in another hypergeometric function. After using the Kummer relation also the y-integration can be done. The final result for A reads

$$\begin{aligned} A &= -\frac{\pi}{\epsilon}\, ds_{12}\, s_{12}^{-1-\epsilon} (1-s_{12})^{1-4\epsilon} \left\{ \frac{\Gamma(1-2\epsilon)\Gamma(-\epsilon)\Gamma(1-\epsilon)}{\Gamma(2-4\epsilon)}\, {}_2F_1(-\epsilon, 1-2\epsilon; 2-4\epsilon; 1-s_{12}) \right. \\ &\quad \left. -(1-s_{12})\, \frac{\Gamma^2(1-\epsilon)\Gamma(1-2\epsilon)}{\Gamma(3-4\epsilon)}\, {}_2F_1(1-\epsilon, 2-2\epsilon; 3-4\epsilon; 1-s_{12}) \right\}. \quad (2.82) \end{aligned}$$

All the divergences have now been extracted in terms of poles and Γ-functions. The remaining task is now to expand the hypergeometric functions in ϵ. This can can be done by means of the `Mathematica` [68] package `HypExp` [69], which we will present and explain in great detail in chapter 3.

2.4.1.4 From NDR to mass regularization

As we have stated earlier, the differential decay width is not an infrared safe object with respect to emission of collinear photons. This means that, as long as the lepton is treated as massless, the sum of virtual and real corrections is not free of collinear divergences. If we had kept the lepton mass different from zero during the whole calculation, the sum of virtual and real corrections would have been finite. However, the computation of the diagrams and the massive phase space integrals in T_V and T_R would have been much more tedious.

The translation of the $1/\epsilon$ pole into a $\ln(m_b^2/m_\ell^2)$-term corresponds to changing the regularization scheme and is complicated by the presence of soft infrared singularities. The correct procedure is to start by constructing an observable that is infrared safe and, consequently, regularization scheme independent. Only at this point we can switch to the m_ℓ regulator and obtain our final result. As an intermediate step, we construct a differential branching ratio where $\hat{s}$ is identified as follows:

$$\hat{s} \;=\; \begin{cases} (p_{\ell_1}+p_{\ell_2}+p_\gamma)^2/m_b^2\,, & \text{if } \vec{p}_\gamma \,||\, (\vec{p}_{\ell_1} \text{ or } \vec{p}_{\ell_2})\,, \\ (p_{\ell_1}+p_{\ell_2})^2/m_b^2\,, & \text{otherwise.} \end{cases} \tag{2.83}$$

In order to switch to this intermediate observable we must subtract the *collinear* decay width differential in the dilepton invariant mass and add the same quantity but remaining differential in the triple invariant.

The calculation of the differential branching ratio in the collinear limit is done with the help of the NDR-scheme splitting function for the massless lepton. The splitting function in this scheme can be derived from Refs. [70, 71] and reads

$$f_\gamma^{(\epsilon)}(x,E) \;=\; 4\widetilde{\alpha}_e \left[\frac{1+(1-x)^2}{x}\left(-\frac{1}{2\epsilon}+\ln\frac{E}{\mu}+\ln(2-2x)\right)-\frac{(2-x)^2}{2x}\ln\frac{2-x}{x}\right]\,, \tag{2.84}$$

where E is the energy of the incoming lepton and xE is the energy of the emitted photon. See Fig. 2.4 for a pictorial view of the kinematics.

The fully differential decay width in the collinear limit is given by (here and in the following we omit the factor $8\,G_F^2|V_{tb}V_{ts}|^2$ stemming from the effective Lagrangian):

$$\begin{aligned} \mathrm{d}\Gamma_{\rm coll}^{(\epsilon)}(\hat{s}_{12},\hat{s}_{1s},\hat{s}_{2s},x) \;&=\; (2m_b)^{-1}\,\left[f_\gamma^{(\epsilon)}(x,E_1)+f_\gamma^{(\epsilon)}(x,E_2)\right]\,|\langle P_9\rangle_{\rm tree}|^2\;dPS_3\,dx \\ &=\; m_b^{-1}\,f_\gamma^{(\epsilon)}(x,E_1)\,|\langle P_9\rangle_{\rm tree}|^2\;dPS_3\,dx\,, \end{aligned} \tag{2.85}$$

where $x,\hat{s}_{12},\hat{s}_{1s},\hat{s}_{2s}\in[0,1]$, $E_1=m_b(1-\hat{s}_{2s})/2$ and we used the $\ell_1\leftrightarrow\ell_2$ symmetry. The collinear decay width differential in the triple invariant ($\hat{s}=(p_{\ell_1}+p_{\ell_2}+p_\gamma)^2/m_b^2$) reads

$$\frac{\mathrm{d}\Gamma_{\rm coll,3}^{(\epsilon)}}{d\hat{s}} = m_b^{-1}\int_0^1 dx\int_0^1 d\hat{s}_{1s}\int_0^1 d\hat{s}_{2s}\,M_3(\hat{s},\hat{s}_{1s},\hat{s}_{2s})\;f_\gamma^{(\epsilon)}(x,E_1)\;|\langle P_9\rangle_{\rm tree}|^2_{\hat{s}_{12}\to\hat{s}}\;. \tag{2.86}$$

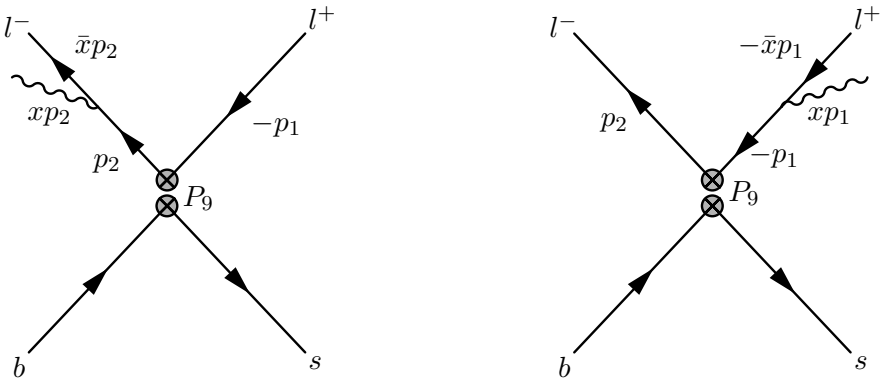

Figure 2.4: Splitting function kinematics. The photon is emitted by a quasi-real lepton.

The collinear decay width differential in the dilepton invariant mass ($\hat{s} = (p_1 + \bar{x}p_2)^2/m_b^2$) reads

$$\frac{\mathrm{d}\Gamma^{(\epsilon)}_{\mathrm{coll},2}}{d\hat{s}} = m_b^{-1} \int_0^{1-\hat{s}} \frac{dx}{\bar{x}} \int_0^1 d\hat{s}_{1s} \int_0^1 d\hat{s}_{2s}\, M_3(\hat{s}/\bar{x}, \hat{s}_{1s}, \hat{s}_{2s})\; f_\gamma^{(\epsilon)}(x, E_1)\;\; |\langle P_9 \rangle_{\mathrm{tree}}|^2_{\hat{s}_{12} \to \hat{s}/\bar{x}}\;, \tag{2.87}$$

where $\bar{x} \equiv 1 - x$, and the non-linear change of variables $\hat{s}_{12} \to \hat{s}/\bar{x}$ also implied a distortion of the x-integration domain. The addition of $\mathrm{d}\Gamma^{(\epsilon)}_{\mathrm{coll},3}/d\hat{s} - \mathrm{d}\Gamma^{(\epsilon)}_{\mathrm{coll},2}/d\hat{s}$ to the results of previous subsections removes the remaining $1/\epsilon$-pole from the differential decay width.

We are now free to convert back this observable to the usual one, in which $\hat{s}$ is always the dilepton invariant mass, using mass regularization. In this context, we need the splitting function in the same scheme [70]:

$$\begin{aligned} f_\gamma^{(m)}(x, E) \;\; &= \;\; 4\tilde{\alpha}_e \Big[\frac{1 + (1-x)^2}{x} \left(\ln \frac{E}{m_\ell} + \ln(2 - 2x) \right) \\ &\qquad -1 + x - \frac{x^2}{2} \ln x - \frac{(2-x)^2}{2} \ln(2 - x) \Big] \,. \end{aligned} \tag{2.88}$$

The original differential decay width is then obtained by adding $\mathrm{d}\Gamma^{(m)}_{\mathrm{coll},2}/d\hat{s} - \mathrm{d}\Gamma^{(m)}_{\mathrm{coll},3}/d\hat{s}$, where $\mathrm{d}\Gamma^{(m)}$ is obtained from $\mathrm{d}\Gamma^{(\epsilon)}$ via $f_\gamma^{(\epsilon)} \to f_\gamma^{(m)}$. Therefore, the total correction term is given by the following double difference:

$$\frac{T_S}{2m_b} \;\; = \;\; \left(\frac{\mathrm{d}\Gamma^{(m)}_{\mathrm{coll},2}}{d\hat{s}} - \frac{\mathrm{d}\Gamma^{(\epsilon)}_{\mathrm{coll},2}}{d\hat{s}} \right) - \left(\frac{\mathrm{d}\Gamma^{(m)}_{\mathrm{coll},3}}{d\hat{s}} - \frac{\mathrm{d}\Gamma^{(\epsilon)}_{\mathrm{coll},3}}{d\hat{s}} \right) \,. \tag{2.89}$$

Note that only the E-independent difference $f_\gamma^{(\epsilon)}(x, E) - f_\gamma^{(m)}(x, E)$ enters in the total correction term. Hence, we can perform separately the $(x,\, \hat{s}_{12})$ and $(\hat{s}_{1s},\, \hat{s}_{2s})$ integrations. The tree level squared matrix element of P_9 integrated over the phase space reads

$$\sigma(\hat{s}_{12}) \equiv \frac{2^{-7+6\epsilon} \pi^{-\frac{5}{2}+2\epsilon} (m_b^2)^{3-2\epsilon} \tilde{\mu}^{4\epsilon}}{\Gamma(\frac{3}{2} - \epsilon)} d\hat{s}_{12}\; \hat{s}_{12}^{-\epsilon}\; (1 - \hat{s}_{12})^{2-2\epsilon}\; \frac{\Gamma(2-\epsilon)}{\Gamma(2-2\epsilon)}\; \frac{2\hat{s}_{12}(1-\epsilon) + 1}{3 - 2\epsilon}\,, \tag{2.90}$$

and the total correction term is finally expressed as

$$T_S = 2\left[\int_0^1 dx\,\left[f_\gamma^{(\epsilon)}(x) - f_\gamma^{(m)}(x)\right]\sigma(\hat{s}) - \int_0^{1-\hat{s}} dx\,\frac{f_\gamma^{(\epsilon)}(x) - f_\gamma^{(m)}(x)}{(1-x)}\sigma\left(\frac{\hat{s}}{1-x}\right)\right]. \tag{2.91}$$

Both integrals in Eq. (2.91) are infrared divergent for $x \to 0$, but their sum is not.

The sum $T_V + T_R + T_S$ is now free of divergences and contains an explicit collinear logarithm $\ln(m_b^2/m_\ell^2)$. The coefficient of this logarithm vanishes when integrated over $\hat{s}_{12}$. This means that if we had considered the total branching ratio instead of the differential one, the sum of $T_V + T_R$ would have been already finite and the inclusion of T_S would have become unnecessary. However, the coefficient of the collinear logarithm is large and positive for low $\hat{s}_{12}$ and large and negative for high $\hat{s}_{12}$. Furthermore, this term renders by far the major contribution to the electromagnetic corrections stemming from the matrix elements. In the sum $T_V + T_R + T_S$ the coefficient of Q_d^2 is up to a color factor proportional to the QCD-function $\omega_{99}^{(1)}(\hat{s})$ from Eq. (A.8), providing another check for our result. Inserting $Q_d = -1/3$ and $Q_l = -1$ finally yields

$$T_V + T_R + T_S = \frac{\widetilde{\alpha}_e\, m_b^6\,(1-\hat{s}_{12})^2\,(1+2\,\hat{s}_{12})}{24\,\pi^3}\omega_{99}^{(\mathrm{em})}(\hat{s}_{12})\,, \tag{2.92}$$

with

$$\begin{aligned}\omega_{99}^{(\mathrm{em})}(\hat{s}) &= \ln\left(\frac{m_b^2}{m_\ell^2}\right)\left[-\frac{1+4\,\hat{s}-8\,\hat{s}^2}{6\,(1-\hat{s})\,(1+2\,\hat{s})} + \ln(1-\hat{s}) - \frac{\left(1-6\,\hat{s}^2+4\,\hat{s}^3\right)\ln\hat{s}}{2\,(1-\hat{s})^2\,(1+2\,\hat{s})}\right] \\ &\quad -\frac{1}{9}\,Li_2(\hat{s}) + \frac{4}{27}\pi^2 - \frac{121-27\,\hat{s}-30\,\hat{s}^2}{72\,(1-\hat{s})\,(1+2\,\hat{s})} - \frac{(41+76\,\hat{s})\,\ln(1-\hat{s})}{36(1+2\,\hat{s})} \\ &\quad +\left(\frac{-3-10\,\hat{s}-17\,\hat{s}^2+14\,\hat{s}^3}{18\,(1-\hat{s})^2\,(1+2\,\hat{s})} + \frac{17\,\ln(1-\hat{s})}{18}\right)\ln\hat{s} - \frac{\left(1-6\,\hat{s}^2+4\,\hat{s}^3\right)\ln^2\hat{s}}{2\,(1-\hat{s})^2\,(1+2\,\hat{s})}\,.\end{aligned} \tag{2.93}$$

The contribution that we have calculated can be effectively taken into account via the following substitution:

$$|C_9(\mu_b)\langle P_9\rangle_{\mathrm{tree}}|^2 \implies |C_9(\mu_b)\langle P_9\rangle_{\mathrm{tree}}|^2\left[1 + 8\,\widetilde{\alpha}_e\,\omega_{99}^{(\mathrm{em})}(\hat{s})\right]. \tag{2.94}$$

2.4.2 Other log-enhanced corrections

The QED corrections to the matrix elements of P_i with $i \neq 9$ contribute to the branching ratio at order $O(\widetilde{\alpha}_s^3\kappa^3)$. Consequently, we include those contributions that are enhanced by an explicit $\ln(m_b^2/m_\ell^2)$. The relevant terms in the amplitude are

$$\mathcal{A} \propto \left[(C_2 + C_F\,C_1)\,\widetilde{\alpha}_s\kappa\,f_2(\hat{s}) + C_9\right]\langle P_9\rangle_{\mathrm{tree}} + C_{10}\langle P_{10}\rangle_{\mathrm{tree}} + C_7\langle P_7\rangle_{\mathrm{tree}}\,, \tag{2.95}$$

where the $f_2(\hat{s})$ is defined in Eq. (2.60). Here we have dropped the NNLO QCD corrections to the matrix elements as well as the terms proportional to the small penguin coefficients

$C_{i(Q)}$. After squaring and under the assumption that C_1 and C_2 are real, we obtain

$$\begin{aligned}
|\mathcal{A}|^2 \;\propto\; & \Big[|C_9|^2 + \widetilde{\alpha}_{\rm s}^2\kappa^2\,(C_2 + C_F\,C_1)^2\,|f_2(\hat{s})|^2 \\
& \qquad +2\,\widetilde{\alpha}_{\rm s}\kappa\,{\rm Re}[f_2(\hat{s})(C_2 + C_F\,C_1)C_9^*]\Big]\;|\langle P_9\rangle_{\rm tree}|^2 \\
& +2\,{\rm Re}\Big[C_7C_9^* + \widetilde{\alpha}_{\rm s}\kappa\,C_7(C_2 + C_F\,C_1)f_2^*(\hat{s})\Big]\;\langle P_7\rangle_{\rm tree}\langle P_9\rangle_{\rm tree}^* \\
& +|C_7|^2\;|\langle P_7\rangle_{\rm tree}|^2 + |C_{10}|^2\;|\langle P_{10}\rangle_{\rm tree}|^2\;. \qquad (2.96)
\end{aligned}$$

The fully differential decay width in the collinear limit now yields

$$\mathrm{d}\Gamma_{\rm coll}^{(m)}(\hat{s}_{12},\hat{s}_{1s},\hat{s}_{2s},x) \;=\; m_b^{-1}\,f_\gamma^{(m)}(x,E_1)\;|\mathcal{A}|^2\;dPS_3\,dx\;. \qquad (2.97)$$

These corrections are induced by collinear photon emission and are given by $\mathrm{d}\Gamma_{\rm coll,2}^{(m)}/d\hat{s} - \mathrm{d}\Gamma_{\rm coll,3}^{(m)}/d\hat{s}$, where we retain only the $\ln(m_b^2/m_\ell^2)$ term in $f_\gamma^{(m)}(x,E)$. The result reads

$$\begin{aligned}
\frac{\mathrm{d}\Delta\Gamma}{d\hat{s}} \;=\; & \frac{G_F^2 m_b^5}{48\pi^3}|V_{tb}V_{ts}|^2(1-\hat{s})^2\widetilde{\alpha}_{\rm s}\kappa\Bigg\{8\,(1+2\hat{s})\Bigg[|C_9|^2\;\omega_{99}^{(\rm em)}(\hat{s}) + |C_{10}|^2\;\omega_{1010}^{(\rm em)}(\hat{s}) \\
& +\widetilde{\alpha}_{\rm s}\kappa\;{\rm Re}\Big[(C_2+C_FC_1)C_9^*\;\omega_{29}^{(\rm em)}(\hat{s})\Big] + \widetilde{\alpha}_{\rm s}^2\kappa^2\;(C_2+C_FC_1)^2\;\omega_{22}^{(\rm em)}(\hat{s})\Bigg] \\
& +96\left[\widetilde{\alpha}_{\rm s}\kappa\;{\rm Re}\,[C_7C_9^*]\;\omega_{79}^{(\rm em)}(\hat{s}) + \widetilde{\alpha}_{\rm s}^2\kappa^2\;{\rm Re}\left[(C_2+C_FC_1)C_7^*\;\omega_{27}^{(\rm em)}(\hat{s})\right]\right] \\
& +8\,(4+\frac{8}{\hat{s}})\widetilde{\alpha}_{\rm s}^2\kappa^2\;|C_7|^2\;\omega_{77}^{(\rm em)}(\hat{s})\Bigg\}\;, \qquad (2.98)
\end{aligned}$$

where $\omega_{99}^{(\rm em)}(\hat{s})$ was already found in the previous section. The other ω-functions are:

$$\omega_{1010}^{(\rm em)}(\hat{s}) \;=\; \ln\left(\frac{m_b^2}{m_\ell^2}\right)\left[-\frac{1+4\,\hat{s}-8\,\hat{s}^2}{6\;(1-\hat{s})\;(1+2\,\hat{s})} + \ln(1-\hat{s}) - \frac{\left(1-6\,\hat{s}^2+4\,\hat{s}^3\right)\;\ln\hat{s}}{2\;(1-\hat{s})^2\;(1+2\,\hat{s})}\right]\;, \qquad (2.99)$$

$$\omega_{77}^{(\rm em)}(\hat{s}) \;=\; \ln\left(\frac{m_b^2}{m_\ell^2}\right)\left[\frac{\hat{s}}{2\,(1-\hat{s})\;(2+\hat{s})} + \ln(1-\hat{s}) - \frac{\hat{s}\;\left(-3+2\,\hat{s}^2\right)}{2\,(1-\hat{s})^2\;(2+\hat{s})}\;\ln(\hat{s})\right]\;, \qquad (2.100)$$

$$\omega_{79}^{(\rm em)}(\hat{s}) \;=\; \ln\left(\frac{m_b^2}{m_\ell^2}\right)\left[-\frac{1}{2\,(1-\hat{s})} + \ln(1-\hat{s}) + \frac{\left(-1+2\,\hat{s}-2\,\hat{s}^2\right)}{2\,(1-\hat{s})^2}\;\ln(\hat{s})\right]\;, \qquad (2.101)$$

$$\omega_{29}^{(\rm em)}(\hat{s}) \;=\; \ln\left(\frac{m_b^2}{m_\ell^2}\right)\left[\frac{\Sigma_1(\hat{s}) + i\,\Sigma_1^I(\hat{s})}{8(1-\hat{s})^2(1+2\hat{s})}\right] + \frac{16}{9}\,\omega_{1010}^{(\rm em)}(\hat{s})\;\ln\Big(\frac{\mu_b}{5{\rm GeV}}\Big)\;, \qquad (2.102)$$

$$\begin{aligned}
\omega_{22}^{(\rm em)}(\hat{s}) \;=\; & \ln\left(\frac{m_b^2}{m_\ell^2}\right)\left[\frac{\Sigma_2(\hat{s})}{8(1-\hat{s})^2(1+2\hat{s})} + \frac{\Sigma_1(\hat{s})}{9(1-\hat{s})^2(1+2\hat{s})}\ln\Big(\frac{\mu_b}{5{\rm GeV}}\Big)\right] \\
& + \frac{64}{81}\,\omega_{1010}^{(\rm em)}(\hat{s})\;\ln^2\Big(\frac{\mu_b}{5{\rm GeV}}\Big)\;, \qquad (2.103)
\end{aligned}$$

$$\omega_{27}^{(\rm em)}(\hat{s}) \;=\; \ln\left(\frac{m_b^2}{m_\ell^2}\right)\left[\frac{\Sigma_3(\hat{s}) + i\,\Sigma_3^I(\hat{s})}{96(1-\hat{s})^2}\right] + \frac{8}{9}\,\omega_{79}^{(\rm em)}(\hat{s})\;\ln\Big(\frac{\mu_b}{5{\rm GeV}}\Big)\;. \qquad (2.104)$$

The functions Σ_i have been evaluated numerically in the low-$\hat{s}$-region (for fixed values of m_b and m_c, see section 2.7):

$$\begin{aligned}
\Sigma_1(\hat{s}) &= 23.787 - 120.948\,\hat{s} + 365.373\,\hat{s}^2 - 584.206\,\hat{s}^3 \,, && (2.105)\\
\Sigma_1^I(\hat{s}) &= 1.653 + 6.009\,\hat{s} - 17.080\,\hat{s}^2 + 115.880\,\hat{s}^3 \,, && (2.106)\\
\Sigma_2(\hat{s}) &= 11.488 - 36.987\,\hat{s} + 255.330\,\hat{s}^2 - 812.388\,\hat{s}^3 + 1011.791\,\hat{s}^4 \,, && (2.107)\\
\Sigma_3(\hat{s}) &= 109.311 - 846.039\,\hat{s} + 2890.115\,\hat{s}^2 - 4179.072\,\hat{s}^3 \,, && (2.108)\\
\Sigma_3^I(\hat{s}) &= 4.606 + 17.650\,\hat{s} - 53.244\,\hat{s}^2 + 348.069\,\hat{s}^3 \,. && (2.109)
\end{aligned}$$

2.5 Collinear logarithms and angular cuts

The explicit logarithm of the lepton mass signals the presence of a collinear singularity whose appearance in the differential branching ratio is strictly related to the definition of the dilepton invariant mass. As explained in Sec. 2.4.1.4, this logarithm disappears if all photons emitted by the final state on-shell leptons are included in the definition of s: $(p_{\ell_1} + p_{\ell_2})^2 \to (p_{\ell_1} + p_{\ell_2} + p_\gamma)^2$.

Let us consider a cone of angular opening θ around an on-shell lepton with momentum p_ℓ. For all photons emitted in this cone we have: $m_\ell^2 \le (p_\ell + p_\gamma)^2 \le \Lambda^2 \simeq 2E_\ell^2(1-\cos\theta)$, where E_ℓ is the energy of the lepton, usually of order $\mathcal{O}(m_b)$. Consequently, the effect of including such photons in the reconstruction of the lepton momentum can be roughly approximated by replacing m_ℓ by some scale of order Λ in the collinear logarithm.

Both Babar and Belle include sufficiently collinear photons in the definition of the lepton momentum. However, the imposed cones are so narrow that the effect for the muons is negligible, i.e. the separation of muons and collinear photons is practically perfect [53][10]. Thus, our expressions containing $\ln(m_b^2/m_\mu^2)$ are directly applicable in this case.

For electrons, the situation is more complicated. In both experiments, the cone is defined in the laboratory frame and has polar and azimuthal angles around 45 mrad and 5 mrad, respectively. Hence, Λ is of the same order as m_μ, which makes the QED corrections for the electrons similar to those for the muons. Nothing more precise can be said without applying dedicated Monte Carlo routines that would take into account the experimental setups in detail.

2.6 Formulae for the branching ratio

In section 2.7, we will express the branching ratio in terms of the quantity $\Phi_{\ell\ell}(\hat{s})/\Phi_u$. In the present section, we express this quantity in terms of the low-scale Wilson coefficients and various functions of $\hat{s}$ that arise from the matrix elements. The main formula reads

$$\frac{\Phi_{\ell\ell}(\hat{s})}{\Phi_u} = \sum_{i\le j} \mathrm{Re}\left[C_i^{\mathrm{eff}}(\mu_b)\, C_j^{\mathrm{eff}*}(\mu_b)\, H_{ij}(\mu_b,\hat{s})\right] \,, \qquad (2.110)$$

where $C_i^{\mathrm{eff}}(\mu_b) \neq C_i(\mu_b)$ only for $i = 7, 8$ (see Eqs. (2.57) and (2.58)). The functions $H_{ij}(\mu_b,\hat{s})$ can be expressed analytically in terms of the coefficients M_i^A listed in Table 2.4

[10] I would also like to thank S. Willocq and my collaborators from [39] for communication on this issue.

and of the following building blocks

$$\begin{aligned}
\mathrm{S}_{99} &= (1-\hat{s})^2(1+2\hat{s})\left\{1+8\,\widetilde{\alpha}_\mathrm{s}\left[\omega_{99}^{(1)}(\hat{s})+u^{(1)}\right]+\kappa\,u^{(\mathrm{em})}+8\,\widetilde{\alpha}_\mathrm{s}\kappa\,\omega_{99}^{(\mathrm{em})}(\hat{s})\right. \\
&\quad \left.+16\,\widetilde{\alpha}_\mathrm{s}^2\left[\omega_{99}^{(2)}(\hat{s})+u^{(2)}+4u^{(1)}\omega_{99}^{(1)}(\hat{s})\right]\right\} \\
&\quad +6\,\frac{\lambda_2}{m_b^2}\,(1-6\hat{s}^2+4\hat{s}^3)\,, \qquad (2.111) \\
\mathrm{S}_{77} &= (1-\hat{s})^2(4+\frac{8}{\hat{s}})\left\{1+8\,\widetilde{\alpha}_\mathrm{s}\left[\omega_{77}^{(1)}(\hat{s})+u^{(1)}\right]+\kappa\,u^{(\mathrm{em})}+8\,\widetilde{\alpha}_\mathrm{s}\kappa\,\omega_{77}^{(\mathrm{em})}(\hat{s})\right\} \\
&\quad +24\,\frac{\lambda_2}{m_b^2}\,(2\hat{s}^2-3)\,, \qquad (2.112) \\
\mathrm{S}_{79} &= 12(1-\hat{s})^2\left\{1+8\,\widetilde{\alpha}_\mathrm{s}\left[\omega_{79}^{(1)}(\hat{s})+u^{(1)}\right]+\kappa\,u^{(\mathrm{em})}+8\,\widetilde{\alpha}_\mathrm{s}\kappa\,\omega_{79}^{(\mathrm{em})}(\hat{s})\right\} \\
&\quad +24\,\frac{\lambda_2}{m_b^2}\,(1-6\hat{s}+4\hat{s}^2)\,, \qquad (2.113) \\
\mathrm{S}_{1010} &= S_{99}+8\,\widetilde{\alpha}_\mathrm{s}\kappa(1-\hat{s})^2(1+2\hat{s})\left[\omega_{1010}^{(\mathrm{em})}(\hat{s})-\omega_{99}^{(\mathrm{em})}(\hat{s})\right]\,. \qquad (2.114)
\end{aligned}$$

The functions $\omega_{ij}^{(k)}$ are listed in appendix A. The functions $\omega_{ij}^{(\mathrm{em})}$ have been given in Eqs. (2.93) and (2.99)–(2.104). The numbers $u^{(1)} = (4\pi^2-25)/12$ and $u^{(2)} \simeq 27.1 + \beta_0 u^{(1)} \ln(\mu_b/m_b)$ originate from the QCD corrections to $b \to X_u e\bar{\nu}$ [72], while the quantity $u^{(\mathrm{em})} = \frac{12}{23}\left(\eta^{-1}-1\right)$ stands for the logarithmically-enhanced QED correction to this decay [73]. The S_{AB} include non-perturbative $\mathcal{O}(\Lambda_{\mathrm{QCD}}^2/m_b^2)$ corrections that one finds by taking the limit $m_c \to 0$ in Eq. (18) of Ref. [44]. They were also calculated in Refs. [43,74].

The explicit expressions for the functions H_{ij} read

$$H_{ij} = \begin{cases} \sum\limits_{A=7,9,10} |M_i^A|^2\; S_{AA} + \;\mathrm{Re}(M_i^7 M_i^{9*})\; S_{79} + \Delta H_{ii}\,, & \text{when } i=j\,, \\ \sum\limits_{A=7,9,10} 2M_i^A M_j^{A*}\; S_{AA} + \left(M_i^7 M_j^{9*} + M_i^9 M_j^{7*}\right)\; S_{79} + \Delta H_{ij}\,, & \text{when } i\neq j\,. \end{cases} \qquad (2.115)$$

It is assumed that all the products in Eq. (2.110) are expanded in $\widetilde{\alpha}_\mathrm{s}$, κ and λ_2, and that higher orders are neglected (see section 2.7). The quantities

$$\Delta H_{ij} = b_{ij} + c_{ij} + e_{ij} \qquad (2.116)$$

that need to be included only for $i = 1,2$ stand for additional bremsstrahlung (b_{ij}), non-perturbative $\mathcal{O}(\Lambda_{\mathrm{QCD}}^2/m_c^2)$ corrections (c_{ij}) and additional $\ln(m_b^2/m_\ell^2)$-enhanced electromagnetic corrections (e_{ij}). Specifically, the non-vanishing e_{ij} that we include read

$$\begin{aligned}
e_{22} &= 8\,(1-\hat{s})^2\,(1+2\hat{s})\,\widetilde{\alpha}_\mathrm{s}^3\kappa^3\,\omega_{22}^{(\mathrm{em})}(\hat{s})\,, \\
e_{27} &= 96\,(1-\hat{s})^2\,\widetilde{\alpha}_\mathrm{s}^3\kappa^3\,\omega_{27}^{(\mathrm{em})}(\hat{s})\,, \\
e_{29} &= 8\,(1-\hat{s})^2\,(1+2\hat{s})\,\widetilde{\alpha}_\mathrm{s}^2\kappa^2\,\omega_{29}^{(\mathrm{em})}(\hat{s})\,, \\
e_{11} &= \tfrac{16}{9}\,e_{22}\,, \\
e_{12} &= \tfrac{8}{3}\,e_{22}\,, \\
e_{1j} &= \tfrac{4}{3}e_{2j}, \qquad \text{for j} = 7,9. \qquad (2.117)
\end{aligned}$$

The $\mathcal{O}(\Lambda^2_{\rm QCD}/m_c^2)$ non-perturbative contributions were calculated in Ref. [75]

$$\begin{aligned}
c_{27} &= -\widetilde{\alpha}_{\rm s}^2\kappa^2\frac{8\lambda_2}{9m_c^2}(1-\hat{s})^2\frac{1+6\hat{s}-\hat{s}^2}{\hat{s}}\,F(r)\,,\\
c_{29} &= -\widetilde{\alpha}_{\rm s}\kappa\frac{8\lambda_2}{9m_c^2}(1-\hat{s})^2(2+\hat{s})\,F(r)\,,\\
c_{22} &= -\widetilde{\alpha}_{\rm s}\kappa\frac{8\lambda_2}{9m_c^2}(1-\hat{s})^2(2+\hat{s})\,{\rm Re}\left(F(r)M_2^{9*}\right)\,,\\
c_{11} &= -\tfrac{2}{9}\,c_{22}\,,\\
c_{12} &= \tfrac{7}{6}\,c_{22}\,,\\
c_{1j} &= -\tfrac{1}{6}\,c_{2j}, \qquad\qquad \text{for j} = 7,9\,,
\end{aligned} \tag{2.118}$$

where $r \equiv 1/y_c = s/(4m_c^2)$. The function $F(r)$ can be found in appendix A.

The finite bremsstrahlung contributions b_{ij} appear at NNLO in Ref. [49], where the notation is very similar to the one proposed here. We do not present these corrections here but do include them in the numerical analysis.

2.7 Branching ratio and numerical results

The content of this section is threefold. We will first describe how to normalize the differential decay width in order to arrive at an expression for the differential branching ratio. Second, we will discuss the $\alpha_s^n\kappa^m$-expansion in more detail. Finally, we will present the numerical results of our phenomenological analysis and give the results for the branching ratio integrated over the low-q^2 region.

The differential (with respect to $\hat{s} = q^2/m^2_{b,\rm pole} \equiv m^2_{\ell\ell}/m^2_{b,\rm pole}$) decay width of $\bar{B} \to X_s\ell^+\ell^-$ can be expressed as follows:

$$\frac{{\rm d}\Gamma(\bar{B}\to X_s\ell^+\ell^-)}{{\rm d}\hat{s}} = \frac{G_F^2 m^5_{b,\rm pole}}{48\pi^3}\,|V_{ts}^*V_{tb}|^2\;\Phi_{\ell\ell}(\hat{s}), \tag{2.119}$$

where the dimensionless function $\Phi_{\ell\ell}(\hat{s})$ is assumed to include both the perturbative and non-perturbative contributions.

In order to minimize the uncertainty stemming from $m^5_{b,\rm pole}$ and the CKM elements, we normalize the rare decay rate to the measured semileptonic one. Furthermore, to avoid introduction of spurious uncertainties due to the perturbative $b \to X_c e\bar{\nu}$ phase-space factor, we follow the analyses of Refs. [52, 76] where

$$C = \left|\frac{V_{ub}}{V_{cb}}\right|^2\frac{\Gamma(\bar{B}\to X_c e\bar{\nu})}{\Gamma(\bar{B}\to X_u e\bar{\nu})}\,, \tag{2.120}$$

was used instead[11]. Consequently, our expression for the $\bar{B} \to X_s\ell^+\ell^-$ branching ratio reads

$$\frac{{\rm d}\mathcal{B}(\bar{B}\to X_s\ell^+\ell^-)}{{\rm d}\hat{s}} = \mathcal{B}(B\to X_c e\bar{\nu})_{\rm exp}\left|\frac{V_{ts}^*V_{tb}}{V_{cb}}\right|^2\frac{4}{C}\,\frac{\Phi_{\ell\ell}(\hat{s})}{\Phi_u}\,, \tag{2.121}$$

[11] I would like to thank Mikołaj Misiak for suggesting this procedure.

$\alpha_s(M_z) = 0.1182 \pm 0.0027$ [78]	$m_e = 0.51099892$ MeV
$\alpha_e(M_z) = 1/127.918$	$m_\mu = 105.658369$ MeV
$s_W^2 \equiv \sin^2\theta_W = 0.2312$	$m_\tau = 1.77699$ GeV
$\lvert V_{ts}^* V_{tb}/V_{cb}\rvert^2 = 0.967 \pm 0.009$ [14]	$m_c(m_c) = (1.224 \pm 0.017 \pm 0.054)$ GeV [79]
$BR(B \to X_c e \bar{\nu})_{\rm exp} = 0.1061 \pm 0.0017$ [80]	$m_b^{1S} = (4.68 \pm 0.03)$ GeV [77]
$M_Z = 91.1876$ GeV	$m_{t,\rm pole} = (172.7 \pm 2.9)$ GeV [81]
$M_W = 80.426$ GeV	$m_B = 5.2794$ GeV
$\lambda_2 \simeq \frac{1}{4}\left(m_{B^*}^2 - m_B^2\right) \simeq 0.12$ GeV^2	$C = 0.58 \pm 0.01$ [77]

Table 2.6: Numerical inputs that we use in the phenomenological analysis. Unless explicitly specified, they are taken from PDG 2004 [10].

where $\Phi_u = 1 + \mathcal{O}(\alpha_s, \alpha_{\rm em}, \Lambda^2/m_b^2)$ is defined by

$$\Gamma(B \to X_u e \bar{\nu}) = \frac{G_F^2 m_{b,\rm pole}^5}{192\pi^3} \lvert V_{ub}\rvert^2 \ \Phi_u. \tag{2.122}$$

Our expressions for the ratio $\Phi_{\ell\ell}(\hat{s})/\Phi_u$ are summarized in section 2.6. Both the perturbative and non-perturbative corrections to this ratio are much better behaved than for $\Phi_{\ell\ell}(\hat{s})$ and Φ_u separately. The factor $C = 0.58 \pm 0.01$ has been recently determined from a global analysis of the semileptonic data [77]. All the input parameters that we use in the numerical calculation are summarized in Table 2.6.

It should be stressed that the pole mass of the b quark that is present in the definition of $\hat{s}$, in the measure $d\hat{s}$ in Eq. (2.121), and in several loop functions, gets analytically converted to the so-called $1S$ mass before any numerical evaluation of the branching ratio is performed. This way one avoids dealing with the renormalon ambiguities in the definition of the pole mass [82]. The formula that relates the pole mass to the $1S$ mass can be found e.g. in section 4 of Ref. [83].

The pole mass of the charm quark is treated similarly since it also suffers from renormalon ambiguities that we want to remove by converting it into a renormalon free mass. However, the situation is more subtle here. Some of the loop functions, e.g. the function $g(y_c)$ from Eq. (2.60), have a discontinuity at $s = 4m_c^2$ which is situated in the low-s region if $m_c < \sqrt{3/2}$ GeV ≈ 1.2247 GeV. Since an expansion on one side of the discontinuity can never converge on the other side we have to make sure that the central value of the charm mass as well as its entire error bar lie completely on either side of the discontinuity. This is not satisfied by the $\overline{MS}$ mass of Table 2.6 but, as it turns out, by the $1S$ mass. The latter therefore enters our calculation as follows. We convert analytically the pole mass of the charm quark into the $1S$ mass by means of the formulas of Ref. [83]. We then convert

numerically the $\overline{MS}$ mass given in Table 2.6 into the $1S$ mass, without passing through any value of the pole mass, following the formulas of Ref. [83]. The number that finally enters our analysis is $m_c^{1S} = 1.504 \pm 0.063$ GeV.

As far as the mass of the top quark is concerned we convert the pole mass to the $\overline{MS}$ mass. To the order we are working, we also take into account electroweak corrections presented in Eq. (31) of Ref. [58].

Let us now explain the details of the α_s and κ expansion that we adopt for calculating our final numerical results. The $b \to s\ell^+\ell^-$ decay amplitude has the following structure (up to an overall factor of G_F):

$$\begin{aligned} \mathcal{A} &= \kappa \left[\mathcal{A}_{LO} + \alpha_s\, \mathcal{A}_{NLO} + \alpha_s^2\, \mathcal{A}_{NNLO} + \mathcal{O}(\alpha_s^3)\right] \\ &\quad +\kappa^2 \left[\mathcal{A}^{em}_{LO} + \alpha_s\, \mathcal{A}^{em}_{NLO} + \alpha_s^2\, \mathcal{A}^{em}_{NNLO} + \mathcal{O}(\alpha_s^3)\right] + \mathcal{O}(\kappa^3)\,. \end{aligned} \tag{2.123}$$

As mentioned in the introduction, $\mathcal{A}_{LO} \sim \alpha_s\, \mathcal{A}_{NLO}$ and $\mathcal{A}^{em}_{LO} \sim \alpha_s\, \mathcal{A}^{em}_{NLO}$. All these terms are included in our calculation in a complete manner, together with the appropriate bremsstrahlung corrections. As far as $\mathcal{A}_{NNLO}$ is concerned, we use the practically complete results of Refs. [45, 47–52]; the only missing parts originate from the unknown two-loop matrix elements of the QCD-penguin operators whose Wilson coefficients are very small.

Among the contributions to $\mathcal{A}^{em}_{NNLO}$, we include only the terms which are either enhanced by an additional factor of $m_t^2/(M_W^2 \sin^2\theta_W)$ (with respect to $\mathcal{A}^{em}_{NLO}$) [52] or contribute to the $\ln(m_b^2/m_\ell^2)$-enhanced terms at the decay width level. The latter terms were calculated for the first time here. They are taken into account in a practically complete manner; the only missing part is proportional to the same tiny Wilson coefficient that is responsible for the smallness of $\mathcal{A}_{LO}$.

The perturbative expansion of the ratio $\Phi_{\ell\ell}(\hat{s})/\Phi_u$ has a similar structure to that of the squared amplitude:

$$\begin{aligned} \mathcal{A}^2 &= \kappa^2 \Big[\mathcal{A}_{LO}^2 + \alpha_s\, 2\mathcal{A}_{LO}\mathcal{A}_{NLO} + \alpha_s^2\, (\mathcal{A}_{NLO}^2 + 2\mathcal{A}_{LO}\mathcal{A}_{NNLO}) \\ &\qquad +\alpha_s^3\, 2(\mathcal{A}_{NLO}\mathcal{A}_{NNLO} + \ldots) + \mathcal{O}(\alpha_s^4))\Big] \\ &+ \kappa^3 \Big[2\mathcal{A}_{LO}\mathcal{A}^{em}_{LO} + \alpha_s\, 2(\mathcal{A}_{NLO}\mathcal{A}^{em}_{LO} + \mathcal{A}_{LO}\mathcal{A}^{em}_{NLO}) \\ &\qquad +\alpha_s^2\, 2(\mathcal{A}_{NLO}\mathcal{A}^{em}_{NLO} + \mathcal{A}_{NNLO}\mathcal{A}^{em}_{LO} + \mathcal{A}_{LO}\mathcal{A}^{em}_{NNLO}) \\ &\qquad +\alpha_s^3\, 2(\mathcal{A}_{NLO}\mathcal{A}^{em}_{NNLO} + \mathcal{A}_{NNLO}\mathcal{A}^{em}_{NLO} + \ldots) + \mathcal{O}(\alpha_s^4)\Big] \\ &+ \mathcal{O}(\kappa^4)\,. \end{aligned} \tag{2.124}$$

In our numerical calculation of $\Phi_{\ell\ell}(\hat{s})/\Phi_u$, we include all the terms that are written explicitly in the above equations. The dots at orders $\kappa^2\alpha_s^3$ and $\kappa^3\alpha_s^3$ stand for terms that are proportional to $\mathcal{A}_{LO}$ and $\mathcal{A}^{em}_{LO}$ and, consequently, can safely be neglected. In the numerical analysis we also include subleading $\Lambda^2_{\rm QCD}/m_c^2$ and $\Lambda^2_{\rm QCD}/m_b^2$ corrections [43, 44, 74, 75] as well as finite bremsstrahlung effects [49].

Our results for the branching ratios integrated in the range $1\ \text{GeV}^2 < m^2_{\ell\ell} < 6\ \text{GeV}^2$

NLO ($\alpha_{em}(\mu_0)$)	1.81×10^{-6}	NLO ($\alpha_{em}(\mu_b)$)	1.68×10^{-6}
NNLO ($\alpha_{em}(\mu_0)$)	1.65×10^{-6}	NNLO ($\alpha_{em}(\mu_b)$)	1.54×10^{-6}
QED (only WC's)	1.56×10^{-6}		
QED (muons)	1.59×10^{-6}	QED (electrons)	1.64×10^{-6}

Table 2.7: Anatomy of QCD and QED corrections.

read

$$\begin{aligned}\mathcal{B}_{\mu\mu} &= \Big[1.59 \pm 0.08_{\rm scale} \pm 0.06_{m_t} \pm 0.024_{C,m_c} \pm 0.015_{m_b} \pm 0.02_{\alpha_s(M_Z)} \\ &\qquad \pm 0.015_{\rm CKM} \pm 0.026_{{\rm BR}_{sl}}\Big] \times 10^{-6} = (1.59 \pm 0.11) \times 10^{-6}\,, \qquad (2.125)\\ \mathcal{B}_{ee} &= \Big[1.64 \pm 0.08_{\rm scale} \pm 0.06_{m_t} \pm 0.025_{C,m_c} \pm 0.015_{m_b} \pm 0.02_{\alpha_s(M_Z)} \\ &\qquad \pm 0.015_{\rm CKM} \pm 0.026_{{\rm BR}_{sl}}\Big] \times 10^{-6} = (1.64 \pm 0.11) \times 10^{-6}\,. \qquad (2.126)\end{aligned}$$

The central values are obtained for the matching scale $\mu_0 = 120$ GeV and the low-energy scale $\mu_b = 5$ GeV. The uncertainty from missing higher order perturbative corrections have been estimated by increasing and decreasing the scales $\mu_{0,b}$ by factors of 2. Uncertainties induced by m_t, m_b, m_c, C, $\alpha_s(M_Z)$, the CKM angles and the semileptonic rate are obtained by varying the various inputs within the errors given in Table 2.6. We assume the errors on C and m_c to be fully correlated. The total error is obtained by adding the individual uncertainties in quadrature. The electron and muon channels receive different contributions because of the $\ln(m_b^2/m_\ell^2)$ present in the bremsstrahlung corrections. The difference gets reduced when the BaBar and Belle angular cuts are included (see section 2.5).

We stress that the indicated uncertainties are only the parametric and perturbative ones. No additional uncertainty for the unknown subleading non-perturbative corrections has been included. In particular, we believe that the uncalculated $\alpha_s(\mu_b)\Lambda_{\rm QCD}/m_{c,b}$ non-perturbative corrections imply an additional uncertainty of around $\sim 5\%$ in the above formula. This issue deserves an independent study.

One should also keep in mind that all the effects of the intermediate ψ and ψ' contributions are assumed to be subtracted on the experimental side. This refers, in particular, to the decays $\psi \to X\ell^+\ell^-$ where low-mass dilepton pairs can be produced. All such decays of the ψ with branching ratios down to 10^{-5} may be relevant. To our knowledge, only $X = \gamma$ has been considered so far in the experimental analyses.

The overall uncertainties in Eqs. (2.125) and (2.126) are somewhat smaller than in Eq. (27) of Ref. [52]. This is mainly due to the improved experimental value of m_t as well as to our use of m_b^{1S} rather than $m_{b,\rm pole}$. The latter possibility was already pointed out in Ref. [52].

In Table 2.7, we show the partial results that we obtain by adding sequentially all the known QCD and QED corrections. The rows denoted by "NLO" and "NNLO" refer to the

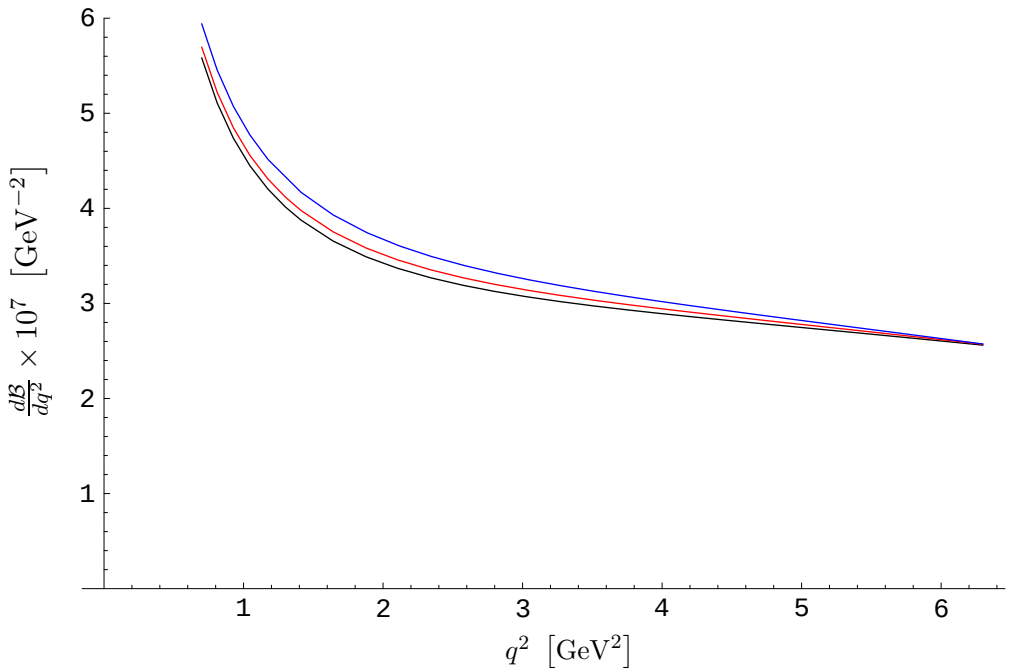

Figure 2.5: Differential branching ratio in the low-q^2 region region with and without $\ln(m_b^2/m_\ell^2)$-corrections. Black curve: "QED only WC's", red curve: "QED (muons)", blue curve: "QED (electrons)".

leading order in QED. The row "QED (only WC's)" contains only those QED corrections that stem from the Wilson coefficients. The row "QED" includes all the electromagnetic corrections (that are different for electrons and muons, as in Eqs. (2.125) and (2.126)). Figure 2.5 shows the differential BR for the cases "QED (only WC's)", "QED (muons)", and "QED (electrons)".

On the experimental side, the branching ratio has been recently measured by both Belle [33] and BaBar [31]. In the low dilepton invariant mass region, 1 GeV^2 $< q^2 <$ 6 GeV^2, the experimental results read

$$\mathcal{B}(B \to X_s \ell^+ \ell^-) = (1.493 \pm 0.504^{+0.411}_{-0.321}) \times 10^{-6} \quad \text{(Belle)} , \tag{2.127}$$

$$\mathcal{B}(B \to X_s \ell^+ \ell^-) = (1.8 \pm 0.7 \pm 0.5) \times 10^{-6} \quad \text{(BaBar)} . \tag{2.128}$$

This leads to a world average

$$\mathcal{B}(B \to X_s \ell^+ \ell^-) = (1.60 \pm 0.51) \times 10^{-6} . \tag{2.129}$$

We see clearly that the SM prediction agrees very well with the experimental results in this region. Had we reversed the sign of the $\bar{B} \to X_s\gamma$ amplitude – which amounts essentially to a change of sign in S_{79} in Eq. (2.113) – the numbers from Eqs. (2.125) and (2.126) would read

$$\mathcal{B}_{\mu\mu} = 3.11 \cdot 10^{-6} \tag{2.130}$$

$$\mathcal{B}_{ee} = 3.19 \cdot 10^{-6} . \tag{2.131}$$

This result will be interpreted in section 2.10.

A numerical formula that gives the branching ratio for non-SM values of the high-scale Wilson coefficients of the operators P_7, P_8, P_9 and P_{10} (see section 2.2) reads

$$\begin{aligned}
\mathcal{B}_{\mu\mu} \;=\; & \Big[\, 2.1913 - 0.001655\, \mathcal{I}(R_{10}) + 0.0005\, \mathcal{I}(R_{10}R_8^*) + 0.0535\, \mathcal{I}(R_7) \\
& + 0.00496\, \mathcal{I}(R_7 R_9^*) + 0.00513\, \mathcal{I}(R_8) + 0.0261\, \mathcal{I}(R_8 R_9^*) - 0.0118\, \mathcal{I}(R_9) \\
& - 0.5426\, \mathcal{R}(R_{10}) + 0.0281\, \mathcal{R}(R_7) + 0.0153\, \mathcal{R}(R_7 R_{10}^*) + 0.06859\, \mathcal{R}(R_7 R_8^*) \\
& - 0.8554\, \mathcal{R}(R_7 R_9^*) - 0.00866\, \mathcal{R}(R_8) + 0.00185\, \mathcal{R}(R_8 R_{10}^*) - 0.0981\, \mathcal{R}(R_8 R_9^*) \\
& + 2.7008\, \mathcal{R}(R_9) - 0.10705\, \mathcal{R}(R_9 R_{10}^*) + 10.7687\, |R_{10}|^2 + 0.2889\, |R_7|^2 \\
& + 0.00381\, |R_8|^2 + 1.4892\, |R_9|^2 + 0.02266\, \mathcal{I}(R_7 R_8^*) \,\Big] \times 10^{-7}\,, \qquad (2.132)
\end{aligned}$$

$$\begin{aligned}
\mathcal{B}_{ee} \;=\; & \Big[\, 2.3278 - 0.001655\, \mathcal{I}(R_{10}) + 0.0005\, \mathcal{I}(R_{10}R_8^*) + 0.0524\, \mathcal{I}(R_7) \\
& + 0.00496\, \mathcal{I}(R_7 R_9^*) + 0.00504\, \mathcal{I}(R_8) + 0.0261\, \mathcal{I}(R_8 R_9^*) - 0.00651\, \mathcal{I}(R_9) \\
& - 0.5426\, \mathcal{R}(R_{10}) - 0.02578\, \mathcal{R}(R_7) + 0.0153\, \mathcal{R}(R_7 R_{10}^*) + 0.0674\, \mathcal{R}(R_7 R_8^*) \\
& - 0.86996\, \mathcal{R}(R_7 R_9^*) - 0.0128\, \mathcal{R}(R_8) + 0.00185\, \mathcal{R}(R_8 R_{10}^*) - 0.09926\, \mathcal{R}(R_8 R_9^*) \\
& + 2.841\, \mathcal{R}(R_9) - 0.10705\, \mathcal{R}(R_9 R_{10}^*) + 11.0367\, |R_{10}|^2 + 0.2813\, |R_7|^2 \\
& + 0.003765\, |R_8|^2 + 1.528\, |R_9|^2 + 0.02266\, \mathcal{I}(R_7 R_8^*) \,\Big] \times 10^{-7}\,, \qquad (2.133)
\end{aligned}$$

where (see Eqs. (2.7), (2.57), (2.58) for the Wilson coefficient definitions)

$$R_{7,8} = \frac{C_{7,8}^{(00)\text{eff}}(\mu_0)}{C_{7,8}^{(00)\text{eff,SM}}(\mu_0)} \qquad \text{and} \qquad R_{9,10} = \frac{C_{9,10}^{(11)}(\mu_0)}{C_{9,10}^{(11)\text{SM}}(\mu_0)}\,. \qquad (2.134)$$

2.8 Logarithmically enhanced corrections to the branching ratio in the high-$\hat{s}$ region

We now turn our attention to the high-$\hat{s}$ region. The basic formulas are the same as in the low-$\hat{s}$ region. The only things that change are some functions that were obtained numerically by a fit in the low-$\hat{s}$ region. This is on the one hand the function $\omega_{99}^{(2)}(\hat{s})$ which can be extracted for the entire $\hat{s}$-region following Refs. [84–86]. More details can be found in appendix A. Furthermore, the functions $F_i^A(\hat{s})$ with $i = 1, 2$ and $A = 7, 9$ from Table 2.4 are only available numerically according to the authors of Ref. [45]. As stated earlier, the functions $F_8^A(\hat{s})$ with $A = 7, 9$ can be found for arbitrary $\hat{s}$ by carrying out the double integral in Eqs. (4.17) and (4.18) of Ref. [45]. As far as the functions $\omega_{ij}^{(\text{em})}(\hat{s})$ in Eq. (2.98) are concerned, exact analytical expressions are known for the functions $\omega_{99}^{(\text{em})}(\hat{s})$, $\omega_{1010}^{(\text{em})}(\hat{s})$, $\omega_{77}^{(\text{em})}(\hat{s})$, and $\omega_{79}^{(\text{em})}(\hat{s})$. Therefore, they hold in the entire q^2-region and can be taken directly from sections 2.4.2 and 2.4.1.4. The functions $\omega_{2j}^{(\text{em})}(\hat{s})$ with $j = 2, 7, 9$,

valid in the high-$\hat{s}$ region, read

$$\omega_{29}^{(\rm em)}(\hat{s}) = \ln\left(\frac{m_b^2}{m_\ell^2}\right)\left[\frac{\Sigma_4(\hat{s})+i\,\Sigma_4^I(\hat{s})}{8(1-\hat{s})^2(1+2\hat{s})}\right]+\frac{16}{9}\,\omega_{1010}^{(\rm em)}(\hat{s})\,\ln\Big(\frac{\mu_b}{5\rm GeV}\Big)\;, \tag{2.135}$$

$$\omega_{22}^{(\rm em)}(\hat{s}) = \ln\left(\frac{m_b^2}{m_\ell^2}\right)\left[\frac{\Sigma_5(\hat{s})}{8(1-\hat{s})^2(1+2\hat{s})}+\frac{\Sigma_4(\hat{s})}{9(1-\hat{s})^2(1+2\hat{s})}\ln\Big(\frac{\mu_b}{5\rm GeV}\Big)\right] + \frac{64}{81}\,\omega_{1010}^{(\rm em)}(\hat{s})\,\ln^2\Big(\frac{\mu_b}{5\rm GeV}\Big)\;, \tag{2.136}$$

$$\omega_{27}^{(\rm em)}(\hat{s}) = \ln\left(\frac{m_b^2}{m_\ell^2}\right)\left[\frac{\Sigma_6(\hat{s})+i\,\Sigma_6^I(\hat{s})}{96(1-\hat{s})^2}\right]+\frac{8}{9}\,\omega_{79}^{(\rm em)}(\hat{s})\,\ln\Big(\frac{\mu_b}{5\rm GeV}\Big)\;. \tag{2.137}$$

They were obtained by a least-squares fit in the high-$\hat{s}$ region (for fixed values of m_b and m_c, see section 2.7). The functions Σ_i, valid in the high-$\hat{s}$ region, read ($\delta = 1-\hat{s}$):

$$\Sigma_4(\hat{s}) = -148.061\,\delta^2+492.539\,\delta^3-1163.847\,\delta^4+1189.528\,\delta^5\;, \tag{2.138}$$

$$\Sigma_4^I(\hat{s}) = -261.287\,\delta^2+1170.856\,\delta^3-2546.948\,\delta^4+2540.023\,\delta^5\;, \tag{2.139}$$

$$\Sigma_5(\hat{s}) = -221.904\,\delta^2+900.822\,\delta^3-2031.620\,\delta^4+1984.303\,\delta^5\;, \tag{2.140}$$

$$\Sigma_6(\hat{s}) = -298.730\,\delta^2+828.0675\,\delta^3-2217.6355\,\delta^4+2241.792\,\delta^5\;, \tag{2.141}$$

$$\Sigma_6^I(\hat{s}) = -528.759\,\delta^2+2095.723\,\delta^3-4681.843\,\delta^4+5036.677\,\delta^5\;. \tag{2.142}$$

The fits are excellent for $\hat{s} > 0.65$. Power corrections $\Lambda_{\rm QCD}^2/m_b^2$ [43,44,74] and $\Lambda_{\rm QCD}^3/m_b^3$ [87, 88] are important in this region. As discussed in section 2.1.1 there is an expansion in inverse powers of $m_b^{\rm eff} = m_b - (q_i^2)^{1/2}$ for the integrated dilepton mass spectrum, where q_i^2 denotes the lower cut in the high-q^2 region [45]. The non-factorizable part of the $\Lambda_{\rm QCD}^2/m_c^2$ are again given in Ref. [75]. Additional effects such as $\bar{\Lambda}/m_b$ corrections arising from the relation between the mass m_b of the b-quark and the mass M_B of the B-meson, and the factorizable part of non-perturbative interactions of intermediate $c\bar{c}$ resonances [46] in the process $\bar{B}\to X_s c\bar{c}\to X_s\ell^+\ell^-$, are discussed in detail in Ref. [45].

2.9 Logarithmically enhanced corrections to the forward backward asymmetry

2.9.1 Derivation of the $\ln(m_b^2/m_\ell^2)$-enhanced QED corrections

In this section we derive the basic formulas that are needed in order to obtain the expressions for the $\ln(m_b^2/m_\ell^2)$-enhanced corrections to the forward backward asymmetry. We shall focus on the unnormalized FBA given by the numerator in Eq. (2.2). It was shown in appendix D of Ref. [43] that the angular forward backward asymmetry with respect to θ_ℓ, the angle in the dilepton c.m.s. between the directions of the momenta of the decaying $\bar{B}$ and the positively charged lepton is equivalent to the energy asymmetry between the two leptons in the restframe of the decaying $\bar{B}$. Events in which $\cos\theta_\ell > 0$ in the dilepton c.m.s. correspond to events in which $E_{\ell^-} > E_{\ell^+}$ measured in the $\bar{B}$-meson restframe, where $E_\pm$ denotes the $\ell^\pm$-energy. Sticking to this frame and defining the scaled energies

$$y_\pm \equiv \frac{2\,E_\pm}{m_b}\;, \tag{2.143}$$

we can write the fully differential FBA as

$$d\mathcal{A}_{FB} \propto \; d\hat{s}\; dy_+\; dy_-\; \delta(1+\hat{s}-y_+-y_-)\; |\mathcal{A}|^2\; \mathrm{sgn}(y_- - y_+). \tag{2.144}$$

We are mainly interested in $\ln(m_b^2/m_\ell^2)$-enhanced electromagnetic corrections. They are again derived by means of the splitting function and we shall adopt the kinematics from Figure 2.4. In the collinear limit the fully differential FBA reads

$$d\mathcal{A}^{(m)}_{FB,\mathrm{coll}} = PF\; dx\; d\hat{s}\; dy_+\; dy_-\; \delta(1+\hat{s}-y_+-y_-)\, f_\gamma^{(m)}(x)\; |\mathcal{A}|^2\; \mathrm{sgn}(y_- - y_+)\;, \tag{2.145}$$

with the pre-factor

$$PF = \frac{G_F^2 m_b |V_{tb}V_{ts}^*|^2}{32\pi^3}\;. \tag{2.146}$$

As in section 2.4.2 we shall only retain the $\ln(m_b^2/m_\ell^2)$-enhanced part of $f_\gamma^{(m)}$, which then becomes independent of E,

$$f_\gamma^{(m)}(x) = 4\,\tilde{\alpha}_e\,\frac{[1+(1-x)^2]}{x}\,\ln\!\left(\frac{m_b}{m_\ell}\right)\;. \tag{2.147}$$

The squared amplitude in Eq. (2.145) is obtained by squaring Eq. (2.95) and collecting all terms relevant for the FBA,

$$\begin{aligned} |\mathcal{A}|^2 \;&=\; 2\,\mathrm{Re}\Big[C_{10}C_9^* + \widetilde{\alpha}_s\kappa\, C_{10}(C_2 + C_F\, C_1) f_2^*(\hat{s})\Big]\; \langle P_{10}\rangle_{\mathrm{tree}}\langle P_9\rangle^*_{\mathrm{tree}} \\ &\quad +2\,\mathrm{Re}[C_{10}C_7^*]\; \langle P_{10}\rangle_{\mathrm{tree}}\langle P_7\rangle^*_{\mathrm{tree}}\;. \end{aligned} \tag{2.148}$$

As before in the case of the branching ratio (section 2.4.1.4) we must consider the difference

$$\frac{d\mathcal{A}^{(m)}_{FB,\mathrm{coll},2}}{d\hat{s}} - \frac{d\mathcal{A}^{(m)}_{FB,\mathrm{coll},3}}{d\hat{s}}\;, \tag{2.149}$$

where we stay differential in the double and in the triple invariant, respectively. At this point more care is required compared to the former calculation. Due to the emergence of the sgn-function in Eq. (2.145) we must distinguish between photon-emission from the ℓ^+ and from the ℓ^- in case of the double invariant. In the former case we have to stay differential in $\hat{s} = (\bar{x}p_1 + p_2)^2$, in the latter in $\hat{s} = (p_1 + \bar{x}p_2)^2$. Also the $y_\pm$ change accordingly. We therefore have

$$\begin{aligned} \frac{d\mathcal{A}^{(m)}_{FB,\mathrm{coll},2,\ell^\pm}}{d\hat{s}} \;&=\; \pm PF\left[\int_0^{1-\sqrt{\hat{s}}} dx \int_{\hat{s}/\bar{x}}^{\frac{\bar{x}+\hat{s}}{\bar{x}(1+\bar{x})}} dy_\pm + \int_{1-\sqrt{\hat{s}}}^{1-\hat{s}} dx \int_{\hat{s}/\bar{x}}^{1} dy_\pm - \int_0^{1-\sqrt{\hat{s}}} dx \int_{\frac{\bar{x}+\hat{s}}{\bar{x}(1+\bar{x})}}^{1} dy_\pm\right] \\ &\quad \times \frac{f_\gamma^{(m)}(x)}{\bar{x}}\; |\mathcal{A}|^2\,\Big|_{\hat{s}\to\hat{s}/\bar{x}\;;\; y_\mp\to 1-y_\pm+\hat{s}/\bar{x}}\;. \end{aligned} \tag{2.150}$$

The two expressions corresponding to upper and lower sign should be equal due to the antisymmetry of $|\mathcal{A}|^2$ in $y_+ \leftrightarrow y_-$. The case of the triple invariant is simpler since we stay differential in $\hat{s} = (p_1+p_2)^2$, namely

$$\frac{d\mathcal{A}^{(m)}_{FB,\mathrm{coll},3,\ell^\pm}}{d\hat{s}} = \pm PF \int_0^1 dx \left[\int_{\hat{s}}^{\frac{1+\hat{s}}{2}} dy_\pm - \int_{\frac{1+\hat{s}}{2}}^{1} dy_\pm\right] f_\gamma^{(m)}(x)\; |\mathcal{A}|^2\,\Big|_{\;y_\mp\to 1-y_\pm+\hat{s}}\;, \tag{2.151}$$

where the expression for the upper and lower sign should again be equal due to the antisymmetry of $|\mathcal{A}|^2$. We finally have to add up the expressions according to Eq. (2.149).

The corrections to the unnormalized FBA read

$$\begin{aligned}\frac{\mathrm{d}\Delta\mathcal{A}}{d\hat{s}} &= \frac{G_F^2 m_b^5}{48\pi^3}|V_{tb}V_{ts}^*|^2(1-\hat{s})^2\widetilde{\alpha}_\mathrm{s}\kappa\Bigg\{-48\left[\widetilde{\alpha}_\mathrm{s}\kappa\,\mathrm{Re}\left[C_7 C_{10}^*\right]\;\omega_{710}^{(\mathrm{em})}(\hat{s})\right]\\ &\quad -24\,\hat{s}\left[\mathrm{Re}\left[C_9 C_{10}^*\right]\;\omega_{910}^{(\mathrm{em})}(\hat{s})+\widetilde{\alpha}_\mathrm{s}\kappa\;\mathrm{Re}\left[(C_2+C_F C_1)C_{10}^*\;\omega_{210}^{(\mathrm{em})}(\hat{s})\right]\right]\Bigg\}\,, \qquad (2.152)\end{aligned}$$

with

$$\omega_{710}^{(\mathrm{em})}(\hat{s}) = \ln\left(\frac{m_b^2}{m_\ell^2}\right)\left[\frac{7-16\sqrt{\hat{s}}+9\,\hat{s}}{4\,(1-\hat{s})}+\ln(1-\sqrt{\hat{s}})+\frac{1+3\,\hat{s}}{1-\hat{s}}\,\ln\left(\frac{1+\sqrt{\hat{s}}}{2}\right)-\frac{\hat{s}\,\ln\hat{s}}{(1-\hat{s})}\right], \qquad (2.153)$$

$$\begin{aligned}\omega_{910}^{(\mathrm{em})}(\hat{s}) &= \ln\left(\frac{m_b^2}{m_\ell^2}\right)\left[-\frac{5-16\sqrt{\hat{s}}+11\,\hat{s}}{4\,(1-\hat{s})}+\ln(1-\sqrt{\hat{s}})\right.\\ &\quad \left.+\frac{1-5\,\hat{s}}{1-\hat{s}}\,\ln\left(\frac{1+\sqrt{\hat{s}}}{2}\right)-\frac{(1-3\,\hat{s})\,\ln\hat{s}}{(1-\hat{s})}\right], \qquad (2.154)\end{aligned}$$

$$\omega_{210}^{(\mathrm{em})}(\hat{s}) = \ln\left(\frac{m_b^2}{m_\ell^2}\right)\left[-\frac{\Sigma_7(\hat{s})+i\,\Sigma_7^I(\hat{s})}{24\,\hat{s}\,(1-\hat{s})^2}\right]+\frac{8}{9}\,\omega_{910}^{(\mathrm{em})}(\hat{s})\,\ln\Big(\frac{\mu_b}{5\mathrm{GeV}}\Big)\,. \qquad (2.155)$$

Again the functions $\omega_{710}^{(\mathrm{em})}(\hat{s})$ and $\omega_{910}^{(\mathrm{em})}(\hat{s})$ are known in the entire q^2-region, whereas the function $\omega_{210}^{(\mathrm{em})}(\hat{s})$ was obtained by a least squares fit. The function Σ_7, valid in the low-$\hat{s}$-region, reads

$$\begin{aligned}\Sigma_7(\hat{s}) &= -0.259023-28.424\,\hat{s}+205.533\,\hat{s}^2-603.219\,\hat{s}^3+722.031\,\hat{s}^4\,, \qquad (2.156)\\ \Sigma_7^I(\hat{s}) &= \left[-12.20658-215.8208\,(\hat{s}-a)+412.1207\,(\hat{s}-a)^2\right](\hat{s}-a)^2\,\theta(\hat{s}-a)\,, \qquad (2.157)\end{aligned}$$

with $a=(4m_c^2/m_b^2)^2\simeq 0.17066$. In the high-$\hat{s}$-region the function Σ_7 reads ($\delta=1-\hat{s}$)

$$\begin{aligned}\Sigma_7(\hat{s}) &= 77.0256\,\delta^2-264.705\,\delta^3+595.814\,\delta^4-610.1637\,\delta^5\,, \qquad (2.158)\\ \Sigma_7^I(\hat{s}) &= 135.858\,\delta^2-618.990\,\delta^3+1325.040\,\delta^4-1277.170\,\delta^5\,. \qquad (2.159)\end{aligned}$$

The fits are excellent for $\hat{s}>0.65$.

2.9.2 Master formula for the FBA and numerical results

In complete analogy to the master formula for the branching ratio in section 2.6 one can derive also a formula that expresses the forward backward asymmetry in terms of the low-scale Wilson coefficients and various building blocks. Stripping off an overall factor of $G_F^2\,m_b^5\,|V_{tb}V_{ts}^*|^2/(48\pi^3)$, we have for the unnormalized FBA

$$\frac{d\mathcal{A}}{d\hat{s}} = \sum_{i\le j}\mathrm{Re}\left[C_i^{\mathrm{eff}}(\mu_b)\;C_j^{\mathrm{eff}*}(\mu_b)\;H_{ij}(\mu_b,\hat{s})\right]\,. \qquad (2.160)$$

Again, the functions $H_{ij}(\mu_b, \hat{s})$ depend on the coefficients M_i^A listed in Table 2.4 and on the following building blocks

$$\begin{aligned} \mathrm{S}_{710} &= -6\,(1-\hat{s})^2 \left\{ 1 + 8\,\widetilde{\alpha}_\mathrm{s}\, f_{710}(\hat{s}) + 8\,\widetilde{\alpha}_\mathrm{s}\kappa\, \omega_{710}^{(\mathrm{em})}(\hat{s}) + \frac{\lambda_1}{m_b^2}\,\frac{3+2\hat{s}+3\hat{s}^2}{6\,(1-\hat{s})^2} \right\} \\ &\quad + 3\,\frac{\lambda_2}{m_b^2}\,(7+10\hat{s}-9\hat{s}^2)\,, \qquad (2.161) \\ \mathrm{S}_{910} &= -3\,\hat{s}\,(1-\hat{s})^2 \left\{ 1 + 8\,\widetilde{\alpha}_\mathrm{s}\, f_{910}(\hat{s}) + 8\,\widetilde{\alpha}_\mathrm{s}\kappa\, \omega_{910}^{(\mathrm{em})}(\hat{s}) + \frac{\lambda_1}{m_b^2}\,\frac{3+2\hat{s}+3\hat{s}^2}{6\,(1-\hat{s})^2} \right\} \\ &\quad + \frac{3\,\lambda_2}{2\,m_b^2}\,\hat{s}\,(9+14\hat{s}-15\hat{s}^2)\,. \qquad (2.162) \end{aligned}$$

The functions $f_{i10}(\hat{s})$ $(i = 7, 9)$ can be found in Eqs. (15) – (17) of Ref. [89]. The functions $\omega_{ij}^{(\mathrm{em})}$ have been given in Eqs. (2.153) and (2.154). The S_{AB} again include non-perturbative $\mathcal{O}(1/m_b^2)$ corrections from Refs. [43, 44, 74]. Contrary to the expression for the BR the quantity λ_1, which is related to the kinetic energy of the b-quark, does not drop out here. This is a small disadvantage since λ_1, contrary to λ_2, is not well known [44]. We shall take $\lambda_1 = -0.27 \pm 0.04$ GeV^2 in our analysis [77]. The explicit expressions for the functions H_{ij} read

$$H_{ij} = \begin{cases} \sum\limits_{A=7,9} \mathrm{Re}(M_i^A M_i^{10*})\, S_{A10} + \Delta H_{ii}\,, & \text{when } i = j \\ \sum\limits_{A=7,9} \left(M_i^A M_j^{10*} + M_i^{10} M_j^{A*} \right) S_{A10} + \Delta H_{ij}\,, & \text{when } i \neq j\,. \end{cases} \qquad (2.163)$$

We again assume that all products in Eq. (2.160) are expanded in $\widetilde{\alpha}_\mathrm{s}$, κ, λ_1 and λ_2, and that higher orders are neglected according to section 2.7.

The quantities

$$\Delta H_{ij} = b_{ij} + c_{ij} + e_{ij} \qquad (2.164)$$

have the same meaning as before. They need to be included only for $i = 1, 2$. The additional $\ln(m_b^2/m_\ell^2)$-enhanced electromagnetic corrections e_{ij} for the FBA read

$$\begin{aligned} e_{210} &= -24\,\hat{s}\,(1-\hat{s})^2\,\widetilde{\alpha}_\mathrm{s}^2\kappa^2\,\omega_{210}^{(\mathrm{em})}(\hat{s}) \\ e_{110} &= \tfrac{4}{3} e_{210}. \qquad (2.165) \end{aligned}$$

The $\mathcal{O}(\Lambda_{\mathrm{QCD}}^2/m_c^2)$ non-perturbative contributions were calculated in Ref. [75]

$$\begin{aligned} c_{210} &= +\widetilde{\alpha}_\mathrm{s}\kappa \frac{\lambda_2}{3m_c^2}(1-\hat{s})^2(1+3\hat{s})\,F(r)\,, \\ c_{110} &= -\tfrac{1}{6}\,c_{210}\,, \qquad (2.166) \end{aligned}$$

where $r \equiv 1/y_c = s/(4m_c^2)$ and the function $F(r)$ is listed in appendix A. The finite bremsstrahlung contributions b_{ij} were calculated in Ref. [90]. Like before, we do not present these corrections here but do include them in the numerical analysis.

In our numerical analysis of the forward backward aymmetry we focus on the extraction of the zero in the low-q^2 region. Contrary to other analyses [52] we will determine the zero from the *unnormalized* FBA [45, 89] and not from the *normalized* one, i.e. we will not

expand the denominator of Eq. (2.2) in the couplings. This has several reasons. First, the unnormalized FBA calculated from the numerator in Eq. (2.2) and the branching ratio determined from the denominator of Eq. (2.2) are independent observables and sensitive to different combinations of Wilson coefficients, as can be seen from Eqs. (2.115) and (2.163). The unnormalized FBA is governed by the axial vector operator P_{10} which is responsible for the asymmetry. The FBA is therefore directly proportional to the Wilson coefficient C_{10}. This feature would get spoilt upon expansion of the denominator. Another reason comes from experiment. We have learnt that the angular asymmetry in the lepton c.m.s. is equivalent to the lepton energy asymmetry in the restframe of the decaying B. Therefore the determination of the FBA amounts to a counting experiment, namely the number of events with $E_{\ell^-} > E_{\ell^+}$ minus the number of events with $E_{\ell^-} < E_{\ell^+}$. Although this is normalized also on the experimental side to the total number of events, the extraction of the zero comes solely from the numerator.

The basic formula for the extraction of the zero is therefore Eq. (2.160). We expand everything in $\widetilde{\alpha}_s$, κ, λ_1 and λ_2, and keep the same terms that were already specified in section 2.7. It is understood that also the conversion of the mass scheme for the botton, the charm and the top quark is performed in the same way as in section 2.7. The results for q_0^2, the zero of the FBA in the low-q^2 region, is

$$q_{0,\mu\mu}^2 = \Big[3.82 \pm 0.09_{\rm scale} \pm 0.004_{m_t} \pm 0.04_{m_c} \pm 0.05_{m_b} \pm 0.11_{\alpha_s(M_Z)}\Big]\,{\rm GeV}^2\,, \quad (2.167)$$

$$q_{0,ee}^2 = \Big[3.67 \pm 0.08_{\rm scale} \pm 0.005_{m_t} \pm 0.04_{m_c} \pm 0.05_{m_b} \pm 0.10_{\alpha_s(M_Z)}\Big]\,{\rm GeV}^2\,. \quad (2.168)$$

The central values as well as the variation of the input parameters and the scales μ_b and μ_0 are the same as in section 2.7. The error due to the uncertainty in λ_1 is negligible. The above error bars on the zero are unnaturally small since accidentally many of the dependences cancel at this point. It is widely accepted that the above scale uncertainty of only $\sim 2.3\%$ can not be regarded as an estimate for unknown higher order terms [91]. As an example, Figure 2.6 shows that in the vicinity of the zero the dependence on the scale μ_b is hardly present, whereas this dependence gets more and more pronounced towards the edges of the low-q^2 region. Below we propose a procedure that gives a more conservative estimate of the total error on the zero.

We consider a fixed value P of the unnormalized FBA, Eq. (2.160). We determine for each parameter-set the value Q^2 for which the unnormalized FBA assumes the value P. The procedure of finding the zero simply corresponds to the special case $P = 0$. It turns out that the further Q^2 departs from the zero the larger get the relative error bars (see also Fig. 2.6). We have for instance (the values of P are not given explicitly)

$$Q_{1,\mu\mu}^2 = \Big[1.50 \pm 0.115_{\rm scale} \pm 0.053_{m_t} \pm 0.034_{m_c} \pm 0.022_{m_b} \pm 0.035_{\alpha_s(M_Z)}\Big]\,{\rm GeV}^2\,, \quad (2.169)$$

$$Q_{1,ee}^2 = \Big[1.50 \pm 0.10_{\rm scale} \pm 0.048_{m_t} \pm 0.032_{m_c} \pm 0.022_{m_b} \pm 0.034_{\alpha_s(M_Z)}\Big]\,{\rm GeV}^2\,, \quad (2.170)$$

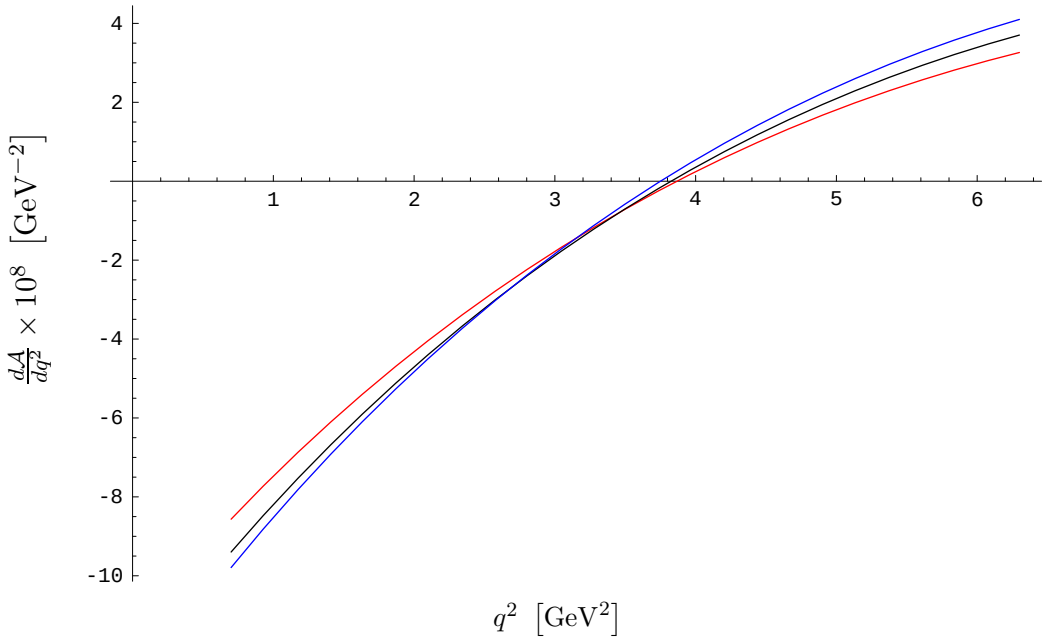

Figure 2.6: Unnormalized FBA as in Eq. (2.160) for the muonic final state with $\mu_b = 2.5$ GeV (red), $\mu_b = 5$ GeV (black) and $\mu_b = 10$ GeV (blue).

$$Q^2_{2,\mu\mu} = \Big[2.50 \pm 0.077_{\text{scale}} \pm 0.03_{m_t} \pm 0.04_{m_c} \pm 0.035_{m_b} \pm 0.06_{\alpha_s(M_Z)}\Big]\,\text{GeV}^2\,, \tag{2.171}$$

$$Q^2_{2,ee} = \Big[2.50 \pm 0.07_{\text{scale}} \pm 0.03_{m_t} \pm 0.04_{m_c} \pm 0.034_{m_b} \pm 0.06_{\alpha_s(M_Z)}\Big]\,\text{GeV}^2\,, \tag{2.172}$$

$$Q^2_{3,\mu\mu} = \Big[5.00 \pm 0.20_{\text{scale}} \pm 0.05_{m_t} \pm 0.055_{m_c} \pm 0.065_{m_b} \pm 0.165_{\alpha_s(M_Z)}\Big]\,\text{GeV}^2\,, \tag{2.173}$$

$$Q^2_{3,ee} = \Big[5.00 \pm 0.21_{\text{scale}} \pm 0.06_{m_t} \pm 0.06_{m_c} \pm 0.065_{m_b} \pm 0.17_{\alpha_s(M_Z)}\Big]\,\text{GeV}^2\,, \tag{2.174}$$

$$Q^2_{4,\mu\mu} = \Big[6.00 \pm 0.38_{\text{scale}} \pm 0.10_{m_t} \pm 0.07_{m_c} \pm 0.075_{m_b} \pm 0.24_{\alpha_s(M_Z)}\Big]\,\text{GeV}^2\,, \tag{2.175}$$

$$Q^2_{4,ee} = \Big[6.00 \pm 0.41_{\text{scale}} \pm 0.12_{m_t} \pm 0.076_{m_c} \pm 0.075_{m_b} \pm 0.26_{\alpha_s(M_Z)}\Big]\,\text{GeV}^2\,. \tag{2.176}$$

The total errors are obtained by adding the individual uncertainties in quadrature. In the cases $Q^2 = 1.50$ GeV^2 and $Q^2 = 6.00$ GeV^2 they are roughly of the same relative size and amount to approximately 8.5%. We shall adopt this error also for the zero and take

$$q^2_{0,\mu\mu} = \Big[3.82 \pm 0.32\Big]\,\text{GeV}^2\,, \tag{2.177}$$

$$q^2_{0,ee} = \Big[3.67 \pm 0.31\Big]\,\text{GeV}^2 \tag{2.178}$$

NLO ($\alpha_{em}(\mu_0)$)	3.39	NLO ($\alpha_{em}(\mu_b)$)	3.39
NNLO ($\alpha_{em}(\mu_0)$)	3.76	NNLO ($\alpha_{em}(\mu_b)$)	3.76
QED (only WC's)	3.93		
QED (muons)	3.82	QED (electrons)	3.67

Table 2.8: Anatomy of QCD and QED corrections for the zero q_0^2 [GeV^2] of the unnormalized FBA.

as the total error bars on the zero.

Table 2.8 shows in complete analogy to Table 2.7 the changes that the zero undergoes when we sequentially add all the known QCD and QED corrections. The rows have the same meaning as in Table 2.7. In the muonic case the position of the zero changes by about -2.8% compared to the "only WC's" case, in the electron case by about -6.6%. However, in the electron case the experimental setups at BaBar and Belle need to be taken into account, see section 2.5. Figure 2.7 shows the unnormalized FBA for the cases "QED (only WC's)", "QED (muons)", and "QED (electrons)".

2.10 Conclusions and Outlook

The search for new physics beyond the Standard Model clearly requires precise determinations of as many observables as possible in order to constrain its parameters with the goal of finding deviations from Standard Model predictions. Such deviations in low-energy decays such as B, D or K-decays would be an indirect signal of physics beyond the SM since the effects of yet unknown particles would become manifest via virtual effects even before energy ranges to produce such particles directly become accessible. Even if no evidence for new physics is found in low-energy observables their precise determination allows to significantly constrain the parameter space of new physics models and allows to explore the flavor structure of new physics models.

In this respect, the loop-induced decays $\bar{B} \to X_s\gamma$ and $\bar{B} \to X_s\ell^+\ell^-$ provide an excellent testing ground since a precise determination of observables associated with these decays is achievable on both the theoretical and experimental side. As far as theory is concerned we have seen that higher order perturbative corrections – together with improved understanding of non-perturbative effects – are indispensable for reaching a precision that can compete with the ever decreasing error bars on the experimental side. In the case of $\bar{B} \to X_s\ell^+\ell^-$ we have motivated the need to include NLO QED corrections to the differential branching ratio and to the forward backward asymmetry. The inclusion of these corrections removes on the one hand the scale ambiguity arising from an overall $\alpha_{em}^2(\mu)$ in these observables by taking into account QED corrections that are enhanced by large logarithms $\ln(M_H^2/M_L^2)$. Further logarithmically enhanced corrections proportional to $\ln(m_b^2/m_\ell^2)$ arise from those parts of QED bremsstrahlung corrections where the emitted photon is collinear to one of the outgoing leptons. The impact on the low-q^2 integrated BR is roughly $+2\%$ in the case of the muonic final state. The impact in case of the electron

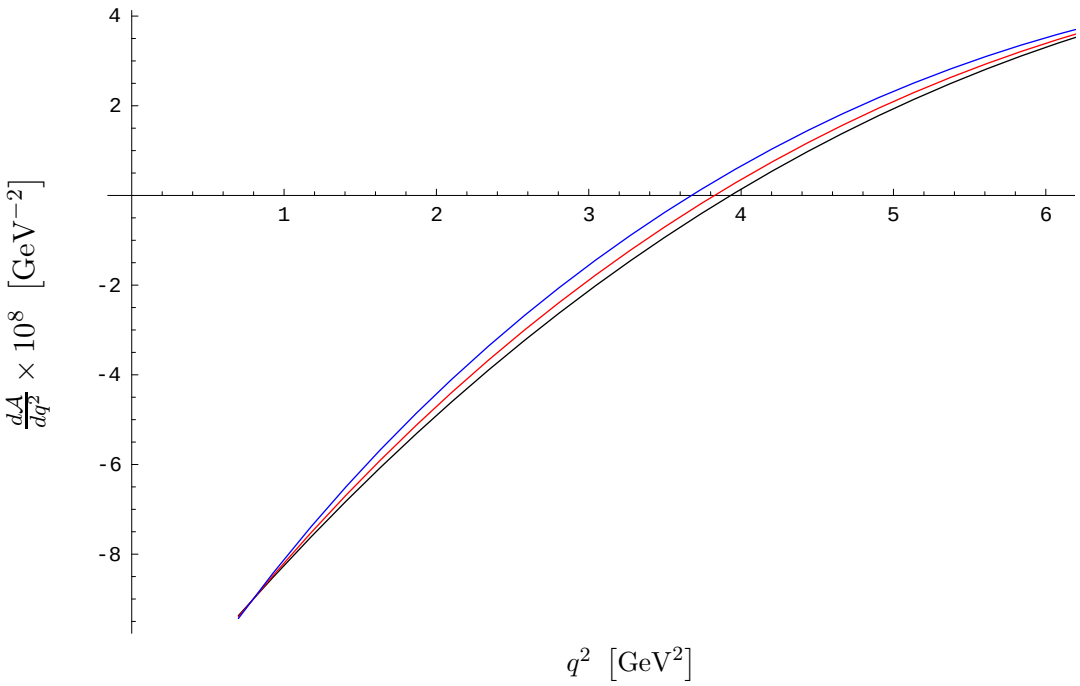

Figure 2.7: Unnormalized FBA as in Eq. (2.160) in the low-q^2 region with and without $\ln(m_b^2/m_\ell^2)$-corrections. Black curve: "QED only WC's", red curve: "QED (muons)", blue curve: "QED (electrons)".

final state depends on the experimental setup, as described in section 2.5. The corrections proportional to $\ln(m_b^2/m_\ell^2)$ in case of the high-q^2 integrated BR are negative since the total effect of this type corrections has to disappear upon integration over the entire phase space available – remember that, contrary to the integrated BR and AFB the differential ones are not infrared safe with respect to emission of collinear photons off leptons. The zero in the low-q^2 region of the unnormalized FBA undergoes a shift of about -2.8% for the muonic final state.

We have seen in sections 2.6, 2.8 and 2.9 that the differential BR is sensitive to the interference term S_{79} of amplitudes proportional to the tree-level matrix elements of P_7 and P_9. The FBA, as can be seen from Eq. (2.163), is on the other hand sensitive to the interference terms S_{710} and S_{910}. The dependence on the corresponding amplitudes – denoted C_7, C_9 and C_{10} here – is pictorially displayed in Figure 2.8.

In the left plot of Figure 2.8 the SM differential BR is shown by the blue curve whereas the case of reversed sign of C_7 – with all other amplitudes held fixed – is drawn by the thin black curve [92]. The enhancement of the BR in the low-s region can be clearly seen whereas the correction to the high-s BR is less pronounced. In the right plot the normalized FBA is shown for the SM case as well as for reversed sign of C_7 (curve 2) [93]. One recognizes immediately that the zero in the low-s region that is present in the SM case has disappeared upon reversing the sign of C_7. Curves 1 and 3 are the versions with the sign of C_{10} being flipped with respect to the curves SM and 2, respectively. This amounts to a flip with respect to the s-axis since the numerator of the FBA is directly proportional to C_{10} whereas the denominator contains C_{10} only via $|C_{10}|^2$.

From this we draw the conclusion that a measurement of the BR and the FBA can

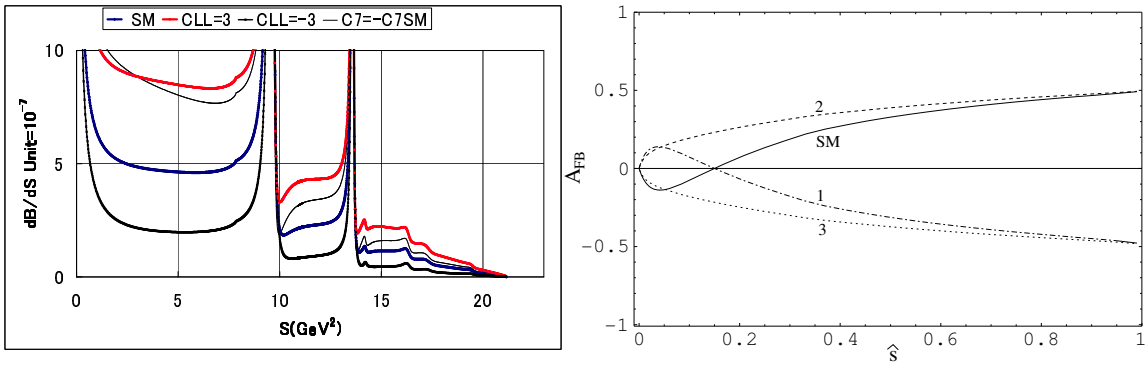

Figure 2.8: Differential branching ratio (left, c.f. [92]) and normalized forward backward asymmetry (right, c.f. [93]) with possible new physics effects. See main text for explanations.

yield useful information on the signs of the amplitudes. This is important information when one is dealing with new physics models since there can be scenarios in which the sign of C_7 gets reversed whereas C_9 and C_{10} receive only small corrections. This has been investigated in the literature [93–96] with the conclusion that extensions of the SM with reversed sign of C_7 but only small corrections to C_9 and C_{10} – like the MSSM with minimal flavor violation at large $\tan\beta$ – are disfavored [95,96]. This conclusion gets also supported by our numerical findings in section 2.7 when we compare Eqs. (2.125), (2.126), (2.130), and (2.131) to Eqs. (2.127) and (2.128). Other calculation associated with $\bar{B} \to X_s \ell^+ \ell^-$ or $\bar{B} \to K^{(*)} \ell^+ \ell^-$ in models beyond the SM have been done in Refs. [96–107].

The forward backward asymmetry has also been measured recently at Babar [32] and Belle [34,35] in the exclusive channel $\bar{B} \to K^* \ell^+ \ell^-$. The measurements are still compatible with either sign of C_7. However, the product of C_9 and C_{10} – which is negative in the SM – is excluded to be positive at 98.2% confidence level [35] under the assumption that corrections to the C_i are of minimal flavor violation type. The statistics in both experiments is still too low to allow for a precise determination of the zero of the FBA. This will become feasible at future experiments like LHCb [108] or at a Super-B factory [92,109, 110]. At LHCb the intension is to measure C_7/C_9 from the exclusive channel $\bar{B} \to K^* \ell^+ \ell^-$ with 13% accuracy with 1 fb^{-1} of data [108]. At a future Super-B factory it will be possible to determine the zero of the inclusive FBA to 7% accuracy with 50 ab^{-1} of data [109].

2.11 Acknowledgements

I would like to thank my collaborators from Ref. [39], notably Enrico Lunghi, Mikołaj Misiak and Daniel Wyler for involving me in this very interesting project. The problem of electromagnetic logarithms $\ln(M_H^2/M_L^2)$ was put forth by Piotr Chankowski. The authors of Ref. [52] provided for useful remarks and a careful reading of the manuscript of Ref. [39]. I would like to thank in particular Enrico Lunghi, Tobias Hurth, and Ulrich Haisch for great support and many useful discussions. Special thanks goes to Thomas Gehrmann and Aude Gehrmann-De Ridder for many discussions and help on the phase space integration, and to Jeffrey Berryhill and Akimasa Ishikawa for information concerning the treatment of collinear photons at BaBar and Belle.

Chapter 3

HypExp, a Mathematica package for expanding hypergeometric functions around integer-valued parameters[1]

3.1 Introduction

As we have seen in the previous chapter, the phase space integration over the four particle final state in $D = 4 - 2\,\epsilon$ dimensions requires the task of expanding hypergeometric functions around integer-valued parameters. This task does not only appear in this context but in many calculations of particle physics, especially during the calculation of radiative corrections to scattering cross sections and decay widths in loop [111–116] or phase space [39, 67, 117] integrals. In the context of dimensional regularisation the arguments of the hypergeometric functions (HF's) have to be expanded in a small parameter (here: ϵ) around integer or rational arguments.

Until recently, the required expansions have been produced case-by-case since a systematic approach was not available. Recently, a general algorithm has been developed [118] for expanding hypergeometric functions and other transcendental functions systematically around their parameters. This algorithm was implemented [119] in the framework of GiNaC [120]. Very recently, a FORM [121] package for expanding transcendental functions has become available [122]. Related work was also presented in Refs. [123, 124].

Until now, an implementation of the expansion of hypergeometric functions with respect to the parameters was missing in the widely used computer algebra systems `Mathematica` [68] and `Maple` [125], allowing to use hypergeometric functions in connection with the multi-purpose features of these programs. To fill this gap, we produced the `Mathematica` package `HypExp` which allows, among other features, to expand hypergeometric functions around integer-valued parameters.

This chapter is organized as follows. We will first describe the `Mathematica` package

[1] The content of this chapter has been published in Ref. [69]

HypExp by listing the commands and providing some examples of its useage. We will also point out some subtleties and give a list of performances and limitations. Afterwards, we will focus on one of the two approaches that were used in order to obtain the expansion of hypergeometric functions around integer-valued parameters, namely the method of integration. We will in particular present the technical details of the algorithm upon which this method is based. Thereafter, we will cover in a short section hypergeometric functions of unit argument, before we state our conclusions.

3.2 The Mathematica package HypExp

Before we start to explain the features of our Mathematica package, we have to set up our notation. The package allows to expand hypergeometric functions of type

$$ {}_JF_{J-1}\left(\{A_1,\ldots,A_J\};\{B_1,\ldots,B_{J-1}\};z\right) \tag{3.1} $$

with

$$ A_i = a_i + \alpha_i\epsilon, \qquad B_i = b_i + \beta_i\epsilon, \qquad a_i, b_i \in \mathbb{Z} \quad \text{and} \quad \alpha_i, \beta_i \in \mathbb{R}\,, \tag{3.2} $$

in the small quantity ϵ to arbitrary order. The expansion works for both symbolic argument z and unit argument. If the argument z is symbolic, it is assumed to be within the set W, where W is defined by

$$ W := \mathbb{C} \setminus V\,, \quad \text{where} \tag{3.3} $$

$$ V := \{z \in \mathbb{R} \,|\, z \geq 1\}\,. \tag{3.4} $$

The results are displayed in terms of rational functions, logarithms, polylogarithms Li_n [126, 127], Nielsen polylogarithms $S_{n,p}$ [128], and harmonic polylogarithms $H_{m_1,\ldots,m_k}$ [129,130].

The package can be obtained from [131]. It should be loaded at the beginning of the session with the following command.[2]

```
<< HypExp'
```

3.2.1 Functions, commands and symbols added

The package HypExp adds two new symbols

- $HypExpPath is the path where the HypExp package is installed.
- $HypExpFailed is the symbol returned by the package in case of failure.

The package adds the following functions.

- HypExp[Hypergeometric2F1[...,x],ϵ,n] gives the ϵ expansion of the enclosed hypergeometric function (HF) to order $\mathcal{O}(\epsilon^n)$. The function HypExp applied to anything else but a HF will leave it intact. Therefore one can map it onto an expression containing hypergeometric functions, and only the HF's will be expanded to the required order in ϵ. This is illustrated by the following example:

[2] Plots taken from Ref. [69] are courtesy of Daniel Maître.

```
(HypExp[#1, ϵ, 1] &) //@
 (Log[1 - ϵ] Hypergeometric2F1[1 + ϵ, 1, 2 - ϵ, x])
```

$$\text{Log}[1-\epsilon]\left(-\frac{\text{Log}[1-x]}{x}+\epsilon\left(\frac{\text{Log}[1-x]}{x}+\frac{\text{Log}[1-x]^2}{x}+\frac{\text{PolyLog}[2,x]}{x}\right)\right)$$

```
(HypExp[#1, ϵ, 1] &) //@ (Log[1 - ϵ]
   HypergeometricPFQ[{1 + 2 ϵ, 1 - ϵ, 2}, {2 - ϵ, 2 + 3 ϵ}, x])
```

$$\text{Log}[1-\epsilon]\left(-\frac{\text{Log}[1-x]}{x}+\epsilon\left(-\frac{2\,\text{Log}[1-x]}{x}-\frac{\text{Log}[1-x]^2}{2x}-\frac{2\,\text{PolyLog}[2,x]}{x}\right)\right)$$

```
Simplify[%]
```

$$-\frac{1}{2x}(\text{Log}[1-\epsilon](\text{Log}[1-x](2+4\epsilon+\epsilon\,\text{Log}[1-x])+4\epsilon\,\text{PolyLog}[2,x]))$$

The result is not given as a `SeriesData` since this would have the effect of forcing the expansion of the rest of the expression. This example also illustrates that the results produced by the package are not simplified, as this might be time consuming and not always appropriate. If one wants to get a compact result, one should use `Simplify` or even `FullSimplify`. The prefactors that accompany the variable ϵ can also be symbolic,

```
(HypExp[#1, ϵ, 1] &) //@ (Log[1 - ϵ]
   HypergeometricPFQ[{1 + α ϵ, 1 - ϵ, 2}, {2 - ϵ, 2 + 3 ϵ}, x])
```

$$\text{Log}[1-\epsilon]\left(\frac{\epsilon\,(\text{Log}[1-x]\,((\alpha-3)\,\text{Log}[1-x]-4)-4\,\text{PolyLog}[2,x])}{2x}-\frac{\text{Log}[1-x]}{x}\right)$$

and the expansion also works for argument $z = 1$.

```
FullSimplify[HypExp[
  Hypergeometric2F1[1 + 3 ϵ, 1 - 2 ϵ, 3 + 2 ϵ, 1], ϵ, 4]]
```

$$\frac{1}{3}(6-6(-6+\pi^2)\epsilon^2-(-468+36\pi^2+\pi^4)\epsilon^4+108\epsilon^3(-1+\text{Zeta}[3]))$$

```
HypExp[HypergeometricPFQ[
  {1 + ϵ, 1 - 2 ϵ, 2 - 3 ϵ}, {2 + 2 ϵ, 2 - ϵ}, 1], ϵ, 2]
```

$$\frac{4}{5}+\frac{1}{5\epsilon}+\left(2-\frac{2\pi^2}{5}\right)\epsilon+\epsilon^2\left(6-\frac{8\pi^2}{5}+\frac{78\,\text{Zeta}[3]}{5}\right)$$

The technicalities of the exansion in the case of the argument being unity are explained in section 3.4.

Besides providing the tools for expanding HF's the package also contains several other useful features, among others the conversion of polylogarithms of different arguments, the evaluation of certain classes of integrals, and the usage of libraries.

- Let us start with the first of the aforementioned points. We will, later on in appendix C.1, Eqs. (C.4) – (C.27), give relations between polylogarithms Li_n and Nielsen polylogarithms $S_{n,p}$ of different arguments. These relations are used internally. By setting the constant `$HypExpPolyLogRules` to `True`, these identities are applied systematically. The default value of `$HypExpPolyLogRules` is `False`. This is also illustrated with an example.

```
$HypExpPolyLogRules = False;

PolyLog[2, z/(z - 1)]
```

$$\text{PolyLog}\left[2,\frac{z}{z-1}\right]$$

```
$HypExpPolyLogRules = True;

PolyLog[2, z/(z - 1)]

-1/2 Log[1 - z]^2 - PolyLog[2, z]
```

We now move on and show how the HypExp package evaluates certain classes of integrals that are, in part, yet unknown to Mathematica.

- The function HypExpInt$[\chi_1, \chi_2, \chi_3, \chi_4, \chi_5, z]$ evaluates integrals of the form

$$I(\chi_1, \chi_2, \chi_3, \chi_4, \chi_5, z) := \int_0^1 du \, \frac{u^{\chi_1} \ln^{\chi_2}(u) \, \ln^{\chi_3}(1-u) \, \ln^{\chi_4}(1-zu)}{(uz-1)^{\chi_5}}, \tag{3.5}$$

with weight

$$w := \chi_2 + \chi_3 + \chi_4 + 1 - \delta_{\chi_5,0} \leq 5. \tag{3.6}$$

All the χ_i are non-negative integers and $z \in W$. Further details on the integrals $I(\chi_1, \chi_2, \chi_3, \chi_4, \chi_5, z)$ and the weight w as well as the origin of the inequality (3.6) can be found in section 3.3.3. The integral can be called with the argument being symbolic:

```
HypExpInt[2, 0, 1, 1, 3, z]
(27 + 2 π^2 - 24 z - 4 π^2 z + 2 π^2 z^2) Log[1 - z] -
 12 (-1 + z)^2 z^3
 (-3 + 4 z) Log[1 - z]^2 + Log[1 - z]^3 - Log[1 - z]^2 Log[z] -
 2 (-1 + z)^2 z^3          3 z^3              2 z^3
 (-3 + 4 z) PolyLog[2, z] - PolyLog[3, 1 - z] +
 2 (-1 + z)^2 z^3           z^3
 3 z + 4 Zeta[3] - 8 z Zeta[3] + 4 z^2 Zeta[3]
 4 (-1 + z)^2 z^3
```

Arguments that match the pattern $z/(z-1)$ are treated with relations between logarithms and polylogarithms of different arguments, appendix C.1, Eqs. (C.1) – (C.27), being already taken into account (if $HypExpPolyLogRules is set to True, see above):

```
HypExpInt[1, 1, 0, 1, 2, z/(z - 1)]
-(6 + π^2) (-1 + z)^2 Log[1 - z] + (-1 + z)^2 Log[1 - z]^3 +
  6 z^2                              6 z^2
 (-1 + z)^2 Log[1 - z]^2 Log[z] - (-1 + z)^2 PolyLog[2, z] +
 2 z^2                            z^2
 (-1 + z)^2 Log[1 - z] PolyLog[2, z] +
 z^2
 (-1 + z)^2 PolyLog[3, 1 - z] - (-1 + z)^2 Zeta[3]
 z^2                            z^2
```

Finally, also all $z \in W$ can be inserted directly. For the special cases $z = 0$ and $z = 1$ the integral simplifies considerably and the restriction $w \leq 5$ can be dropped.

```
HypExpInt[2, 4, 1, 1, 3, 1]
3 π^4/2 + π^6/6 - 42 Zeta[3] + 22 π^2 Zeta[3] + 2/3 π^4 Zeta[3] -
 108 Zeta[3]^2 - 348 Zeta[5] + 16 π^2 Zeta[5] - 240 Zeta[7]
```

In the case $z = 1$ we refer the reader also to the next paragraph and to section 3.3.3.3.

- The function HypExpU$[n, m, p]$ evaluates integrals of the form

$$U(n,m,p) := \int_0^1 du\, \ln^n(u) \cdot \ln^m(1-u) \cdot u^p \tag{3.7}$$

with $p \in \mathbb{Z}$ and n, m being non-negative integers. The only additional constraint on the parameters is that the condition $m + p \geq 0$ has to be satisfied in order to yield a convergent integral.

```
HypExpU[4, 3, -2]
2 π^4 + π^6/3 - 144 Zeta[3] + 48 π^2 Zeta[3] + 18/5 π^4 Zeta[3] -
 216 Zeta[3]^2 - 576 Zeta[5] + 72 π^2 Zeta[5] - 1152 Zeta[7]
```

For further details on the integrals $U(n, m, p)$ we refer the reader to section 3.3.3.3.

We finally turn our attention to the third of the above points, namely the usage of libraries. Since the computation of the expansion for high orders and large parameters is quite time consuming, it is of interest to store the results that have been already calculated and reuse them, instead of recalculating them. Several different libraries can be found at [131]. Further libraries can be added, depending on the needs and on the amount of available disk space.

- HypExpIsKnownToOrder$[a_1, \ldots, a_J, b_1, \ldots, b_{J-1}, n]$ returns True if the expansion of the hypergeometric function with parameters corresponding to the first arguments of the function is available in the library to the order n.
- HypExpAddToLib$[a_1, \ldots, a_J, b_1, \ldots, b_{J-1}, n]$ adds an expansion to the library.

Further notes on how to install, use and extend the libraries are given in [69, 131].

3.2.2 Functions modified

The package also updates Series to allow it to expand compound expressions containing hypergeometric functions. The difference between this and the mapping with HypExp is that the other functions of ϵ are also expanded, as shown by the following example:

```
Series[
 Log[1 - ϵ] Hypergeometric2F1[ϵ + 1, 1, 2 - ϵ, x], {ϵ, 0, 2}]
Log[1 - x] ϵ
---------- +
    x
 (-Log[1 - x]/(2 x) - Log[1 - x]^2/x - PolyLog[2, x]/x) ϵ^2 + O[ϵ]^3
Series[Log[1 - ϵ] HypergeometricPFQ[
   {2 ϵ + 1, 1 - ϵ, 2}, {2 - ϵ, 3 ϵ + 2}, x], {ϵ, 0, 2}]
Log[1 - x] ϵ
---------- +
    x
 (5 Log[1 - x]/(2 x) + Log[1 - x]^2/(2 x) + 2 PolyLog[2, x]/x) ϵ^2 + O[ϵ]^3
```

This allows to work with the expansion of HF's as Mathematica users are used to. We also updated the series expansion of the regularized hypergeometric functions since they are nothing else but hypergeometric functions divided by Γ-functions.

Since the incomplete B function is a special case of a HF,

$$B(z,a,b) = \frac{z^a}{a}\, {}_2F_1(a, 1-b, a+1, z), \quad a \neq 0, -1, -2, \ldots \tag{3.8}$$

it is also possible to expand it around integer-valued parameters with the HypExp package, as shown by the following example.

```
Series[Beta[x, 1 + 2 ϵ, 2 - ϵ], {ϵ, 0, 1}]
(x - x^2/2) +
 (-3 x/2 + x^2/4 + 1/2 Log[1 - x] - x Log[1 - x] + 1/2 x^2 Log[1 - x] +
    2 x Log[x] - x^2 Log[x]) ϵ + O[ϵ]^2
```

3.2.3 Note on the expansion for negative parameters

Let us state here a small subtlety that arises from the way in which Mathematica deals with hypergeometric functions in the case of negative parameters. Let us consider, for example, ${}_2F_1(-m+\alpha, b, -m-l+\beta; x)$ for m, l, b being positive integers and α, β small. Using the definition one gets

$$ {}_2F_1(-m+\alpha, b, -m-l+\beta; x) = \sum_{n=0}^{\infty} \frac{(-m+\alpha)_n (b)_n}{(-m-l+\beta)_n n!} x^n \; . \tag{3.9} $$

The term $n = m + l + 1$ of the above expression reads

$$ \frac{(-m+\alpha)\cdots(-1+\alpha)\alpha\cdots(l+\alpha)\;(b)_{m+l+1}}{(-m-l+\beta)(-m-l+\beta+1)\ldots(-1+\beta)\beta} \; \frac{x^{m+l+1}}{(m+l+1)!} \; . \tag{3.10} $$

This and all further terms contain the ratio α/β. If one wants to define a value for ${}_2F_1(-m, b, -m-l; x)$ one has to take the limit of Eq. (3.9) for α and β going to zero. The result depends on the way one approches $(0,0)$ with α and β. In [132], one can find the formula

$$ {}_2F_1(-m, b, -m-l; x) = \sum_{n=0}^{\infty} \frac{(-m)_n (b)_n}{(-l-m)_n n!} x^n \tag{3.11} $$

which is also the result Mathematica gives. This corresponds to a trajectory in the (α, β)-plane going along the β axis. Taking a trajectory along the α axis would lead to a $1/\beta$ pole. Approaching (0,0) along any other sloped straight line gives a result of the form

$$ f_1(x) + \frac{\alpha}{\beta} f_2(x) \tag{3.12} $$

where $f_1(x)$ is just the result of Eq. (3.11) and $f_2(x)$ happens to be the second solution of the hypergeometric differential equation

$$ x(1-x)\, w''(x) + (B_1 - (A_1 + A_2 + 1)x)\; w'(x) - A_1\, A_2\, w(x) = 0 \tag{3.13} $$

with

$$ A_1 = -m \, , \qquad A_2 = b \, , \qquad B_1 = -m - l \, . \tag{3.14} $$

Since the use of the Kummer identity (3.22)

$$ {}_2F_1(A_1, A_2; B_1; x) = (1-x)^{B_1 - A_1 - A_2}\; {}_2F_1(B_1 - A_1, B_1 - A_2; B_1; x) \tag{3.15} $$

induces a rotation in the (α, β) plane and since Mathematica always chooses the trajectory along the β axis, the result for the HF and its Kummer transform will not be identical

in Mathematica for our chosen example. This feature can occur whenever we encounter a ratio α/β in the series representation of a hypergeometric function ${}_2F_1$.

We conclude this subsection with an example which also shows that HypExp takes this feature properly into account.

```
Hypergeometric2F1[-1 + α ϵ, 2, -2 + β ϵ, x];

Limit[%, ϵ → 0]

x + 1

Hypergeometric2F1[-1 + α ϵ, 2, -2 + β ϵ, x] /. {Hypergeometric2F1[a_, b_, c_, x_] :>
    (1 - x)^(c - b - a) * Hypergeometric2F1[c - a, c - b, c, x]};

Limit[%, ϵ → 0]

 2 x - 1
(x - 1)^3

(*Kill kernel, business as usual*)

<< HypExp'

Collect[HypExp[Hypergeometric2F1[-1 + α ϵ, 2, -2 + β ϵ, x], ϵ, 0], α, Simplify]

 (x - 2) α x^3
-(-------------) + x + 1
 (x - 1)^3 β
```

3.2.4 Performances and limitations

The limits are set by the CPU and the amount of memory available. In all practical cases known to us, however, the result is given in a reasonable time. The following table shows the CPU time dependence for the expansion of some hypergeometric functions to different orders on a 3 GHz processor/1.5 GB RAM machine.

order	2	3	4	5
${}_2F_1(1+\epsilon, 1-\epsilon; 2+2\epsilon, x)$	< 1 s	< 1 s	< 1 s	7 s
${}_2F_1(1+\alpha_1\epsilon, 1+\alpha_2\epsilon; 2+\beta_1\epsilon, x)$	< 1 s	< 1 s	< 1 s	6 s
${}_3F_2(1+2\epsilon, 1-\epsilon, 2-3\epsilon; 1+3\epsilon, 2+\epsilon, x)$	< 1 s	< 1 s	< 1 s	3 s
${}_3F_2(1+\alpha_1\epsilon, 1+\alpha_2\epsilon, 2+\alpha_3\epsilon;$ $1+\beta_1\epsilon, 2+\beta_2\epsilon, x)$	< 1 s	< 1 s	1.5 s	3 s
${}_4F_3(1+\alpha_1\epsilon, 2+\alpha_2\epsilon, 3+\alpha_3\epsilon, 4+\alpha_4\epsilon;$ $\beta_1\epsilon, 1+\beta_2\epsilon, 1+\beta_3\epsilon, x)$	12 s	20 s	50 s	140 s

The package was developed in Mathematica 5.0 and should work on newer versions.

3.3 Method of integration

So far we described the functions of the HypExp package in great detail and illustrated their usage by means of several examples. We will now be dealing with the method of integration, one of the approaches that was used to derive the expansion of hypergeometric functions around integer-valued parameters.

Among the hypergeometric functions (HF), the ordinary Gauß-hypergeometric function

$$ {}_2F_1\left(A_1, A_2; B_1; z\right) \tag{3.16}$$

appears most frequently in scientific calculations, and it is therefore worth to focus in particular on this type of functions [132]. We will calculate the ϵ-expansion of the ${}_2F_1$-functions up to and including order $\mathcal{O}(\epsilon^4)$ by means of the algorithm described below which is based on the well-known integral representation of the ${}_2F_1$-functions. Applying this method to this subset of functions has by all means its benefits since it is fast and efficient. However, going to higher orders in the ϵ-expansion or to higher ${}_JF_{J-1}$-functions quickly reveals that the nested sums method, which is the other approach applied in Ref. [69], is in general more powerful. Nevertheless, applying several independent methods also provides useful consistency checks.

3.3.1 ${}_2F_1$-algorithm

We use the notation introduced at the beginning of section 3.2 in Eqs. (3.1) – (3.4). Furthermore, we state that the mapping

$$f(z) := \frac{z}{z-1} \tag{3.17}$$

as a Moebius transformation is a bijective mapping and satisfies

$$f(V) = V \quad f(W) = W\,, \quad \text{and} \quad f(f(z)) = z\,, \tag{3.18}$$

where W and V are defined in Eqs. (3.3) and (3.4). We finally turn our attention to the ${}_2F_1$-functions. We will first collect some useful formulas [132,133] that will allow us to shift each of the parameters up or down by integer units. For the parameters A_i , $(i = 1, 2)$, we use

$$\begin{aligned}(B_1 - A_1)\,{}_2F_1(\mathbf{A_1} - \mathbf{1}, A_2; B_1; z) \\ + \left[2A_1 - B_1 - (A_1 - A_2)z\right]\,{}_2F_1(\mathbf{A_1}, A_2; B_1; z) \\ + A_1(z-1)\,{}_2F_1(\mathbf{A_1} + \mathbf{1}, A_2; B_1; z) = 0\end{aligned} \tag{3.19}$$

and from symmetries a similar equation in which A_1 and A_2 are interchanged. Whenever we refer to Eq. (3.19) it should be clear from the context whether we intend to shift A_1 or A_2. The parameter B_1 finally can be shifted up or down by means of

$$\begin{aligned}B_1(B_1-1)(z-1)\,{}_2F_1(A_1, A_2; \mathbf{B_1} - \mathbf{1}; z) \\ + B_1\left[B_1 - 1 - (2B_1 - A_1 - A_2 - 1)z\right]\,{}_2F_1(A_1, A_2; \mathbf{B_1}; z) \\ + (B_1 - A_1)(B_1 - A_2)z\,{}_2F_1(A_1, A_2; \mathbf{B_1} + \mathbf{1}; z) = 0\,.\end{aligned} \tag{3.20}$$

There is yet another class of relations between ${}_2F_1$-functions, namely the relations of Gauß between contiguous functions [132]. Their inclusion would lead only to a minor simplicifation here, and thus we let them serve as a check for our results rather than implementing them in our algorithm.

From the relations (3.19) and (3.20) we conclude that the knowledge of the ϵ-expansions of the ${}_2F_1$-functions whose integer parts $\{a_1, a_2, b_1\}$ of the parameters read

$$\begin{array}{lll}\{0,0,0\} & \{0,1,0\} & \{0,0,1\} \\ \{1,1,0\} & \{0,1,1\} & \{1,1,1\}\end{array} \tag{3.21}$$

is sufficient in order to derive the ϵ-expansion of *any* ${}_2F_1$-function with $\{a_1, a_2, b_1\}$ being integer-valued. But even this small set of functions can be reduced further by means of Kummer relations [132, 133]. The relevant Kummer relations read

$$
\begin{aligned}
{}_2F_1(A_1, A_2; B_1; z) &= (1-z)^{B_1-A_1-A_2}\, {}_2F_1(B_1-A_1, B_1-A_2; B_1; z)\,, && (3.22)\\
{}_2F_1(A_1, A_2; B_1; z) &= (1-z)^{-A_1}\, {}_2F_1(A_1, B_1-A_2; B_1; \frac{z}{z-1})\,, && (3.23)\\
{}_2F_1(A_1, A_2; B_1; z) &= (1-z)^{-A_2}\, {}_2F_1(B_1-A_1, A_2; B_1; \frac{z}{z-1})\,, && (3.24)
\end{aligned}
$$

and relate both the functions $\{0,1,1\}$ and $\{1,1,1\}$ to the function $\{0,0,1\}$, such that we can get along with a mere four functions, namely

$$\{0,0,0\} \quad \{0,1,0\} \quad \{0,0,1\} \quad \{1,1,0\}\,. \tag{3.25}$$

For completeness, we mention that Eq. (3.22) holds true for all $z \in \mathbb{C}$, whereas Eqs. (3.23) and (3.24) are only valid for $z \in W$.

The sets (3.21) and (3.25) of basic hypergeometric functions have, however, one major drawback. In order to express a general ${}_2F_1$-function solely in terms of functions from these sets, repeated application of Eqs. (3.19) and (3.20) is required and additional negative powers of ϵ might be generated in prefactors via this procedure. It is therefore necessary to know the ϵ-expansions of the basic hypergeometric functions to *higher* order than is sought by the ${}_2F_1$-function in question.

In order to avoid this disturbing feature we consider an extended set of basic hypergeometric functions. The extended set has three major subsets. In the first subset we collect those basic HF's that contain only positive integer parts, namely

$$
\begin{aligned}
&\{0,0,0\} \quad \{0,1,0\} \quad \{0,0,1\} \quad \{1,1,0\}\\
&\{0,1,1\} \quad \{1,1,1\} \quad \{0,1,2\} \quad \{1,1,2\}\,.
\end{aligned}
\tag{3.26}
$$

The second subset contains those basic HF's in which $b_1 = 0$. It reads

$$\{-1,-1,0\} \quad \{-1,0,0\} \quad \{-1,1,0\}\,. \tag{3.27}$$

The third subset finally contains those basic HF's in which $b_1 = -1$:

$$
\begin{aligned}
&\{-2,-2,-1\} \quad \{-2,-1,-1\} \quad \{-2,0,-1\}\\
&\{-2,1,-1\} \quad \{-1,-1,-1\} \quad \{-1,0,-1\}\\
&\{-1,1,-1\} \quad \{0,0,-1\} \quad \{0,1,-1\} \quad \{1,1,-1\}\,.
\end{aligned}
\tag{3.28}
$$

Although some functions in this set might not be considered independent since they are related via Kummer relations, we will consider this set as basic since it allowed us to efficiently and conveniently implement the algorithm described below. The goal of the latter is to express a general ${}_2F_1$-function entirely in terms of functions from the set (3.26) – (3.28) by repeated application of equations (3.19) and (3.20) as well as the Kummer relations (3.22) – (3.24). Before we start, we mention that throughout the algorithm we make use of the symmetry $A_1 \leftrightarrow A_2$ after each step in order to ensure that we always have $a_1 \leq a_2$.

1. We start the reduction of our ${}_2F_1$-function in question by applying Kummer relations such that the sum
$$|a_1| + |a_2| + |b_1| \tag{3.29}$$
gets minimized. Especially for high absolute values of the parameters this procedure shortens the algorithm significantly.

2. Then, if $b_1 < -1$, we shift B_1 up by applying (3.20) repeatedly (rep.) to all HF's with $b_1 < -1$. This step ensures that from now on we only have to deal with functions in which $b_1 \geq -1$.

For the rest of the algorithm we distinguish two cases, namely $b_1 = -1$ and $b_1 \geq 0$. The further steps for $b_1 = -1$ and $b_1 \geq 0$ are illustrated by the flow-charts in Figures 3.1 and 3.2 respectively. The ambitious reader is invited to verify that at the end of this algorithm only ${}_2F_1$-functions from the set (3.26) – (3.28) appear and that no negative power of ϵ has been generated at any intermediate step. To conclude this section we remark that for the most frequent case in which the three parameters a_1, a_2, and b_1 are all non-negative, only the last column of Figure 3.2 has to be considered.

3.3.2 Expansion of the basic ${}_2F_1$-functions

Now that we went through the algorithm for the ${}_2F_1$-functions in great detail we have to explain how the ϵ-expansions of the basic HF's from the set (3.26) – (3.28) are obtained.

For the functions in Eq. (3.26) we adopt the integral representation [132]
$${}_2F_1(A_1, A_2; B_1; z) = \frac{\Gamma(B_1)}{\Gamma(A_2)\Gamma(B_1 - A_2)} \int_0^1 du \, \frac{u^{A_2-1} \, (1-u)^{B_1-A_2-1}}{(1-zu)^{A_1}} \,, \tag{3.30}$$
which we must restrict to $z \in W$ and $B_1 > A_2 > 0$. Since this approach will be based on the requirement that the integration over u and the expansion in ϵ commute, we have to set up the additional condition $b_1 > a_2 > 0$. One recognizes immediately that from the set (3.26) only the functions $\{0, 1, 2\}$ and $\{1, 1, 2\}$ satisfy the latter inequality. The parameters A_2 and B_1 of the other six functions first have to be shifted up by means of Eqs. (3.19) and (3.20) until a convergent integral representation is obtained for each of them. The subsequent expansion of the integral representation in ϵ and how one solves the occurring integrals is covered in section 3.3.3.

The functions in Eqs. (3.27) and (3.28), all of which contain at least one negative parameter, are now, for the sake of obtaining *their* ϵ-expansion, expressed in terms of functions from the set (3.26). This is again done by appropriate application of the Kummer relations (3.22) – (3.24) as well as Eqs. (3.19) and (3.20).

The shift of parameters as described in the preceding two paragraphs is now unavoidably accompanied by the advent of negative powers of ϵ in certain prefactors. To be more precise, we must expand the functions $\{1, 1, 0\}$ and $\{1, 1, 2\}$ up to and including order $\mathcal{O}(\epsilon^4)$ and the other six functions of Eq. (3.26) to order $\mathcal{O}(\epsilon^5)$ in order to guarantee that all functions from the set (3.26) – (3.28) can be expanded up to and including order $\mathcal{O}(\epsilon^4)$. This might at first glance seem peculiar, but it turns out that at the respective highest order in ϵ the occurring functions are the same. We conclude from this that, with the tools provided here, it is in principle possible to expand a certain class of ${}_2F_1$-functions even to order $\mathcal{O}(\epsilon^5)$.

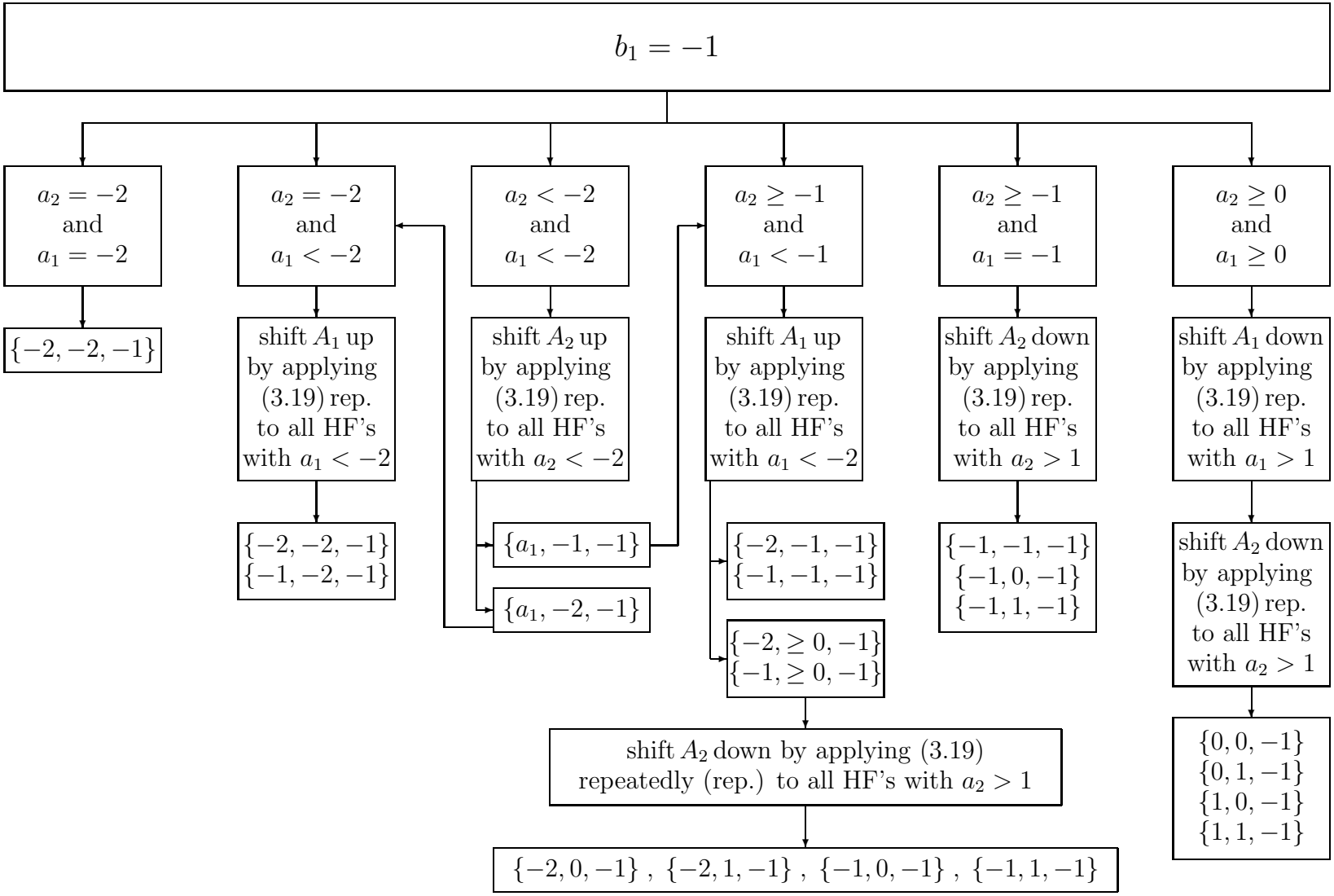

Figure 3.1: ${}_2F_1$-algorithm for $b_1 = -1$

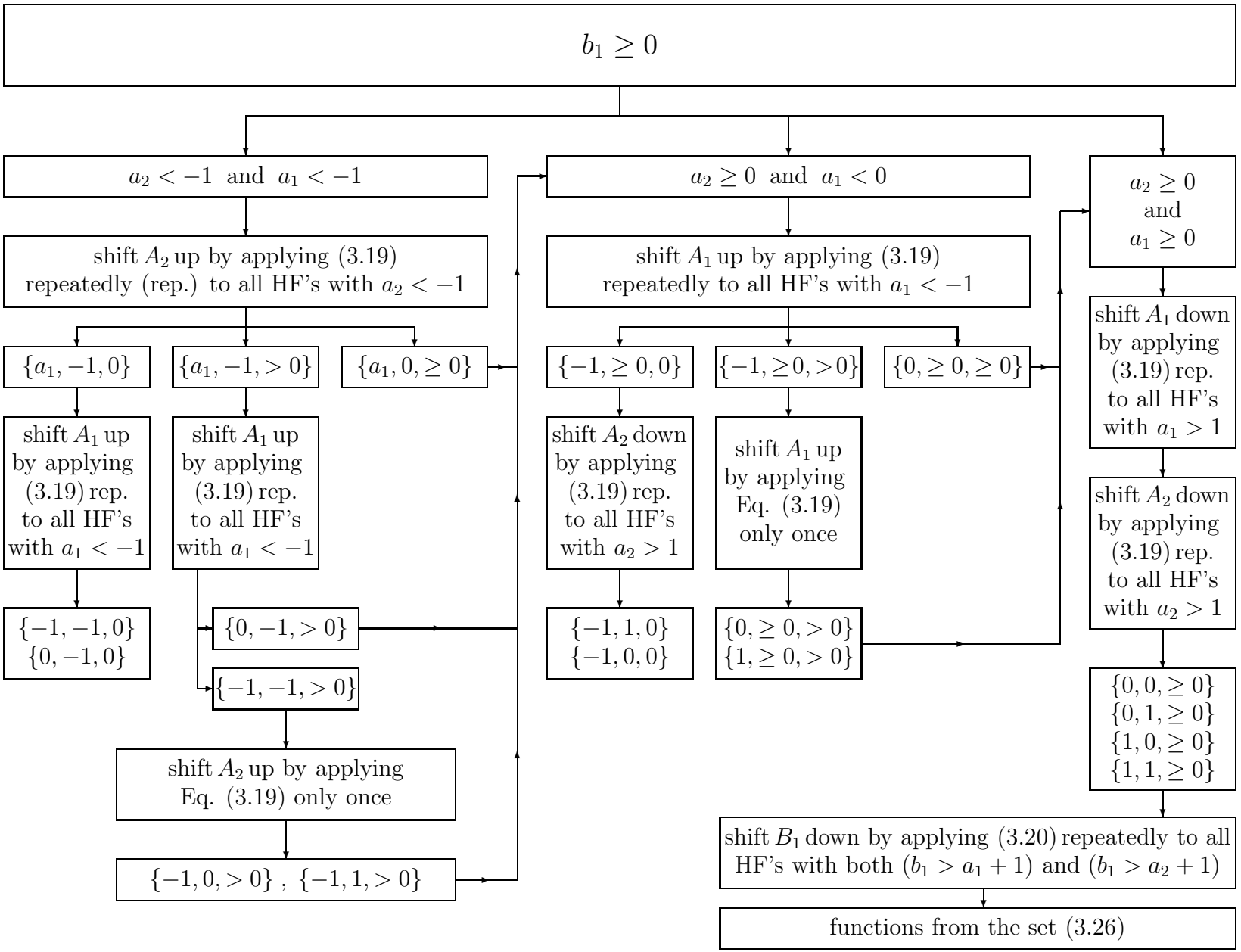

Figure 3.2: ${}_2F_1$-algorithm for $b_1 \geq 0$

3.3.3 Integrals and their algorithm

3.3.3.1 General aspects

Expressing a HF ${}_2F_1\left(a_1+\alpha_1\,\epsilon, a_2+\alpha_2\,\epsilon; b_1+\beta_1\,\epsilon; z\right)$ with $b_1 > a_2 > 0$ in terms of its integral representation according to Eq. (3.30) and subsequently expanding in ϵ yields integrals that have the general form

$$I\left(\chi_1,\chi_2,\chi_3,\chi_4,\chi_5,z\right) := \int_0^1 du\, \frac{u^{\chi_1}\,\ln^{\chi_2}(u)\,\ln^{\chi_3}(1-u)\,\ln^{\chi_4}(1-zu)}{(uz-1)^{\chi_5}}\,, \tag{3.31}$$

where the χ_i are non-negative integers and $z \in W$. The results of these integrals contain rational functions, logarithms, polylogarithms Li_n [126, 127], Nielsen polylogarithms $S_{n,p}$ [128], and harmonic polylogarithms $H_{m_1,\ldots,m_k}$ [129, 130]. Relations between polylogarithms Li_n and Nielsen polylogarithms $S_{n,p}$ of different arguments can be found in appendix C.1.

Let us define the *weight* w of the integral by

$$w := \chi_2+\chi_3+\chi_4+1-\delta_{\chi_5,0}\,. \tag{3.32}$$

The weight w is related to the weight of the harmonic polylogarithms [129, 130], namely any integral of weight w can be expressed in terms of harmonic polylogarithms of weight w or less. In order to guarantee that the ϵ-expansion of *any* ${}_2F_1$-function up to order $\mathcal{O}(\epsilon^n)$ can be performed, the computation of all integrals with weight w up to $n+1$ is required, this being the reason for the inequality (3.6).

3.3.3.2 Description of the algorithm

In order to make the computation more efficient we now show that any of the integrals $I\left(\chi_1,\chi_2,\chi_3,\chi_4,\chi_5,z\right)$ can be expressed in terms of integrals with $\chi_1 = \chi_5 = 0$ and of at most the same weight as the original one:

1. In the case $\chi_1 \leq \chi_5$, the integral $I\left(\chi_1,\chi_2,\chi_3,\chi_4,\chi_5,z\right)$ can, via the replacement
$$u = \frac{1}{z}(uz-1)+\frac{1}{z} \tag{3.33}$$
in the numerator and subsequent cancellation of the corresponding denominators, be expressed as a linear combination of integrals of the form
$$I\left(0,\chi_2,\chi_3,\chi_4,\chi_5,z\right),\, I\left(0,\chi_2,\chi_3,\chi_4,\chi_5-1,z\right),\, \ldots,\, I\left(0,\chi_2,\chi_3,\chi_4,\chi_5-\chi_1,z\right)\,. \tag{3.34}$$

2. In the case $\chi_1 > \chi_5$, we can apply the same steps as before and eventually arrive at integrals of the form
$$I\left(\chi_1-\chi_5,\chi_2,\chi_3,\chi_4,0,z\right),\, I\left(\chi_1-\chi_5-1,\chi_2,\chi_3,\chi_4,0,z\right),\, \ldots,\, I\left(0,\chi_2,\chi_3,\chi_4,0,z\right),\, I\left(0,\chi_2,\chi_3,\chi_4,1,z\right),\, \ldots,\, I\left(0,\chi_2,\chi_3,\chi_4,\chi_5,z\right)\,. \tag{3.35}$$
In other words, the replacement rule (3.33) for u yields integrals in which at least one of the entries χ_1 and χ_5 is zero.

3. We continue our reduction by manipulating integrals of the form $I(\chi_1, \chi_2, \chi_3, \chi_4, 0, z)$ with $\chi_1 > 0$. By recalling the relation

$$\int_0^1 du \, \frac{d}{du} \left[u^{\chi_1} (1-u) \ln^{\chi_2}(u) \, \ln^{\chi_3}(1-u) \, \ln^{\chi_4}(1-zu) \right] = 0 \tag{3.36}$$

and explicitly taking the derivative of the product, one derives the relation

$$\begin{aligned}
&(\chi_1 + 1) \, I(\chi_1, \chi_2, \chi_3, \chi_4, 0, z) = \\
&\quad \chi_1 \, I(\chi_1 - 1, \chi_2, \chi_3, \chi_4, 0, z) - \chi_2 \, I(\chi_1, \chi_2 - 1, \chi_3, \chi_4, 0, z) \\
&\quad + \chi_2 \, I(\chi_1 - 1, \chi_2 - 1, \chi_3, \chi_4, 0, z) - \chi_3 \, I(\chi_1, \chi_2, \chi_3 - 1, \chi_4, 0, z) \\
&\quad + z \, \chi_4 \, I(\chi_1, \chi_2, \chi_3, \chi_4 - 1, 1, z) - z \, \chi_4 \, I(\chi_1 + 1, \chi_2, \chi_3, \chi_4 - 1, 1, z) \; .
\end{aligned} \tag{3.37}$$

Repeated application of steps 1. — 3. finally yields an expression which contains only integrals with $\chi_1 = 0$ and of at most the same weight as the integral we started with.

4. The remaining task is now to subsequently lower χ_5. By repeated application of the relations

$$\begin{aligned}
I(0, \chi_2, \chi_3, \chi_4, \chi_5, z) = &- \sum_{k=0}^{\chi_5 - 1} \left[\binom{\chi_5}{k} \, I(0, \chi_2, \chi_3, \chi_4, k, z) \right] \\
&+ \frac{(-z)^{\chi_5}}{(\chi_5 - 1)!} \cdot \sum_{v=0}^{\chi_4} \left\{ \frac{\chi_4!}{(\chi_4 - v + 1)!} \left[\sum_{j=1}^{\chi_5 - 1} \binom{\chi_5 - 1}{j} \, (-1)^j \, j^{-v} \right] \right. \\
&\left. \times \frac{d^{\chi_5}}{dz^{\chi_5}} I(0, \chi_2, \chi_3, \chi_4 - v + 1, 0, z) \right\}
\end{aligned} \tag{3.38}$$

for $\chi_5 > 1$ and

$$\begin{aligned}
I(0, \chi_2, \chi_3, \chi_4, 1, z) = &- I(0, \chi_2, \chi_3, \chi_4, 0, z) \\
&+ \frac{z}{\chi_4 + 1} \cdot \frac{d}{dz} I(0, \chi_2, \chi_3, \chi_4 + 1, 0, z)
\end{aligned} \tag{3.39}$$

one eventually arrives at an expression of the desired form. The original integral $I(\chi_1, \chi_2, \chi_3, \chi_4, \chi_5, z)$ is now represented in terms of integrals with $\chi_1 = \chi_5 = 0$ and derivatives thereof. The derivatives are only applied in the end when the integrals on which they act are found as an explicit function of z.

5. From the above considerations we conclude that the basic integrals are those with $\chi_1 = \chi_5 = 0$. These integrals must now be found as an explicit function of z. They are combinations of rational functions, logarithms, polylogarithms Li_n, Nielsen polylogarithms $S_{n,p}$, and harmonic polylogarithms $H_{m_1,\ldots,m_k}$. They are then plugged into the derived expression for the original integral $I(\chi_1, \chi_2, \chi_3, \chi_4, \chi_5, z)$. Subsequently, the derivatives are carried out.

As far as the evaluation of the basic integrals $I\,(0,\chi_2,\chi_3,\chi_4,0,z)$ is concerned, we now show that integrals with $\chi_2 < \chi_3$ can be obtained easily once the ones with $\chi_2 > \chi_3$ are known. This is due to the fact that the transformation $u \to 1-u$ in the integrand of (3.31) allows us to represent integrals with $\chi_2 < \chi_3$ in terms of integrals with $\chi_2 > \chi_3$. By means of the relation

$$\ln\left[1-z(1-u)\right] = \ln\left(1-z\right) + \ln(1-\frac{z}{z-1}\,u)\,, \tag{3.40}$$

which holds true for all $z \in W$ and $0 < u < 1$, one easily derives the formula

$$I\,(0,\chi_2,\chi_3,\chi_4,0,z) = \sum_{m=0}^{\chi_4} \binom{\chi_4}{m} \cdot \ln^{\chi_4-m}\left(1-z\right) \cdot I(0,\chi_3,\chi_2,m,0,\frac{z}{z-1}). \tag{3.41}$$

Since this formula also transforms the argument z, we derived relations between polylogarithms that allow to simplify these arguments again. Details on the argument transformations of the polylogarithms can be found in section 3.2.1 and in appendix C.1.

To summarize, for a given weight w the set of basic integrals consists of all

$$I\,(0,\chi_2,\chi_3,\chi_4,0,z) \qquad \text{with} \quad \chi_2+\chi_3+\chi_4 = w\,. \tag{3.42}$$

Their evaluation yields – to some extent complicated – expressions of z that contain rational functions, logarithms, polylogarithms Li_n, Nielsen polylogarithms $S_{n,p}$, and harmonic polylogarithms $H_{m_1,\ldots,m_k}$. Integrals of (3.42) with $\chi_2 < \chi_3$ can be reexpressed in terms of integrals with $\chi_2 > \chi_3$ and argument $z/(z-1)$ and are therefore easily obtained once the argument transformations of the polylogarithms are taken into account.

We implemented this algorithm in the function `HypExpInt`. This function gives back the result of any integral I with

$$w = \chi_2+\chi_3+\chi_4+1-\delta_{\chi_5,0} \leq 5 \tag{3.43}$$

as an explicit function of z and is explained in detail in section 3.2.1. For the actual calculation of the ϵ-expansion of ${}_2F_1$-functions we need a bit less than is provided by the algorithm and by the function `HypExpInt`. We have:

$$\chi_1 \;\leq\; 2\,, \tag{3.44}$$

$$\chi_5 \;\leq\; 1\,. \tag{3.45}$$

The first inequality arises from the fact that we have to shift up the parameters A_2 and B_1 of our basic hypergeometric functions, Eq. (3.26), via the relations (3.19) and (3.20) in order to obtain convergent integral representations. In this procedure, $b_1 - 2$, which eventually determines the highest value for χ_1 to occur, assumes values up to 2. Similarly, the parameter a_1 determines the highest value for χ_5 that can show up. With this in mind one derives the second inequality directly from the collection (3.26) of basic hypergeometric functions.

3.3.3.3 Integrals of unit argument

Putting $z = 1$ in the integrals $I\,(\chi_1,\chi_2,\chi_3,\chi_4,\chi_5,z)$ immediately turns our attention to an other type of integrals that we considered useful to implement. We define the function

$U(n,m,p)$ by

$$U(n,m,p) := \int_0^1 du\, \ln^n(u) \cdot \ln^m(1-u) \cdot u^p \tag{3.46}$$

with $p \in \mathbb{Z}$ and n, m being non-negative integers. In order to yield a convergent integral the inequality $m+p \geq 0$ has to be satisfied. We demonstrate below how *any* convergent integral $U(n,m,p)$ can be expressed in terms of $U(0,0,0)$ and integrals of the form $U(n,m,-1)$.

1. We start by considering the case $p < -1$; $n > 0$ and $m+p \geq 0$. Repeated application of

$$\begin{aligned} U(n,m,p) &= -\frac{n}{p+1} \cdot U(n-1,m,p) + \frac{m}{p+1} \cdot U(m-1,n,-1) \\ &\quad + \frac{m}{p+1} \sum_{\tau=1}^{-p-1} U(n,m-1,-\tau) \end{aligned} \tag{3.47}$$

   leaves us with integrals of the form $U(n,m,-1)$ and $U(0,m,p)$, where the latter type still happens to have $p < -1$ and $m+p \geq 0$. These integrals get reduced via the recursion relation

$$U(0,m,p) = \frac{m}{p+1} \sum_{\kappa=1}^{-p-1} U(0,m-1,-\kappa) \tag{3.48}$$

   to integrals with $p = -1$.

2. We now proceed with the case $p = 0$, in which the function U is symmetric in $n \leftrightarrow m$ and therefore $n \geq m$ can always be achieved. Applying this in turn with the formula

$$\begin{aligned} U(n,m,0) &= -n \sum_{\sigma=0}^{m} \frac{(-1)^{m-\sigma}\, m!}{\sigma!}\, U(n-1,\sigma,0) \\ &\quad + n \sum_{\lambda=1}^{m} \frac{(-1)^{m-\lambda}\, m!}{\lambda!}\, U(n-1,\lambda,-1) \end{aligned} \tag{3.49}$$

   for $\{n,m\} \neq \{0,0\}$ eventually yields integrals of the desired form.

3. In the case $p > 0$ we apply the same trick as in step 3 of section 3.3.3.2 and derive from

$$\int_0^1 du\, \frac{d}{du} \left[u^p (1-u) \ln^n(u)\, \ln^m(1-u)\right] = 0 \tag{3.50}$$

   the recurrence relation

$$\begin{aligned} (p+1)\, U(n,m,p) &= p\, U(n,m,p-1) + n\, U(n-1,m,p-1) \\ &\quad - n\, U(n-1,m,p) - m\, U(n,m-1,p)\ . \end{aligned} \tag{3.51}$$

Repeated application of these steps finally yields an expression which only contains integrals of the demanded form.

$U(0,0,0)$ is trivially found to be unity. A nice algorithm for the computation of integrals of the form $U(n,m,-1)$ is given in section 7.9.5 of Ref. [126] and will not be repeated here.

The evaluation of integrals $U\,(n,m,p)$ with $p \in \mathbb{Z}$ and n, m being non-negative integers can be called with the function `HypExpU`, and an example can be found in section 3.2.1.

The connection to $I\,(\chi_1,\chi_2,\chi_3,\chi_4,\chi_5,z)$ in $z=1$ is given by

$$I\,(\chi_1,\chi_2,\chi_3,\chi_4,\chi_5,1) = \sum_{j=0}^{\chi_1}(-1)^{j-\chi_5}\left(\begin{array}{c}\chi_1\\ j\end{array}\right) U\,(\chi_3+\chi_4,\chi_2,j-\chi_5) \tag{3.52}$$

for $\chi_2 \geq \chi_5$. By means of this relation the function `HypExpInt` can be directly called with unit argument, see section 3.2.1.

3.4 Hypergeometric functions of unit argument

The hypergeometric series

$${}_JF_{J-1}\,(\{A_1,\ldots,A_J\};\{B_1,\ldots,B_{J-1}\};z) = \sum_{n=0}^{\infty}\frac{(A_1)_n\ldots(A_J)_n}{(B_1)_n\ldots(B_{J-1})_n}\,\frac{z^n}{n!} \tag{3.53}$$

converges in $z=1$ only if the condition

$$\sum_{t=1}^{J-1}B_t - \sum_{r=1}^{J}A_r > 0 \tag{3.54}$$

is satisfied. This implies that, if

$$s \equiv \sum_{t=1}^{J-1}b_t - \sum_{r=1}^{J}a_r > 0\;, \tag{3.55}$$

the expansion in ϵ commutes with the procedure of taking the limit $z \to 1$, and the series expansion of the function ${}_JF_{J-1}\,(\{A_1,\ldots,A_J\};\{B_1,\ldots,B_{J-1}\};1)$ around $\epsilon = 0$ has a well-defined finite radius of convergence. We therefore call the case $s > 0$ *non-critical*.

The case $s \leq 0$, on the other hand, will be referred to as *critical* since this case requires more care and additional explanation on its treatment. By means of an algorithm based on partial fractions it is possible to express a hypergeometric function (HF) ${}_JF_{J-1}$ of unit argument and value s in terms of $J-1$ hypergeometric functions ${}_JF_{J-1}$, also of unit argument, but of value $s+1$ or higher. We outline this procedure for the case in which no two of the B_i are equal. Assuming that all occurring infinite sums converge, we start with the series expansion (3.53) of the function

$${}_JF_{J-1}\,(\{A_1+1,\ldots,A_J+1\};\{B_1+1,\ldots,B_{J-1}+1\};1) \tag{3.56}$$

and multiply and divide therein by the fraction

$$\frac{(A_1+n)\cdot\ldots\cdot(A_J+n)}{(B_1+n)\cdot\ldots\cdot(B_{J-1}+n)}\;. \tag{3.57}$$

The inverse of the above expression gets combined appropriately with the Γ-functions of the Pochhammer symbols, whereas the multiplied one gets expanded into partial fractions, yielding

$$n - \sum_{\mu=1}^{J-1} B_\mu + \sum_{\varrho=1}^{J} A_\varrho + \sum_{\tau=1}^{J-1} \frac{\prod_{\sigma=1}^{J}(B_\tau - A_\sigma)}{(B_\tau + n) \cdot \prod_{\lambda=1;\lambda\neq\tau}^{J-1}(B_\tau - B_\lambda)} \; . \tag{3.58}$$

The term linear in n gives back the function (3.56), which then cancels on both sides of the equation. The constant term is proportional to the function

$${}_JF_{J-1}\left(\{A_1, \ldots, A_J\}; \{B_1, \ldots, B_{J-1}\}; 1\right) \tag{3.59}$$

for which we are seeking and for which we can now solve the equation. Each term of the last sum in (3.58) contains a HF of value $s+1$. After some intermediate steps, we arrive at

$$\begin{aligned} &\left[\sum_{\mu=1}^{J-1} B_\mu - \sum_{\varrho=1}^{J} A_\varrho\right] {}_JF_{J-1}\left(\{A_1, \ldots, A_J\}; \{B_1, \ldots, B_{J-1}\}; 1\right) \\ &= \sum_{\tau=1}^{J-1} \frac{\prod_{\sigma=1}^{J}(B_\tau - A_\sigma)}{\prod_{\lambda=1;\lambda\neq\tau}^{J-1}(B_\tau - B_\lambda)} \cdot \frac{1}{B_\tau} \\ &\quad \times {}_JF_{J-1}\left(\{A_1, \ldots, A_J\}; \{B_1, \ldots, B_{\tau-1}, B_\tau + 1, B_{\tau+1}, \ldots, B_{J-1}\}; 1\right) \; . \end{aligned} \tag{3.60}$$

The case in which there is any combination of equal B_i's can be treated analogously. The linear and the constant term in the expression (3.58) remain unchanged, only the last sum will look different, and the final expression (3.60) will contain HF's of value $s+1$ or higher.

Repeated application of this algorithm allows to express a critical HF as a linear combination of non-critical ones, the two expressions being related via analytic continuation.

Since the analytic continuation is unique and the expression obtained by the algorithm has a well-defined expansion around $\epsilon = 0$, we can associate the expansion at hand also with the original critical HF. In this sense the ϵ-expansion of a critical HF has to be understood and the user must be aware of this feature. The same phenomenon happens, by the way, for the well-known Γ-function.

The special case $J = 2$ is simpler due to the following identity:

$${}_2F_1\left(A_1, A_2; B_1; 1\right) = \frac{\Gamma(B_1)\,\Gamma(B_1 - A_1 - A_2)}{\Gamma(B_1 - A_1)\,\Gamma(B_1 - A_2)} \; . \tag{3.61}$$

Again, the series expansions of the Γ-functions have to be understood in the sense of analytic continuation.

The crucial property of a critical function is that ϵ does not drop out of the expression on the left-hand side of Eq. (3.54). This means that

$$\sum_{t=1}^{J-1} \beta_t - \sum_{r=1}^{J} \alpha_r \neq 0 \tag{3.62}$$

has to be satisfied in the case $s \leq 0$. If $s \leq 0$ and (3.62) yields zero, the series (3.53) is divergent for all values of ϵ and no remedy can be found.

The way in which the HFs of unit argument are implemented in the package is described in section 3.2.1.

3.5 Conclusions

In this chapter we presented the `Mathematica` package `HypExp` for expanding arbitrary hypergeometric functions ${}_JF_{J-1}$ to arbitrary order in a small quantity around integer-valued parameters. These expansions are required for example in the computation of multi-loop or multi-particle phase space integrals in dimensionally regularized quantum field theory.

A first application was already presented in the phase space integration of the bremsstrahlung calculation in chapter 2. Additional ones will follow in chapters 4 and 5,namely on the one hand the ϵ-expansion of the two-loop quark and gluon form factors whose exact analytic expressions contain hypergeometric functions in addition to Γ-functions. On the other hand the master integrals that contribute to the same form factors at three-loop precision.

Acknowledgements

A special thanks goes to Daniel Maître for a wonderful cooperation during all stages of development of this package and for providing the bigger part of the implementation. I would like to thank Thomas Gehrmann and Alejandro Daleo for useful discussions, a careful reading of the manuscript of Ref. [69], and for patiently testing early versions of the package. I also wish to thank Gudrun Heinrich for independent numerical checks of the series expansions using the sector decomposition [134] method described in [135–137].

Chapter 4

Two-Loop Quark and Gluon Form Factors in Dimensional Regularisation[1]

4.1 Introduction

In this chapter, we present a first application of the `HypExp` package presented in chapter 3, namely the two-loop corrections to the massless quark form factor $\gamma^* \to q\bar{q}$ and gluon form factor $H \to gg$ (effective vertex) to all orders in the dimensional regularisation parameter $\epsilon = (4-d)/2$. The all-order results contain Γ-functions in combination with hypergeometric functions of unit argument. Using the `HypExp` package, these all-order results can be expanded to any desired order, yielding Laurent expansions in ϵ.

The infrared pole structure of renormalised multi-loop amplitudes in dimensional regularisation with $d = 4 - 2\epsilon$ space-time dimensions can be predicted from an infrared factorisation formula, which was first conjectured in [138], where it was formulated up to two loops. A proof of the formula, together with an explicit formulation up to three loops was derived later in [139]. The simplest multi-loop amplitudes where the infrared factorisation formula can be applied are three-point functions, involving two partons coupled to an external current: the quark form factor $\gamma^* \to q\bar{q}$ and the gluon form factor $H \to gg$. The QCD corrections to these form factors can in particular be used to fix a priori unknown constants in the infrared factorisation formula, thus enabling an unambiguous prediction for multi-loop amplitudes involving more than two external partons.

In the infrared factorisation formula for a given form factor (or more generally for a given multi-leg amplitude) at a certain number of loops, infrared singularity operators act on the form factor evaluated with a lower number of loops. The infrared singularity operators contain explicit infrared poles $1/\epsilon^2$ and $1/\epsilon$. They do therefore project subleading terms in ϵ from the lower order form factors.

At present, two-loop corrections to the massless quark [140–142] and gluon [143] form factors are known to order ϵ^0. Two-loop corrections to this order were also obtained for massive quarks [144–146]. The infrared structure of the massless form factors and infrared cancellations with real radiation contributions are described in detail in [147–150]. Very recently, results to order ϵ^2 were obtained for the quark form factor [151].

[1] The content of this chapter has been published in Ref. [116]

The calculation of these corrections proceeds through a reduction [115, 152–155] of all two-loop Feynman integrals appearing in the form factors to a small set of master integrals. The reduction is exact in ϵ, such that the evaluation of the form factors is limited only by the order to which the master integrals can be computed. The massless two-loop form factors contain three two-loop master integrals, which can be computed either using various analytical methods [113] or numerically order-by-order in their Laurent expansion using the sector decomposition [134] algorithm [135–137]. Up to now, exact expressions were known only for two of these master integrals, while the third (the so-called two-loop crossed triangle graph) was known only as a Laurent expansion up to finite terms [111, 112, 156].

In this chapter, we derive an exact expression for the two-loop crossed triangle graph in terms of generalised hypergeometric functions of unit argument in section 4.2. Using the `HypExp`-package [69, 131] for the Laurent expansion of generalised hypergeometric functions, this can be expanded to any desired order in ϵ. Together with the exact expressions for the one- and two-loop quark and gluon form factors in section 4.3, this allows the expansion of these form factors to higher orders in ϵ. For illustration, we list the one-loop form factors to order ϵ^4 and the two-loop form factors to order ϵ^2 in section 4.4; these orders appear for example in the ultraviolet renormalisation and infrared factorisation of the corresponding three-loop from factors. Finally, section 4.5 contains conclusions and an outlook.

4.2 Two-loop master integrals

The virtual two-loop vertex master integrals were first derived to order ϵ^0 in [111, 112, 156] in the context of the calculation of the two-loop quark form factor [140–142]. All but the crossed triangle graph A_6 can be expressed in terms of Γ-functions to all orders in ϵ.

Factoring out a common

$$S_\Gamma = \left(\frac{(4\pi)^\epsilon}{16\pi^2\,\Gamma(1-\epsilon)}\right), \tag{4.1}$$

and introducing $q^2 = (p_1+p_2)^2$, they read

$A_{2,\mathrm{LO}}$ =

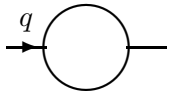

$$= \int \frac{\mathrm{d}^d k}{(2\pi)^d} \frac{1}{k^2(k-p_1-p_2)^2}$$
$$= S_\Gamma \left(-q^2 - i0\right)^{-\epsilon} \frac{\Gamma(1+\epsilon)\Gamma^3(1-\epsilon)}{\Gamma(2-2\epsilon)} \frac{i}{\epsilon}, \tag{4.2}$$

A_3 =

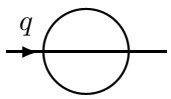

$$= \int \frac{\mathrm{d}^d k}{(2\pi)^d} \int \frac{\mathrm{d}^d l}{(2\pi)^d} \frac{1}{k^2 l^2 (k-l-p_1-p_2)^2}$$
$$= S_\Gamma^2 \left(-q^2 - i0\right)^{1-2\epsilon} \frac{\Gamma(1+2\epsilon)\Gamma^5(1-\epsilon)}{\Gamma(3-3\epsilon)} \frac{-1}{2(1-2\epsilon)\epsilon}, \tag{4.3}$$

$$
\begin{aligned}
A_4 \;=\; & \\
&= \int \frac{\mathrm{d}^d k}{(2\pi)^d} \int \frac{\mathrm{d}^d l}{(2\pi)^d} \frac{1}{k^2 l^2 (k-p_1-p_2)^2 (k-l-p_1)^2} \\
&= S_\Gamma^2 \left(-q^2 - i0\right)^{-2\epsilon} \frac{\Gamma(1-2\epsilon)\Gamma(1+\epsilon)\Gamma^4(1-\epsilon)\Gamma(1+2\epsilon)}{\Gamma(2-3\epsilon)} \frac{-1}{2(1-2\epsilon)\epsilon^2} \,. \qquad (4.4)
\end{aligned}
$$

No exact expression for A_6 was known up to now. Following the steps outlined in [111, 112, 156], we obtain

$$
\begin{aligned}
A_6 \;=\; & \\
&= \int \frac{\mathrm{d}^d k}{(2\pi)^d} \int \frac{\mathrm{d}^d l}{(2\pi)^d} \frac{1}{k^2 l^2 (k-p_1-p_2)^2 (k-l)^2 (k-l-p_2)^2 (l-p_1)^2} \\
&= S_\Gamma^2 \left(-q^2 - i0\right)^{-2-2\epsilon} \left[- \frac{\Gamma^3(1-\epsilon)\,\Gamma(1+\epsilon)\,\Gamma^4(1-2\epsilon)\,\Gamma^3(1+2\epsilon)}{\epsilon^4\,\Gamma^2(1-4\epsilon)\,\Gamma(1+4\epsilon)} \right. \\
&\quad + \frac{\Gamma^4(1-\epsilon)\,\Gamma(1+\epsilon)\,\Gamma(1-2\epsilon)\,\Gamma(1+2\epsilon)}{2\,\epsilon^4\,\Gamma(1-3\epsilon)}\; {}_3F_2(1,-4\epsilon,-2\epsilon;1-3\epsilon,1-2\epsilon;1) \\
&\quad - \frac{4\,\Gamma^4(1-\epsilon)\,\Gamma(1-2\epsilon)\,\Gamma(1+2\epsilon)}{\epsilon^2\,(1+\epsilon)\,(1+2\epsilon)\,\Gamma(1-4\epsilon)}\; {}_3F_2(1,1,1+2\epsilon;2+\epsilon,2+2\epsilon;1) \\
&\quad \left. - \frac{\Gamma^5(1-\epsilon)\,\Gamma(1+2\epsilon)}{2\,\epsilon^4\,\Gamma(1-3\epsilon)}\; {}_4F_3(1,1-\epsilon,-4\epsilon,-2\epsilon;1-3\epsilon,1-2\epsilon,1-2\epsilon;1) \right] \,. \qquad (4.5)
\end{aligned}
$$

While $A_{2,LO}$, A_3 and A_4 can be expanded using any standard computer algebra programme, the expansion of A_6 requires the expansion of generalised hypergeometric functions in their parameters. For this purpose the `HypExp` [69, 131] package is well suited, and it allows us to derive the eighth-order expansion

$$
\begin{aligned}
A_6 \;=\; & S_\Gamma^2 \left(-q^2 - i0\right)^{-2-2\epsilon} \left[- \frac{1}{\epsilon^4} + \frac{5\pi^2}{6\epsilon^2} + \frac{27}{\epsilon}\zeta_3 + \frac{23\pi^4}{36} + \left(117\zeta_5 - 8\pi^2\zeta_3\right)\epsilon \right. \\
& + \left(\frac{19\pi^6}{315} - 267\zeta_3^2\right)\epsilon^2 + \left(-\frac{109\pi^4}{10}\zeta_3 - 40\pi^2\zeta_5 - 6\zeta_7\right)\epsilon^3 \\
& \left. + \left(44\pi^2\zeta_3^2 - \frac{1073\pi^8}{3024} - 2466\,\zeta_3\,\zeta_5 + 264\zeta_{5,3}\right)\epsilon^4 + \mathcal{O}(\epsilon^5) \right] \,, \qquad (4.6)
\end{aligned}
$$

where we encountered a multiple zeta value [157] (see also appendix B.4) in the last term.

4.3 Quark and gluon form factors at two loops

The tree-level quark and gluon form factors are obtained by normalising the corresponding tree-level vertex functions to unity:

$$
F_q^{(0l)} = 1 \,, \qquad F_g^{(0l)} = 1 \,. \qquad (4.7)
$$

The unrenormalised one-loop and two-loop form factors are calculated from the relevant Feynman diagrams. Using integration-by-parts [152, 153] and Lorentz invariance [115] identities (which can be solved symbolically for massless two-loop vertex integrals, see the appendix of [158]), these can be reduced [115, 154, 155] to the master integrals listed in section 4.2.

The unrenormalised one-loop quark and gluon form factors read[2]:

$$F_q^{(1l,B)} = -ig^2\,\frac{N^2-1}{N}\,\frac{d^2-7d+16}{2\,(d-4)}\,A_{2,\mathrm{LO}}\,, \tag{4.8}$$

$$F_g^{(1l,B)} = ig^2\,N\,\frac{d^3-16d^2+68d-88}{(d-4)\,(d-2)}\,A_{2,\mathrm{LO}}\,, \tag{4.9}$$

where $N = 3$ is the number of colours and g is the bare QCD coupling parameter.

The unrenormalised two-loop quark and gluon form factors for N_F massless quark flavours are [147, 149]:

$$\begin{aligned}
F_q^{(2l,B)} = g^4\,\frac{N^2-1}{N}\Bigg\{ & -\frac{N^2-1}{N}\,\frac{(d^2-7d+16)^2}{4\,(d-4)^2}\,A_{2,\mathrm{LO}}^2 \\
& +N\,\frac{(d^5-18d^4+138d^3-552d^2+1144d-980)\,(3d-8)}{2\,(d-3)\,(d-4)^3}\,\frac{A_3}{q^2} \\
& +\frac{1}{N}\,\frac{(9d^6-358d^5+4309d^4-24466d^3+72896d^2-110064d+66080)\,(3d-8)}{16(d-3)(d-4)^3(2d-7)}\,\frac{A_3}{q^2} \\
& +N\,\frac{3d^6-82d^5+819d^4-4030d^3+10344d^2-12824d+5632}{4\,(d-1)\,(d-4)^2\,(3d-8)}\,A_4 \\
& -\frac{1}{N}\,\frac{(21d^6-789d^5+9422d^4-53864d^3+163200d^2-253472d+159232)}{16\,(3d-8)\,(2d-7)\,(d-4)^2}\,A_4 \\
& +N_F\,\frac{(3d^3-31d^2+110d-128)\,(d-2)}{2\,(d-1)\,(d-4)\,(3d-8)}\,A_4 \\
& -\frac{1}{N}\,\frac{d^3-20d^2+104d-176}{32\,(2d-7)}(q^2)^2\,A_6\Bigg\}\,,
\end{aligned} \tag{4.10}$$

$$\begin{aligned}
F_g^{(2l,B)} = g^4\Bigg\{ & -N^2\,\frac{(d^3-16d^2+68d-88)^2}{(d-4)^2\,(d-2)^2}\,A_{2,\mathrm{LO}}^2 \\
& -N^2\,\frac{1}{2\,(d-1)\,(d-2)^2\,(d-3)\,(d-4)^3\,(2d-5)\,(2d-7)}\Big(192d^{10}-6947d^9 \\
& \quad +105470d^8-907248d^7+4958664d^6-18113645d^5+44930982d^4 \\
& \quad -74791460d^3+79854504d^2-49204128d+13194496\Big)\,\frac{A_3}{q^2} \\
& -N\,N_F\,\frac{2d^6-45d^5+377d^4-1610d^3+3868d^2-5136d+3008}{(d-1)\,(d-2)\,(d-3)\,(d-4)^2}\,\frac{A_3}{q^2} \\
& +\frac{N_F}{N}\,\frac{1}{4\,(d-2)\,(d-3)\,(d-4)^2\,(2d-5)\,(2d-7)}\Big(70d^7-1663d^6+16290d^5 \\
& \quad -86031d^4+266004d^3-483356d^2+479360d-200704\Big)\,\frac{A_3}{q^2}
\end{aligned}$$

[2]Eqs. (4.8) – (4.11) are courtesy of Thomas Gehrmann, see also Refs. [147, 149].

$$
\begin{aligned}
&-N^2\,\frac{1}{2\,(d-1)\,(d-2)^2\,(d-4)^2\,(2d-5)\,(2d-7)}\,\Big(108d^8-2661d^7+28822d^6\\
&\qquad -177546d^5+674735d^4-1607602d^3+2325996d^2-1848920d+607968\Big)\,A_4\\
&+N\,N_F\,\frac{2d^4-28d^3+130d^2-228d+104}{(d-1)\,(d-2)\,(d-4)}\,A_4\\
&-\frac{N_F}{N}\,\frac{(46d^4-545d^3+2395d^2-4606d+3248)\,(d-6)}{4\,(d-2)\,(d-4)\,(2d-5)\,(2d-7)}\,A_4\\
&-N^2\,\frac{3\,(3d-8)\,(d-3)}{4\,(2d-5)\,(2d-7)}(q^2)^2\,A_6\\
&-\frac{N_F}{N}\,\frac{(d-4)\,(2d^3-25d^2+94d-112)}{8\,(d-2)\,(2d-5)\,(2d-7)}(q^2)^2\,A_6\Big\}\,. \qquad (4.11)
\end{aligned}
$$

The renormalised form factors are obtained by introducing the renormalised QCD coupling constant and the renormalised effective coupling of H to the gluon field strength [143], and subsequent expansion in powers of the renormalised coupling.

4.4 Expansion of two-loop form factors

The renormalised form factors are expanded in the renormalised coupling constant. In the $\overline{\rm MS}$ scheme, the bare coupling $\alpha_0 = g^2/(4\pi)$ is related to the renormalised coupling $\alpha_s \equiv \alpha_s(\mu^2)$, evaluated at the renormalisation scale μ^2 by

$$
\alpha_0\mu_0^{2\epsilon}S_\epsilon = \alpha_s\mu^{2\epsilon}\left[1-\frac{11N-2N_F}{6\epsilon}\left(\frac{\alpha_s}{2\pi}\right)+\mathcal{O}(\alpha_s^2)\right]\,, \qquad (4.12)
$$

where

$$
S_\epsilon = (4\pi)^\epsilon e^{-\epsilon\gamma} \qquad \text{with the Euler constant } \gamma = 0.5772\ldots
$$

and μ_0^2 is the mass parameter introduced in dimensional regularisation to maintain a dimensionless coupling in the QCD Lagrangian density. For simplicity, we set $\mu^2 = q^2$. If the squared momentum transfer q^2 is space-like ($q^2 < 0$), the form factors are real, while they acquire imaginary parts for time-like q^2. These imaginary parts (and corresponding real parts) arise from the ϵ-expansion of

$$
\Delta(q^2) = (-\mathrm{sgn}(q^2) - i0)^{-\epsilon}\,. \qquad (4.13)
$$

The renormalised form factors can then be written as

$$
F_{q,g}(q^2) = 1+\left(\frac{\alpha_s}{2\pi}\,\Delta(q^2)\right)F_{q,g}^{(1)}+\left(\frac{\alpha_s}{2\pi}\,\Delta(q^2)\right)^2F_{q,g}^{(2)}+\mathcal{O}(\alpha_s^3)\,. \qquad (4.14)
$$

Expanding the first and second order coefficients of the form factors to ϵ^4 and ϵ^2

respectively, we obtain:

$$
\begin{aligned}
F_q^{(1)} &= \left(N-\frac{1}{N}\right)\left[-\frac{1}{2\epsilon^2}-\frac{3}{4\epsilon}-2+\frac{\pi^2}{24}+\left(-4+\frac{\pi^2}{16}+\frac{7}{6}\zeta_3\right)\epsilon\right.\\
&+\left(-8+\frac{\pi^2}{6}+\frac{7}{4}\zeta_3-\frac{47\pi^4}{2880}\right)\epsilon^2\\
&+\left(-16-\frac{7\pi^2}{72}\zeta_3+\frac{14}{3}\zeta_3+\frac{31}{10}\zeta_5+\frac{\pi^2}{3}+\frac{47\pi^4}{1920}\right)\epsilon^3\\
&\left.+\left(-32-\frac{7\pi^2}{48}\zeta_3+\frac{28}{3}\zeta_3-\frac{49}{36}\zeta_3^2+\frac{93}{20}\zeta_5+\frac{2\pi^2}{3}+\frac{47\pi^4}{720}+\frac{949\pi^6}{241920}\right)\epsilon^4\right]+\mathcal{O}(\epsilon^5)\,,
\end{aligned}
\tag{4.15}
$$

$$
\begin{aligned}
F_g^{(1)} &= N\left[-\frac{1}{\epsilon^2}-\frac{11}{6\epsilon}+\frac{\pi^2}{12}+\left(-1+\frac{7}{3}\zeta_3\right)\epsilon+\left(-3+\frac{47\pi^4}{1440}\right)\epsilon^2\right.\\
&+\left(-7-\frac{7\pi^2}{36}\zeta_3+\frac{31}{5}\zeta_5+\frac{\pi^2}{12}\right)\epsilon^3\\
&\left.+\left(-15+\frac{7}{3}\zeta_3-\frac{49}{18}\zeta_3^2+\frac{\pi^2}{4}+\frac{949\pi^6}{120960}\right)\epsilon^4\right]+\frac{N_F}{3\epsilon}+\mathcal{O}(\epsilon^5)\,,
\end{aligned}
\tag{4.16}
$$

$$
\begin{aligned}
F_q^{(2)} &= \left(N-\frac{1}{N}\right)\left\{N\left[\frac{1}{8\epsilon^4}+\frac{17}{16\epsilon^3}+\frac{433}{288\epsilon^2}\right.\right.\\
&+\frac{1}{\epsilon}\left(\frac{4045}{1728}-\frac{11\pi^2}{96}+\frac{7}{24}\zeta_3\right)+\left(-\frac{9083}{10368}-\frac{521\pi^2}{1728}+\frac{13}{18}\zeta_3+\frac{23\pi^4}{2880}\right)\\
&+\left(-\frac{1244339}{62208}-\frac{11\pi^2}{48}\zeta_3+\frac{4235}{432}\zeta_3+\frac{163}{40}\zeta_5-\frac{10427\pi^2}{10368}+\frac{29\pi^4}{1440}\right)\epsilon\\
&+\left(-\frac{36528395}{373248}-\frac{77\pi^2}{432}\zeta_3+\frac{109019}{2592}\zeta_3-\frac{403}{72}\zeta_3^2+\frac{529}{30}\zeta_5\right.\\
&\left.\left.\left.-\frac{181451\pi^2}{62208}+\frac{8759\pi^4}{51840}+\frac{47\pi^6}{7560}\right)\epsilon^2\right]\\
&+\frac{1}{N}\left[-\frac{1}{8\epsilon^4}-\frac{3}{8\epsilon^3}+\frac{1}{\epsilon^2}\left(-\frac{41}{32}+\frac{\pi^2}{48}\right)\right.\\
&+\frac{1}{\epsilon}\left(-\frac{221}{64}+\frac{4}{3}\zeta_3\right)+\left(-\frac{1151}{128}-\frac{17\pi^2}{192}+\frac{29}{8}\zeta_3+\frac{13\pi^4}{576}\right)\\
&+\left(-\frac{5741}{256}-\frac{7\pi^2}{18}\zeta_3+\frac{839}{48}\zeta_3+\frac{23}{10}\zeta_5-\frac{71\pi^2}{128}+\frac{19\pi^4}{320}\right)\epsilon\\
&+\left(-\frac{27911}{512}-\frac{9\pi^2}{16}\zeta_3+\frac{6989}{96}\zeta_3-\frac{163}{9}\zeta_3^2+\frac{231}{40}\zeta_5\right.\\
&\left.\left.-\frac{613\pi^2}{256}+\frac{3401\pi^4}{11520}-\frac{223\pi^6}{17280}\right)\epsilon^2\right]\\
&+N_F\left[-\frac{1}{8\epsilon^3}-\frac{1}{18\epsilon^2}+\frac{1}{\epsilon}\left(\frac{65}{432}+\frac{\pi^2}{48}\right)+\left(\frac{4085}{2592}+\frac{23\pi^2}{432}+\frac{1}{36}\zeta_3\right)\right.
\end{aligned}
$$

$$+\left(\frac{108653}{15552}-\frac{119}{108}\zeta_3+\frac{497\pi^2}{2592}+\frac{\pi^4}{1440}\right)\epsilon$$
$$+\left(\frac{2379989}{93312}-\frac{5\pi^2}{54}\zeta_3-\frac{3581}{648}\zeta_3-\frac{59}{60}\zeta_5+\frac{9269\pi^2}{15552}-\frac{145\pi^4}{10368}\right)\epsilon^2\Bigg]\Bigg\}+\mathcal{O}(\epsilon^3)\,, \tag{4.17}$$

$$\begin{aligned}
F_g^{(2)} &= N^2\left[\frac{1}{2\epsilon^4}+\frac{77}{24\epsilon^3}+\frac{1}{\epsilon^2}\left(\frac{175}{72}-\frac{\pi^2}{24}\right)\right.\\
&+\frac{1}{\epsilon}\left(-\frac{119}{54}-\frac{25}{12}\zeta_3-\frac{11\pi^2}{144}\right)+\left(\frac{8237}{648}-\frac{33}{4}\zeta_3+\frac{67\pi^2}{144}-\frac{7\pi^4}{240}\right)\\
&+\left(\frac{200969}{3888}+\frac{23\pi^2}{72}\zeta_3-\frac{1139}{108}\zeta_3+\frac{71}{20}\zeta_5+\frac{53\pi^2}{108}-\frac{1111\pi^4}{8640}\right)\epsilon\\
&+\left(\frac{4082945}{23328}-\frac{11\pi^2}{216}\zeta_3-\frac{13109}{162}\zeta_3+\frac{901}{36}\zeta_3^2-\frac{341}{20}\zeta_5\right.\\
&\left.\left.+\frac{85\pi^2}{1296}-\frac{1943\pi^4}{8640}+\frac{257\pi^6}{6720}\right)\epsilon^2\right]\\
&+N\,N_F\left[-\frac{7}{12\epsilon^3}-\frac{13}{12\epsilon^2}+\frac{1}{\epsilon}\left(\frac{155}{216}+\frac{\pi^2}{72}\right)\right.\\
&+\left(-\frac{5905}{1296}+\frac{1}{2}\zeta_3-\frac{5\pi^2}{72}\right)+\left(-\frac{162805}{7776}-\frac{95}{54}\zeta_3-\frac{11\pi^2}{432}+\frac{7\pi^4}{1440}\right)\epsilon\\
&\left.+\left(-\frac{3663205}{46656}+\frac{31\pi^2}{108}\zeta_3+\frac{274}{81}\zeta_3-\frac{9}{10}\zeta_5+\frac{883\pi^2}{2592}-\frac{73\pi^4}{2592}\right)\epsilon^2\right]\\
&+\frac{N_F}{N}\left[-\frac{1}{8\epsilon}+\left(\frac{67}{48}-\zeta_3\right)+\left(\frac{2027}{288}-\frac{23}{6}\zeta_3-\frac{7\pi^2}{144}-\frac{\pi^4}{54}\right)\epsilon\right.\\
&\left.+\left(\frac{47491}{1728}+\frac{5\pi^2}{18}\zeta_3-\frac{281}{18}\zeta_3-4\zeta_5-\frac{209\pi^2}{864}-\frac{23\pi^4}{324}\right)\epsilon^2\right]+N_F^2\,\frac{1}{9\epsilon^2}+\mathcal{O}(\epsilon^3)\,.
\end{aligned} \tag{4.18}$$

4.5 Conclusions and outlook

In this chapter, we computed the two-loop quark and gluon form factors to all orders in the dimensional regularisation parameter ϵ. The principal ingredient to this calculation is the two-loop crossed triangle graph A_6, for which we computed an exact expression in terms of generalised hypergeometric functions of unit argument, which can be expanded to any desired order in ϵ using the `HypExp`-package.

A potential application of the form factors derived here is the extraction of the complete set of infrared pole terms of the genuine three-loop quark form factor from the recently derived three-loop splitting and coefficient functions in deep inelastic scattering [159–162]. In turn, these allow to fix the yet unknown hard radiation constants in the infrared factorisation formula at three loops. Parts of these constants were derived previously from $\mathcal{N}=4$ supersymmetry relations [163, 164].

The two-loop vertex master integrals feature as subtopologies in the reduction of the three-loop form factor contributions, appearing if one of the three loops is disconnected from the others by pinching the connecting propagators. In this case, their terms to ϵ^2 are required.

The calculation presented here illustrates the applicability of the `HypExp`-package in the calculation of multi-loop corrections in quantum field theory. Functions similar to those which were expanded here appear also in multi-particle phase space integrals in massless [67] and massive decay processes [39]. Since all these integrals correspond to particular cuts of multi-loop two-point functions, one might expect that three-loop and four-loop two-point functions could also be expanded using `HypExp` to high orders in ϵ, as required for multi-loop calculations of fully inclusive observables [165].

While finalising the paper to this chapter, an independent paper addressing very similar issues appeared. In Ref. [151], Moch, Vermaseren and Vogt compute the two-loop quark form factor to order ϵ^2 and apply it in the extraction of the pole parts of the three-loop quark form factor from deep inelastic coefficient functions. In this paper, the hard radiation constants for infrared factorisation at three-loops and related resummation coefficients are extracted for processes involving quarks only. Expanding our unrenormalised quark form factor (4.10) to order ϵ^2, we confirm the result (B.1) of Ref. [151].

Acknowledgements

I wish to thank Gudrun Heinrich for independent numerical checks of the `HypExp` Laurent expansions using the sector decomposition [134] method described in [135–137].

Chapter 5

Scalar Three-Loop Master Integrals in Massless QCD[1]

5.1 Introduction

In this chapter we evaluate scalar three-loop master integrals with three external legs, an incoming, off-shell one and two outgoing ones, both of the latter being on-shell. The two on-shell legs are considered massless as well as all internal propagators. The computation will be done in dimensional regularization, with $D = 4-2\epsilon$ being the number of dimensions. Dimensional regularization does not introduce any dimensionful parameter, hence there is only one single scale $q^2 = (p_1 + p_2)^2$, with p_1 and p_2 being the momenta of the external on-shell lines. Dimensional regularization will be used to regularize both ultra-violet and infrared singularities, which in the final result show up as poles in ϵ.

The three-loop master integrals are major ingredients to the quark form factor $\gamma^* \to q\,\bar{q}$ and gluon form factor $H \to gg$ to three-loop precision. The three-loop form factors contribute to NNNLO corrections to $gg \to H$ and $q\bar{q} \to W$, Z (Drell-Yan process). Starting from these form factors, the total cross section for these processes can be computed in a soft plus virtual approximation (cf. Refs. [167–169] for the NNLO $gg \to H$ case).

As we have already mentioned in the last chapter, further applications are related to the resummation of infrared and collinear contributions to the form factors via evolution equations in q^2. The connection between resummation and higher order perturbative results has been already pointed out in Ref. [151], where also the implications of the structure function F_2 in photon-exchange DIS [161] on the quark form factor and its resummation was worked out. Furthermore, the form factors allow to extract some resummation coefficients in the Collins-Soper-Sterman formalism [170, 171] – e.g. for the p_T-distribution of Z-bosons at small p_T.

There are in total 16 master integrals of the considered type. They can be obtained from Ref. [172] by cutting internal lines of the two point four loop integrals in such a way as to produce three-loop three point functions. By doing this, we keep only diagrams which do not factorize into a two loop times a one loop integral or into a one loop integral to the third power. The diagrams are displayed pictorially in Figure 5.1. The number of propagators ranges from five to nine. Six of the diagrams contain bubble insertions (diagrams $A_{5,1}$, $A_{5,2}$, $A_{6,1}$, $A_{6,3}$, $A_{7,1}$, $A_{7,2}$), whereas the other ten are of genuine three-

[1]The content of this chapter appeared, in part, in Ref. [166]

loop type. Seven of the diagrams ($A_{5,1}$, $A_{5,2}$, $A_{6,1}$, $A_{6,2}$, $A_{6,3}$, $A_{7,3}$, $A_{9,1}$) have a planar topology, the remaining nine are crossed.

The evaluation of the corresponding integrals gets considerably more complicated with increasing number of propagators, the absence of bubble insertions and/or the advent of crossed topologies. Another citerion is that diagrams in which the outermost vertex of an outgoing line connects only three lines are simpler than those in which four lines – none of which belonging to a bubble insertion – are connected. In this work, the results of all diagrams with at most seven propagators will be presented (with the exception of $A_{7,5}$).

As is obvious, the scale q^2 factors out of each integral after integration over the loop momenta. The remaining integral over Feynman parameters therefore contains – besides the Feynman parameters themselves – the regulator ϵ as the only parameter. It turns out that we will be able to obtain the results of some of the diagrams (namely $A_{5,1}$, $A_{5,2}$, $A_{6,1}$, $A_{6,3}$, $A_{7,1}$, $A_{7,2}$, $A_{7,4}$) in a closed form. The corresponding expressions will contain Γ-functions and hypergeometric functions of unit argument. As has been discussed in great datail in previous chapters, these all-order results can be expanded in a Laurent series in ϵ by means of `Mathematica` [68] and the dedicated package `HypExp` [69].

Of the integrals that can – to our knowledge – not be displayed in a closed form, we give intermediate results from which the coefficients of the Laurent expansions in ϵ can be obtained in an analytic form. In order to extract the three-loop form factors to order $\mathcal{O}(\epsilon^0)$, we need to compute all those coefficients of the master integrals with values of the Riemann ζ-function [132, 173, 174] up to and including transcendentality six.

As important checks for our findings we have on the one hand the independent computations of Refs. [166, 175]. On the other hand, all coefficients of the Laurent series expansions can be computed numerically using the sector decomposition [134] method of Refs. [135–137]. The comparison between analytical and numerical results for the coefficients gives agreement with a precision of well below 1%.

5.2 Master Integrals

In this section we list the results we obtained for the three-loop master integrals. The labelling of the diagrams is according to Figure 5.1. The results for the diagrams $A_{5,1}$, $A_{5,2}$, and $A_{6,1}$ can be given for arbitrary propagator powers ν_i. The values of the ν_i are assumed to be such that the arguments of all occurring Γ-functions are different from $0, -1, -2, \ldots$.

In our first diagram, namely $A_{5,1}$, we label the powers of the sloped propagators by ν_1 and ν_2, whereas ν_3, ν_4, and ν_5 are associated with the three propagators that form the twofold bubble insertion. The form of the diagram immediately suggests that the result must be completely symmetric in $\{\nu_1, \nu_2\}$ as well as in $\{\nu_3, \nu_4, \nu_5\}$. The calculation leads to

$$\begin{aligned} A_{5,1}\left[\nu_i\right] &= \int\frac{d^Dk}{(2\pi)^D}\int\frac{d^Dl}{(2\pi)^D}\int\frac{d^Dm}{(2\pi)^D}\,\frac{1}{[(k+p_1)^2]^{\nu_1}\,[(k-p_2)^2]^{\nu_2}\,[l^2]^{\nu_3}\,[(k+l+m)^2]^{\nu_4}\,[m^2]^{\nu_5}} \\ &= \frac{i\,(-1)^{1-N}}{(4\pi)^{3D/2}}\,\left[-\,q^2-i\,\eta\right]^{3D/2-N}\,\frac{\Gamma(\frac{D}{2}-\nu_3)\,\Gamma(\frac{D}{2}-\nu_4)\,\Gamma(\frac{D}{2}-\nu_5)}{\Gamma(\nu_1)\,\Gamma(\nu_2)\,\Gamma(\nu_3)\,\Gamma(\nu_4)\,\Gamma(\nu_5)} \\ &\quad\times\frac{\Gamma(N-\frac{3\,D}{2})\,\Gamma(\nu_{345}-D)\,\Gamma(\frac{3\,D}{2}-N+\nu_1)\,\Gamma(\frac{3\,D}{2}-N+\nu_2)}{\Gamma(\frac{3\,D}{2}-\nu_{345})\,\Gamma(2D-N)}\;, \end{aligned} \tag{5.1}$$

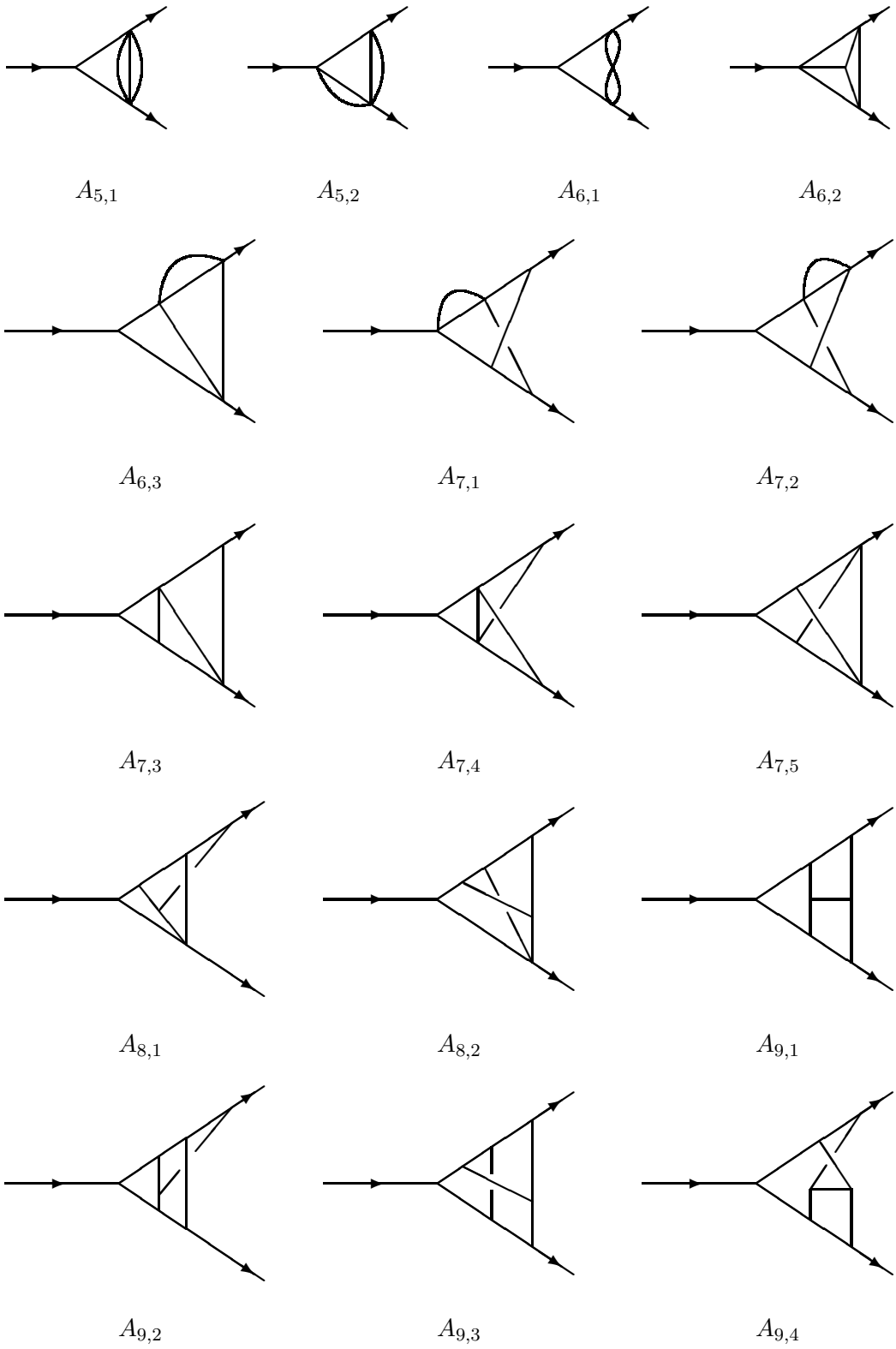

Figure 5.1: Three-loop master integrals with massless propagators. The incoming momentum is $q = p_1 + p_2$. Outgoing lines are considered on-shell and massless, i.e. $p_1^2 = p_2^2 = 0$.

where we introduced the short-hand notations

$$\nu_{ijk\ldots} = \nu_i + \nu_j + \nu_k + \ldots \tag{5.2}$$
$$N = \nu_{12345} \ . \tag{5.3}$$

In the above equation (5.1), $\eta > 0$ is an infinitesimal quantity that indicates the way in which the analytical continuation has to be performed in the case $q^2 > 0$.

In the special case in which all ν_i are equal to unity, the result simplifies considerably. Defining the prefactor S_Γ as

$$S_\Gamma = \frac{1}{(4\pi)^{D/2}\,\Gamma(1-\epsilon)} \ , \tag{5.4}$$

we have

$$A_{5,1}\,[\nu_i = 1] = i\,S_\Gamma^3\,\left[-\,q^2 - i\,\eta\right]^{1-3\,\epsilon}\,\frac{\Gamma^6(1-\epsilon)\,\Gamma(2\,\epsilon)\,\Gamma(3\,\epsilon)\,\Gamma(1-3\,\epsilon)}{(1-2\,\epsilon)\,(2-3\,\epsilon)\,\Gamma(3-4\,\epsilon)} \ . \tag{5.5}$$

In the next diagram, $A_{5,2}$, the power of the upper sloped propagator is labeled by ν_1. ν_2 and ν_3 are the powers of the propagators of the lower bubble insertion, whereas ν_4 and ν_5 are associated with the propagators of the vertical bubble. From the form of the diagram we can read off that the result will be symmetric in $\{\nu_2, \nu_3\}$ as well as in $\{\nu_4, \nu_5\}$. It reads

$$\begin{aligned} A_{5,2}\,[\nu_i] &= \int\frac{d^Dk}{(2\pi)^D}\int\frac{d^Dl}{(2\pi)^D}\int\frac{d^Dm}{(2\pi)^D}\,\frac{1}{[(k+p_1)^2]^{\nu_1}\,[(l-k+p_2)^2]^{\nu_2}\,[l^2]^{\nu_3}\,[(k+m)^2]^{\nu_4}\,[m^2]^{\nu_5}} \\ &= \frac{i\,(-1)^{1-N}}{(4\pi)^{3D/2}}\,\left[-\,q^2 - i\,\eta\right]^{3D/2-N}\,\frac{\Gamma(\frac{D}{2}-\nu_2)\,\Gamma(\frac{D}{2}-\nu_3)\,\Gamma(\frac{D}{2}-\nu_4)\,\Gamma(\frac{D}{2}-\nu_5)}{\Gamma(\nu_1)\,\Gamma(\nu_2)\,\Gamma(\nu_3)\,\Gamma(\nu_4)\,\Gamma(\nu_5)} \\ &\quad\times\frac{\Gamma(N-\frac{3\,D}{2})\,\Gamma(D-\nu_{145})\,\Gamma(\nu_{45}-\frac{D}{2})\,\Gamma(\frac{3\,D}{2}-N+\nu_1)}{\Gamma(D-\nu_{23})\,\Gamma(D-\nu_{45})\,\Gamma(2D-N)} \ . \end{aligned} \tag{5.6}$$

Again, the case in which all ν_i are equal to unity is much simpler, namely

$$A_{5,2}\,[\nu_i = 1] = -i\,S_\Gamma^3\,\left[-\,q^2 - i\,\eta\right]^{1-3\,\epsilon}\,\frac{\Gamma^7(1-\epsilon)\,\Gamma(\epsilon)\,\Gamma(3\,\epsilon)\,\Gamma(1-3\,\epsilon)}{(1-2\,\epsilon)\,\Gamma(2-2\,\epsilon)\,\Gamma(3-4\,\epsilon)} \ . \tag{5.7}$$

The last diagram with two bubble insertions is $A_{6,1}$. Again, ν_1 and ν_2 are the powers of the sloped propagators. ν_3 and ν_4 form the powers of the upper bubble insertion, whereas ν_5 and ν_6 are given to the lower one. The diagram also adopts several symmetries, namely in $\{\nu_1, \nu_2\}$, $\{\nu_3, \nu_4\}$, $\{\nu_5, \nu_6\}$, and, in addition, in $\{\{\nu_3, \nu_4\}, \{\nu_5, \nu_6\}\}$. One finds

$$\begin{aligned} A_{6,1}\,[\nu_i] &= \int\frac{d^Dk}{(2\pi)^D}\int\frac{d^Dl}{(2\pi)^D}\int\frac{d^Dm}{(2\pi)^D}\,\frac{1}{[(k+p_1)^2]^{\nu_1}\,[(k-p_2)^2]^{\nu_2}} \\ &\qquad\times\frac{1}{[l^2]^{\nu_3}\,[(l+k)^2]^{\nu_4}\,[m^2]^{\nu_5}\,[(m+k)^2]^{\nu_6}} \\ &= \frac{i\,(-1)^{1-N}}{(4\pi)^{3D/2}}\,\left[-\,q^2 - i\,\eta\right]^{3D/2-N}\,\frac{\Gamma(\frac{D}{2}-\nu_3)\,\Gamma(\frac{D}{2}-\nu_4)\,\Gamma(\frac{D}{2}-\nu_5)\,\Gamma(\frac{D}{2}-\nu_6)}{\Gamma(\nu_1)\,\Gamma(\nu_2)\,\Gamma(\nu_3)\,\Gamma(\nu_4)\,\Gamma(\nu_5)\,\Gamma(\nu_6)} \\ &\quad\times\frac{\Gamma(N-\frac{3\,D}{2})\,\Gamma(\nu_{34}-\frac{D}{2})\,\Gamma(\nu_{56}-\frac{D}{2})\,\Gamma(\frac{3\,D}{2}-N+\nu_1)\,\Gamma(\frac{3\,D}{2}-N+\nu_2)}{\Gamma(D-\nu_{34})\,\Gamma(D-\nu_{56})\,\Gamma(2D-N)} \ , \end{aligned} \tag{5.8}$$

where this time we have

$$N \;=\; \nu_{123456} \;. \tag{5.9}$$

Finally, we again give the result for the case in which all ν_i are equal to unity.

$$A_{6,1}\left[\nu_i = 1\right] \;=\; -i\,S_\Gamma^3\,\left[-\,q^2 - i\,\eta\right]^{-3\,\epsilon}\,\frac{\Gamma^7(1-\epsilon)\,\Gamma^2(\epsilon)\,\Gamma(3\,\epsilon)\,\Gamma^2(1-3\,\epsilon)}{\Gamma^2(2-2\,\epsilon)\,\Gamma(2-4\,\epsilon)} \;. \tag{5.10}$$

Since from now on the diagrams will become more and more complicated, we restrain ourselves to the case in which the powers of all propagators are equal to unity.

The next diagram to be considered is $A_{6,2}$. It will not be displayed in a closed form. Instead, we will derive a twofold Mellin-Barnes representation [113, 176, 177] from which the coefficients of the Laurent series expansion about $\epsilon = 0$ can be computed in an analytic form. Starting with

$$A_{6,2} \;=\; \int\frac{d^Dk}{(2\pi)^D}\int\frac{d^Dl}{(2\pi)^D}\int\frac{d^Dm}{(2\pi)^D}\;\frac{1}{(k+p_1)^2\;(k+l-p_2)^2\;l^2\;m^2\;(m-k)^2\;(m-k-l)^2}\;, \tag{5.11}$$

we integrate over the loop momenta in the order m, k, and l, thereby introducing five Feynman parameters that arise from the procedure of combining the six propagators. Two of the Feynman parameter integrals can be done explicitly, yielding an expression that contains a triple integral over a Meijer-G function [132, 174, 178–180] (see also appendix B.3) and that reads

$$\begin{aligned} A_{6,2} \;=\;& -i\,S_\Gamma^3\,\left[-\,q^2 - i\,\eta\right]^{-3\,\epsilon}\,\frac{\Gamma^3(1-\epsilon)\,\Gamma(3\,\epsilon)}{\Gamma(1-2\,\epsilon)\,\Gamma(2-4\,\epsilon)} \\ & \times\int\limits_0^1 dx\,dy\,dz\;x^{-\epsilon}\,(1-x)^{-3\,\epsilon}\,y^{-\epsilon}\,(1-y)^{-3\,\epsilon}\,z^{-2\,\epsilon}\,(1-z)^{-2\,\epsilon} \\ & \times G_{33}^{32}\left(x\,z + y\,(1-z)\,\middle|\,\begin{matrix}\{-1+4\,\epsilon, -1+4\,\epsilon\}\;,\;\{3\,\epsilon\} \\ \{-1+3\,\epsilon, -1+2\,\epsilon, 0\}\;,\;\{\}\end{matrix}\right) \;. \end{aligned} \tag{5.12}$$

We now make use of the contour integral representation of the Meijer-G function, Eq. (B.14), and subsequently decompose the argument via the Mellin-Barnes representation, Eq. (B.6). The integrals over x, y, and z can then be done in terms of Γ-functions. This leads us to the following double Mellin-Barnes representation for $A_{6,2}$,

$$\begin{aligned} A_{6,2} \;=\;& -i\,S_\Gamma^3\,\left[-\,q^2 - i\,\eta\right]^{-3\,\epsilon}\,\frac{\Gamma^3(1-\epsilon)\,\Gamma(3\,\epsilon)\,\Gamma^2(1-3\,\epsilon)}{\Gamma(1-2\,\epsilon)\,\Gamma(2-4\,\epsilon)}\int\limits_{c_1-i\,\infty}^{c_1+i\,\infty}\frac{dw_1}{2\pi i}\int\limits_{c_2-i\,\infty}^{c_2+i\,\infty}\frac{dw_2}{2\pi i} \\ & \times\frac{\Gamma(-1+3\,\epsilon-w_1)\,\Gamma(-1+2\,\epsilon-w_1)\,\Gamma(2-4\,\epsilon+w_1)\,\Gamma(-w_2)\,\Gamma(w_2-w_1)}{\Gamma(3\,\epsilon-w_1)\,\Gamma(2-4\,\epsilon+w_2)\,\Gamma(2-4\,\epsilon+w_1-w_2)} \\ & \times\Gamma(1-\epsilon+w_2)\,\Gamma(1-\epsilon+w_1-w_2)\,\Gamma(1-2\,\epsilon+w_2)\,\Gamma(1-2\,\epsilon+w_1-w_2) \;. \end{aligned} \tag{5.13}$$

In the above equation (5.13) the contour integrals in the complex plane are along curves that separate poles of the form $\Gamma(a - w_i)$ (right poles) from the ones arising in $\Gamma(b + w_i)$ (left poles). The most convenient choice for these curves are straight lines parallel to the imaginary axis, i. e. the real parts along the curves are constant. According to Refs. [176, 177], these real parts, together with the parameter ϵ, must be chosen in such a way as to have positive arguments in all occurring Γ-functions in order to separate left and right poles in the desired way. One verifies easily that

$$c_1 = -\frac{6}{5}\,, \qquad c_2 = -\frac{1}{2}\,, \qquad -\frac{1}{15} < \epsilon < \frac{3}{20} \tag{5.14}$$

is an appropriate choice in Eq. (5.13). From the fact that the origin lies within the allowed region for ϵ we learn that the Mellin-Barnes integration does not produce any more poles in ϵ than the one that is already present in the prefactor. Therefore the expansion in ϵ commutes with the contour integrations. Proceeding in this way, the Mellin-Barnes integrations can be done order by order in ϵ. During this procedure, the contours can be closed at infinity to either side of the complex plane and the residues inside the respective encircled region can be summed. In addition, the formulas in the appendices D and E of Ref. [113] as well as appendix B.4 of this thesis prove extremely useful. The final result for $A_{6,2}$ is

$$\begin{aligned} A_{6,2} \;=\;& i\,S_\Gamma^3\left[-q^2 - i\,\eta\right]^{-3\,\epsilon} \\ & \times \left[-\frac{2\,\zeta_3}{\epsilon} - 18\,\zeta_3 - \frac{7\pi^4}{180} + \left(-122\,\zeta_3 - \frac{7\pi^4}{20} + \frac{2\pi^2}{3}\,\zeta_3 - 10\,\zeta_5\right)\epsilon \right. \\ & \left. + \left(-738\,\zeta_3 - \frac{427\pi^4}{180} + 6\pi^2\,\zeta_3 - 90\,\zeta_5 + \frac{163\pi^6}{7560} + 76\,\zeta_3^2\right)\epsilon^2 + \mathcal{O}(\epsilon^3)\right]\,. \end{aligned} \tag{5.15}$$

The next three diagrams to be considered are $A_{6,3}$, $A_{7,1}$, and $A_{7,2}$, each of which contains a single bubble insertion. After integrating out the bubble insertion we are left over with an effective two loop diagram of one less propagator. However, one of the propagators in the effective two loop graph will carry a power that is different from unity. The two-loop crossed vertex graphs with powers different from unity were discussed previously in Ref. [181].

While computing the effective two loop diagrams, it turns out that, after integrating over the loop momenta, also all integrals over Feynman parameters can be carried out in a closed form. The respective results contain Γ-functions in combination with hypergeometric functions of unit argument. We used the aforementioned `Mathematica` [68] package `HypExp` [69] for expanding the all-order results into their respective Laurent series expansions about $\epsilon = 0$. The explicit result for $A_{6,3}$ reads

$$\begin{aligned} A_{6,3} \;=\;& \int\frac{d^Dk}{(2\pi)^D}\int\frac{d^Dl}{(2\pi)^D}\int\frac{d^Dm}{(2\pi)^D}\,\frac{1}{k^2\,(k-q)^2\,(k-l)^2\,(l-p_1)^2\,(m-l)^2\,m^2} \\ =\;& -i\,S_\Gamma\,\frac{\Gamma(\epsilon)\,\Gamma^3(1-\epsilon)}{\Gamma(2-2\,\epsilon)}\cdot I_5(\epsilon) \end{aligned} \tag{5.16}$$

with

$$\begin{aligned}
I_5(\alpha) &= -(-1)^\alpha \int\frac{d^Dk}{(2\pi)^D}\int\frac{d^Dl}{(2\pi)^D}\;\frac{1}{k^2\;(k-q)^2\;(k-l)^2\;(l-p_1)^2\;[l^2]^\alpha} \\
&= S_\Gamma^2\;\left[-q^2-i\,\eta\right]^{-\alpha-2\,\epsilon}\frac{\Gamma^3(1-\epsilon)\,\Gamma(1-\alpha-\epsilon)\,\Gamma(1-\alpha-2\,\epsilon)}{\Gamma(\alpha)\,\Gamma(2-\alpha-2\,\epsilon)\,\Gamma(2-\alpha-3\,\epsilon)} \\
&\quad\times\left[\frac{\Gamma(1-\alpha-2\,\epsilon)\,\Gamma(\alpha+2\,\epsilon)\,\Gamma(\alpha+\epsilon)\,\Gamma(\alpha)\,\Gamma(1-\alpha-\epsilon)}{\Gamma(1-\epsilon)}\right. \\
&\quad\left.+\frac{\Gamma(\alpha+2\,\epsilon-1)\,\Gamma(1-\epsilon)}{(1-2\,\epsilon)}\;{}_3F_2(1,1-\epsilon,1-2\,\epsilon\,;\,2-2\,\epsilon,2-\alpha-2\,\epsilon\,;\,1)\right]\,.
\end{aligned} \tag{5.17}$$

Substituting $\alpha=\epsilon$ in Eq. (5.17) leads to the following series expansion for $A_{6,3}$

$$\begin{aligned}
A_{6,3} &= i\,S_\Gamma^3\left[-q^2-i\,\eta\right]^{-3\,\epsilon} \\
&\quad\times\left[-\frac{1}{6\,\epsilon^3}-\frac{3}{2\,\epsilon^2}-\left(\frac{55}{6}+\frac{\pi^2}{6}\right)\frac{1}{\epsilon}-\frac{95}{2}-\frac{3\,\pi^2}{2}+\frac{17\,\zeta_3}{3}\right. \\
&\quad+\left(-\frac{1351}{6}-\frac{55\,\pi^2}{6}-\frac{\pi^4}{90}+51\,\zeta_3\right)\epsilon \\
&\quad+\left(-\frac{2023}{2}-\frac{95\,\pi^2}{2}-\frac{\pi^4}{10}+\frac{935\,\zeta_3}{3}+\frac{10\,\pi^2\,\zeta_3}{3}+65\,\zeta_5\right)\epsilon^2 \\
&\quad+\left(-\frac{26335}{6}-\frac{1351\,\pi^2}{6}-\frac{11\,\pi^4}{18}+\frac{7\,\pi^6}{54}\right. \\
&\quad\left.\left.+1615\,\zeta_3+30\,\pi^2\,\zeta_3-\frac{268\,\zeta_3^2}{3}+585\,\zeta_5\right)\epsilon^3+\mathcal{O}(\epsilon^4)\right]\;.
\end{aligned} \tag{5.18}$$

The above Eq. (5.17) can be used for two other cross checks. First, we can consider the limit $\alpha\to 0$. This is done by setting $\alpha=\xi\,\epsilon$, followed by the series expansion in ϵ. Finally, we set $\xi=0$. The result has to coincide – up to a global sign – with the series expansion of the two loop integral A_4 of Eq. (4.4). The second check is performed by the limit $\alpha\to 1$, in which case we have to find the result for the two loop five propagator integral that is obtained out of $A_{6,3}$ by removing the bubble. Both checks were found to be fulfilled on the level of the series expansions. The calculation of $I_5(\epsilon)$ by sector decomposition provided an additional check.

We now proceed with the integral $A_{7,1}$, which assumes the form

$$\begin{aligned}
A_{7,1} &= \int\frac{d^Dk}{(2\pi)^D}\int\frac{d^Dl}{(2\pi)^D}\int\frac{d^Dm}{(2\pi)^D}\;\frac{1}{m^2\;(m-k)^2\;(k-q)^2\;(k-l)^2\;(k-l-p_2)^2\;l^2\;(l-p_1)^2} \\
&= -i\,S_\Gamma\,\frac{\Gamma(\epsilon)\,\Gamma^3(1-\epsilon)}{\Gamma(2-2\,\epsilon)}\cdot I_6(\epsilon)
\end{aligned} \tag{5.19}$$

with

$$
\begin{aligned}
I_6(\alpha) &= -(-1)^\alpha \int\frac{d^Dk}{(2\pi)^D}\int\frac{d^Dl}{(2\pi)^D}\,\frac{1}{[k^2]^\alpha\,(k-q)^2\,(k-l)^2\,(k-l-p_2)^2\,l^2\,(l-p_1)^2} \\
&= S_\Gamma^2\,\left[-q^2-i\,\eta\right]^{-1-\alpha-2\,\epsilon}\,\Gamma^2(1-\epsilon)\,\Gamma^2(-\epsilon) \\
&\quad\times\left[\frac{\Gamma(-\epsilon)\,\Gamma(2\,\epsilon)}{2\,\Gamma(1-3\,\epsilon)}\,{}_4F_3(\alpha,1-\alpha-4\,\epsilon,1-\epsilon,-2\,\epsilon\,;\,1-3\,\epsilon,1-2\,\epsilon,1-2\,\epsilon\,;\,1)\right. \\
&\qquad+\frac{\Gamma(1-2\,\epsilon)\,\Gamma(1-\alpha-2\,\epsilon)\,\Gamma(2+\epsilon)\,\Gamma(\alpha+2\,\epsilon)}{\Gamma(\alpha)\,\Gamma(2-\epsilon)\,\Gamma(1-\alpha-4\,\epsilon)} \\
&\qquad\quad\times{}_4F_3(1,1,1-2\,\epsilon,2+\epsilon\,;\,2,2,2-\epsilon\,;\,1) \\
&\qquad-\frac{2\,\Gamma(-2\,\epsilon)\,\Gamma(1+\alpha+2\,\epsilon)\,\Gamma(2+\epsilon)\,\Gamma(1-\alpha-2\,\epsilon)}{\Gamma(\alpha)\,\Gamma(2-\epsilon)\,\Gamma(1-\alpha-4\,\epsilon)} \\
&\qquad\quad\times{}_4F_3(1,1,1+\alpha+2\,\epsilon,2+\epsilon\,;\,2,2,2-\epsilon\,;\,1) \\
&\qquad-\frac{\Gamma(\alpha+2\,\epsilon)\,\Gamma(2-\alpha-\epsilon)}{(1-\alpha-2\,\epsilon)^2\,\Gamma(\alpha)\,\Gamma(2-\alpha-3\,\epsilon)} \\
&\quad\times{}_4F_3(1,1-\alpha-2\,\epsilon,1-\alpha-4\,\epsilon,2-\alpha-\epsilon\,;\,2-\alpha-2\,\epsilon,2-\alpha-2\,\epsilon,2-\alpha-3\,\epsilon\,;\,1) \\
&\qquad+\frac{\Gamma(-2\,\epsilon)\,\Gamma(1+2\,\epsilon)\,\Gamma(2+\epsilon)\,\Gamma(1+\alpha+2\,\epsilon)\,\Gamma(2-\alpha-2\,\epsilon)}{\Gamma(\alpha)\,\Gamma(1-\alpha-4\,\epsilon)\,\Gamma(2-\epsilon)\,\Gamma(2+2\,\epsilon)} \\
&\qquad\quad\left.\times{}_5F_4(1,1,2-\alpha-2\,\epsilon,1+\alpha+2\,\epsilon,2+\epsilon\,;\,2,2,2-\epsilon,2+2\,\epsilon\,;\,1)\right]\,. \qquad (5.20)
\end{aligned}
$$

Again, we have to plug in $\alpha=\epsilon$ in Eq. (5.20) in order to obtain the series expansion for $A_{7,1}$. It reads

$$
\begin{aligned}
A_{7,1} &= i\,S_\Gamma^3\,\left[-q^2-i\,\eta\right]^{-1-3\,\epsilon} \\
&\quad\times\left[\frac{1}{4\,\epsilon^5}+\frac{1}{2\,\epsilon^4}+\left(1-\frac{\pi^2}{6}\right)\frac{1}{\epsilon^3}+\left(2-\frac{\pi^2}{3}-10\,\zeta_3\right)\frac{1}{\epsilon^2}\right. \\
&\qquad+\left(4-\frac{2\,\pi^2}{3}-\frac{11\,\pi^4}{45}-20\,\zeta_3\right)\frac{1}{\epsilon} \\
&\qquad+\left(8-\frac{4\,\pi^2}{3}-\frac{22\,\pi^4}{45}-40\,\zeta_3+\frac{14\,\pi^2\,\zeta_3}{3}-88\,\zeta_5\right) \\
&\qquad+\left(16-\frac{8\,\pi^2}{3}-\frac{44\,\pi^4}{45}-\frac{943\,\pi^6}{7560}-80\,\zeta_3\right. \\
&\qquad\quad\left.\left.+\frac{28\,\pi^2\,\zeta_3}{3}+196\,\zeta_3^2-176\,\zeta_5\right)\epsilon+\mathcal{O}(\epsilon^2)\right]\,. \qquad (5.21)
\end{aligned}
$$

The integral $I_6(\alpha)$ provides another cross check since for $\alpha=1$ we have to reproduce the integral A_6 of Eq. (4.5). This we checked to be the case on the level of the series expansion.

As we proceed, the expressions for the integrals become more and more lengthy. The

result for the integral $A_{7,2}$ reads

$$\begin{aligned} A_{7,2} &= \int\frac{d^Dk}{(2\pi)^D}\int\frac{d^Dl}{(2\pi)^D}\int\frac{d^Dm}{(2\pi)^D}\;\frac{1}{k^2\;(k-q)^2\;(l-p_1)^2\;(k-l)^2\;(k-l-p_2)^2\;m^2\;(m-l)^2} \\ &= -i\,S_\Gamma\,\frac{\Gamma(\epsilon)\,\Gamma^3(1-\epsilon)}{\Gamma(2-2\,\epsilon)}\cdot J_6(\epsilon) \end{aligned} \tag{5.22}$$

with

$$\begin{aligned} J_6(\alpha) &= -(-1)^\alpha\int\frac{d^Dk}{(2\pi)^D}\int\frac{d^Dl}{(2\pi)^D}\;\frac{1}{k^2\;[l^2]^\alpha\;(k-q)^2\;(l-p_1)^2\;(k-l)^2\;(k-l-p_2)^2} \\ &= S_\Gamma^2\,\left[-\,q^2-i\,\eta\right]^{-1-\alpha-2\,\epsilon}\,\Gamma(1-\epsilon)\,\Gamma(-\epsilon)\,\Gamma(1-\alpha-\epsilon) \\ &\quad\times\Bigg[-\frac{\Gamma(1-\alpha-2\,\epsilon)\,\Gamma(\alpha+\epsilon)\,\Gamma(\alpha+2\,\epsilon)\,\Gamma(1-\epsilon)\,\Gamma(-\epsilon)\,\Gamma^2(\epsilon)}{4\,\Gamma(\alpha)\,\Gamma(1-\alpha-4\,\epsilon)\,\Gamma(2\,\epsilon)} \\ &\qquad+\frac{\Gamma(1-\alpha-2\,\epsilon)\,\Gamma(\alpha+\epsilon)\,\Gamma(\alpha+2\,\epsilon)\,\Gamma(-2\,\epsilon)}{\epsilon\,\Gamma(\alpha)\,\Gamma(1-\alpha-4\,\epsilon)} \\ &\qquad-\frac{\Gamma^2(1-\alpha-2\,\epsilon)\,\Gamma(\alpha+\epsilon)\,\Gamma^2(\alpha+2\,\epsilon)\,\Gamma(\alpha+4\,\epsilon)}{\Gamma(\alpha)\,\Gamma(1+2\,\epsilon)} \\ &\qquad-\frac{\Gamma(1-\alpha-2\,\epsilon)\,\Gamma(1-\epsilon)\,\Gamma(\alpha+\epsilon)\,\Gamma(\alpha+2\,\epsilon-1)}{\Gamma(\alpha)\,\Gamma(2-\alpha-3\,\epsilon)} \\ &\qquad\quad\times{}_3F_2(1,1-\alpha-2\,\epsilon,1-\alpha-4\,\epsilon\,;\,2-\alpha-2\,\epsilon,2-\alpha-3\,\epsilon\,;\,1) \\ &\qquad+\frac{\Gamma(\alpha-1)\,\Gamma(1-\alpha-2\,\epsilon)\,\Gamma(1-\epsilon)\,\Gamma(-2\,\epsilon)\,\Gamma(1+\epsilon)\,\Gamma(1+2\,\epsilon)}{\Gamma(\alpha)\,\Gamma(1-\alpha-4\,\epsilon)\,\Gamma(2-\alpha-\epsilon)} \\ &\qquad\quad\times{}_3F_2(1-\alpha,1+\epsilon,1+2\,\epsilon\,;\,2-\alpha,2-\alpha-\epsilon\,;\,1) \\ &\qquad+\frac{\Gamma(1-\epsilon)\,\Gamma(-2\,\epsilon)\,\Gamma(1+\epsilon)\,\Gamma(1+2\,\epsilon)\,\Gamma(\alpha+\epsilon)\,\Gamma(\alpha+2\,\epsilon)}{(\alpha+4\,\epsilon)\,\Gamma(\alpha)\,\Gamma(1-\alpha-3\,\epsilon)\,\Gamma(1+\alpha+3\,\epsilon)} \\ &\qquad\quad\times{}_3F_2(1+\epsilon,1+2\,\epsilon,\alpha+4\,\epsilon\,;\,1+\alpha+3\,\epsilon,1+\alpha+4\,\epsilon\,;\,1) \\ &\qquad+\frac{\Gamma(1-2\,\epsilon)\,\Gamma(1-\alpha-2\,\epsilon)\,\Gamma(1-\epsilon)\,\Gamma(1+\alpha+\epsilon)\,\Gamma(\alpha+2\,\epsilon)}{\Gamma(1+\alpha)\,\Gamma(1-\alpha-4\,\epsilon)\,\Gamma(2-\epsilon)} \\ &\qquad\quad\times{}_4F_3(1,1,1-2\,\epsilon,1+\alpha+\epsilon\,;\,2,1+\alpha,2-\epsilon\,;\,1) \\ &\qquad+\frac{\Gamma^2(1-\epsilon)\,\Gamma(2\,\epsilon)\,\Gamma(\alpha+\epsilon)\,\Gamma(\alpha+2\,\epsilon)}{(\alpha+2\,\epsilon)\,\Gamma(\alpha)\,\Gamma(1-\alpha-3\,\epsilon)\,\Gamma(1+\alpha+\epsilon)\,\Gamma(1+2\,\epsilon)} \\ &\qquad\quad\times{}_4F_3(1,1,1-\epsilon,\alpha+2\,\epsilon\,;\,1-2\,\epsilon,1+\alpha+\epsilon,1+\alpha+2\,\epsilon\,;\,1) \\ &\qquad+\frac{\Gamma(1-\alpha-2\,\epsilon)\,\Gamma^2(1-\epsilon)\,\Gamma(\alpha+2\,\epsilon-1)}{\Gamma(2-\alpha-3\,\epsilon)\,\Gamma(1-2\,\epsilon)} \\ &\qquad\times{}_4F_3(1,1-\alpha-4\,\epsilon,1-\alpha-2\,\epsilon,1-\epsilon\,;\,2-\alpha-2\,\epsilon,2-\alpha-3\,\epsilon,1-2\,\epsilon\,;\,1) \\ &\qquad+\frac{\alpha\,\Gamma(1-\alpha-2\,\epsilon)\,\Gamma(-2\,\epsilon)\,\Gamma(\alpha+\epsilon)\,\Gamma(\alpha+2\,\epsilon)}{\Gamma(\alpha)\,\Gamma(1-\alpha-4\,\epsilon)}\;{}_3F_2(1,1,1+\alpha\,;\,2,2\,;\,1) \\ &\qquad-\frac{\Gamma(1-\alpha-2\,\epsilon)\,\Gamma(-2\,\epsilon)\,\Gamma(\alpha+\epsilon)\,\Gamma(1+\alpha+2\,\epsilon)}{\Gamma(\alpha)\,\Gamma(1-\alpha-4\,\epsilon)} \\ &\qquad\quad\times{}_3F_2(1,1,1+\alpha+2\,\epsilon\,;\,2,2\,;\,1)\Bigg]\,. \end{aligned} \tag{5.23}$$

Details about the calculation of Eq. (5.23) can be found in Ref. [175]. Useful formulas that got applied at intermediate steps were taken from Refs. [132,133,174]. Setting $\alpha = \epsilon$ leads to the following series expansion of $A_{7,2}$,

$$\begin{aligned}
A_{7,2} &= i\,S_\Gamma^3\left[-q^2 - i\,\eta\right]^{-1-3\,\epsilon} \\
&\quad \times \left[\frac{\pi^2}{12\,\epsilon^3} + \left(\frac{\pi^2}{6} + 2\,\zeta_3\right)\frac{1}{\epsilon^2} + \left(\frac{\pi^2}{3} + \frac{83\,\pi^4}{720} + 4\,\zeta_3\right)\frac{1}{\epsilon}\right. \\
&\quad + \left(\frac{2\,\pi^2}{3} + \frac{83\,\pi^4}{360} + 8\,\zeta_3 - \frac{5\,\pi^2\,\zeta_3}{3} + 15\,\zeta_5\right) \\
&\quad + \left(\frac{4\,\pi^2}{3} + \frac{83\,\pi^4}{180} + \frac{2741\,\pi^6}{90720} + 16\,\zeta_3\right. \\
&\quad \left.\left. - \frac{10\,\pi^2\,\zeta_3}{3} - 73\,\zeta_3^2 + 30\,\zeta_5\right)\epsilon + \mathcal{O}(\epsilon^2)\right] \quad . \qquad (5.24)
\end{aligned}$$

We finally state that the expression (5.23) for $J_6(\alpha)$ can again be used for several cross checks. First, in the limit $\alpha \to 1$ we have to obtain the same result as for A_6 of Eq. (4.5) or $I_6(1)$ of Eq. (5.20). The check is done by first considering $\alpha = 1 + \chi\,\epsilon$ in (5.23) followed by a subsequent expansion in ϵ. In the end, the limit $\chi \to 0$ is carried out. A second check is provided by the limit $\alpha \to 0$. We again set $\alpha = \eta\,\epsilon$ and carry out the series expansion, followed by letting $\eta \to 0$. The result has to be the same – up to a global sign – as the series expansion of $I_5(1)$ of Eq. (5.17). All checks have been verified on the level of the respective series expansions.

We now leave the bubble insertion-type integrals and will first turn our attention to integral $A_{7,3}$. This integral will be displayed, similarly to the integral $A_{6,2}$, as a multiple Mellin-Barnes representation, namely

$$\begin{aligned}
A_{7,3} &= \int\frac{d^Dk}{(2\pi)^D}\int\frac{d^Dl}{(2\pi)^D}\int\frac{d^Dm}{(2\pi)^D}\;\frac{1}{k^2\;(k+q)^2\;(l-k-p_2)^2\;(l-p_2)^2\;(m+l)^2\;m^2\;(m-p_1)^2} \\
&= i\,S_\Gamma^3\left[-q^2 - i\,\eta\right]^{-1-3\,\epsilon}\frac{\Gamma^4(1-\epsilon)\,\Gamma(-\epsilon)}{\Gamma(1-2\,\epsilon)\,\Gamma(1-3\,\epsilon)}\int\limits_{c_1-i\,\infty}^{c_1+i\,\infty}\frac{dw_1}{2\pi i}\int\limits_{c_2-i\,\infty}^{c_2+i\,\infty}\frac{dw_2}{2\pi i}\int\limits_{c_3-i\,\infty}^{c_3+i\,\infty}\frac{dw_3}{2\pi i}\;\frac{\Gamma(-w_1)}{\Gamma(1-w_1)} \\
&\quad \times\frac{\Gamma(-3\,\epsilon-w_3)\,\Gamma(1+2\,\epsilon+w_1+w_2)\,\Gamma(1+w_1+w_2)\,\Gamma(-2\,\epsilon-w_2)\,\Gamma(-\epsilon-w_1)}{\Gamma(1-3\,\epsilon-w_3)\,\Gamma(2-2\,\epsilon+w_1+w_2)} \\
&\quad \times\Gamma(-w_3)\,\Gamma(\epsilon-w_1-w_2+w_3)\,\Gamma(1-\epsilon+w_2)\,\Gamma(1+w_3)\,\Gamma(-\epsilon+w_1-w_3) \quad . \qquad (5.25)
\end{aligned}$$

The contour integrals are again along straight lines in the complex plane parallel to the imaginary axis, and we must, just as before, choose the real parts of the integration variables such as to have positive arguments in all occurring Γ-functions. This is achieved by choosing

$$c_1 = -\frac{3}{20}\,, \qquad c_2 = -\frac{3}{5}\,, \qquad c_3 = -\frac{1}{2}\,, \qquad -\frac{1}{8} < \epsilon < \frac{3}{20}. \qquad (5.26)$$

Just as before in $A_{6,2}$, we have the origin within the allowed region for ϵ and therefore the Mellin-Barnes integration does not give rise to any additional poles in ϵ. We can thus again perform the contour integrations order by order in ϵ. Since the leading coefficient turns out to have already transcendentality five, we only need to compute the first two terms in the expansion. They come out as

$$A_{7,3} = i\,S_\Gamma^3\left[-\,q^2 - i\,\eta\right]^{-1-3\,\epsilon}\left[\left(-\frac{\pi^2\,\zeta_3}{6} - 10\,\zeta_5\right)\frac{1}{\epsilon} - \frac{119\,\pi^6}{2160} - \frac{31}{2}\,\zeta_3^2 + \mathcal{O}(\epsilon)\right]. \quad (5.27)$$

The next diagram we consider is $A_{7,4}$. One could think that it is quite difficult since it does lack both a bubble insertion and a planar topology. However, it turns out to be simpler than the planar diagram $A_{7,3}$, yes it can even be displayed in a closed form. The main reason for this is the fact that at the outer vertices of both outgoing lines only three lines meet. This property is absent in both $A_{6,2}$ and $A_{7,3}$, both of which did not reveal a closed form but only a multiple Mellin-Barnes representation. For $A_{7,4}$, we find

$$\begin{aligned}
A_{7,4} &= \int\frac{d^Dk}{(2\pi)^D}\int\frac{d^Dl}{(2\pi)^D}\int\frac{d^Dm}{(2\pi)^D}\,\frac{1}{k^2\,(k-q)^2\,(m+l-k)^2\,l^2\,(l-p_1)^2\,m^2\,(m-p_2)^2} \\
&= i\,S_\Gamma^3\left[-\,q^2 - i\,\eta\right]^{-1-3\,\epsilon}\cdot 2\cdot\Gamma^4(1-\epsilon)\,\Gamma^2(-\epsilon) \\
&\quad\times\left[\frac{\Gamma(1-\epsilon)\,\Gamma(3\,\epsilon)}{(1-3\,\epsilon)^2\,\Gamma(2-4\,\epsilon)}\;{}_4F_3(1,1-\epsilon,1-3\,\epsilon,2-6\,\epsilon\,;\,2-3\,\epsilon,2-3\,\epsilon,2-4\,\epsilon\,;\,1)\right. \\
&\qquad -\frac{\Gamma(1-3\,\epsilon)\,\Gamma(2-3\,\epsilon)\,\Gamma(3\,\epsilon)\,\Gamma(1+2\,\epsilon)}{\Gamma(2-\epsilon)\,\Gamma(2-6\,\epsilon)} \\
&\qquad\quad\times{}_4F_3(1,1,1+2\,\epsilon,2-3\,\epsilon\,;\,2,2,2-\epsilon\,;\,1) \\
&\qquad +\frac{\Gamma^2(1-3\,\epsilon)\,\Gamma(1+2\,\epsilon)\,\Gamma(1+3\,\epsilon)}{\Gamma(2-\epsilon)\,\Gamma(2-6\,\epsilon)} \\
&\qquad\quad\left.\times{}_4F_3(1,1,1+2\,\epsilon,1+3\,\epsilon\,;\,2,2,2-\epsilon\,;\,1)\right] \\
&= i\,S_\Gamma^3\left[-\,q^2 - i\,\eta\right]^{-1-3\,\epsilon} \\
&\quad\times\left[\frac{6\,\zeta_3}{\epsilon^2} + \left(\frac{11\,\pi^4}{90} + 36\,\zeta_3\right)\frac{1}{\epsilon} + \left(\frac{11\,\pi^4}{15} + 216\,\zeta_3 - 2\,\pi^2\,\zeta_3 + 46\,\zeta_5\right)\right. \\
&\qquad\left. + \left(\frac{22\,\pi^4}{5} - \frac{19\,\pi^6}{270} + 1296\,\zeta_3 - 12\,\pi^2\,\zeta_3 - 282\,\zeta_3^2 + 276\,\zeta_5\right)\epsilon + \mathcal{O}(\epsilon)^2\right]. \quad (5.28)
\end{aligned}$$

The most important check for our analytical findings is the numerical computation of the coefficients that arise in the ϵ-expansion of the master integrals. All coefficients have been computed numerically using the sector decomposition [134] method of Refs. [135–137]. The checks in the case of integrals with bubble insertions have also been done for some ϵ-dependent values of α (see $I_5(\alpha)$, $I_6(\alpha)$ and $J_6(\alpha)$ in section 5.2) as well as for ϵ-dependent values of the ν_i (see $A_{5,1}$, $A_{5,2}$ and $A_{6,1}$). The agreement between numerical and analytical

results is, for reasonable computer run-times (up to a few days), well below 1%, in most cases even well below 1 per mill.

5.3 Conclusions and outlook

In this chapter, as well as in chapter 4, we have calculated higher order contributions to the quark form factor $\gamma^* \to q\bar{q}$ and gluon form factor $H \to gg$ which appear in several precision observables of QCD. At this, we applied two techniques in order to obtain expansions to sufficiently high orders in the dimensional regularisation parameter ϵ.

On the one hand, there are certain master integrals in which all integrations over loop momenta and Feynman parameters can be done in a closed form. The results contain only ϵ-dependent hypergeometric functions and Γ-functions and are thus valid to all orders in ϵ. The newly developed `Mathematica` package `HypExp` serves to perform the expansion in a Laurent series about $\epsilon = 0$.

On the other hand, of the master integrals that – to our knowledge – do not adopt a closed all-order representation, we derived a Mellin Barnes represenation in which the contour integrations in the complex plane commute with the expansion in ϵ, enabling us to perform the analytic computation of the coefficients order by order in ϵ.

Of the remaining three-loop master integrals in Fig. 5.1 a method of appropriately combining conventional Feynman parameterization with Mellin-Barnes integrations will be a reasonable choice that should finally enable us to extract the Laurent series of all diagrams. At this, all coefficients up to and including transcendentality six are required.

Acknowledgements

I would like to thank Gudrun Heinrich for patiently performing the computation of all numerical coefficients using the sector decomposition [134] method of Refs. [135–137]. I also appreciated the enjoyable cooperation with Cedric Studerus, Daniel Maître, and Thomas Gehrmann.

Appendix A

Auxiliary quantities for $\bar{B} \to X_s \ell^+ \ell^-$

The loop functions that appear in chapter 2 are:

$$A(x) = \frac{-3x^3+2x^2}{2(x-1)^4}\ln x + \frac{8x^3+5x^2-7x}{12(x-1)^3}, \tag{A.1}$$

$$Y(x) = \frac{3x^2}{8(x-1)^2}\ln x + \frac{x^2-4x}{8(x-1)}, \tag{A.2}$$

$$W(x) = \frac{-32x^4+38x^3+15x^2-18x}{18(x-1)^4}\ln x + \frac{-18x^4+163x^3-259x^2+108x}{36(x-1)^3}, \tag{A.3}$$

$$S(x) = \frac{3x^3}{2(x-1)^3}\ln x + \frac{x^3-11x^2+4x}{4(x-1)^2}, \tag{A.4}$$

$$X(x) = \frac{3x^2-6x}{8(x-1)^2}\ln x + \frac{x^2+2x}{8(x-1)}, \tag{A.5}$$

$$E(x) = \frac{x(18-11x-x^2)}{12(1-x)^3} + \frac{x^2(15-16x+4x^2)}{6(1-x)^4}\ln x - \frac{2}{3}\ln x\,. \tag{A.6}$$

The following function appears in the matrix elements of the four-quark operators:

$$g(y) = \frac{20}{27} + \frac{4}{9}y - \frac{2}{9}(2+y)\sqrt{|1-y|}\begin{cases} \ln\left|\frac{1+\sqrt{1-y}}{1-\sqrt{1-y}}\right| - i\pi, & \text{when } y<1, \\ 2\arctan\frac{1}{\sqrt{y-1}}, & \text{when } y \geq 1\,, \end{cases} \tag{A.7}$$

The $\omega_{ij}^{(n)}$ functions that include the sum of infrared divergent virtual and real contributions to the matrix elements of P_7, P_9 and P_{10} are:

$$\begin{aligned}
\omega_{99}^{(1)}(\hat{s}) &= -\frac{4}{3}Li_2(\hat{s}) - \frac{2}{3}\ln(1-\hat{s})\ln\hat{s} - \frac{2}{9}\pi^2 - \frac{5+4\hat{s}}{3(1+2\hat{s})}\ln(1-\hat{s}) \\
&\quad -\frac{2\hat{s}(1+\hat{s})(1-2\hat{s})}{3(1-\hat{s})^2(1+2\hat{s})}\ln\hat{s} + \frac{5+9\hat{s}-6\hat{s}^2}{6(1-\hat{s})(1+2\hat{s})}\,, \qquad \text{(A.8)} \\
\omega_{99}^{(2)}(\hat{s}) &= -19.2 + 6.1\hat{s} + (37.9 + 17.2\ln\hat{s})\hat{s}^2 - 18.7\hat{s}^3\,, \qquad \text{(A.9)} \\
\omega_{1010}^{(1)}(\hat{s}) &= \omega_{99}^{(1)}(\hat{s})\,, \qquad \text{(A.10)} \\
\omega_{77}^{(1)}(\hat{s}) &= -\frac{4}{3}Li_2(\hat{s}) - \frac{2}{3}\ln(1-\hat{s})\,\ln\hat{s} - \frac{2}{9}\pi^2 - \frac{(8+\hat{s})}{3\,(2+\hat{s})}\ln(1-\hat{s}) \\
&\quad -\frac{2\,\hat{s}\,\left(2-2\,\hat{s}-\hat{s}^2\right)}{3\,(1-\hat{s})^2\,(2+\hat{s})}\ln\hat{s} - \frac{16-11\,\hat{s}-17\,\hat{s}^2}{18\,(1-\hat{s})\,(2+\hat{s})} - \frac{8}{3}\ln(\frac{\mu_b}{m_b})\,, \qquad \text{(A.11)} \\
\omega_{79}^{(1)}(\hat{s}) &= -\frac{4}{3}Li_2(\hat{s}) - \frac{2}{3}\ln(1-\hat{s})\,\ln\hat{s} - \frac{2}{9}\pi^2 - \frac{(2+7\hat{s})}{9\hat{s}}\ln(1-\hat{s}) \\
&\quad -\frac{2\,\hat{s}\,(3-2\hat{s})}{9\,(1-\hat{s})^2}\ln\hat{s} + \frac{5-9\hat{s}}{18\,(1-\hat{s})} - \frac{4}{3}\ln(\frac{\mu_b}{m_b})\,. \qquad \text{(A.12)}
\end{aligned}$$

The function $\omega_{99}^{(1)}(\hat{s})$ has been extracted [54, 55] from the $\mathcal{O}(\alpha_s)$ corrections [182] to the semileptonic decay. The functions $\omega_{77}^{(1)}(\hat{s})$ and $\omega_{79}^{(1)}(\hat{s})$ have been calculated in Ref. [48]. Note that $\omega_{77}^{(1)}(\hat{s})$ in the $\hat{s} \to 0$ limit reproduces the $\mathcal{O}(\alpha_s)$ correction [183–185] to the matrix element of P_7 in the $b \to X_s\gamma$ decay. The function $\omega_{99}^{(2)}(\hat{s})$ was extracted [52] from the $\mathcal{O}(\alpha_s^2)$ corrections [84, 186] to the spectrum of the $b \to X_u e\bar{\nu}$ decay. The approximate formula in Eq. (A.9) is valid in the range $0 < \hat{s} < 0.4$. A somewhat more precise approximation can be extracted from $\mathcal{O}(\alpha_s^2)$ corrections to heavy-to light decays [85, 86] and can be used in further analyses. Also a formula for the high-$\hat{s}$ region can be obtained following Refs. [84, 86]. The function $\omega_{99}^{(2)}(\hat{s})$ is proportional to the ratio X_2/X_0 in these references, where one has to keep track of different normalizations that are used in [84–86].

The function $F(r)$ that arises in the the $\mathcal{O}(1/m_c^2)$ non-perturbative corrections reads [75]

$$F(r) = \frac{3}{2r}\begin{cases} \frac{1}{\sqrt{r(1-r)}}\arctan\sqrt{\frac{r}{1-r}} - 1, & \text{when } 0 < r < 1, \\ \frac{1}{2\sqrt{r(r-1)}}\left(\ln\frac{1-\sqrt{1-1/r}}{1+\sqrt{1-1/r}} + i\pi\right) - 1, & \text{when } r > 1. \end{cases} \qquad \text{(A.13)}$$

The numerical diagonalization of the matrix $\hat{W}^{(10)}$ yields:

$$\begin{aligned}
a_i &= \Big[-1.04348, -0.899395, -0.521739, -0.521739, -0.422989, 0.408619, \\
&\qquad 0.26087, 0.26087, 0.26087, 0.145649, 0.130435, 0, 0\Big] \qquad \text{(A.14)}
\end{aligned}$$

and

$$\hat{V} = \begin{pmatrix}
0 & 0 & 0.942522 & 0.0253179 & 0 & 0 \\
0 & 0 & -0.314174 & -0.0084393 & 0 & 0 \\
-0.0109144 & -0.160583 & 0.0349082 & -0.0961354 & 0.917797 & -0.922049 \\
-0.0654862 & -0.984073 & -0.104725 & 0.288406 & -0.266582 & 0.331368 \\
0.000682148 & 0.00725171 & -0.00872705 & 0.0240338 & -0.153681 & 0.130848 \\
0.00409289 & 0.0759058 & 0.0261812 & -0.0721015 & 0.250927 & 0.151325 \\
0 & 0 & 0 & 0 & 0 & 0 \\
0 & 0 & 0 & 0 & 0 & 0 \\
0.163715 & 0 & 0 & 0.291219 & 0 & 0 \\
0.982293 & 0 & 0 & -0.873658 & 0 & 0 \\
-0.0102322 & 0 & 0 & -0.0728048 & 0 & 0 \\
-0.0613933 & 0 & 0 & 0.218414 & 0 & 0 \\
0 & 0 & 0 & 0 & 0 & 0
\end{pmatrix}$$

$$\begin{pmatrix}
0.00100213 & -0.83105 & 0.00542193 & 0 & 0 & 0 & 0 \\
0.00066809 & -0.554033 & 0.00361462 & 0 & 0 & 0 & 0 \\
-0.0255649 & -0.0263825 & 0.0632231 & 0.726443 & 0.0531116 & 0 & 0 \\
-0.0383473 & -0.0395738 & 0.0948347 & -0.684418 & -0.0398337 & 0 & 0 \\
0.00639122 & 0.00659563 & -0.0158058 & -0.0368909 & -0.00331947 & 0 & 0 \\
0.00958682 & 0.00989345 & -0.0237087 & 0.0499047 & 0.00248961 & 0 & 0 \\
0 & 0 & 0 & 0 & 0 & 1. & 0 \\
0 & 0 & 0 & 0 & 0 & 0 & 1. \\
-0.53753 & 0 & 0 & 0 & -0.796674 & 0 & 0 \\
-0.806295 & 0 & 0 & 0 & 0.597505 & 0 & 0 \\
0.134383 & 0 & 0 & 0 & 0.0497921 & 0 & 0 \\
0.201574 & 0 & 0 & 0 & -0.0373441 & 0 & 0 \\
0 & 0 & 0.993053 & 0 & 0 & 0 & 0
\end{pmatrix} \tag{A.15}$$

Appendix B

Useful formulas

B.1 Loop integrals

In this section we collect the most important formulas that are needed for the loop integrals of the previous chapters. We start with two formulas for collecting propagators of loop integrals via Feynman parameters.

$$\frac{1}{a^n\,b^m} = \frac{\Gamma(n+m)}{\Gamma(n)\,\Gamma(m)} \int\limits_0^1 dx \frac{x^{n-1}\,(1-x)^{m-1}}{[a\,x+b\,(1-x)]^{n+m}}\;, \tag{B.1}$$

$$\begin{aligned}\frac{1}{A_1^{m_1}\,A_2^{m_2}\,\cdots\,A_n^{m_n}} &= \frac{\Gamma(\sum_{i=1}^n m_i)}{\Gamma(m_1)\,\Gamma(m_2)\,\cdots\,\Gamma(m_n)} \\ &\times \int\limits_0^1 dx_1 dx_2 \cdots dx_n \frac{x_1^{m_1-1}\,x_2^{m_2-1}\,\cdots\,x_n^{m_n-1}\,\delta(1-\sum_{i=1}^n x_i)}{(x_1\,A_1+x_2\,A_2+\ldots+x_n\,A_n)^{m_1+m_2+\ldots+m_n}}\;.\end{aligned} \tag{B.2}$$

Integrals over loop momenta are done by means of the following two formulas [2,3].

$$\int\frac{d^Dk}{(2\pi)^D}\;\frac{1}{[k^2-m^2+i\eta]^n} = \frac{i\,(-1)^{-n}}{(4\pi)^{D/2}}\frac{\Gamma(n-\frac{D}{2})}{\Gamma(n)}\frac{1}{(m^2-i\eta)^{n-\frac{D}{2}}}\;, \tag{B.3}$$

$$\begin{aligned}&\int\frac{d^Dk}{(2\pi)^D}\;\frac{1}{\left[(k-q)^2-m_1^2+i\eta\right]^{n_1}\;\left[k^2-m_2^2+i\eta\right]^{n_2}} \\ &= \frac{i\,(-1)^{-n_1-n_2}}{(4\pi)^{D/2}}\frac{\Gamma(n_1+n_2-\frac{D}{2})}{\Gamma(n_1)\,\Gamma(n_2)}\int\limits_0^1 dx\;\frac{x^{n_1-1}\;(1-x)^{n_2-1}}{\left[m_1^2\,x+m_2^2\,(1-x)-q^2\,x\,(1-x)-i\eta\right]^{n_1+n_2-\frac{D}{2}}}\;.\end{aligned} \tag{B.4}$$

At this point we want to state a small but useful formula by means of which we can extract the right powers of minus one. For infinitesimally small $\eta > 0$, we have

$$\frac{1}{(-\chi\pm i\,\eta)^m} = \frac{(-1)^{\mp m}}{(\chi\mp i\,\eta)^m}\;. \tag{B.5}$$

It is often necessary to decompose propagators via a Mellin Barnes representation. The two main relations read

$$\frac{1}{(A_1+A_2)^\alpha} = \int\limits_{c-i\,\infty}^{c+i\,\infty} \frac{dw}{2\pi i}\, A_1^w\, A_2^{-\alpha-w}\, \frac{\Gamma(-w)\,\Gamma(\alpha+w)}{\Gamma(\alpha)}\,, \tag{B.6}$$

$$\begin{aligned}\frac{1}{(A_1+A_2+\ldots+A_m)^\alpha} &= \int\limits_{c_1-i\,\infty}^{c_1+i\,\infty} \frac{dw_1}{2\pi i} \cdots \int\limits_{c_{m-1}-i\,\infty}^{c_{m-1}+i\,\infty} \frac{dw_{m-1}}{2\pi i}\, A_1^{w_1} \cdots A_{m-1}^{w_{m-1}}\, A_m^{-\alpha-w_1-\ldots-w_{m-1}} \\ &\quad \times \frac{\Gamma(-w_1)\cdots\Gamma(-w_{m-1})\,\Gamma(\alpha+w_1+\ldots+w_{m-1})}{\Gamma(\alpha)}\,. \end{aligned} \tag{B.7}$$

As described in chapter 5, the integration contours are such as to separate left poles of the Γ-function from right ones. The Feynman parameters that are introduced by Eq. (B.2) can, after integration over the loop momentum and subsequent factorization via Mellin Barnes representations, be integrated out via the relation

$$\int\limits_0^1 dx_1 dx_2 \cdots dx_n\, x_1^{a_1-1}\, x_2^{a_2-1} \cdots x_n^{a_n-1}\, \delta(1-\sum_{i=1}^n x_i) = \frac{\Gamma(a_1)\,\Gamma(a_2)\cdots\Gamma(a_n)}{\Gamma(a_1+a_2+\ldots+a_n)}\,. \tag{B.8}$$

The last step of computing a loop integral is quite often a single or multiple Mellin Barnes integration. At this stage, the lemmata of Barnes [187,188] are very useful,

$$\begin{aligned}&\int\limits_{c-i\,\infty}^{c+i\,\infty} \frac{dz}{2\pi i}\, \Gamma(\lambda_1+z)\,\Gamma(\lambda_2+z)\,\Gamma(\lambda_3-z)\,\Gamma(\lambda_4-z) = \\ &\qquad \frac{\Gamma(\lambda_1+\lambda_3)\,\Gamma(\lambda_1+\lambda_4)\,\Gamma(\lambda_2+\lambda_3)\,\Gamma(\lambda_2+\lambda_4)}{\Gamma(\lambda_1+\lambda_2+\lambda_3+\lambda_4)}\,, \end{aligned} \tag{B.9}$$

$$\begin{aligned}&\int\limits_{c-i\,\infty}^{c+i\,\infty} \frac{dz}{2\pi i}\, \frac{\Gamma(\lambda_1+z)\,\Gamma(\lambda_2+z)\,\Gamma(\lambda_3+z)\,\Gamma(\lambda_4-z)\,\Gamma(\lambda_5-z)}{\Gamma(\lambda_1+\lambda_2+\lambda_3+\lambda_4+\lambda_5+z)} = \\ &\qquad \frac{\Gamma(\lambda_1+\lambda_4)\,\Gamma(\lambda_2+\lambda_4)\,\Gamma(\lambda_3+\lambda_4)\,\Gamma(\lambda_1+\lambda_5)\,\Gamma(\lambda_2+\lambda_5)\,\Gamma(\lambda_3+\lambda_5)}{\Gamma(\lambda_1+\lambda_2+\lambda_4+\lambda_5)\,\Gamma(\lambda_1+\lambda_3+\lambda_4+\lambda_5)\,\Gamma(\lambda_2+\lambda_3+\lambda_4+\lambda_5)}\,. \end{aligned} \tag{B.10}$$

As usual, the integration curves have to separate left poles of the Γ-function from right ones. Various corollaries of Eqs. (B.9) and (B.10) can be found in Appendix D of Ref. [113].

B.2 Hypergeometric functions

In this section we list representations of hypergeometric functions ${}_JF_{J-1}$ based on sums and integrals. We start with an infinite sum,

$${}_JF_{J-1}(A_1,\ldots,A_J\,;\,B_1,\ldots,B_{J-1}\,;\,z) = 1 + \sum_{n=1}^\infty \frac{(A_1)_n\cdots(A_J)_n}{(B_1)_n\cdots(B_{J-1})_n}\frac{z^n}{n!}\,, \tag{B.11}$$

with $|z| < 1$. The Pochhammer symbols $(a)_n$ are defined as

$$\begin{aligned}
(a)_0 &\equiv 1 \qquad\qquad \text{for all } a \in \mathbb{C}\,, \\
(a)_n &= \frac{\Gamma(a+n)}{\Gamma(a)} \quad \text{for } a \in \mathbb{C} \setminus -\mathbb{N}_0\,, \quad n \in \mathbb{N}\,, \\
(a)_n &= a\,(a+1)\cdots(a+n-2)\,(a+n-1) \quad \text{for } a \in -\mathbb{N}_0\,, \quad n \in \mathbb{N}\,. \qquad \text{(B.12)}
\end{aligned}$$

From the last equation in (B.12) we learn that the series in (B.11) truncates and gives a polynomial of finite degree if one (or more) of the A_i is zero or a negative integer. We remind the reader about the subtlety that arises when one has to deal with negative parameters, see section 3.2.3.

The hypergeometric functions ${}_JF_{J-1}$ also adopt an integral representation along the real axis,

$$\begin{aligned}
&{}_JF_{J-1}(A_1,\ldots,A_J\,;\,B_1,\ldots,B_{J-1}\,;\,z) \;=\; \\
&\left[\prod_{i=1}^{J-1}\frac{\Gamma(B_i)}{\Gamma(A_i)\,\Gamma(B_i-A_i)}\right]\int_0^1 dt_1\cdots dt_{J-1}\,\frac{\prod_{k=1}^{J-1} t_k^{A_k-1}\,(1-t_k)^{B_k-A_k-1}}{(1-z\,t_1\cdots t_{J-1})^{A_J}}\,. \qquad \text{(B.13)}
\end{aligned}$$

B.3 MeijerG functions

We now turn our attention to another class of formulas, namely the MeijerG function [132, 133, 174, 178–180], and list its most important properties together with relations to other functions. The primary definition of the MeijerG function is

$$G^{m,n}_{p,q}\left(z\,\middle|\,\begin{matrix}\{a_1,\ldots,a_n\}\,,\{a_{n+1},\ldots,a_p\}\\ \{b_1,\ldots,b_m\}\,,\{b_{m+1},\ldots,b_q\}\end{matrix}\right)=\int_L\frac{ds}{2\pi i}\,\frac{\prod_{j=1}^{m}\Gamma(b_j-s)\prod_{k=1}^{n}\Gamma(1-a_k+s)}{\prod_{j=m+1}^{q}\Gamma(1-b_j+s)\prod_{k=n+1}^{p}\Gamma(a_k-s)}\,z^s \qquad \text{(B.14)}$$

or equivalently

$$G^{m,n}_{p,q}\left(z\,\middle|\,\begin{matrix}\{a_1,\ldots,a_n\}\,,\{a_{n+1},\ldots,a_p\}\\ \{b_1,\ldots,b_m\}\,,\{b_{m+1},\ldots,b_q\}\end{matrix}\right)=\int_L\frac{ds}{2\pi i}\,\frac{\prod_{j=1}^{m}\Gamma(b_j+s)\prod_{k=1}^{n}\Gamma(1-a_k-s)}{\prod_{j=m+1}^{q}\Gamma(1-b_j-s)\prod_{k=n+1}^{p}\Gamma(a_k+s)}\,z^{-s}. \qquad \text{(B.15)}$$

One of the choices for the path L is as usual from $-i\,\infty$ to $+i\,\infty$ such that all poles of Γ-functions that run to the left are separated from those that run to the right. There are, however, two more possibilities for the choice of the path L. They can be found, together with convergence conditions, in Ref. [132]. From the defining equations, we derive the

following relations for argument transformations

$$z^\sigma\, G_{p,q}^{m,n}\left(z \,\middle|\, \begin{matrix}\{a_1,\ldots,a_n\}\,,\{a_{n+1},\ldots,a_p\}\\ \{b_1,\ldots,b_m\}\,,\{b_{m+1},\ldots,b_q\}\end{matrix}\right) \;=\; G_{p,q}^{m,n}\left(z \,\middle|\, \begin{matrix}\{a_1+\sigma,\ldots,a_n+\sigma\}\,,\{a_{n+1}+\sigma,\ldots,a_p+\sigma\}\\ \{b_1+\sigma,\ldots,b_m+\sigma\}\,,\{b_{m+1}+\sigma,\ldots,b_q+\sigma\}\end{matrix}\right), \tag{B.16}$$

$$G_{p,q}^{m,n}\left(\frac{1}{z} \,\middle|\, \begin{matrix}\{a_1,\ldots,a_n\}\,,\{a_{n+1},\ldots,a_p\}\\ \{b_1,\ldots,b_m\}\,,\{b_{m+1},\ldots,b_q\}\end{matrix}\right) \;=\; G_{q,p}^{n,m}\left(z \,\middle|\, \begin{matrix}\{1-b_1,\ldots,1-b_m\}\,,\{1-b_{m+1},\ldots,1-b_q\}\\ \{1-a_1,\ldots,1-a_n\}\,,\{1-a_{n+1},\ldots,1-a_p\}\end{matrix}\right). \tag{B.17}$$

Two formulas that can be used to express hypergeometric functions in terms of MeijerG functions are

$${}_pF_{p-1}(a_1,\ldots,a_p\,;\,b_1,\ldots,b_{p-1}\,;\,-z) \;=\; \frac{\Gamma(b_1)\cdots\Gamma(b_{p-1})}{\Gamma(a_1)\cdots\Gamma(a_p)}\, G_{p,p}^{1,p}\left(z \,\middle|\, \begin{matrix}\{1-a_1,\ldots,1-a_p\}\,,\{\}\\ \{0\}\,,\{1-b_1,\ldots,1-b_{p-1}\}\end{matrix}\right), \tag{B.18}$$

$$(1-z)^{a+b-c}\,{}_2F_1(a,b\,;\,c\,;\,z) \;=\; \frac{\Gamma(c)}{\Gamma(c-a)\,\Gamma(c-b)}\, G_{2,2}^{1,2}\left(-z \,\middle|\, \begin{matrix}\{a-c+1,b-c+1\}\,,\{\}\\ \{0\}\,,\{1-c\}\end{matrix}\right). \tag{B.19}$$

Equation (B.18) also allows to easily establish a contour integral representation for hypergeometric functions. On the other hand, we can express MeijerG functions in terms of hypergeometric functions. If no two b_j, $j=1,\ldots,m$ differ by an integer, we have

$$G_{p,q}^{m,n}\left(z \,\middle|\, \begin{matrix}\{a_1,\ldots,a_n\}\,,\{a_{n+1},\ldots,a_p\}\\ \{b_1,\ldots,b_m\}\,,\{b_{m+1},\ldots,b_q\}\end{matrix}\right) \;=$$

$$\sum_{h=1}^{m} \frac{\prod_{j=1}^{m}{}' \Gamma(b_j-b_h)\prod_{k=1}^{n}\Gamma(1+b_h-a_k)}{\prod_{j=m+1}^{q}\Gamma(1+b_h-b_j)\prod_{k=n+1}^{p}\Gamma(a_k-b_h)}\, z^{b_h}$$

$$\times\, {}_pF_{q-1}(1+b_h-a_1,\ldots,1+b_h-a_p\,;\,1+b_h-b_1,\ldots,*,\ldots,1+b_h-b_q\,;\,(-1)^{p-m-n}\,z)\,, \tag{B.20}$$

where $p < q$ or $p = q$ and $|z| < 1$. Similarly, if no two a_k, $k = 1, \ldots, n$ differ by an integer, we have

$$G^{m,n}_{p,q}\left(z \,\middle|\, \begin{matrix}\{a_1,\ldots,a_n\}\,,\{a_{n+1},\ldots,a_p\}\\ \{b_1,\ldots,b_m\}\,,\{b_{m+1},\ldots,b_q\}\end{matrix}\right) \;=$$

$$\sum_{h=1}^{n} \frac{\prod_{j=1}^{n}{}' \Gamma(a_h - a_j) \prod_{k=1}^{m} \Gamma(b_k - a_h + 1)}{\prod_{j=n+1}^{p} \Gamma(a_j - a_h + 1) \prod_{k=m+1}^{q} \Gamma(a_h - b_k)}\, z^{a_h - 1}$$

$$\times {}_qF_{p-1}(1 + b_1 - a_h, \ldots, 1 + b_q - a_h\,;\, 1 + a_1 - a_h, \ldots, *, \ldots, 1 + a_p - a_h\,;\, (-1)^{q-m-n}\,\frac{1}{z})\,, \tag{B.21}$$

where $q < p$ or $q = p$ and $|z| > 1$. The symbol $\prod'$ means that the factor $j = h$ is omitted. The corresponding term is also left out in the hypergeometric function, as is indicated by an asteriks. Eqs. (B.20) and (B.21) also hold for unit argument if the convergence condition (3.54) is satisfied.

The full power of the MeijerG functions is revealed once we consider integrations over this type of functions.

$$\int_0^1 dx\, x^{\rho-1}\,(1-x)^{\sigma-1}\, G^{m,n}_{p,q}\left(\alpha\, x \,\middle|\, \begin{matrix}\{a_1,\ldots,a_n\}\,,\{a_{n+1},\ldots,a_p\}\\ \{b_1,\ldots,b_m\}\,,\{b_{m+1},\ldots,b_q\}\end{matrix}\right) \;=$$

$$\Gamma(\sigma)\, G^{m,n+1}_{p+1,q+1}\left(\alpha \,\middle|\, \begin{matrix}\{1-\rho, a_1,\ldots,a_n\}\,,\{a_{n+1},\ldots,a_p\}\\ \{b_1,\ldots,b_m\}\,,\{b_{m+1},\ldots,b_q, 1-\rho-\sigma\}\end{matrix}\right)\,, \tag{B.22}$$

$$\int_0^\infty dx\, x^{\rho-1}\,(x+\beta)^{-\sigma}\, G^{m,n}_{p,q}\left(\alpha\, x \,\middle|\, \begin{matrix}\{a_1,\ldots,a_n\}\,,\{a_{n+1},\ldots,a_p\}\\ \{b_1,\ldots,b_m\}\,,\{b_{m+1},\ldots,b_q\}\end{matrix}\right) \;=$$

$$\frac{\beta^{\rho-\sigma}}{\Gamma(\sigma)}\, G^{m+1,n+1}_{p+1,q+1}\left(\alpha\,\beta \,\middle|\, \begin{matrix}\{1-\rho, a_1,\ldots,a_n\}\,,\{a_{n+1},\ldots,a_p\}\\ \{\sigma-\rho, b_1,\ldots,b_m\}\,,\{b_{m+1},\ldots,b_q\}\end{matrix}\right)\,, \tag{B.23}$$

and finally the queen of all integration formulas

$$\int_0^\infty dx\, G^{m,n}_{p,q}\left(\alpha\, x \,\middle|\, \begin{matrix}\{a_1,\ldots,a_n\}\,,\{a_{n+1},\ldots,a_p\}\\ \{b_1,\ldots,b_m\}\,,\{b_{m+1},\ldots,b_q\}\end{matrix}\right) G^{k,l}_{r,s}\left(\beta\, x \,\middle|\, \begin{matrix}\{c_1,\ldots,c_l\}\,,\{c_{l+1},\ldots,c_r\}\\ \{d_1,\ldots,d_k\}\,,\{d_{k+1},\ldots,d_s\}\end{matrix}\right)$$

$$= \alpha^{-1}\, G^{k+n,l+m}_{q+r,p+s}\left(\frac{\beta}{\alpha} \,\middle|\, \begin{matrix}\{-b_1,\ldots,-b_m,c_1,\ldots,c_l\}\,,\{c_{l+1},\ldots,c_r,-b_{m+1},\ldots,-b_q\}\\ \{-a_1,\ldots,-a_n,d_1,\ldots,d_k\}\,,\{d_{k+1},\ldots,d_s,-a_{n+1},\ldots,-a_p\}\end{matrix}\right). \tag{B.24}$$

Again, for conditions of validity for these integration formulas, see [174] and references therein.

B.4 Infinite summation of polygamma functions

This section is devoted to a list of formulas that allow to analytically compute infinite sums over polygamma functions $\psi^{(k)}(n)$, as this is required during the summation of residues in Mellin-Barnes integrals. The polygamma functions are defined as

$$\begin{aligned} \psi^{(0)}(z) &= \frac{d}{dz} \ln\left[\Gamma(z)\right] , \\ \psi^{(k)}(z) &= \frac{d}{dz} \psi^{(k-1)}(z) \quad \text{for} \quad k = 1, 2, \dots \quad . \end{aligned} \tag{B.25}$$

For positive, integer-valued arguments, the values of the polygamma functions read

$$\begin{aligned} \psi^{(0)}(n) &= -\gamma_E + \sum_{i=1}^{n-1} \frac{1}{i} , \\ \psi^{(k)}(n) &= (-1)^k \, k! \cdot \left[-\zeta_{k+1} + \sum_{i=1}^{n-1} \frac{1}{i^{k+1}} \right] \quad \text{for} \quad k = 1, 2, \dots \quad . \end{aligned} \tag{B.26}$$

Before we start the list of formulas, we introduce a short-hand notation. Let

$$f(\{deg_1, pow_1\}, \dots, \{deg_j, pow_j\}, p) \equiv \sum_{n=1}^{\infty} \frac{\left[\psi^{(deg_1)}(n)\right]^{pow_1} \cdots \left[\psi^{(deg_j)}(n)\right]^{pow_j}}{n^p} , \tag{B.27}$$

so for instance

$$f(\{0,1\},\{1,2\},3) \equiv \sum_{n=1}^{\infty} \frac{\psi^{(0)}(n) \, \left[\psi^{(1)}(n)\right]^2}{n^3} . \tag{B.28}$$

B.4.1 Summation with $p = 1$

$$f(\{1,1\},1) = 2\,\zeta_3 , \tag{B.29}$$

$$f(\{2,1\},1) = -\frac{\pi^4}{36} , \tag{B.30}$$

$$f(\{3,1\},1) = -\pi^2\,\zeta_3 + 18\,\zeta_5 , \tag{B.31}$$

$$f(\{4,1\},1) = -\frac{2\,\pi^6}{45} + 12\,\zeta_3^2 , \tag{B.32}$$

$$f(\{1,2\},1) = \frac{\pi^2\,\zeta_3}{6} + \zeta_5 , \tag{B.33}$$

$$f(\{0,1\},\{1,1\},1) = \frac{\pi^4}{72} - 2\,\gamma_E\,\zeta_3 , \tag{B.34}$$

$$f(\{0,1\},\{2,1\},1) = \frac{\gamma_E\,\pi^4}{36} + \frac{2\,\pi^2\,\zeta_3}{3} - 8\,\zeta_5 , \tag{B.35}$$

$$f(\{0,1\},\{3,1\},1) = \frac{\pi^6}{72} + \gamma_E\,\pi^2\,\zeta_3 - 9\,\zeta_3^2 - 18\,\gamma_E\,\zeta_5 , \tag{B.36}$$

$$f(\{1,1\},\{2,1\},1) = -\frac{\pi^6}{360} - \zeta_3^2 , \tag{B.37}$$

$$f(\{0,1\},\{1,2\},1) = \frac{\pi^6}{240} - \frac{\gamma_E\,\pi^2\,\zeta_3}{6} - \frac{5\,\zeta_3^2}{2} - \gamma_E\,\zeta_5 , \tag{B.38}$$

$$f(\{0,2\},\{2,1\},1) = -\frac{\gamma_E^2\,\pi^4}{36} - \frac{\pi^6}{90} - \frac{4\,\gamma_E\,\pi^2\,\zeta_3}{3} + 7\,\zeta_3^2 + 16\,\gamma_E\,\zeta_5 . \tag{B.39}$$

B.4.2 Summation with $p > 1$

$$f(\{0,1\},p) = \mathrm{MZV}(\{p,1\}) - \gamma_E\,\zeta_p\;, \tag{B.40}$$

$$f(\{j,1\},p) = (-1)^j\;j!\;[\mathrm{MZV}(\{p,j+1\}) - \zeta_{j+1}\,\zeta_p] \quad \text{for} \quad j \geq 1\;, \tag{B.41}$$

$$f(\{0,2\},p) = -2\,\gamma_E\,\mathrm{MZV}(\{p,1\}) + \mathrm{MZV}(\{p,2\}) + 2\,\mathrm{MZV}(\{p,1,1\}) + \gamma_E^2\,\zeta_p\;, \tag{B.42}$$

$$f(\{1,2\},p) = -\frac{\pi^2\,\mathrm{MZV}(\{p,2\})}{3} + \mathrm{MZV}(\{p,4\}) + 2\,\mathrm{MZV}(\{p,2,2\}) + \frac{\pi^4\,\zeta_p}{36}\;, \tag{B.43}$$

$$f(\{2,2\},p) = 4\,\mathrm{MZV}(\{p,6\}) + 8\,\mathrm{MZV}(\{p,3,3\}) - 8\,\mathrm{MZV}(\{p,3\})\,\zeta_3 + 4\,\zeta_3^2\,\zeta_p\;, \tag{B.44}$$

$$\begin{aligned} f(\{0,3\},p) = {} & 3\,\gamma_E^2\,\mathrm{MZV}(\{p,1\}) - 3\,\gamma_E\,\mathrm{MZV}(\{p,2\}) + \mathrm{MZV}(\{p,3\}) \\ & -6\,\gamma_E\,\mathrm{MZV}(\{p,1,1\}) + 3\,\mathrm{MZV}(\{p,1,2\}) + 3\,\mathrm{MZV}(\{p,2,1\}) \\ & +6\,\mathrm{MZV}(\{p,1,1,1\}) - \gamma_E^3\,\zeta_p\;, \end{aligned} \tag{B.45}$$

$$\begin{aligned} f(\{1,3\},p) = {} & -\frac{\pi^4\,\mathrm{MZV}(\{p,2\})}{12} + \frac{\pi^2\,\mathrm{MZV}(\{p,4\})}{2} - \mathrm{MZV}(\{p,6\}) \\ & +\pi^2\,\mathrm{MZV}(\{p,2,2\}) - 3\,\mathrm{MZV}(\{p,2,4\}) - 3\,\mathrm{MZV}(\{p,4,2\}) \\ & -6\,\mathrm{MZV}(\{p,2,2,2\}) + \frac{\pi^6\,\zeta_p}{216}\;, \end{aligned} \tag{B.46}$$

$$\begin{aligned} f(\{0,4\},p) = {} & -4\,\gamma_E^3\,\mathrm{MZV}(\{p,1\}) + 6\,\gamma_E^2\,\mathrm{MZV}(\{p,2\}) - 4\,\gamma_E\,\mathrm{MZV}(\{p,3\}) \\ & +\mathrm{MZV}(\{p,4\}) + 12\,\gamma_E^2\,\mathrm{MZV}(\{p,1,1\}) - 12\,\gamma_E\,\mathrm{MZV}(\{p,1,2\}) \\ & +4\,\mathrm{MZV}(\{p,1,3\}) - 12\,\gamma_E\,\mathrm{MZV}(\{p,2,1\}) + 6\,\mathrm{MZV}(\{p,2,2\}) \\ & +4\,\mathrm{MZV}(\{p,3,1\}) - 24\,\gamma_E\,\mathrm{MZV}(\{p,1,1,1\}) + 12\,\mathrm{MZV}(\{p,1,1,2\}) \\ & +12\,\mathrm{MZV}(\{p,1,2,1\}) + 12\,\mathrm{MZV}(\{p,2,1,1\}) + 24\,\mathrm{MZV}(\{p,1,1,1,1\}) \\ & +\gamma_E^4\,\zeta_p\;, \end{aligned} \tag{B.47}$$

$$
\begin{aligned}
f(\{0,5\},p) &= 5\,\gamma_E^4\,\mathrm{MZV}(\{p,1\}) - 10\,\gamma_E^3\,\mathrm{MZV}(\{p,2\}) + 10\,\gamma_E^2\,\mathrm{MZV}(\{p,3\}) \\
&\quad -5\,\gamma_E\,\mathrm{MZV}(\{p,4\}) + \mathrm{MZV}(\{p,5\}) - 20\,{\gamma_E}^3\,\mathrm{MZV}(\{p,1,1\}) \\
&\quad +30\,\gamma_E^2\,\mathrm{MZV}(\{p,1,2\}) - 20\,\gamma_E\,\mathrm{MZV}(\{p,1,3\}) + 5\,\mathrm{MZV}(\{p,1,4\}) \\
&\quad +30\,\gamma_E^2\,\mathrm{MZV}(\{p,2,1\}) - 30\,\gamma_E\,\mathrm{MZV}(\{p,2,2\}) + 10\,\mathrm{MZV}(\{p,2,3\}) \\
&\quad -20\,\gamma_E\,\mathrm{MZV}(\{p,3,1\}) + 10\,\mathrm{MZV}(\{p,3,2\}) + 5\,\mathrm{MZV}(\{p,4,1\}) \\
&\quad +60\,\gamma_E^2\,\mathrm{MZV}(\{p,1,1,1\}) - 60\,\gamma_E\,\mathrm{MZV}(\{p,1,1,2\}) \\
&\quad +20\,\mathrm{MZV}(\{p,1,1,3\}) - 60\,\gamma_E\,\mathrm{MZV}(\{p,1,2,1\}) \\
&\quad +30\,\mathrm{MZV}(\{p,1,2,2\}) + 20\,\mathrm{MZV}(\{p,1,3,1\}) \\
&\quad -60\,\gamma_E\,\mathrm{MZV}(\{p,2,1,1\}) + 30\,\mathrm{MZV}(\{p,2,1,2\}) \\
&\quad +30\,\mathrm{MZV}(\{p,2,2,1\}) + 20\,\mathrm{MZV}(\{p,3,1,1\}) \\
&\quad -120\,\gamma_E\,\mathrm{MZV}(\{p,1,1,1,1\}) + 60\,\mathrm{MZV}(\{p,1,1,1,2\}) \\
&\quad +60\,\mathrm{MZV}(\{p,1,1,2,1\}) + 60\,\mathrm{MZV}(\{p,1,2,1,1\}) - \gamma_E^5\,\zeta_p \\
&\quad +60\,\mathrm{MZV}(\{p,2,1,1,1\}) + 120\,\mathrm{MZV}(\{p,1,1,1,1,1\})\ , \qquad \text{(B.48)}
\end{aligned}
$$

$$
\begin{aligned}
f(\{0,1\},\{1,1\},p) &= \frac{\pi^2\,\mathrm{MZV}(\{p,1\})}{6} + \gamma_E\,\mathrm{MZV}(\{p,2\}) - \mathrm{MZV}(\{p,3\}) \\
&\quad -\mathrm{MZV}(\{p,1,2\}) - \mathrm{MZV}(\{p,2,1\}) - \frac{\gamma_E\,\pi^2\,\zeta_p}{6}\ , \qquad \text{(B.49)}
\end{aligned}
$$

$$
\begin{aligned}
f(\{0,1\},\{2,1\},p) &= -2\,\gamma_E\,\mathrm{MZV}(\{p,3\}) + 2\,\mathrm{MZV}(\{p,4\}) + 2\,\mathrm{MZV}(\{p,1,3\}) \\
&\quad +2\,\mathrm{MZV}(\{p,3,1\}) - 2\,\mathrm{MZV}(\{p,1\})\,\zeta_3 + 2\,\gamma_E\,\zeta_3\,\zeta_p\ , \qquad \text{(B.50)}
\end{aligned}
$$

$$
\begin{aligned}
f(\{0,1\},\{3,1\},p) &= \frac{\pi^4\,\mathrm{MZV}(\{p,1\})}{15} + 6\,\gamma_E\,\mathrm{MZV}(\{p,4\}) - 6\,\mathrm{MZV}(\{p,5\}) \\
&\quad -6\,\mathrm{MZV}(\{p,1,4\}) - 6\,\mathrm{MZV}(\{p,4,1\}) - \frac{\gamma_E\,\pi^4\,\zeta_p}{15}\ , \qquad \text{(B.51)}
\end{aligned}
$$

$$
\begin{aligned}
f(\{0,1\},\{4,1\},p) &= -24\,\gamma_E\,\mathrm{MZV}(\{p,5\}) + 24\,\mathrm{MZV}(\{p,6\}) + 24\,\mathrm{MZV}(\{p,1,5\}) \\
&\quad +24\,\mathrm{MZV}(\{p,5,1\}) - 24\,\mathrm{MZV}(\{p,1\})\,\zeta_5 + 24\,\gamma_E\,\zeta_5\,\zeta_p\,, \qquad \text{(B.52)} \\
f(\{1,1\},\{2,1\},p) &= \frac{\pi^2\,\mathrm{MZV}(\{p,3\})}{3} - 2\,\mathrm{MZV}(\{p,5\}) - 2\,\mathrm{MZV}(\{p,2,3\}) \\
&\quad -2\,\mathrm{MZV}(\{p,3,2\}) + 2\,\mathrm{MZV}(\{p,2\})\,\zeta_3 - \frac{\pi^2\,\zeta_3\,\zeta_p}{3}\,, \qquad \text{(B.53)} \\
f(\{1,1\},\{3,1\},p) &= -\frac{\pi^4\,\mathrm{MZV}(\{p,2\})}{15} - \pi^2\,\mathrm{MZV}(\{p,4\}) + 6\,\mathrm{MZV}(\{p,6\}) \\
&\quad +6\,\mathrm{MZV}(\{p,2,4\}) + 6\,\mathrm{MZV}(\{p,4,2\}) + \frac{\pi^6\,\zeta_p}{90}\,, \qquad \text{(B.54)} \\
f(\{0,2\},\{1,1\},p) &= -\frac{\gamma_E\,\pi^2\,\mathrm{MZV}(\{p,1\})}{3} - \gamma_E^2\,\mathrm{MZV}(\{p,2\}) + \frac{\pi^2\,\mathrm{MZV}(\{p,2\})}{6} \\
&\quad +2\,\gamma_E\,\mathrm{MZV}(\{p,3\}) - \mathrm{MZV}(\{p,4\}) + \frac{\pi^2\,\mathrm{MZV}(\{p,1,1\})}{3} \\
&\quad +2\,\gamma_E\,\mathrm{MZV}(\{p,1,2\}) - 2\,\mathrm{MZV}(\{p,1,3\}) + 2\,\gamma_E\,\mathrm{MZV}(\{p,2,1\}) \\
&\quad -2\,\mathrm{MZV}(\{p,2,2\}) - 2\,\mathrm{MZV}(\{p,3,1\}) - 2\,\mathrm{MZV}(\{p,1,1,2\}) \\
&\quad -2\,\mathrm{MZV}(\{p,1,2,1\}) - 2\,\mathrm{MZV}(\{p,2,1,1\}) + \frac{\gamma_E^2\,\pi^2\,\zeta_p}{6}\,, \qquad \text{(B.55)} \\
f(\{0,2\},\{2,1\},p) &= 2\,\gamma_E^2\,\mathrm{MZV}(\{p,3\}) - 4\,\gamma_E\,\mathrm{MZV}(\{p,4\}) + 2\,\mathrm{MZV}(\{p,5\}) \\
&\quad -4\,\gamma_E\,\mathrm{MZV}(\{p,1,3\}) + 4\,\mathrm{MZV}(\{p,1,4\}) + 2\,\mathrm{MZV}(\{p,2,3\}) \\
&\quad -4\,\gamma_E\,\mathrm{MZV}(\{p,3,1\}) + 2\,\mathrm{MZV}(\{p,3,2\}) + 4\,\mathrm{MZV}(\{p,4,1\}) \\
&\quad +4\,\mathrm{MZV}(\{p,1,1,3\}) + 4\,\mathrm{MZV}(\{p,1,3,1\}) + 4\,\mathrm{MZV}(\{p,3,1,1\}) \\
&\quad +4\,\gamma_E\,\mathrm{MZV}(\{p,1\})\,\zeta_3 - 2\,\mathrm{MZV}(\{p,2\})\,\zeta_3 - 4\,\mathrm{MZV}(\{p,1,1\})\,\zeta_3 \\
&\quad -2\,\gamma_E^2\,\zeta_3\,\zeta_p\,, \qquad \text{(B.56)}
\end{aligned}
$$

$$
\begin{aligned}
f(\{0,2\},\{3,1\},p) &= -\frac{2\,\gamma_E\,\pi^4\,\mathrm{MZV}(\{p,1\})}{15} + \frac{\pi^4\,\mathrm{MZV}(\{p,2\})}{15} - 6\,\gamma_E^2\,\mathrm{MZV}(\{p,4\}) \\
&\quad +12\,\gamma_E\,\mathrm{MZV}(\{p,5\}) - 6\,\mathrm{MZV}(\{p,6\}) + \frac{2\,\pi^4\,\mathrm{MZV}(\{p,1,1\})}{15} \\
&\quad +12\,\gamma_E\,\mathrm{MZV}(\{p,1,4\}) - 12\,\mathrm{MZV}(\{p,1,5\}) - 6\,\mathrm{MZV}(\{p,2,4\}) \\
&\quad +12\,\gamma_E\,\mathrm{MZV}(\{p,4,1\}) - 6\,\mathrm{MZV}(\{p,4,2\}) - 12\,\mathrm{MZV}(\{p,5,1\}) \\
&\quad -12\,\mathrm{MZV}(\{p,1,1,4\}) - 12\,\mathrm{MZV}(\{p,1,4,1\}) \\
&\quad -12\,\mathrm{MZV}(\{p,4,1,1\}) + \frac{\gamma_E^2\,\pi^4\,\zeta_p}{15}\,, \qquad \text{(B.57)} \\
f(\{0,1\},\{1,2\},p) &= \frac{\pi^4\,\mathrm{MZV}(\{p,1\})}{36} + \frac{\gamma_E\,\pi^2\,\mathrm{MZV}(\{p,2\})}{3} - \frac{\pi^2\,\mathrm{MZV}(\{p,3\})}{3} \\
&\quad -\gamma_E\,\mathrm{MZV}(\{p,4\}) + \mathrm{MZV}(\{p,5\}) - \frac{\pi^2\,\mathrm{MZV}(\{p,1,2\})}{3} \\
&\quad +\mathrm{MZV}(\{p,1,4\}) - \frac{\pi^2\,\mathrm{MZV}(\{p,2,1\})}{3} - 2\,\gamma_E\,\mathrm{MZV}(\{p,2,2\}) \\
&\quad +2\,\mathrm{MZV}(\{p,2,3\}) + 2\,\mathrm{MZV}(\{p,3,2\}) + \mathrm{MZV}(\{p,4,1\}) \\
&\quad +2\,\mathrm{MZV}(\{p,1,2,2\}) + 2\,\mathrm{MZV}(\{p,2,1,2\}) + 2\,\mathrm{MZV}(\{p,2,2,1\}) \\
&\quad -\frac{\gamma_E\,\pi^4\,\zeta_p}{36}\,, \qquad \text{(B.58)} \\
f(\{0,2\},\{1,2\},2) &= \frac{101\,\gamma_E^2\,\pi^6}{22680} + \frac{769\,\pi^8}{756000} - \frac{37\,\mathrm{MZV}(\{5,3\})}{5} - \frac{\gamma_E\,\pi^4\,\zeta_3}{10} - \gamma_E^2\,\zeta_3^2 \\
&\quad +\frac{2\,\pi^2\,\zeta_3^2}{3} + \frac{\gamma_E\,\pi^2\,\zeta_5}{6} - 15\,\zeta_3\,\zeta_5 + \frac{77\,\gamma_E\,\zeta_7}{8}\,, \qquad \text{(B.59)} \\
f(\{0,1\},\{1,1\},\{2,1\},2) &= -\frac{9139\,\pi^8}{6804000} + \frac{38\,\mathrm{MZV}(\{5,3\})}{5} + \frac{13\,\gamma_E\,\pi^4\,\zeta_3}{180} \\
&\quad -\frac{5\,\pi^2\,\zeta_3^2}{3} - \frac{2\,\gamma_E\,\pi^2\,\zeta_5}{3} + 29\,\zeta_3\,\zeta_5 + \frac{19\,\gamma_E\,\zeta_7}{8}\,, \qquad \text{(B.60)}
\end{aligned}
$$

$$
\begin{aligned}
f(\{0,3\},\{1,1\},p) &= \frac{\gamma_E^2\,\pi^2\,\mathrm{MZV}(\{p,1\})}{2} + \gamma_E^3\,\mathrm{MZV}(\{p,2\}) - \frac{\gamma_E\,\pi^2\,\mathrm{MZV}(\{p,2\})}{2} \\
&\quad -3\,\gamma_E^2\,\mathrm{MZV}(\{p,3\}) + \frac{\pi^2\,\mathrm{MZV}(\{p,3\})}{6} + 3\,\gamma_E\,\mathrm{MZV}(\{p,4\}) \\
&\quad -\mathrm{MZV}(\{p,5\}) - \gamma_E\,\pi^2\,\mathrm{MZV}(\{p,1,1\}) - 3\,\gamma_E^2\,\mathrm{MZV}(\{p,1,2\}) \\
&\quad +\frac{\pi^2\,\mathrm{MZV}(\{p,1,2\})}{2} + 6\,\gamma_E\,\mathrm{MZV}(\{p,1,3\}) - 3\,\mathrm{MZV}(\{p,1,4\}) \\
&\quad -3\,\gamma_E^2\,\mathrm{MZV}(\{p,2,1\}) + \frac{\pi^2\,\mathrm{MZV}(\{p,2,1\})}{2} + 6\,\gamma_E\,\mathrm{MZV}(\{p,2,2\}) \\
&\quad -4\,\mathrm{MZV}(\{p,2,3\}) + 6\,\gamma_E\,\mathrm{MZV}(\{p,3,1\}) - 4\,\mathrm{MZV}(\{p,3,2\}) \\
&\quad -3\,\mathrm{MZV}(\{p,4,1\}) + \pi^2\,\mathrm{MZV}(\{p,1,1,1\}) + 6\,\gamma_E\,\mathrm{MZV}(\{p,1,1,2\}) \\
&\quad -6\,\mathrm{MZV}(\{p,1,1,3\}) + 6\,\gamma_E\,\mathrm{MZV}(\{p,1,2,1\}) - 6\,\mathrm{MZV}(\{p,1,2,2\}) \\
&\quad -6\,\mathrm{MZV}(\{p,1,3,1\}) + 6\,\gamma_E\,\mathrm{MZV}(\{p,2,1,1\}) - 6\,\mathrm{MZV}(\{p,2,1,2\}) \\
&\quad -6\,\mathrm{MZV}(\{p,2,2,1\}) - 6\,\mathrm{MZV}(\{p,3,1,1\}) - 6\,\mathrm{MZV}(\{p,1,1,1,2\}) \\
&\quad -6\,\mathrm{MZV}(\{p,1,1,2,1\}) - 6\,\mathrm{MZV}(\{p,1,2,1,1\}) \\
&\quad -6\,\mathrm{MZV}(\{p,2,1,1,1\}) - \frac{\gamma_E^3\,\pi^2\,\zeta_p}{6}\,, \qquad \text{(B.61)} \\
f(\{0,3\},\{2,1\},2) &= \frac{167\,\gamma_E^2\,\pi^6}{7560} + \frac{3113\,\pi^8}{567000} + \frac{28\,\mathrm{MZV}(\{5,3\})}{5} + \gamma_E^3\,\pi^2\,\zeta_3 \\
&\quad +\frac{7\,\gamma_E\,\pi^4\,\zeta_3}{12} - 15\,\gamma_E^2\,\zeta_3^2 - \frac{3\,\pi^2\,\zeta_3^2}{2} - 9\,\gamma_E^3\,\zeta_5 \\
&\quad +\frac{9\,\gamma_E\,\pi^2\,\zeta_5}{2} - 25\,\zeta_3\,\zeta_5 - \frac{903\,\gamma_E\,\zeta_7}{8}\,, \qquad \text{(B.62)} \\
f(\{0,4\},\{1,1\},2) &= \frac{7\,\gamma_E^4\,\pi^4}{360} - \frac{\gamma_E^2\,\pi^6}{168} - \frac{48493\,\pi^8}{13608000} + \frac{43\,\mathrm{MZV}(\{5,3\})}{5} \\
&\quad -\frac{4\,\gamma_E^3\,\pi^2\,\zeta_3}{3} - \frac{2\,\gamma_E\,\pi^4\,\zeta_3}{5} + 6\,\gamma_E^2\,\zeta_3^2 + \pi^2\,\zeta_3^2 \\
&\quad +14\,\gamma_E^3\,\zeta_5 - \frac{10\,\gamma_E\,\pi^2\,\zeta_5}{3} + 17\,\zeta_3\,\zeta_5 + \frac{307\,\gamma_E\,\zeta_7}{4}\,. \qquad \text{(B.63)}
\end{aligned}
$$

The list of equations presented here has a certain overlap with the content of Appendix C in [113]. On the other hand, most of our relations are more general. All infinite sums

have been obtained by an algorithm based on the nested sums [118, 189] method[1]. The Riemann ζ-function [132, 173, 174] is defined by

$$\zeta_p \equiv \sum_{i=1}^{\infty} \frac{1}{i^p} \quad \text{for} \quad Re(p) > 1. \tag{B.64}$$

The multiple zeta values [157] "MZV" that occur frequently in the above equtions are defined by

$$\mathrm{MZV}(\{m_1, \ldots, m_n\}) \equiv \sum_{i_1=1}^{\infty} \frac{1}{i_1^{m_1}} \sum_{i_2=1}^{i_1-1} \frac{1}{i_2^{m_2}} \cdots \sum_{i_{n-1}=1}^{i_{n-2}-1} \frac{1}{i_{n-1}^{m_{n-1}}} \sum_{i_n=1}^{i_{n-1}-1} \frac{1}{i_n^{m_n}}\,. \tag{B.65}$$

They can often be converted to values of the Riemann ζ-function by means of available computer algebra packages [122, 130].

[1] I would like to thank Daniel Maître for providing a `Mathematica` [68] routine by means of which it was possible to extract the presented infinite sums.

Appendix C

Relations between polylogarithms

In this appendix we collect useful relations among logarithms, polylogarithms Li_n, and Nielsen polylogarithms $S_{n,p}$ as well as some additional integrals. As stated earlier in section 3.2.1, the automatic application of these relations in the `Mathematica` package `HypExp` is optional and controlled by the value of `$HypExpPolyLogRules`. The relations are based on [126, 128] and hold at least for all $z \in W$, where W is defined in Eq. (3.3).

C.1 Relations between logarithms and polylogarithms

$$\ln(\frac{z}{z-1}) = \ln(-z) - \ln(1-z) \tag{C.1}$$

$$\ln(\frac{1}{1-z}) = -\ln(1-z) \tag{C.2}$$

$$\ln(\frac{z}{1-z}) = -\ln(1-z) + \ln(z) \tag{C.3}$$

$$Li_2(1-z) = -Li_2(z) + \frac{\pi^2}{6} - \ln(z)\,\ln(1-z) \tag{C.4}$$

$$Li_2(\frac{z}{z-1}) = -Li_2(z) - \frac{1}{2}\ln^2(1-z) \tag{C.5}$$

$$Li_2(\frac{1}{1-z}) = Li_2(z) - \frac{1}{2}\,\ln^2(1-z) + \frac{\pi^2}{6} + \ln(1-z)\,\ln(-z) \tag{C.6}$$

$$Li_2(\frac{1}{z}) = -\frac{1}{2}\ln^2(-\frac{1}{z}) - \frac{\pi^2}{6} - Li_2(z) \tag{C.7}$$

$$Li_2(\frac{z-1}{z}) = \frac{1}{2}\,\ln^2(-\frac{1}{z}) + \frac{\pi^2}{3} - \ln(\frac{1}{z})\,\ln(\frac{z-1}{z}) + Li_2(z) \tag{C.8}$$

$$\begin{aligned} Li_3(\frac{z}{z-1}) = {} & -Li_3(z) - Li_3(1-z) + \zeta(3) + \frac{\pi^2}{6}\,\ln(1-z) \\ & -\frac{1}{2}\,\ln(z)\,\ln^2(1-z) + \frac{1}{6}\,\log^3(1-z) \end{aligned} \tag{C.9}$$

$$\begin{aligned} Li_3(\frac{1}{1-z}) = {} & \frac{1}{6}\,\ln^3(1-z) - \frac{1}{2}\,\ln(-z)\,\ln^2(1-z) + \frac{1}{2}\,\ln(z)\,\ln^2(1-z) \\ & -\frac{\pi^2}{3}\,\ln(1-z) + Li_3(1-z) \end{aligned} \tag{C.10}$$

$$Li_3(\frac{1}{z}) = Li_3(z) - \frac{\pi^2}{6}\ln(-\frac{1}{z}) - \frac{1}{6}\ln^3(-\frac{1}{z}) \tag{C.11}$$

$$\begin{aligned} Li_3(\frac{z-1}{z}) &= -Li_3(z) - Li_3(1-z) + \zeta(3) - \frac{1}{6}\ln^3(\frac{1-z}{z}) - \frac{\pi^2}{6}\ln(\frac{1-z}{z}) \\ &\quad + \frac{1}{6}\ln^3(1-z) + \frac{\pi^2}{6}\ln(1-z) - \frac{1}{2}\ln^2(1-z)\ln(z) \end{aligned} \tag{C.12}$$

$$\begin{aligned} Li_4(\frac{1}{1-z}) &= -\frac{1}{24}\ln^4(1-z) + \frac{1}{6}\ln(-z)\ln^3(1-z) - \frac{1}{6}\ln(z)\ln^3(1-z) \\ &\quad + \frac{\pi^2}{6}\ln^2(1-z) + \frac{\pi^4}{45} - Li_4(1-z) \end{aligned} \tag{C.13}$$

$$Li_4(\frac{z-1}{z}) = -Li_4(\frac{z}{z-1}) - \frac{1}{24}\ln^4(\frac{1-z}{z}) - \frac{\pi^2}{12}\ln^2(\frac{1-z}{z}) - \frac{7\pi^4}{360} \tag{C.14}$$

$$\begin{aligned} Li_5(\frac{1}{1-z}) &= \frac{1}{120}\ln^5(1-z) - \frac{1}{24}\ln(-z)\ln^4(1-z) + \frac{1}{24}\ln(z)\ln^4(1-z) \\ &\quad - \frac{\pi^2}{18}\ln^3(1-z) - \frac{\pi^4}{45}\ln(1-z) + Li_5(1-z) \end{aligned} \tag{C.15}$$

$$\begin{aligned} S_{2,2}(z) &= \frac{1}{24}\ln^4(1-z) - \frac{1}{6}\ln(z)\ln^3(1-z) + \frac{\pi^2}{12}\ln^2(1-z) \\ &\quad - Li_3(z)\ln(1-z) + \zeta(3)\ln(1-z) - Li_4(1-z) + Li_4(z) \\ &\quad + Li_4(\frac{z}{z-1}) + \frac{\pi^4}{90} \end{aligned} \tag{C.16}$$

$$\begin{aligned} S_{2,2}(1-z) &= -\frac{1}{24}\ln^4(1-z) + \frac{1}{6}\ln(z)\ln^3(1-z) - \frac{1}{4}\ln^2(z)\ln^2(1-z) \\ &\quad - \frac{\pi^2}{12}\ln^2(1-z) + \frac{\pi^2}{6}\ln(z)\ln(1-z) - \ln(z)\,Li_3(1-z) \\ &\quad + Li_4(1-z) - Li_4(z) - Li_4(\frac{z}{z-1}) + \zeta(3)\ln(z) - \frac{\pi^4}{120} \end{aligned} \tag{C.17}$$

$$\begin{aligned} S_{2,2}(\frac{z}{z-1}) &= \frac{1}{12}\ln^4(1-z) - \frac{1}{3}\ln(z)\ln^3(1-z) + \frac{\pi^2}{12}\ln^2(1-z) - \frac{\pi^4}{90} \\ &\quad - Li_3(1-z)\ln(1-z) - Li_3(z)\ln(1-z) \\ &\quad + Li_4(1-z) + Li_4(z) + Li_4(\frac{z}{z-1}) \end{aligned} \tag{C.18}$$

$$\begin{aligned} S_{2,2}(\frac{1}{1-z}) &= \frac{1}{3}\ln(z)\ln^3(1-z) - \frac{1}{6}\ln(-z)\ln^3(1-z) - \frac{\pi^2}{12}\ln^2(1-z) \\ &\quad - \frac{1}{2}\ln(-z)\ln(z)\ln^2(1-z) + \frac{1}{4}\ln^2(-z)\ln^2(1-z) - Li_4(z) \\ &\quad - Li_4(1-z) - Li_4(\frac{z}{z-1}) + Li_3(1-z)\ln(1-z) \end{aligned}$$

$$
\begin{aligned}
&+\frac{\pi^2}{6}\ln(-z)\ln(1-z)+\frac{\pi^4}{72}-\zeta(3)\ln(1-z)\\
&-\ln(-z)Li_3(1-z)+\zeta(3)\ln(-z)
\end{aligned}
\tag{C.19}
$$

$$
\begin{aligned}
S_{2,3}(z) &= \frac{1}{8}\ln(z)\ln^4(1-z)-\frac{1}{30}\ln^5(1-z)-\frac{\pi^2}{18}\ln^3(1-z)\\
&+\frac{1}{2}Li_3(z)\ln^2(1-z)+\left[Li_4(1-z)-Li_4(\frac{z}{z-1})\right]\ln(1-z)\\
&-\frac{\zeta(3)}{2}\ln^2(1-z)-Li_5(z)-Li_5(1-z)-Li_5(\frac{z}{z-1})\\
&+S_{3,2}(z)+\zeta(5)
\end{aligned}
\tag{C.20}
$$

$$
\begin{aligned}
S_{2,3}(1-z) &= \frac{1}{24}\ln(z)\ln^4(1-z)-\frac{1}{6}\ln^2(z)\ln^3(1-z)+\frac{1}{6}\ln^3(z)\ln^2(1-z)\\
&+\frac{\pi^2}{12}\ln(z)\ln^2(1-z)-\frac{\pi^2}{12}\ln^2(z)\ln(1-z)-Li_4(z)\ln(1-z)\\
&+\zeta(3)\ln(z)\ln(1-z)+\frac{\pi^4}{90}\ln(1-z)+\frac{\pi^4}{90}\ln(z)-\frac{\zeta(3)}{2}\ln^2(z)\\
&+\frac{1}{2}\ln^2(z)Li_3(1-z)-\ln(z)Li_4(1-z)+\ln(z)Li_4(z)\\
&+\ln(z)Li_4(\frac{z}{z-1})-S_{3,2}(z)+2\,\zeta(5)-\frac{\pi^2}{6}\zeta(3)
\end{aligned}
\tag{C.21}
$$

$$
\begin{aligned}
S_{2,3}(\frac{1}{1-z}) &= -\frac{1}{60}\ln^5(1-z)+\frac{1}{8}\ln(z)\ln^4(1-z)+\frac{1}{12}\ln^2(-z)\ln^3(1-z)\\
&-\frac{1}{3}\ln(-z)\ln(z)\ln^3(1-z)-\frac{\pi^2}{36}\ln^3(1-z)-\frac{\pi^4}{90}\ln(-z)\\
&-\frac{1}{12}\ln^3(-z)\ln^2(1-z)+\frac{\pi^2}{12}\ln(-z)\ln^2(1-z)-\frac{\zeta(3)}{2}\ln^2(-z)\\
&+\frac{1}{4}\ln^2(-z)\ln(z)\ln^2(1-z)-\frac{\pi^2}{12}\ln^2(-z)\ln(1-z)\\
&+\frac{1}{2}Li_3(1-z)\ln^2(1-z)-\ln(-z)\ln(1-z)Li_3(1-z)\\
&-Li_4(1-z)\ln(1-z)-Li_4(\frac{z}{z-1})\ln(1-z)-\frac{\pi^4}{90}\ln(1-z)\\
&+\frac{1}{2}\ln^2(-z)Li_3(1-z)+\ln(-z)Li_4(1-z)+\ln(-z)Li_4(z)\\
&+\ln(-z)Li_4(\frac{z}{z-1})+Li_5(1-z)-2\,Li_5(z)-2\,Li_5(\frac{z}{z-1})\\
&+S_{3,2}(z)+\zeta(5)-\frac{\pi^2}{6}\zeta(3)
\end{aligned}
\tag{C.22}
$$

$$
\begin{aligned}
S_{2,3}(\frac{z}{z-1}) &= \frac{1}{24}\,\ln^5(1-z) - \frac{1}{6}\,\ln(z)\,\ln^4(1-z) + \frac{\pi^2}{18}\,\ln^3(1-z) + 2\,\zeta(5) \\
&\quad -\frac{1}{2}\,Li_3(1-z)\,\ln^2(1-z) - \frac{1}{2}\,Li_3(z)\,\ln^2(1-z) - S_{3,2}(z) \\
&\quad +\frac{\zeta(3)}{2}\ln^2(1-z) + \left[Li_4(1-z) + Li_4(\frac{z}{z-1})\right]\ln(1-z) \\
&\quad +\frac{\pi^4}{90}\,\ln(1-z) - 2\,Li_5(1-z) + Li_5(z) + Li_5(\frac{z}{z-1})
\end{aligned}
\tag{C.23}
$$

$$
\begin{aligned}
S_{3,2}(1-z) &= -\frac{1}{120}\,\ln^5(1-z) + \frac{1}{24}\,\ln(z)\,\ln^4(1-z) - \frac{1}{12}\ln^2(z)\ln^3(1-z) \\
&\quad -\frac{\pi^2}{36}\,\ln^3(1-z) + \frac{\pi^2}{12}\,\ln(z)\,\ln^2(1-z) - Li_4(z)\,\ln(1-z) \\
&\quad +\zeta(3)\ln(z)\ln(1-z) - \frac{\pi^4}{120}\ln(1-z) + \frac{\pi^4}{90}\ln(z) \\
&\quad -\ln(z)Li_4(1-z) + Li_5(z) + Li_5(1-z) + Li_5(\frac{z}{z-1}) \\
&\quad -\frac{\pi^2\zeta(3)}{6} + \zeta(5) - S_{3,2}(z)
\end{aligned}
\tag{C.24}
$$

$$
\begin{aligned}
S_{3,2}(\frac{z}{z-1}) &= \frac{1}{60}\,\ln^5(1-z) - \frac{1}{24}\,\ln(z)\,\ln^4(1-z) + \frac{\pi^2}{36}\,\ln^3(1-z) + \zeta(5) \\
&\quad +\frac{\zeta(3)}{2}\ln^2(1-z) + \left[Li_4(\frac{z}{z-1}) - Li_4(z)\right]\ln(1-z) + 2Li_5(z) \\
&\quad +\frac{\pi^4}{90}\,\ln(1-z) - Li_5(1-z) + 2\,Li_5(\frac{z}{z-1}) - S_{3,2}(z)
\end{aligned}
\tag{C.25}
$$

$$
\begin{aligned}
S_{3,2}(\frac{1}{1-z}) &= \frac{1}{24}\,\ln(-z)\,\ln^4(1-z) - \frac{1}{12}\,\ln(z)\,\ln^4(1-z) \\
&\quad -\frac{1}{12}\,\ln^2(-z)\,\ln^3(1-z) + \frac{1}{6}\,\ln(-z)\,\ln(z)\,\ln^3(1-z) \\
&\quad +\frac{\pi^2}{36}\,\ln^3(1-z) - \frac{\pi^2}{12}\,\ln(-z)\,\ln^2(1-z) + \frac{\zeta(3)}{2}\,\ln^2(1-z) \\
&\quad -Li_4(1-z)\ln(1-z) + Li_4(z)\ln(1-z) - \frac{\pi^2}{6}\,\zeta(3) \\
&\quad -\frac{\pi^4}{72}\ln(1-z) - \frac{\pi^4}{90}\ln(-z) + \ln(-z)Li_4(1-z) + 2Li_5(1-z) \\
&\quad -Li_5(z) - Li_5(\frac{z}{z-1}) + S_{3,2}(z) - \zeta(3)\ln(-z)\ln(1-z)
\end{aligned}
\tag{C.26}
$$

$$
S_{3,2}(-1) = \frac{\pi^2}{12}\,\zeta(3) - \frac{29}{32}\,\zeta(5) \tag{C.27}
$$

There exist also relations between harmonic polylogarithms $H_{m_1,\ldots,m_k}$ of different arguments. These are implemented in the `HPL` package and described in Ref. [130].

C.2 Additional integrals

This subsection is devoted to some additional integrals yet unknown to `Mathematica`. They are, however, not implemented in the `HypExp` package.

$$\int_0^1 du\,\frac{\ln(1-u)\,\ln^2(1-zu)}{u} = -\frac{\pi^4}{45} + \frac{\pi^2}{2}\,\ln^2(1-z) + \frac{1}{12}\,\ln^4(1-z)$$
$$-\frac{5}{3}\,\ln(z)\,\ln^3(1-z) - 2\,\ln^2(1-z)\,Li_2(z) - [Li_2(z)]^2$$
$$-4\,\ln(1-z)\,Li_3(1-z) - 2\,\ln(1-z)\,Li_3(z) + 2\,Li_4(1-z) + 2\,Li_4(z)$$
$$+2\,Li_4(\frac{z}{z-1}) + 2\,\zeta(3)\,\ln(1-z) \quad \text{(C.28)}$$

$$\int_0^1 du\,\frac{\ln(u)\,\ln(1-u)\,\ln(1-zu)}{u} = \frac{\pi^4}{90} + \frac{\pi^2}{12}\,\ln^2(1-z) + \frac{1}{24}\,\ln^4(1-z)$$
$$-\frac{1}{6}\,\ln(z)\,\ln^3(1-z) + \frac{\pi^2}{6}\,Li_2(z) - \frac{1}{2}\,[Li_2(z)]^2 - \ln(1-z)\,Li_3(z)$$
$$-Li_4(1-z) - Li_4(z) + Li_4(\frac{z}{z-1}) + \zeta(3)\,\ln(1-z) \quad \text{(C.29)}$$

$$\int_0^1 du\,\frac{\ln^2(u)\,\ln(1-zu)}{1-u} = -[Li_2(z)]^2 - 2\,\ln(1-z)\,Li_3(z)$$
$$+2\,Li_4(z) + 2\,\zeta(3)\,\ln(1-z) \quad \text{(C.30)}$$

$$\int_0^1 du\,\frac{\ln^2(u)\,\ln(1-u)\,\ln(1-zu)}{u} = -4\,\mathrm{HPL}(\{3,2\},z) - 10\,S_{3,2}(z) - \frac{\pi^2}{3}\,Li_3(z)$$
$$+2\,Li_2(z)\,Li_3(z) + 6\,Li_5(z) - 2\,\zeta(3)\,Li_2(z) \quad \text{(C.31)}$$

$$\int_0^1 du\,\frac{Li_2(u)}{1-uz} = -\frac{\pi^2}{3}\,\frac{\ln(1-z)}{z} + \frac{\ln(z)\,\ln^2(1-z)}{2\,z} + \frac{\ln(1-z)\,Li_2(z)}{z}$$
$$+\frac{Li_3(1-z)}{z} - \frac{Li_3(z)}{z} - \frac{\zeta(3)}{z} \quad \text{(C.32)}$$

$$\int_0^1 du\,\frac{\ln(1-uz)\,Li_2(u)}{1-uz} = \frac{\pi^4}{90\,z} - \frac{\pi^2}{3}\,\frac{\ln^2(1-z)}{z} - \frac{\ln^4(1-z)}{24\,z}$$
$$+\frac{5}{6}\,\frac{\ln(z)\,\ln^3(1-z)}{z} + \frac{\ln^2(1-z)\,Li_2(z)}{z} + \frac{[Li_2(z)]^2}{2\,z}$$
$$+2\,\frac{\ln(1-z)\,Li_3(1-z)}{z} + \frac{\ln(1-z)\,Li_3(z)}{z} - \frac{Li_4(1-z)}{z}$$
$$-\frac{Li_4(z)}{z} - \frac{1}{z}\,Li_4(\frac{z}{z-1}) - \zeta(3)\,\frac{\ln(1-z)}{z} \quad \text{(C.33)}$$

$$\int_0^z dw\,\frac{\ln^2(w)\,\ln^2(1-w)}{w} = -\frac{2\pi^4}{45}\ln(z) - \frac{\pi^2}{3}\ln(z)\ln^2(1-z)$$
$$+\frac{\pi^2}{3}\,\ln(1-z)\,\ln^2(z) + \frac{2}{3}\,\ln^3(1-z)\,\ln^2(z) - \ln^2(1-z)\,\ln^3(z)$$
$$-2\,\ln(1-z)\,\ln^2(z)\,Li_2(z) - 2\,\ln^2(z)\,Li_3(1-z) + 4\,\ln(1-z)\,\ln(z)\,Li_3(z)$$
$$+4\,\ln(z)\,Li_4(1-z) - 4\,\ln(z)\,Li_4(z) - 4\,\ln(z)\,Li_4(\frac{z}{z-1}) + 4\,S_{3,2}(z)$$
$$-\frac{1}{6}\ln(z)\ln^4(1-z) - 4\,\zeta(3)\,\ln(1-z)\,\ln(z) + 2\,\zeta(3)\,\ln^2(z) \quad \text{(C.34)}$$

$$\int_0^z dw\,\frac{\ln^2(w)\,\ln^2(1-w)}{1-w} = -\frac{2\pi^2}{9}\,\ln^3(1-z) - \frac{2}{15}\,\ln^5(1-z) - \frac{2\pi^4}{45}\,\ln(z)$$
$$+\frac{\pi^2}{3}\,\ln(z)\,\ln^2(1-z) + \frac{1}{2}\,\ln(z)\ln^4(1-z) - \frac{5}{3}\,\ln^3(1-z)\,\ln^2(z)$$
$$-2\,\ln(z)\,\ln^2(1-z)\,Li_2(z) - 4\,\ln(z)\,\ln(1-z)\,Li_3(1-z) + 2\,\ln^2(1-z)\,Li_3(z)$$
$$+4\,\ln(1-z)\,Li_4(1-z) + 4\,\ln(z)\,Li_4(1-z) - 4\,\ln(1-z)\,Li_4(\frac{z}{z-1})$$
$$-4\,Li_5(1-z) - 4\,Li_5(z) - 4\,Li_5(\frac{z}{z-1}) + 4\,S_{3,2}(z) - 2\,\zeta(3)\,\ln^2(1-z) + 4\,\zeta(5) \quad \text{(C.35)}$$

$$\int_0^z dw\,\frac{\ln(w)\,Li_2(w)}{1-w} = \frac{\pi^2}{6}\ln^2(1-z) + \frac{1}{12}\ln^4(1-z) - \frac{\pi^2}{3}\ln(z)\ln(1-z)$$
$$-\frac{1}{3}\,\ln(z)\,\ln^3(1-z) + \ln^2(z)\,\ln^2(1-z) + \ln(z)\,\ln(1-z)\,Li_2(z)$$
$$-\frac{1}{2}\,[Li_2(z)]^2 + 2\,\ln(z)\,Li_3(1-z) - 2\,\ln(1-z)\,Li_3(z) - 2\,Li_4(1-z)$$
$$+2\,Li_4(z) + 2\,Li_4(\frac{z}{z-1}) + 2\,\zeta(3)\,\ln(1-z) - 2\,\zeta(3)\,\ln(z) + \frac{\pi^4}{45} \quad \text{(C.36)}$$

$$\int_0^z dw\,[Li_2(w)]^2 = 6\,z + 6\,\ln(1-z) - \frac{2\pi^2}{3}\,\ln(1-z) - 6\,z\,\ln(1-z) - 2\,\ln^2(1-z)$$
$$+2\,z\,\ln^2(1-z) + 2\,\ln(z)\,\ln^2(1-z) - 2\,z\,Li_2(z) + 2\,\ln(1-z)\,Li_2(z)$$
$$+2\,z\,\ln(1-z)\,Li_2(z) + z\,[Li_2(z)]^2 + 4\,Li_3(1-z) - 4\,\zeta(3) \quad \text{(C.37)}$$

$$\int_0^z dw\,\frac{[Li_2(w)]^2}{w} \;=\; 2\,\mathrm{HPL}(\{3,2\},z) + 4\,S_{3,2}(z) \quad \text{(C.38)}$$

$$\int_0^z dw\,\frac{[Li_2(w)]^2}{w^2} = -\frac{2\pi^2}{3}\,\ln(1-z) + 2\,\ln^2(1-z) - \frac{2\,\ln^2(1-z)}{z} + 4\,Li_2(z)$$
$$+ 2\,\ln^2(1-z)\,\ln(z) + 2\,\ln(1-z)\,Li_2(z) + \frac{2\,\ln(1-z)\,Li_2(z)}{z}$$
$$- \frac{[Li_2(z)]^2}{z} + 4\,Li_3(1-z) + 2\,Li_3(z) - 4\,\zeta(3) \quad \text{(C.39)}$$

$$\int_0^z dw\,\frac{Li_3(w)}{(1-w)^2} = \frac{\pi^2}{3}\,\ln(1-z) - \ln(z)\,\ln^2(1-z) - \ln(1-z)\,Li_2(z)$$
$$-2\,Li_3(1-z) + \frac{z\,Li_3(z)}{1-z} + 2\,\zeta(3) \quad \text{(C.40)}$$

$$\int_0^z dw\,\frac{Li_4(w)}{(1-w)^2} = \frac{1}{2}\,[Li_2(z)]^2 + \ln(1-z)\,Li_3(z) + \frac{z\,Li_4(z)}{1-z} \quad \text{(C.41)}$$

$$\int_0^z dw\,Li_4(\frac{w}{w-1}) = \frac{\pi^2}{6}\,\ln^2(1-z) + \frac{1}{24}\ln^4(1-z) - \frac{1}{2}\,\ln(z)\ln^3(1-z)$$
$$- \frac{1}{2}\,\ln^2(1-z)\,Li_2(z) - \frac{1}{2}[Li_2(z)]^2 - \ln(1-z)\,Li_3(1-z)$$
$$- \ln(1-z)\,Li_3(z) + z\,Li_4(\frac{z}{z-1}) + \zeta(3)\,\ln(1-z) \quad \text{(C.42)}$$

Defining

$$I_n^p(z) := \int_0^1 du\,\frac{z\,Li_p(u)}{(1-zu)^n}\,, \qquad n \in \mathbb{N}^{\geq 1}\,, \qquad p \in \mathbb{N}^{\geq 2}\,, \quad \text{(C.43)}$$

we have

$$I_1^p(z) = -\zeta_p\,\ln(1-z) - (-1)^p\,[Li_{p+1}(z) + \mathrm{HPL}(\{p,1\},z)]$$
$$+ \sum_{i=2}^{p-1}(-1)^{p-i}\,\zeta_i\,Li_{p+1-i}(z)\,, \quad \text{(C.44)}$$

where the last sum only contributes if $p > 2$. Moreover, we have

$$I_{n+1}^p(z) = \left[1 - \frac{1}{n} + \frac{z}{n}\,\frac{d}{dz}\right] I_n^p(z) \qquad \text{for } n > 1\,. \quad \text{(C.45)}$$

Integrals of the type

$$\int_0^1 du\,\frac{z\,\ln^q(u)\,Li_p(u)}{(1-zu)^n}\,, \qquad n, q \in \mathbb{N}^{\geq 1}\,, \qquad p \in \mathbb{N}^{\geq 2} \quad \text{(C.46)}$$

can also be solved. We apply the following steps:

1. Consider $n = 1$ and write $z/(1-zu) = \sum_{j=1}^{\infty} z^j\, u^{j-1}$.
2. Run the `Mathematica` command `Integrate`$\big[$`u`$^{\mathrm{j}-1}$ `Log[u]`$^{\mathrm{q}}$ `PolyLog[p, u]`$, \{\mathrm{u}, 0, 1\}\big]$ or a similar command in your most favorite computer algebra system. Here, j ist symbolic but p and q are numerical.
3. The resulting terms are of the form $z^j\ \psi^{(i)}(j)/j^k$ (or similar) and can be summed by means of the nested sums algorithm. As a final result one obtains harmonic polylogarithms of argument z.
4. Higher powers of n in the denominator of (C.46) are obtained by differentiation with respect to z similar to (C.45).

Further techniques are series representations of logarithms and polylogarithms as well as auxiliary – single or multiple – differentiation or integration with respect to z prior to integration over u. For instance, if we differentiate the integral

$$\int_0^1 du\, \frac{\ln^2(1-u)\, \ln^2(1-zu)}{u} \tag{C.47}$$

with respect to z, we can apply the function `HypExpInt` from the `HypExp` package on the resulting expression. Subsequently, we integrate again with respect to z and determine the additive constant. The integrals

$$\int_0^1 du\, \frac{\ln^2(1-u)\, \ln(u)\, \ln(1-zu)}{u} \quad \text{and} \quad \int_0^1 du\, \frac{\ln(1-u)\, \ln(u)\, \ln^2(1-zu)}{u} \tag{C.48}$$

can be treated analogously. The integral $\displaystyle\int_0^1 du\, \ln^2(u)\, \ln^4(1-zu)$ – and therefore also associated ones that have this integral as a basic integral in the sense of section 3.3.3 – can also be computed by means of the above mentioned techniques.

Finally, we want to state a useful trick for double integrals over the unit square. We consider

$$\int_0^1 dt_1 \int_0^1 dt_2\, g(t_1, v)\, f(t_1\, t_2, x). \tag{C.49}$$

v and x stand for any combination of residual variables. If neither of the integrations can be performed, one can substitute $t_2 = w/t_1$ and interchange the order of integration. One obtains

$$\int_0^1 dw\, f(w, x) \int_w^1 dt_1\, \frac{g(t_1, v)}{t_1}\,. \tag{C.50}$$

Oftentimes, the expression $g(t_1, v)/t_1$ is rather simple and one integration (over t_1) can be carried out at this stage. The further procedure depends on whether we have to integrate – at least over a subset – of the x's and the v's, or if one seeks for a function of all x's and the v's. In the former case, similar tricks as the one presented here might be applied to appropriate combinations of the remaining integration variables. In the latter case, one has to head for the integration over w.

Bibliography

[1] S. Weinberg, "The Quantum Theory of Fields", Vol. 1-3 , Cambridge University Press.

[2] M.E. Peskin and D.V. Schroeder, An Introduction to Quantum Field Theory (Westview Press, 1995).

[3] J. Donoghue, E. Golowich and B. Holstein, Dynamics of the Standard Model (Cambridge University Press, 1992).

[4] S.L. Glashow, J. Iliopoulos and L. Maiani, Phys. Rev. D2 (1970) 1285.

[5] N. Cabibbo, Phys. Rev. Lett. 10 (1963) 531.

[6] M. Kobayashi and T. Maskawa, Prog. Theor. Phys. 49 (1973) 652.

[7] A.J. Buras, (1998), hep-ph/9806471.

[8] L. Wolfenstein, Phys. Rev. Lett. 51 (1983) 1945.

[9] A.J. Buras, M.E. Lautenbacher and G. Ostermaier, Phys. Rev. D50 (1994) 3433, hep-ph/9403384.

[10] Particle Data Group, S. Eidelman et. al, Phys. Lett. B592 (2004) 1.

[11] `http://pdg.lbl.gov`.

[12] R. Fleischer, Lect. Notes Phys. 647 (2004) 42, hep-ph/0210323.

[13] R. Fleischer, (2006), hep-ph/0608010.

[14] CKMfitter Group, J. Charles et al., Eur. Phys. J. C 41 (2005) 1, hep-ph/0406184.

[15] CDF - Run II, A. Abulencia et al., Phys. Rev. Lett. 97 (2006) 062003, hep-ex/0606027.

[16] CDF, A. Abulencia et al., Phys. Rev. Lett. 97 (2006) 242003, hep-ex/0609040.

[17] D0, V.M. Abazov et al., Phys. Rev. Lett. 97 (2006) 021802, hep-ex/0603029.

[18] M. Beneke et al., Phys. Rev. Lett. 83 (1999) 1914, hep-ph/9905312.

[19] M. Beneke et al., Nucl. Phys. B591 (2000) 313, hep-ph/0006124.

[20] M. Beneke et al., Nucl. Phys. B606 (2001) 245, hep-ph/0104110.

[21] C.W. Bauer et al., Phys. Rev. D63 (2001) 114020, hep-ph/0011336.

[22] C.W. Bauer, D. Pirjol and I.W. Stewart, Phys. Rev. D65 (2002) 054022, hep-ph/0109045.

[23] C.W. Bauer, D. Pirjol and I.W. Stewart, Phys. Rev. D66 (2002) 054005, hep-ph/0205289.

[24] M. Beneke et al., Nucl. Phys. B643 (2002) 431, hep-ph/0206152.

[25] R.J. Hill and M. Neubert, Nucl. Phys. B657 (2003) 229, hep-ph/0211018.

[26] M. Beneke and T. Feldmann, Phys. Lett. B553 (2003) 267, hep-ph/0211358.

[27] D. Pirjol and I.W. Stewart, Phys. Rev. D67 (2003) 094005, hep-ph/0211251.

[28] T. Mannel, W. Roberts and Z. Ryzak, Nucl. Phys. B355 (1991) 38.

[29] T. Mannel, W. Roberts and Z. Ryzak, Nucl. Phys. B368 (1992) 204.

[30] A.V. Manohar and M.B. Wise, Camb. Monogr. Part. Phys. Nucl. Phys. Cosmol. 10 (2000) 1.

[31] BABAR, B. Aubert et al., Phys. Rev. Lett. 93 (2004) 081802, hep-ex/0404006.

[32] BABAR, B. Aubert et al., Phys. Rev. D73 (2006) 092001, hep-ex/0604007.

[33] Belle, M. Iwasaki et al., Phys. Rev. D72 (2005) 092005, hep-ex/0503044.

[34] The Belle Collaboration, K. Abe et al., (2005), hep-ex/0508009.

[35] A. Ishikawa et al., Phys. Rev. Lett. 96 (2006) 251801, hep-ex/0603018.

[36] A.J. Buras et al., Phys. Rev. Lett. 95 (2005) 261805, hep-ph/0508165.

[37] A.J. Buras et al., JHEP 11 (2006) 002, hep-ph/0603079.

[38] M. Gorbahn and U. Haisch, Phys. Rev. Lett. 97 (2006) 122002, hep-ph/0605203.

[39] T. Huber et al., Nucl. Phys. B740 (2006) 105, hep-ph/0512066.

[40] A. Ali and G. Hiller, Phys. Rev. D60 (1999) 034017, hep-ph/9807418.

[41] K.S.M. Lee and I.W. Stewart, Phys. Rev. D74 (2006) 014005, hep-ph/0511334.

[42] K.S.M. Lee et al., Phys. Rev. D74 (2006) 011501, hep-ph/0512191.

[43] A. Ali et al., Phys. Rev. D55 (1997) 4105, hep-ph/9609449.

[44] G. Buchalla and G. Isidori, Nucl. Phys. B525 (1998) 333, hep-ph/9801456.

[45] A. Ghinculov et al., Nucl. Phys. B685 (2004) 351, hep-ph/0312128.

[46] F. Kruger and L.M. Sehgal, Phys. Lett. B380 (1996) 199, hep-ph/9603237.

[47] C. Bobeth, M. Misiak and J. Urban, Nucl. Phys. B574 (2000) 291, hep-ph/9910220.

[48] H.H. Asatryan et al., Phys. Rev. D65 (2002) 074004, hep-ph/0109140.

[49] H.H. Asatryan et al., Phys. Rev. D66 (2002) 034009, hep-ph/0204341.

[50] P. Gambino, M. Gorbahn and U. Haisch, Nucl. Phys. B673 (2003) 238, hep-ph/0306079.

[51] M. Gorbahn and U. Haisch, Nucl. Phys. B713 (2005) 291, hep-ph/0411071.

[52] C. Bobeth et al., JHEP 04 (2004) 071, hep-ph/0312090.

[53] J. Berryhill and A. Ishikawa, private communication .

[54] M. Misiak, Nucl. Phys. B393 (1993) 23, [Erratum-ibid. B439 (1995) 461].

[55] A.J. Buras and M. Münz, Phys. Rev. D52 (1995) 186, hep-ph/9501281.

[56] P. Gambino and U. Haisch, JHEP 10 (2001) 020, hep-ph/0109058.

[57] G. Buchalla, A.J. Buras and M.K. Harlander, Nucl. Phys. B337 (1990) 313.

[58] G. Buchalla and A.J. Buras, Phys. Rev. D57 (1998) 216, hep-ph/9707243.

[59] A.J. Buras, P. Gambino and U.A. Haisch, Nucl. Phys. B570 (2000) 117, hep-ph/9911250.

[60] T. van Ritbergen, J.A.M. Vermaseren and S.A. Larin, Phys. Lett. B400 (1997) 379, hep-ph/9701390.

[61] M. Czakon, Nucl. Phys. B710 (2005) 485, hep-ph/0411261.

[62] A.J. Buras, M. Jamin and M.E. Lautenbacher, Nucl. Phys. B400 (1993) 75, hep-ph/9211321.

[63] K.G. Chetyrkin, M. Misiak and M. Munz, Nucl. Phys. B520 (1998) 279, hep-ph/9711280.

[64] K. Baranowski and M. Misiak, Phys. Lett. B483 (2000) 410, hep-ph/9907427.

[65] H.H. Asatrian et al., Phys. Lett. B507 (2001) 162, hep-ph/0103087.

[66] K.G. Chetyrkin, M. Misiak and M. Münz, Phys. Lett. B400 (1997) 206, Phys. Lett. B425 (1998) 414 (E), [hep-ph/9612313].

[67] A. Gehrmann-De Ridder, T. Gehrmann and G. Heinrich, Nucl. Phys. B682 (2004) 265, hep-ph/0311276.

[68] *MATHEMATICA 5.0*, Copyright 2003 by Wolfram Research.

[69] T. Huber and D. Maître, Comput. Phys. Commun. 175 (2006) 122, hep-ph/0507094.

[70] H. Terazawa, Rev. Mod. Phys. 45 (1973) 615.

[71] B. Mele and P. Nason, Nucl. Phys. B361 (1991) 626.

[72] T. van Ritbergen, Phys. Lett. B454 (1999) 353, hep-ph/9903226.

[73] A. Sirlin, Nucl. Phys. B196 (1982) 83.

[74] A.F. Falk, M.E. Luke and M.J. Savage, Phys. Rev. D49 (1994) 3367, hep-ph/9308288.

[75] G. Buchalla, G. Isidori and S.J. Rey, Nucl. Phys. B511 (1998) 594, hep-ph/9705253.

[76] P. Gambino and M. Misiak, Nucl. Phys. B611 (2001) 338, hep-ph/0104034.

[77] C.W. Bauer et al., Phys. Rev. D70 (2004) 094017, hep-ph/0408002.

[78] S. Bethke, Nucl. Phys. Proc. Suppl. 135 (2004) 345, hep-ex/0407021.

[79] A.H. Hoang and A.V. Manohar, Phys. Lett. B633 (2006) 526, hep-ph/0509195.

[80] BABAR, B. Aubert et al., Phys. Rev. Lett. 93 (2004) 011803, hep-ex/0404017.

[81] CDF collaboration, (2005), hep-ex/0507091.

[82] A.H. Hoang, Z. Ligeti and A.V. Manohar, Phys. Rev. D59 (1999) 074017, hep-ph/9811239.

[83] A.H. Hoang, (2000), hep-ph/0008102.

[84] A. Czarnecki and K. Melnikov, Phys. Rev. Lett. 88 (2002) 131801, hep-ph/0112264.

[85] I. Blokland et al., Phys. Rev. Lett. 93 (2004) 062001, hep-ph/0403221.

[86] I. Blokland et al., Phys. Rev. D71 (2005) 054004, hep-ph/0503039.

[87] C.W. Bauer and C.N. Burrell, Phys. Lett. B469 (1999) 248, hep-ph/9907517.

[88] C.W. Bauer and C.N. Burrell, Phys. Rev. D62 (2000) 114028, hep-ph/9911404.

[89] H.M. Asatrian et al., Phys. Rev. D66 (2002) 094013, hep-ph/0209006.

[90] H.M. Asatrian et al., Mod. Phys. Lett. A19 (2004) 603, hep-ph/0311187.

[91] U. Haisch and T. Hurth, private communication .

[92] SuperKEKB Physics Working Group, A.G. Akeroyd et al., (2004), hep-ex/0406071.

[93] A. Ali et al., Phys. Rev. D66 (2002) 034002, hep-ph/0112300.

[94] P.L. Cho, M. Misiak and D. Wyler, Phys. Rev. D54 (1996) 3329, hep-ph/9601360.

[95] P. Gambino, U. Haisch and M. Misiak, Phys. Rev. Lett. 94 (2005) 061803, hep-ph/0410155.

[96] C. Bobeth et al., Nucl. Phys. B726 (2005) 252, hep-ph/0505110.

[97] C. Bobeth et al., Phys. Rev. D64 (2001) 074014, hep-ph/0104284.

[98] C. Bobeth, A.J. Buras and T. Ewerth, Nucl. Phys. B713 (2005) 522, hep-ph/0409293.

[99] S. Schilling et al., Phys. Lett. B616 (2005) 93, hep-ph/0407323.

[100] Z.j. Xiao and L.x. Lu, Phys. Rev. D74 (2006) 034016, hep-ph/0605076.

[101] P. Colangelo et al., Phys. Rev. D73 (2006) 115006, hep-ph/0604029.

[102] S. Bertolini et al., Nucl. Phys. B353 (1991) 591.

[103] T. Goto et al., Phys. Rev. D55 (1997) 4273, hep-ph/9609512.

[104] J.L. Hewett and J.D. Wells, Phys. Rev. D55 (1997) 5549, hep-ph/9610323.

[105] C.S. Huang, W. Liao and Q.S. Yan, Phys. Rev. D59 (1999) 011701, hep-ph/9803460.

[106] Y.G. Kim, P. Ko and J.S. Lee, Nucl. Phys. B544 (1999) 64, hep-ph/9810336.

[107] E. Lunghi et al., Nucl. Phys. B568 (2000) 120, hep-ph/9906286.

[108] P. Koppenburg and J.H. Lopes, CERN Workshop "Flavour in the era of the LHC", Nov. 7-10, 2005, `http://flavlhc.web.cern.ch/flavlhc/`.

[109] J. Hewett (ed.) et al., (2004), hep-ph/0503261.

[110] J. Albert et al., (2005), physics/0512235.

[111] W.L. van Neerven, Nucl. Phys. B268 (1986) 453.

[112] G. Kramer and B. Lampe, J. Math. Phys. 28 (1987) 945.

[113] V.A. Smirnov, Evaluating Feynman Integrals (Springer Tracts of Modern Physics, Heidelberg, 2004).

[114] J. Fleischer, F. Jegerlehner and O.V. Tarasov, Nucl. Phys. B672 (2003) 303, hep-ph/0307113.

[115] T. Gehrmann and E. Remiddi, Nucl. Phys. B580 (2000) 485, hep-ph/9912329.

[116] T. Gehrmann, T. Huber and D. Maître, Phys. Lett. B622 (2005) 295, hep-ph/0507061.

[117] S. Weinzierl, JHEP 0303 (2003) 062, hep-ph/0302180.

[118] S. Moch, P. Uwer and S. Weinzierl, J. Math. Phys. 43 (2002) 3363, hep-ph/0110083.

[119] S. Weinzierl, Comput. Phys. Commun. 145 (2002) 357, math-ph/0201011.

[120] C. Bauer, A. Frink and R. Kreckel, (2000), cs.sc/0004015.

[121] J.A.M. Vermaseren, (2000), math-ph/0010025.

[122] S. Moch and P. Uwer, Comp. Phys. Commun. 174 (2006) 759, math-ph/0508008.

[123] M.Y. Kalmykov, Nucl. Phys. Proc. Suppl. 135 (2004) 280, hep-th/0406269.

[124] S. Weinzierl, J. Math. Phys. 45 (2004) 2656, hep-ph/0402131.

[125] *Maple 7*, Copyright 2001 by Waterloo Maple Software and the University of Waterloo.

[126] L. Lewin, Polylogarithms and associated functions (North Holland, Amsterdam, 1981).

[127] A.B. Goncharov, Math. Res. Lett. 497 (1998), math-ph/0010025.

[128] N. Nielsen, Nova Acta Leopoldina (Halle) 90 (1909) 123.

[129] E. Remiddi and J.A.M. Vermaseren, Int. J. Mod. Phys. A15 (2000) 725, hep-ph/9905237.

[130] D. Maître, Comp. Phys. Commun. 174 (2006) 222, hep-ph/0507152.

[131] `http://www-theorie.physik.unizh.ch/~maitreda/HypExp/`.

[132] A. Erdélyi (ed.), Higher transcendental functions, Vol. 1, (McGraw-Hill, New York, 1953) .

[133] `http://functions.wolfram.com`.

[134] K. Hepp, Commun. Math. Phys. 2 (1966) 301.

[135] T. Binoth and G. Heinrich, Nucl. Phys. B585 (2000) 741, hep-ph/0004013.

[136] T. Binoth and G. Heinrich, Nucl. Phys. B680 (2004) 375, hep-ph/0305234.

[137] T. Binoth and G. Heinrich, Nucl. Phys. B693 (2004) 134, hep-ph/0402265.

[138] S. Catani, Phys. Lett. B427 (1998) 161, hep-ph/9802439.

[139] G. Sterman and M.E. Tejeda-Yeomans, Phys. Lett. B552 (2003) 48, hep-ph/0210130.

[140] G. Kramer and B. Lampe, Z. Phys. C34 (1987) 497; C42 (1989) 504(E).

[141] T. Matsuura and W.L. van Neerven, Z. Phys. C38 (1988) 623.

[142] T. Matsuura, S.C. van der Maarck and W.L. van Neerven, Nucl. Phys. B319 (1989) 570.

[143] R.V. Harlander, Phys. Lett. B492 (2000) 74, hep-ph/0007289.

[144] W. Bernreuther et al., Nucl. Phys. B706 (2005) 245, hep-ph/0406046.

[145] W. Bernreuther et al., Nucl. Phys. B712 (2005) 229, hep-ph/0412259.

[146] W. Bernreuther et al., Nucl. Phys. B723 (2005) 91, hep-ph/0504190.

[147] A. Gehrmann-De Ridder, T. Gehrmann and E.W.N. Glover, Nucl. Phys. B691 (2004) 195, hep-ph/0403057.

[148] A. Gehrmann-De Ridder, T. Gehrmann and E.W.N. Glover, Phys. Lett. B612 (2005) 36, hep-ph/0501291.

[149] A. Gehrmann-De Ridder, T. Gehrmann and E.W.N. Glover, Phys. Lett. B612 (2005) 49, hep-ph/0502110.

[150] A. Gehrmann-De Ridder, T. Gehrmann and E.W.N. Glover, JHEP 09 (2005) 056, hep-ph/0505111.

[151] S. Moch, J.A.M. Vermaseren and A. Vogt, JHEP 08 (2005) 049, hep-ph/0507039.

[152] F.V. Tkachov, Phys. Lett. B100 (1981) 65.

[153] K.G. Chetyrkin and F.V. Tkachov, Nucl. Phys. B192 (1981) 159.

[154] S. Laporta, Int. J. Mod. Phys. A15 (2000) 5087, hep-ph/0102033.

[155] C. Anastasiou and A. Lazopoulos, JHEP 0407 (2004) 046, hep-ph/0404258.

[156] R.J. Gonsalves, Phys. Rev. D28 (1983) 1542.

[157] J.M. Borwein et al., Transactions of the American Mathematical Society, Volume 353, Number 3, year 2001, pages 907-941, arXiv:math.CA/9910045.

[158] C. Anastasiou et al., Nucl. Phys. B580 (2000) 577, hep-ph/0003261.

[159] S. Moch, J.A.M. Vermaseren and A. Vogt, Nucl. Phys. B688 (2004) 101, hep-ph/0403192.

[160] S. Moch, J.A.M. Vermaseren and A. Vogt, Nucl. Phys. B691 (2004) 129, hep-ph/0404111.

[161] S. Moch, J.A.M. Vermaseren and A. Vogt, Nucl. Phys. B724 (2005) 3, hep-ph/0504242.

[162] S. Moch, J.A.M. Vermaseren and A. Vogt, Nucl. Phys. B726 (2005) 317, hep-ph/0506288.

[163] A.V. Kotikov et al., Phys. Lett. B595 (2004) 521, hep-th/0404092.

[164] Z. Bern, L.J. Dixon and V.A. Smirnov, Phys. Rev. D72 (2005) 085001, hep-th/0505205.

[165] S. Bekavac, Comput. Phys. Commun. 175 (2006) 180, hep-ph/0505174.

[166] T. Gehrmann et al., Phys. Lett. B640 (2006) 252, hep-ph/0607185.

[167] R.V. Harlander and W.B. Kilgore, Phys. Rev. D64 (2001) 013015, hep-ph/0102241.

[168] R.V. Harlander and W.B. Kilgore, Phys. Rev. Lett. 88 (2002) 201801, hep-ph/0201206.

[169] R.V. Harlander and W.B. Kilgore, JHEP 10 (2002) 017, hep-ph/0208096.

[170] J.C. Collins, D.E. Soper and G. Sterman, Phys. Lett. B134 (1984) 263.

[171] J.C. Collins, D.E. Soper and G. Sterman, Nucl. Phys. B250 (1985) 199.

[172] P.A. Baikov, Phys. Lett. B634 (2006) 325, hep-ph/0507053.

[173] G.F.B. Riemann, Monatsber. Königl. Preuss. Akad. Wiss. Berlin (Nov. 1859) 671.

[174] A. Erdélyi (ed.), Tables of Integral Transforms, Vol. 2, (McGraw-Hill, New York, 1954) .

[175] C. Studerus, (2006), Bachelor Arbeit, Universität Zürich.

[176] C. Anastasiou and A. Daleo, JHEP 10 (2006) 031, hep-ph/0511176.

[177] J.B. Tausk, Phys. Lett. B469 (1999) 225, hep-ph/9909506.

[178] C.S. Meijer, Nieuw Arch. Wiskunde (2) 18 (1936) 10.

[179] C.S. Meijer, Proc. Nederl. Akad. Wetensch. 44 (1941) 1062.

[180] C.S. Meijer, Proc. Nederl. Akad. Wetensch. 49 (1946), 344-456, 457-469, 632-641, 765-772, 936-943, 1063-1072, 1165-1175.

[181] S. Moch, Nucl. Instrum. Meth. A559 (2006) 285, math-ph/0509058.

[182] M. Jeżabek and J.H. Kühn, Nucl. Phys. B 320 (1989) 20.

[183] A. Ali and C. Greub, Z. Phys. C49 (1991) 431.

[184] A. Ali and C. Greub, Phys. Lett. B259 (1991) 182.

[185] A. Ali and C. Greub, Phys. Lett. B361 (1995) 146, hep-ph/9506374.

[186] K.G. Chetyrkin et al., Phys. Rev. D60 (1999) 114015, hep-ph/9906273.

[187] E.W. Barnes, Proc. London Math. Soc. 6 (1908) 141.

[188] W.N. Bailey, Generalised Hypergeometric Series (Cambridge, England: University Press, 1935).

[189] J.A.M. Vermaseren, Int. J. Mod. Phys. A14 (1999) 2037, hep-ph/9806280.

Acknowledgements

Now that I have come close to the completion of my Ph.D. I can without any doubt say that going to Zürich and joining the University's Institute for Theoretical Physics was one of the best decisions I have ever made. I am therefore greatful to many people who had a great share in letting my time in Zürich become a very successful and worthwile one.

First of all I would like to thank my advisor Daniel Wyler for his support and guidance during the last three years. I profited a lot from his vast knowlegde of physics. His door was always open for discussions, and I enjoyed both physics and non-physics conversations with him. I am greatful that he was always available when he was needed, even at unearthly hours. I would also like to thank him for giving me the opportunity to attend several workshops and conferences.

No lesser thank goes to Thomas Gehrmann from whom I also benefited a lot. He taught me many interesting aspects of physics, and I enjoyed working with him and learning from him. He also showed me many computational techniques, was very patient, and always open for questions and discussions of any kind.

I am deeply indebted to Enrico Lunghi, without whom the project on rare B-decays would not have been possible. I appreciated his guidance and support at any stage of our collaboration a lot. I admire his drive and I wonder what the source of his countless good and motivating ideas might be. I hope that our collaboration will continue beyond the completion of this thesis.

Furthermore, I would like to thank various people for support during my research and during my applications, most notably Mikołaj Misiak, Thomas Mannel, John Donoghue, Tobias Hurth, and Bastian Kubis. I also enjoyed many useful discussions on physics with the postdocs, Ph. D. and diploma students of the Institute, among others Sabine Schilling, Ulrich Haisch, Alejandro Daleo, Gudrun Heinrich, Werner Porod, and Ayres Freitas.

I would like to thank Ulrich Straumann for joining the committee and for useful discussions, and Christoph Greub for providing a survey.

I would also like to thank the University of Zürich and the Schweizerischer Nationalfonds for financial support; our system administrators Roland Bernet, Douglas Potter and Marco Miranda for quick help in case of computer problems; and Daniela Montavon, Esther Meier, and Suzanne Wilde-Duvernay for the excellent administration.

A special thank goes to my office mates Daniel Maître and Tobias Kaufmann for an enjoyable atmosphere and for help and discussions on computers, physics and beyond.

I enjoyed in particular our pizza, beer, and cards (Doppelkopf) sessions at Incrocio, starring Andreas "mit Piech zum Siech" Kaiser, Christoph "Propeller" Meier, Tobias "ja, ebbe, hä" Kaufmann, Daniel "Al Capone" Maître, Tobias "jetzt geht's dabei" Goerdt, Enrico "the dark Lord of coffee" Lunghi, Beat Tödtli "Fussballgott", Eva "Verdura" Poulsen, Daniel "Re" Egli, Christian "WM-Experte" Kurz, Ayres "DoKo-Champ" Freitas, Uli "wenn ich was Grünes will, mach' ich mir 'n Beck's auf" Haisch, Alejandro "God of Sports" Daleo, Simone "Minestrone" Weinmann, David Noth and many more.

My entire time in Zürich was accompanied by music. I would like to thank the Stadtharmonie Zürich Oerlikon-Seebach and the MHZ Oberstrass for letting me join their ensembles. Highlights such as concerts at Tonhalle Zürich and KKL Luzern, the Sechseläuten parade and the concert trip to Singapore are unforgettable.

I am very grateful to my family and friends and in particular my girlfriend Cornelia for their love and care and for their support during my entire studies.

CURRICULUM VITAE

Personal Data

Name	:	HUBER
First name	:	Tobias
Date of birth	:	July 21, 1976
Place of birth	:	D-77704 Oberkirch
Nationality	:	German

Education

10/2003 - 9/2006:	PhD in Theoretical Physics, Dr. sc. nat., University of Zürich, Switzerland PhD thesis: Radiative Corrections to Rare B-Decays, Computational Tools, and Higher Order Perturbative Calculations Thesis supervisor: Prof. Dr. Daniel Wyler
10/1997 - 8/2001 and 9/2002 - 3/2003:	Diploma in Physics, University of Karlsruhe, Germany Diploma thesis: Baryon Form Factors and Baryon Decays in Chiral Perturbation Theory Thesis supervisor: Prof. Dr. Thomas Mannel
8/2001 - 8/2002:	Master of Science University of Massachusetts, Amherst, MA, USA Master thesis: Chiral Nucleon Form Factors and Long Distance Regularization Thesis supervisor: Prof. Dr. John F. Donoghue
9/1987 - 6/1996:	Hans Furler Gymnasium, Oberkirch, Germany June 1996: Abitur

Teaching Experience

10/2003 - 9/2006:	Teaching Assistant, Theoretical Physics Courses (Electrodynamics, Quantum Mechanics, Methods of Mathematical Physics, General Relativity), University of Zürich
4/2001 - 7/2001 and 9/2002 - 9/2003:	Teaching Assistant, Theoretical Physics Courses (Classical Mechanics, Electrodynamics), University of Karlsruhe
5/2002 - 8/2002:	Teacher of the physics section of two MCAT test preparation courses, "The Princeton Review", Amherst, MA, USA

4/1999 - 3/2001:	Teaching Assistant, Mathematics (Analysis, Linear Algebra) University of Karlsruhe

Awards and Scholarships

7/1999 - 3/2003:	Demy of "Studienstiftung des deutschen Volkes" (German National Academic Foundation)
1995:	Third Prize, "Bundeswettbewerb Mathematik" (National competition in Mathematics)
1993:	First Prize, "Landeswettbewerb Mathematik" (Regional competition in Mathematics)
1992:	Third Prize, "Landeswettbewerb Mathematik" (Regional competition in Mathematics)

Languages

German:	First language
English:	fluent
French:	good
Italian	

RESEARCH STATUS

Publications and Preprints:

1.) Gehrmann, T., Heinrich, G., Huber, T., and Studerus, C.
Master Integrals for Massless Three-Loop Form Factors: One-Loop and Two-Loop Insertions
Phys. Lett. B640 (2006), 252-259, [arXiv:hep-ph/0607185]

2.) Huber, T., Lunghi, E., Misiak, M., and Wyler, D.
Electromagnetic logarithms in $\bar{B} \to X_s\, l^+ l^-$
Nucl. Phys. B740 (2006), 105-137, [arXiv:hep-ph/0512066]

3.) Huber, T., and Maître, D.
HypExp, a Mathematica package for expanding hypergeometric functions around integer-valued parameters
Comput. Phys. Commun. 175 (2006), 122-144, [arXiv:hep-ph/0507094]

4.) Gehrmann, T., Huber, T., and Maître, D.
Two-loop quark and gluon form factors in dimensional regularisation
Phys. Lett. B622 (2005), 295-302, [arXiv:hep-ph/0507061]

5.) Donoghue, J. F., Holstein, B. R., Huber, T., and Ross, A.
Long distance effects and strangeness in the nucleon
Fizika B14 (2005), 217-244, [arXiv:hep-ph/0412035]

In Preparation:

1.) Huber, T., Hurth, T., and Lunghi, E.
Logarithmically Enhanced Corrections to the Decay Rate and Forward Backward Asymmetry in $\bar{B} \to X_s\, l^+ l^-$

2.) Gehrmann, T., Heinrich, G., Huber, T., and Maître, D.
Complete Set of Master Integrals for Massless Three-Loop Form Factors

Conference Proceedings:

1.) Huber, T., and Schilling, S.
$\bar{B} \to X_s\, l^+ l^-$ in the standard model and in two-Higgs-doublet models
in: *Proceedings of the 40th "Rencontres de Moriond on QCD and High Energy Hadronic Interactions"*
La Thuile, Aosta Valley, Italy, March 12th – 19th, 2005,
eds.: Étienne Augé and Jean Trân Thanh Vân. *[arXiv:hep-ph/0512067]*